UNIVERSITY OF LEEDS

Using earth system modelling to understand abrupt climate changes in the last glacial period: transient events and ocean oscillations

Brooke Snoll

Submitted in accordance with the requirements for the degree of Doctor of Philosophy

The University of Leeds

Faculty of Environment

School of Earth and Environment

February 2025

Intellectual Property

The candidate confirms that the work submitted is their own, except where work which has formed as part of jointly authored publications has been included. The contribution of the candidate and the other authors to this work has been explicitly indicated below. The candidate confirms that appropriate credit has been given within the thesis where reference has been made to the work of others.

The work in Chapter 2 of this thesis was published in Climate of the Past as part of the 'Paleoclimate Modelling Intercomparison Project phase 4 (PMIP4) (CP/GMD inter-journal SI)' special issue as follows: Brooke Snoll, Ruza F. Ivanovic, Lauren J. Gregoire, Sam Sherriff-Tadano, Laurie Menviel, Takashi Obase, Ayako Abe-Ouchi, Nathaelle Bouttes, Chengfei He, Feng He, Marie Kapsch, Uwe Mikolajewicz, Juan Muglia, and Paul Valdes: A multi-model assessment of the early last deglaciation (PMIP4 LDv1): a meltwater perspective, Clim. Past, 20, 789–815, https://doi.org/10.5194/cp-20-789-2024, 2024. The study conception was developed by the PMIP4 Working Group, consisting of RI, LM, TO, AAO, NB, MK, UM, and PV. BS, LG, SST, and RI contributed to the study design, with LM, TO, and AAO providing additional feedback and close communication with BS. The design of the experiments and running of them was performed by RI, LG, LM, TO, AAO, NB, CH, FH, MK, UM, JM, and PV. Material preparation and data collection was performed by BS. The manuscript was prepared by BS with contributions from all co-authors, who read and approved the final manuscript.

The work in Chapter 3 was submitted for publication to Critical Insights in Climate Change with authorship of Brooke Snoll, Ruza F. Ivanovic, Lauren J. Gregoire, Sam Sherriff-Tadano, and Yvan Romé and with the provisional title 'Competing effects of sea ice change control the pace and amplitude of millennial-scale climate oscillations'. The study conception was developed by BS, RI, LG, and SST. BS, RI, LG, and SST contributed to the study design with YR providing additional feedback and close communication with BS. BS, RI, and LG designed the experiments, and BS performed them. Material preparation and data analysis was performed by BS. The manuscript was prepared by BS with contributions from all co-authors, who read and approved the submitted manuscript.

The work in Chapter 4 of this thesis is awaiting review by the co-authors before submission to The Cryosphere with authorship of Brooke Snoll, Ruza F. Ivanovic, Lauren J. Gregoire, Sam Sherriff-Tadano, and Violet Patterson. The study conception was developed by BS, RI, and LG. BS, RI, LG, and SST contributed to the study design. BS, RI, and LG designed the experiments, and BS performed them with assistance from VP. Material preparation and data

analysis was performed by BS. The manuscript was prepared by BS with contributions from RI, LG, and SST, who read and approved a previous version of this manuscript.

Signed 

Acknowledgments

There are many people who I would like to acknowledge for their fundamental role in the completion of this thesis. First, I would like to thank Ruza Ivanovic and Lauren Gregoire for their continuous encouragement and positivity throughout their supervision. Despite adversities that have arose in the last few years, they always found the time to support me through my PhD and create a wonderful and welcoming research space that I will be endlessly grateful for. I would also like to thank Sam Sherriff-Tadano for his additional supervision that always brought new and exciting ideas to the research and an uplifting and optimistic attitude wherever he went. Finally, thank you to Dan Hill for agreeing to assist me at a time when I needed some additional supervision.

This thesis is the result of the many incredible collaborators I have been fortunate enough to work with, including but not limited to Laurie Menviel, Takashi Obase, Ayako Abe-Ouchi, the rest of the PMIP4 Working Group, Yvan Romé, and Violet Patterson. I would also like to recognise the invaluable assistance of the CEMAC team in Leeds, and in particular Richard Rigby and Julia Tindall, for all the computational and model running support they provided.

The last few years would have been more difficult if not for the my colleagues and friends at and beyond the University. Thank you to the Climate-Ice group members, including Yvan, Violet, Laura, Jonathan, Oliver, and Sam, as well as the Physical Climate Change group for creating a supportive space to share my work and learn about others'. Thank you Priestley 11.06, the best office in the School of Earth and Environment, for creating a reason for me to come to the office, despite the *occasional* rowdiness.

I would like to extend special thanks to the morning gym crew, Molly Asher, Roxanne Bottomley, and Sicily Fiennes, who were the only reason I ever got to the office before 9 am. Thank you all for your unwavering support, working with me in various locations, and providing wholesome escapes from the thesis outside of working hours. Thank you to the Republica 11s for keeping me active in more ways than one and cultivating an inviting and inclusive space to play the sport I love and spend time with wonderful people.

Thank you to my mother and John for their continuous support and compassion even from thousands of miles away. Finally, I would like to thank Mows for their encouragement, care, and help that got me through my PhD. Thank you for listening to my endless rants and bad stories and at least trying to sound interested, being accommodating of my work schedule, and always believing in me. I would also like to acknowledge Babs for supporting Mows through

my PhD and for nothing else.

This project was funded by the Natural Environment Research Council (NERC) Panorama Doctoral Training Partnership (DTP) under grant NE/S007458/1.

Abstract

The Last Glacial Period and ensuing deglaciation were marked by rapid transitions between cold and warm climates. Despite decades of research, uncertainty remains about the mechanisms driving these events, though it is widely agreed that reorganisations of the Atlantic Meridional Overturning Circulation (AMOC) play a crucial role. However, the precise climatic controls on AMOC remain unclear.

To explore AMOC evolution and its role in abrupt climate change, I employ earth system modelling. First, I compare transient simulations of the last deglaciation under various meltwater scenarios to assess the influence of ice sheet meltwater on the occurrence of abrupt events like Heinrich Stadial 1. Finding that most models fail to produce an abrupt interstadial-stadial switch when forced by current reconstructions of ice sheet meltwater, I then investigate AMOC oscillations in glacial climate simulations with a constant meltwater flux. By varying background conditions, I determine that CO_2 and orbital changes strongly influence the periodicity, magnitude, and occurrence of AMOC oscillations. Lastly, using a coupled climate-ice sheet model, I examine how the Bølling Warming impacts Northern Hemisphere ice sheets, revealing that surface ablation increases due to the abrupt warming, but the scale of this melt is modulated by ocean forcing and initial ice sheet topography.

The results of this thesis demonstrate the sensitivity of the AMOC to subtle shifts in background conditions. These findings underscore the need for further high-resolution climate and ice sheet simulations to unravel the chain of events governing past abrupt climate transitions in the Last Glacial Period.

Contents

List of Figures

List of Tables

Abbreviations

AABW AntArctic Bottom Water
AICC2012 Antarctic ice core chronology
AMOC Atlantic Meridional Overturning Circulation
AOGCM Atmosphere-Ocean General Circulation Model
BRIDGE Bristol Research Initiative for the Dynamic Global Environment
CMIP Coupled Model Intercomparison Project
D-O Dansgaard-Oeschger
EIS Eurasian Ice Sheer
EMIC Earth System Model of Intermediate Complexity
ESM Earth System Model
FAMOUS FAst Met Office/UK Universities Simulator
GCM General Circulation Model
GIN Greenland-Iceland-Nordic
GrIS Greenland Ice Sheet
HadCM3 Hadley Centre Climate Model 3
HS1 Heinrich Stadial 1
IPCC Intergovernmental Panel on Climate Change
IRD Ice-Rafted Debris
ka BP thousand years before present
LDv1 Last Deglaciation version 1 protocol
LGM Last Glacial Maximum
MIS3 Marine Isotope Stage 3
MLD Mixed Layer Depth
MOSES2 Met Office Surface Exchange Scheme 2
m SLE metres sea level equivalent
MWP1a Meltwater Pulse 1a
NADW North Atlantic Deep Water
NAIS North American Ice Sheet
NATL North Atlantic
PMIP4 Palaeoclimate Modelling Intercomparison Project 4
ppb[v] parts per billion [by volume]
ppm[v] parts per million [by volume]
SAT Surface Air Temperature
SIC Sea Ice Concentration
SST Sea Surface Temperature
Sv Sverdrup
TRIFFID Top-down Representation of Interactive Foliage and Flora including Dynamics

CHAPTER 1

Introduction

1.1 Scientific context for the thesis

1.1.1 The Last Glacial Period

The most recent glacial period, the *Last Glacial Period*, occurred between 115 and 11.7 thousand years ago (ka BP; with present being 1950 CE) and began at the end of the Last Interglacial. Variations in the Earth's orbit, or Milankovic cycles, have caused historical cycles between glacial and interglacial periods through the orbital elements of eccentricity, obliquity, and precession (Berger 1988). The transition from the Last Interglacial to the Last Glacial Period coincides with decreasing Northern Hemisphere summer insolation, a result of the combined impact of changing eccentricity and precession.

Also known as the Last Ice Age, the Last Glacial Period was colder and drier than modern day with extensive ice sheets (Figure 1.1) across northern North America, a culmination of the Cordilleran and Laurentide ice sheets, Eurasia, covering the Barents and Kara Seas, Scandinavia, and even Ireland and northern Britain at times (Dyke 2004; Peltier et al. 2015; Svendsen 2004; Tarasov et al. 2012), and with larger Antarctic and Greenland ice sheets than today (Argus et al. 2014; Briggs et al. 2014; Lambeck et al. 2014). Atmospheric CO_2 concentrations, measured from trapped gases in ice cores from the Greenland and Antarctic ice sheets, were low compared to interglacial periods (e.g., modern day) with concentrations as low as 180 parts per million (ppm; Siegenthaler et al. 2005; Kawamura et al. 2007; Bereiter et al. 2015) during the Last Glacial Period. Methane and nitrous oxide, also correlated with glacial-interglacial cycles, varied between 350 and 400 parts per billion by volume (ppbv) for CH_4 (Loulergue et al. 2008) and around 200 ppbv for N_2O (Schilt et al. 2010).

As a whole, the Last Glacial Period is characterised by rapid climate transitions between cold (stadial) and warm (interstadial) states originally described from Greenland ice cores and ice-rafted deposits in the Atlantic Ocean (Dansgaard et al. 1982; Bond et al. 1993; Grootes et al. 1993), but now evident in surface air temperature proxy records world-wide, such as in European pollen records (e.g., Fletcher et al. 2010), sediment cores of South America (e.g., Fritz et al. 2010), vegetation records from North America (e.g., Jiménez-Moreno et al. 2010), stalagmite

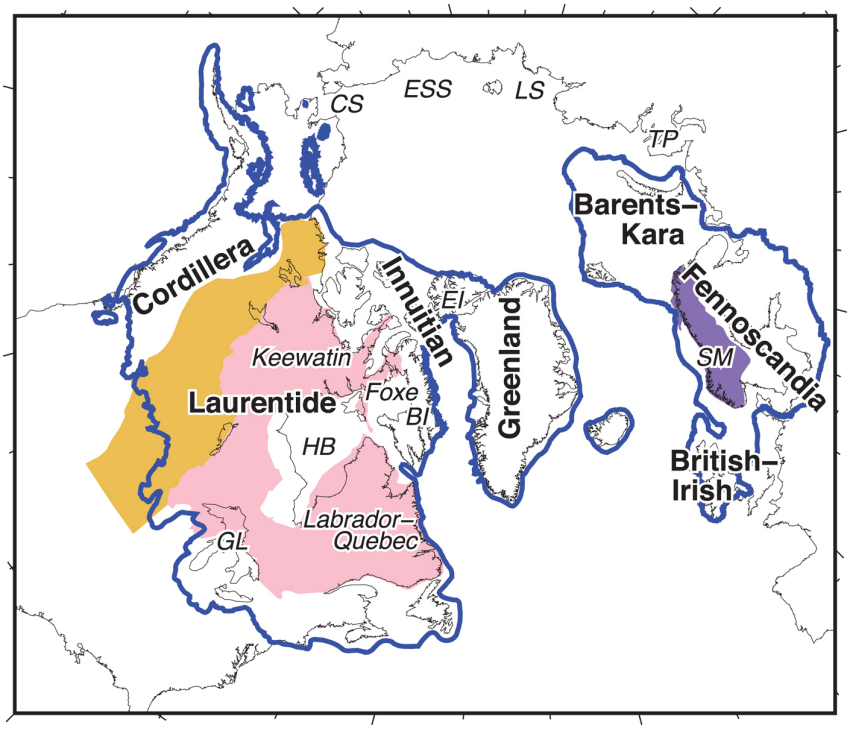

Figure 1.1: Location of Northern Hemisphere ice sheets at the Last Glacial Maximum (21 ka BP): Cordillera[n], Laurentide, Innuitian, Greenland, Barents-Kara, Fennoscandia and British-Irish Ice Sheets (blue line; Dyke 2004; Hughes et al. 2016; Gowan et al. 2016). The locations of the three domes of Laurentide Ice Sheet: Labrador-Quebec, Keewatin and Foxe. The areas mentioned in this study include the Hudson Bay (HB), the Great Lakes (GL), Baffin Island (BI), Ellesmere Island (EI), Taimyr Peninsula (TP), Laptev Sea (LS), East Siberian Sea (ESS) and Chukchi Sea (CS). The yellow area is the Interior Plains, the pink area is the Canadian Shield and the purple area is the Scandinavia Mountains (SM). Taken from Niu et al. (2019).

and loess records in Asia (e.g., Wang et al. 2008; Yang and Ding 2014) and oxygen-isotope records in Greenland (Wolff et al. 2010; Buizert et al. 2018) anti-phased with variability in Antarctica (EPICA Community Members et al. 2006; Buizert et al. 2015).

1.1.1.1 Abrupt climate events during the glacial period

The most commonly referred to example of abrupt climate changes during the Last Glacial Period are Dansgaard-Oeschger (D-O) cycles, or millennial-scale climate oscillations of up to 10-15 °C in the high northern latitudes (Huber et al. 2006; Kindler et al. 2014; Andersen et al. 2006). These events are documented most frequently during a period known as Marine Isotope Stage 3 (between 60 and 25 ka BP; Sanchez Goñi and Harrison 2010), as recorded from Greenland ice cores (Figure 1.2e) and more globally, including the Tropics (Deplazes et al. 2013; Adolphi et al. 2018), North and South America (Wang et al. 2004; Asmerom et al. 2010; Deplazes et al. 2013; Vanneste et al. 2015), and Eurasia (e.g., Wang et al. 2008; Rousseau et al. 2017), but also asynchronously recorded in Antarctica (e.g., Blunier et al. 1998; EPICA Community Members et al. 2006; Markle et al. 2017). The anti-phasing between Greenland and Antarctic temperatures is called the 'bipolar see-saw', or the concept that meridional heat transport leads to asynchronous temperature changes in the hemispheres (Stocker 1998).

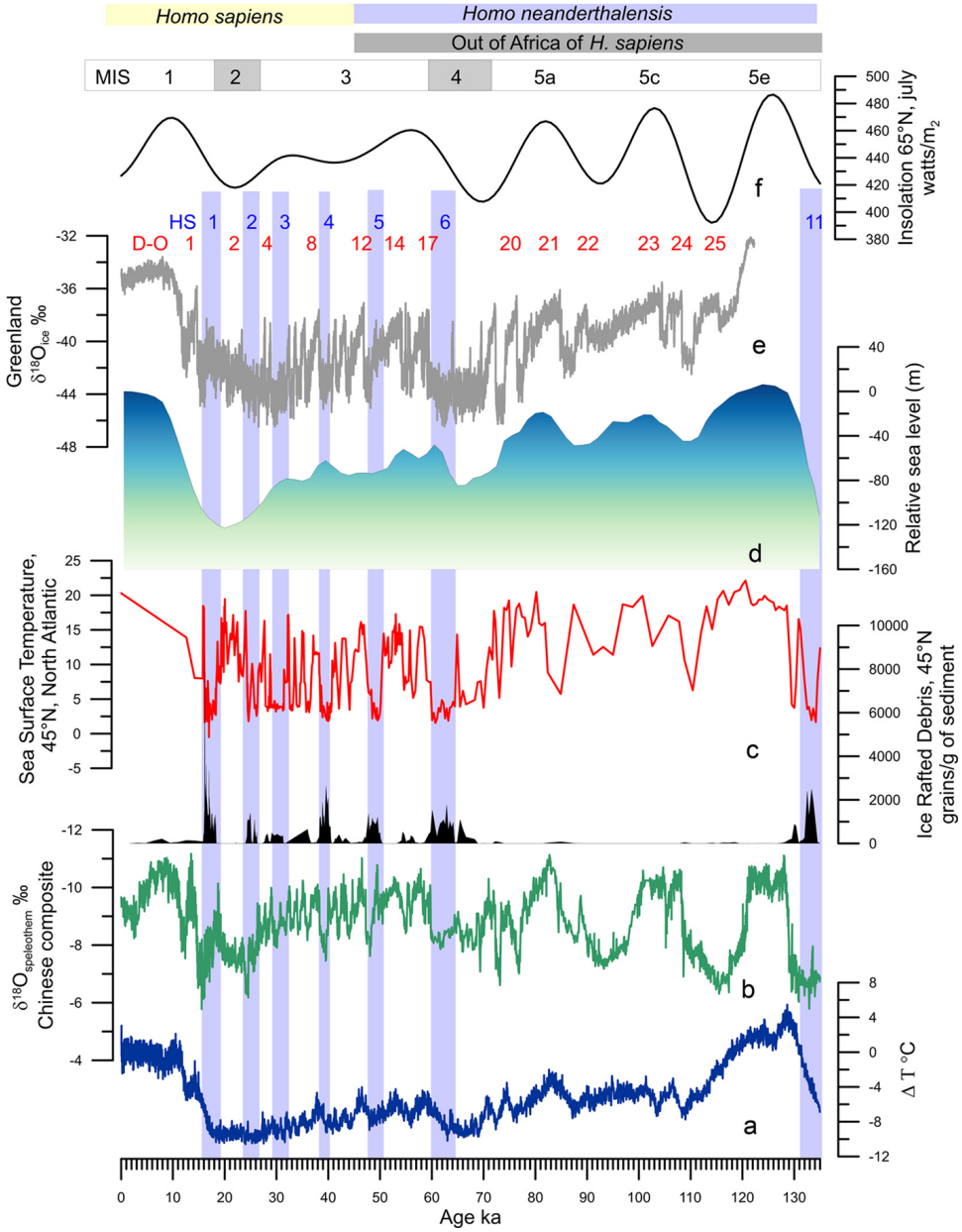

Figure 1.2: Climate variability during the Last Glacial Period. (a) Antarctic temperature anomalies (Jouzel et al. 2007). (b) Composite of Chinese speleothem record from the Sanbao and Dongge Caves (Cheng et al. 2016)[1]. (c) Ice-rafted debris and sea surface temperatures reconstructed from foraminifera[2] of core MD04-2845 (45° N, 5° W; Sánchez Goñi et al. 2008). (d) Relative sea level changes (Waelbroeck et al. 2002) to modern day. (e) Greenland ice core $\delta^{18}O$[1] (Rasmussen et al. 2014). (f) Insolation variation in July at 65° N (Berger and Loutre 1991). Taken from Goñi (2020).

[1]Oxygen isotopes trapped in the ice cores are used as a proxy for temperature by observing the change in ^{18}O ($\delta\ ^{18}O$). In a warmer climate, there are more heavy isotopes in the ice core as more ^{18}O has the energy to evaporate out of the ocean and precipitate onto the ice sheet.

[2]The ratio of magnesium (Mg) to calcium (Ca) in planktic and benthic foraminifera shells measures the occurrence of Mg substituting in for a Ca atom in the formation of calcium carbonate, $CaCO_3$. The substitution is ocean temperature dependent–temperature increases give rise to an increase in magnesium concentrations (Nürnberg et al. 1996)

.

There were ∼25 D-O cycles during the Last Glacial Period, commonly described as having an average periodicity of ∼1,500 years (Schulz 2002; Rahmstorf 2002), though D-O cycles are irregular and have a periodicity of anywhere between 400 and 2,600 years (Wolff et al. 2010). Similar to the saw-tooth pattern of the glacial-interglacial cycles, an ordinary D-O cycle consists of an abrupt warming into the warm interstadial phase followed by a relatively slower cooling into the cold and relatively stable stadial phase (Figure 1.2; Thomas et al. 2009). The transition from the cold to the warm phase can increase temperatures by up to 16.5°C in Greenland (Kindler et al. 2014) with an average warming duration of ∼60 years (Lohmann and Ditlevsen 2019). At the beginning of each interstadial, there is a warm overshoot phase in the Atlantic Meridional Overturning Circulation (AMOC) and corresponding North Atlantic surface temperatures (Knorr and Lohmann 2003; Dokken et al. 2013; Dima et al. 2018) in which the AMOC first surpasses and then subsequently rebounds to settle in a quasi-equilibrium state of AMOC strength (Dima et al. 2018).

Stadial phases of D-O cycles are sometimes paired with a Heinrich event–a massive armada of icebergs calved from the Laurentide ice sheet (Hemming 2004; Hodell et al. 2017). Heinrich events are identified in deep sea core records in the North Atlantic (Bond and Lotti 1995) where the event is captured by a layer of rocky debris transported from the Laurentide ice sheet into the North Atlantic Ocean between the latitudes of 40° and 55° N (i.e., the Ruddiman belt; Ruddiman 1977) via icebergs. The stadial phases that contain Heinrich events are called Heinrich Stadials. Early research hypothesised that the melting of the icebergs initiated a strong disruption of the AMOC and caused surface ocean cooling in the North Atlantic and surface air cooling in the surrounding areas (discussed more in section 1.1.2.1; Bond et al. 1992; Bard et al. 2000). However, high latitude North Atlantic surface ocean temperature and ice-rafted debris proxy data demonstrate that, at least in some cases, surface ocean cooling occurred hundreds of years earlier than the iceberg events (Barker et al. 2015).

1.1.1.2 The last deglaciation

Between 26 ka BP (Peltier and Fairbanks 2006) and 19 ka BP (Clark et al. 2009; Lambeck et al. 2014; Mix et al. 2001), the ice sheets reached a maximum extent (Figure 1.1) and sea level hit a minimum (Figure 1.2d). At the *Last Glacial Maximum* (LGM), global mean surface temperatures were also estimated to be between 4 and 7 °C lower than present-day (Annan et al. 2022; Liu et al. 2023).

After 19 ka BP, the Earth started warming towards its present state initiated by a gradual increase in boreal summer insolation (Figure 1.3c; Berger 1978). Subsequently, as greenhouse gas concentrations also rose (Loulergue et al. 2008; Schilt et al. 2010; Bereiter et al. 2015), the vast ice sheets began melting and sea levels began to rise (Figure 1.2d and 1.3g). This period, known as the *last deglaciation* is defined by a major, long-term (order of 10,000 years) climate transition from the most recent cold glacial to the current warm interglacial state (known as the Holocene; beginning around 11.7 ka BP), as well as many short-term, decadal- to millennial-scale warmings and coolings.

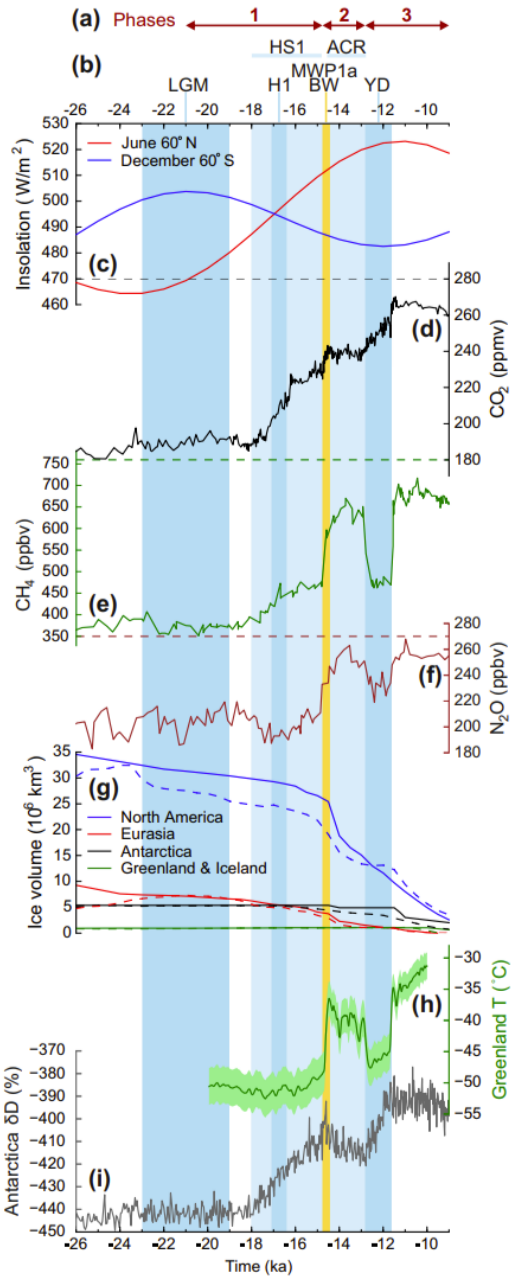

Figure 1.3: The last deglaciation: forcing and events. (a) Phases of the PMIP protocol core experiments. (b) Climate events and periods. (c) June insolation at 60° N (red) and December insolation at 60°] S (blue) from Berger (1978). (d) Atmospheric carbon dioxide concentration in Antarctica from Bereiter et al. (2015). (e) Atmospheric methane concentration in Antarctica from Loulergue et al. (2008). (f) Atmospheric nitrous oxide concentration in Antarctica from Schilt et al. (2010). Dashed lines shown pre-industrial levels in (c)-(e). (g) Volume of the ice sheets according to ICE-6G_C ice sheet reconstruction (solid lines; Argus et al. 2014; Peltier et al. 2015) and the GLAC-1D reconstruction (dashed lines; Briggs et al. 2014; Tarasov and Peltier 2002; Tarasov et al. 2012). (h) Greenland temperature reconstruction from Buizert et al. (2014). (i) Antarctica δD[1] from Jouzel et al. (2007).

[1]Similar to with oxygen isotopes, hydrogen isotopes (^{1}H and ^{2}H; ^{2}H is also knows as deuterium or D) can be used as a proxy for temperature, with higher temperatures leading to a greater relative abundance of lighter hydrogen isotopes in an ice core.

1.1.1.2.1 Heinrich Stadial 1

The first short-term climate event to occur during the last deglaciation is Heinrich Stadial 1 (HS1; between ∼18 and 14.7 ka BP; Martin et al. 2023). HS1 is defined by cooler temperatures (Shakun et al. 2012) and weak ocean circulation (Ng et al. 2018), contradictory to what would be expected during the onset of the deglaciation. With the increasing insolation, temperatures were expected to rise globally, but instead surface temperatures in the Northern Hemisphere remained cold (Bard et al. 2000; Buizert et al. 2018; Pedro et al. 2022). Pre-HS1, between 20 and 19 ka BP, massive meltwater discharges from the Eurasian ice sheet occurred (Ménot et al. 2006; Toucanne et al. 2015) that could have resulted in a slowed down AMOC and colder temperatures (section 1.1.2.2). In addition, HS1 is associated with two climatic episodes (Broecker and Putnam 2012; Huang et al. 2019) that consisted of freshwater discharges from the Eurasian ice sheet (∼18.2 ka BP; e.g., Ménot et al. 2006; Stanford et al. 2011) and a massive ice rafting episode from the Laurentide ice sheet (known as Heinrich event 1, ∼16.2 ka BP; Hemming 2004; Hodell et al. 2017). This additional meltwater discharge could have provided the means to prolong the weakening of the AMOC for thousands of years (Solas et al. 2011; Barker et al. 2015).

1.1.1.2.2 Bølling-Allerød Warming

After HS1, an abrupt transition to an interstadial state was triggered known as the Bølling-Allerød Warming (abbreviated to Bølling warming; ∼14.7 ka BP in Greenland; Severinghaus and Brook 1999; Lea et al. 2003; Buizert et al. 2018). The Bølling interstadial, the first warming event of the last deglaciation in the Northern Hemisphere, was originally described in three parts: the Bølling and Allerød warm interstadials separated by the Older Dryas cold stadial (Figure 1.3h; section 1.1.1.2.4). In Greenland, temperatures increased about 8-10 °C in a few decades (Steffensen et al. 2008; Buizert et al. 2018) coincident with a cold event recorded in Antarctica, known as the Antarctic Cold Reversal (Blunier et al. 1997; Stenni et al. 2001; Pedro et al. 2016), with a mechanism linked to the bipolar see-saw (Menviel et al. 2011). The interstadial is synchronous with an increase of boreal summer insolation (Berger and Loutre 1991) and significant ice volume loss. The transition from HS1 to the Bølling Warming and on to the Younger Dryas stadial (section 1.1.1.2.4) is often considered to be the most recent D-O event (Figure 1.2e; Su et al. 2016).

1.1.1.2.3 Meltwater Pulse 1a

The Bølling Warming also coincides with a notable abrupt meltwater event, called Meltwater Pulse 1a (MWP1a; ∼14.7 to 14.3 ka BP; Fairbanks 1989; Deschamps et al. 2012; Lambeck et al. 2014). MWP1a consisted of sea level rise of 8-22 metres in ∼350 years or less (Deschamps et al. 2012; Liu et al. 2016), although, the origin of the meltwater pulse has long been debated. The primary source of the meltwater discharge is thought to have originated from the saddle collapse between the Laurentide and Cordilleran ice sheets that likely occurred between 16 and 14 ka BP (Dyke 2004; Gregoire et al. 2012; Gregoire et al. 2016), with additional contributions from Antarctica (Peltier 2005; Briggs et al. 2014; Golledge et al. 2014) and Eurasia (Brendryen

et al. 2020; Lin et al. 2021; Coonin et al. 2025).

1.1.1.2.4 Older and Younger Dryas

After the abrupt warming event at 14.7 ka BP, two stadial periods occur before then end of the last deglaciation. The Older Dryas occurred between the Bølling and Allerød interstadial at ∼14 ka BP and is characterised by a glacial re-advance (Mangerud 1970). After the Allerød interstadial, at 12.9 ka BP, another abrupt cooling phase is recorded in Greenland and Antarctic ice cores, known as the Younger Dryas (Broecker et al. 2010; Murton et al. 2010; Liu et al. 2012) and thought to be caused by the release of freshwater from the proglacial Lake Agassiz, located along the southwestern front of the retreating Laurentide ice sheet (Broecker et al. 2010; Murton et al. 2010). The stadial period lasted ∼1,200 years before the last deglaciation terminated and the climate entered into the Holocene.

1.1.2 Mechanisms of abrupt climate change and the AMOC

Despite decades of research on D-O cycles and other abrupt climate changes, uncertainty still remains as to the mechanisms and drivers of these transitions. Because the bipolar see-saw mechanism is linked to meridional heat transport of the AMOC (Broecker 1998; Rahmstorf 2002) and proxy records for the AMOC often are coincident with North Atlantic temperature changes (McManus et al. 2004; Ng et al. 2018), connections have been drawn between the AMOC and abrupt climate change events.

1.1.2.1 Atlantic Meridional Overturning Circulation

The AMOC is the Atlantic component of the global meridional overturning circulation, or global network of ocean currents previously known as the Conveyor (Broecker 1997; Rahmstorf 2002). The global meridional overturning circulation connects the different ocean basins and their respective ocean circulations: the Pacific meridional overturning circulation, the Atlantic meridional overturning circulation, the Indian Ocean meridional overturning circulation, and the Antarctica circumpolar current in the Southern Ocean (Rahmstorf 2002). The overturning system is governed by wind-driven currents and tides (on inter-annual timescales) alongside buoyancy fluxes (on inter-annual to decadal timescales) driven by the thermohaline circulation (Buckley and Marshall 2016; Jackson et al. 2022). The density of water, and therefore its buoyancy, is determined by its temperature and salinity (where colder and more saline waters have a higher density).

In the modern ocean, the buoyancy fluxes allow for light, warm, but also high-salinity waters originating from the Gulf of Mexico and the tropics to be transported northward into the North Atlantic. As this water reaches the high latitudes, it loses heat to the atmosphere and becomes more dense, attaining critical density in sites such as the Irminger and Nordic Seas (Figure 1.4). At these locations, called deep water formation sites, the upper cell of the AMOC sinks and forms North Atlantic Deep Water (NADW; Cheng et al. 2007), which subsequently returns southwards, reaching the Antarctic circumpolar current. In the Southern Ocean, the deep water mixes with other deep water masses and is upwelled at the surface where it might circulate into

other ocean basins or sink again through the process of brine rejection to create Antarctic Bottom Water (AABW), very dense water that layers the Atlantic Ocean floor. Brine rejection is the process of freshwater production by expelling salt as water freezes into sea ice (Nebbia and Menozzi 1968).

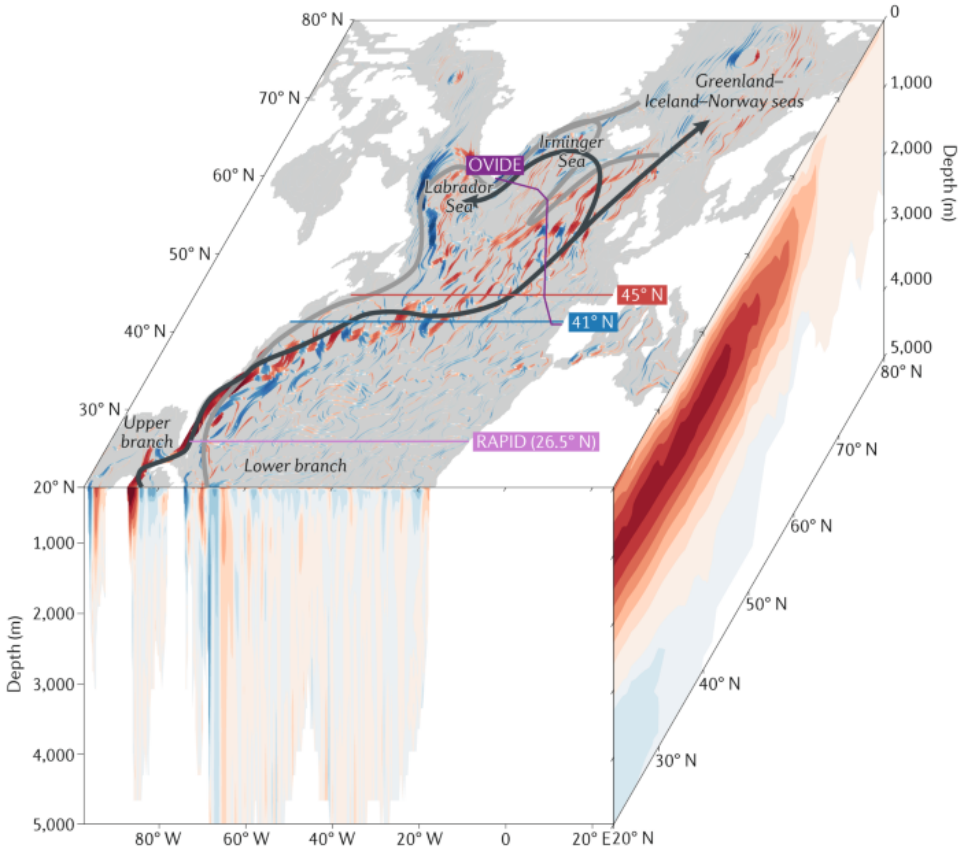

Figure 1.4: Schematic of the Atlantic Meridional Overturning Circulation (AMOC). In the surface panel (top), surface currents are indicated in black arrows, and the return deep currents are represented by grey arrows. Sinking is plotted in red and upwelling in blue. The right-hand panel shows the zonally integrated meridional circulation (or the AMOC streamfunction). Red colours indicate clockwise motion, and blue colours indicate anti-clockwise motion. Taken from Jackson et al. (2022).

However, the shape and strength of the AMOC has very likely changed throughout its history and has shown frequent variability (Lynch-Stieglitz 2017; Ng et al. 2018). Reconstructions of the past AMOC demonstrate its ability to not only transition rapidly out of a weak state to a strong state (and vice versa) but also to remain in a specific state for a prolonged period of time. Stommel (1961) was first to demonstrate the existence of multiple equilibria in the ocean circulation using a simple non-linear two-box model. As modelling advanced, this conclusion was followed by hysteresis modelling of the AMOC, a concept first tested by Rahmstorf (1996) and continually tested with increasingly efficient and more complex models to understand the impact of external forcings on the AMOC. The two equilibria are referred to as a 'strong', warm, or interstadial AMOC mode, and a 'weak', cold, or stadial AMOC mode, as defined by Böhm et al. (2015) (Figure 1.5). In the warm mode, deep water formation is active in the North Atlantic and NADW occupies a large fraction of the deep Atlantic basin (i.e., down to

~5,000 metres depth). In the cold mode, NADW is recorded at shallower depths than modern day and instead, the deeper layers of the Atlantic basin are blanketed by the expansion of deep water convected from the Southern Ocean (Antarctic Bottom Water). There is also evidence for a third mode, an 'off' AMOC mode, as a potential result of meltwater discharges, where the AMOC has collapsed and no deep water forms in the North Atlantic. Antarctic Bottom Water fills out the entire Atlantic basin and temperatures decrease across the North Atlantic region.

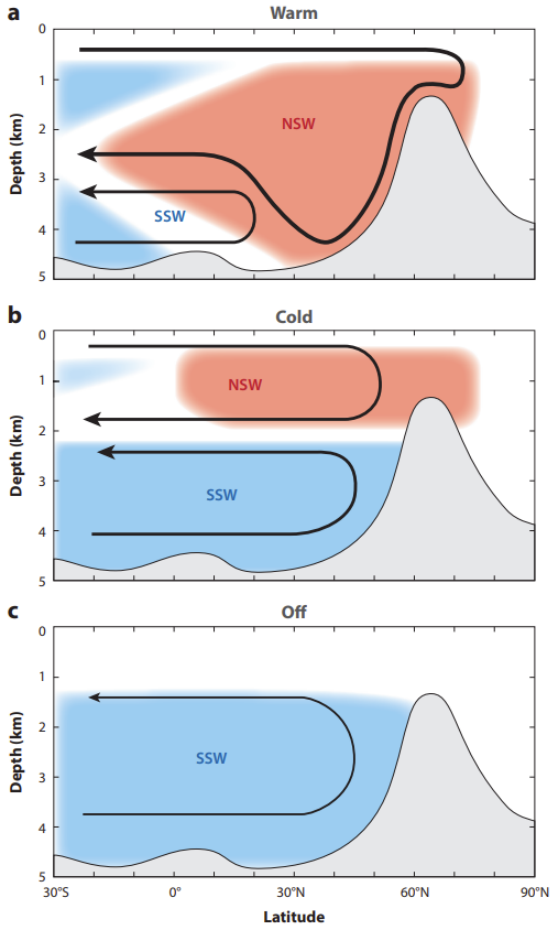

Figure 1.5: Modes of the AMOC. NSW (in red) stands for Northern Source Water and represents the warm Atlantic waters that form North Atlantic Deep Water (NADW). SSW (in blue) stands for Southern Source Water and represents the Antarctic Bottom Water. The water mass, circulation, and depth indicate typical observations for each mode–warm, cold, and off. Taken from (Lynch-Stieglitz 2017).

There is still debate, however, on how to interpret geological records of AMOC strength, especially during the Last Glacial Maximum (LGM) and how the initial state of the AMOC impacts the subsequent climate change of the last deglaciation. Some interpretations have suggested a weaker and shallower AMOC than present-day during the LGM (e.g., Lynch-Stieglitz et al. 2007; Menviel et al. 2012; Böhm et al. 2015; Lynch-Stieglitz 2017; Menviel et al. 2017; Muglia and Schmittner 2021; Wilmes et al. 2021; Pöppelmeier et al. 2023b). Whilst other ocean circulation proxy studies (e.g., McManus et al. 2004; Gherardi et al. 2005; Gherardi et al. 2009; Ivanovic et al. 2018a; Ng et al. 2018) demonstrated a consensus of a vigorous but shallower AMOC in the latter stages of the LGM and in the early last deglaciation (relative to the mod-

ern day). Recent modelling also has shown between a deep and strong ocean circulation at the LGM (e.g., Menviel et al. 2011; He et al. 2021; Sherriff-Tadano et al. 2021; Kapsch et al. 2022; Snoll et al. 2022) due to the presence of thick ice sheets (Oka et al. 2012; Sherriff-Tadano et al. 2018; Galbraith and Lavergne 2019) and a shallow AMOC of similar strength to present-day (e.g., Gu et al. 2020; Zhu et al. 2021).

Coming out of the LGM, different conclusions can be drawn from the reconstructions as to the AMOC during Heinrich Stadial 1 (i.e., collapsed; Gherardi et al., 2005, weakened but persistent; Bradtmiller et al., 2014, or still active; Repschläger et al., 2021) depending on the proxy used, location of the sediment cores, and the interpretation of the proxy and its accuracy in representing the AMOC. However, a study combining all thirty-three available deglacial AMOC proxy records demonstrates that there is large consensus in the AMOC pattern of change despite the diverse oceanographic and sedimentary settings (Ng et al. 2018). This compilation concludes on an AMOC weakening during Heinrich Stadial 1 as well as an AMOC resumption in strength at the onset of the Bølling Warming. The AMOC then weakened again during the Younger Dryas before resuming in strength once more whilst transitioning into the Holocene interstadial.

Since the start of the 21st century, observations of the modern AMOC have been made through measuring water velocity across the entire water column using full-depth moorings (Frajka-Williams et al. 2019). The location of the RAPID array, 26.5° N, is often used as the representative location of the AMOC due to the large northward heat transport by the ocean at this latitude. Between 2004, when RAPID array measurements began, and present-day, the estimated AMOC strength was measured as $\sim$16.9 $\pm$ 4.6 Sverdrup (Sv; 1 Sv = 1 million cubic metres per second). The OSNAP array, located in the subpolar North Atlantic with sections in the Iceland, Irminger, and Labrador sea basins, is used to infer overturning in deep water formation sites. Initial results from the OSNAP array show that the majority of overturning occurs north of the eastern part of OSNAP, i.e., along the western boundaries of the Iceland and Irminger Seas (Lozier et al. 2019; Petit et al. 2020). The Labrador Sea, in the west, contributes significantly less to overturning than that of the eastern basins (Pickart and Spall 2007).

1.1.2.2 Meltwater and the AMOC

Despite our increased understanding of the AMOC, the mechanisms behind the switches between different AMOC modes and their potential relation to abrupt climate changes is still largely unknown. One compelling link between AMOC transitions and abrupt climate events is the impact of freshwater fluxes on the ability for deep water formation to occur. Previous studies have shown that the AMOC pattern can be easily perturbed by changes in meltwater input into the North Atlantic. For example, if freshwater is deposited into the critical convection sites in the subpolar North Atlantic, i.e., the Labrador Sea and Nordic Seas, locations of high sensitivity to wind patterns and sea ice formation, the circulation strength can be disrupted (**rahmstorf˙decadal˙1999**). This is because freshwater, in contrast to saline water, is significantly less dense, and can, therefore, decrease sea water's density and hinder deep water formation and the amount of heat transported northward. In some cases where meltwater fluxes are applied to the North Atlantic in model simulations, rapid decreases of $\sim$10 °C or more in

annual Greenland surface air temperature occur (e.g., Ganopolski and Rahmstorf 2001; Knutti et al. 2004; Otto-Bliesner and Brady 2010; Brown and Galbraith 2016). However, the response to a freshwater flux is model dependent, and there is evidence to show that climate models are too sensitive to fluxes in some instances (He and Clark 2022) or, alternatively, have too muted of a response in others (Valdes 2011; Liu et al. 2014).

There are also strong indications that the impact of oceanic freshwater fluxes is highly dependent on the location that they enter the ocean (depth and latitude/longitude) and at what magnitude and speed, as it determines the efficiency of convection disruption (e.g., Stocker et al. 2007; Roche et al. 2007; Roche et al. 2010; Smith and Gregory 2009; Otto-Bliesner and Brady 2010; Condron and Winsor 2012; Ivanovic et al. 2017; Romé et al. 2022). For example, in contrast to the effect of North Atlantic freshwater 'hosing', where a uniform freshwater flux between 0.1 Sv and 0.4 Sv was released in the Ruddiman belt to represent melt Heinrich events, on the Northern Hemisphere, a freshwater perturbation in the Southern Ocean can induce a non-linear response in the Southern Hemisphere ocean circulation dependent on the magnitude of freshwater discharge and speed at which it is dispersed (Swingedouw et al. 2009; Menviel et al. 2010). However, the Southern Hemisphere ocean circulation has previously been shown to weaken due to meltwater discharge in the Southern Ocean (Stouffer et al. 2007; Menviel et al. 2010), coincident with either a cooling in the Southern Hemisphere whilst the climate in the Northern Hemisphere warms (Weaver 2003; Menviel et al. 2010), or climate changes that are restricted to the Southern Hemisphere (Ivanovic et al. 2018b; Yeung et al. 2019). Regions in the the North Atlantic that are closest to deep water formation sites tend to have the strongest impact in slowing down Atlantic ocean circulation (i.e., off the coast of Ireland and Norway; Smith and Gregory 2009; Roche et al. 2010), whereas Southern and Pacific Ocean deposits have no or limited effect.

The locations of meltwater input is especially important to consider when reflecting on the impact of MWP1a. Despite the use of transient simulations of the last deglaciation and the ample observable data to tune and set-up the model simulations with, the coincident timing of MWP1a and the Bølling warming, has led to difficulty reconciling a strong AMOC (associated with the Bølling warming) with a large freshwater release (associated with MWP1a) using current climate models. Only the transient simulation of Obase and Abe-Ouchi (2019) has successfully simulated a weak AMOC during the onset of the last deglaciation and Heinrich Stadial 1 and the abrupt increase at the Bølling warming without releasing (and then stopping) an unrealistically large amount of freshwater.

There is a longstanding view that a strong freshwater discharge is *necessary* to trigger the transition between strong and weak AMOC modes (Paillard and Labeyriet 1994; Vidal et al. 1997). Freshwater hosing experiments were successful in demonstrating AMOC shifts in general circulation models in the context of D-O cycles (e.g., Ganopolski and Rahmstorf 2001; Knutti et al. 2004; Kageyama et al. 2013; Brown and Galbraith 2016), however the forcing used was often much larger than estimates of meltwater input from Heinrich events (i.e., between 0.1 and 1 Sv as opposed to 0.02-0.08 Sv; Roberts et al. 2014).

1.1.2.3 The cryosphere

1.1.2.3.1 Sea ice

Sea ice in the Nordic Seas has proven to be crucial to the transition between stadial and interstadial phases (e.g., Li et al. 2010; Dokken et al. 2013; Vettoretti and Peltier 2016; Li and Born 2019). Li et al. (2010) show in their simulation that sea ice removal from the Nordic Seas causes 10 °C of winter warming and a 50% increase in snow accumulation at the Greenland Summit. Dokken et al. (2013) find similar results from the marine proxy record, determining that a decrease in sea ice cover during interstadial conditions increases evaporation in that area, and leads to more precipitation over the Eurasian ice sheet. As the ice sheet increases in size, it calves more, sending icebergs into the Arctic, providing a source of freshwater and a mechanism to transition to stadial conditions. When in a stadial phase, sea ice concentration increases, inhibiting wind mixing and transfer of heat between the ocean and atmosphere. Ocean waters, therefore, remain insulated and warm, causing deep water formation to decrease, and stratification of water layers to weaken. This leads to the warmer waters melting the sea ice above it, starting a transition to interstadial conditions (Dokken et al. 2013). Through this process, the abrupt changes in sea ice concentration in this region are correlated with the abrupt changes in the climate, such as D-O cycles.

1.1.2.3.2 Ice sheets

Past ice sheet growth and retreat is constrained by well-documented geological data (e.g., Hughes et al. 2016; Batchelor et al. 2019; Gowan et al. 2021) such as from moraines, debris left behind by a moving glacier, and striations, a groove cut into the bedrock by gravel and rocks carried by glacial ice and meltwater (Stokes et al. 2015). However, reconstructing ice thickness remains challenging and is only constrained by relative sea level records utilising the highly uncertain method of Glacial Isostatic Adjustment (GIA) modelling of the solid earth (Pollard et al. 2023) to infer ice thickness from the rate of rebound since the deglaciation. In combination with records of ice sheet extent, this method has been utilised to develop the ice sheet reconstructions used in palaeoclimate simulations and this thesis (e.g., GLAC-1D and ICE6-G_C; Tarasov et al. 2012; Peltier et al. 2015). A meltwater flux is a derivate of ice thickness changes, and therefore, even more difficult to constrain. Few studies have attempted to reconstruct meltwater fluxes with geochemical traces (Toucanne et al. 2015; Wickert 2016) and suffer from large uncertainties and insufficient data coverage.

It is important to have an accurate representation of past ice sheets because ice sheet topography not only contributes to freshwater input through meltwater, calving, and iceberg melt, but ice sheets also impact wind patterns and strength due to their high elevation. The direction of wind flow, along with its speed, can also affect the strength of AMOC and its transportation of heat throughout the Atlantic Ocean (Zhang et al. 2014). Higher ice sheet elevations enhance surface wind and therefore wind-driven oceanic transport, moving salt into areas of deep water formation and increasing surface salinity in North Atlantic areas, in turn promoting AMOC strengthening (Oka et al. 2012; Muglia and Schmittner 2015; Sherriff-Tadano et al. 2018).

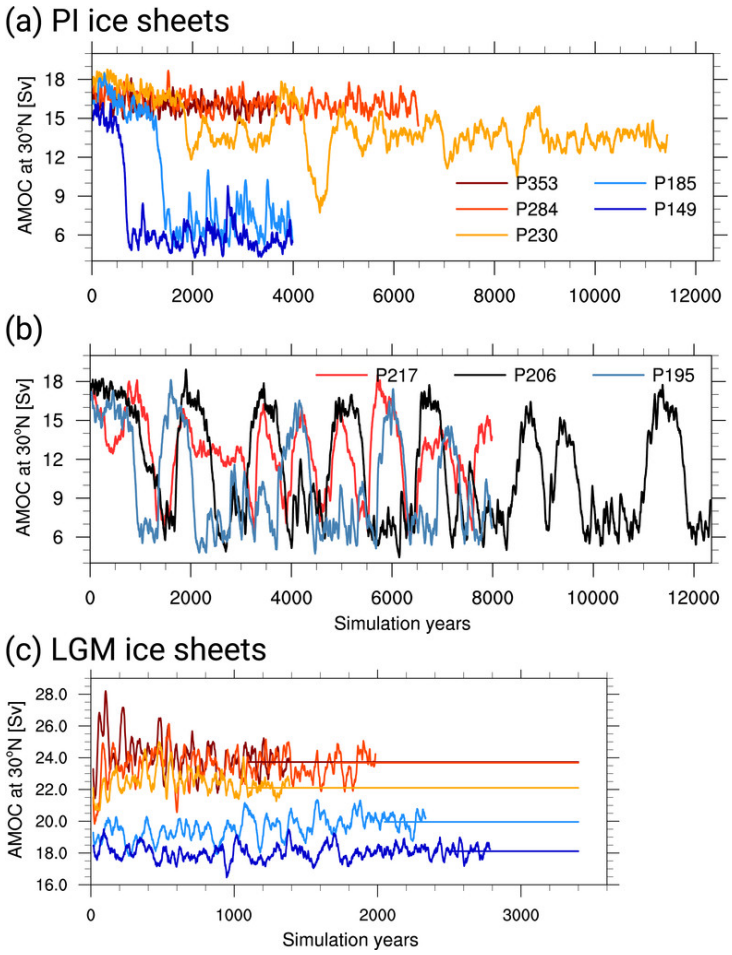

Figure 1.6: Example of millennial-scale variability, or abrupt AMOC oscillations, in a general circulation model. Maximum overturning circulation at 30° N in the Atlantic ocean for simulations described by Klockmann et al. (2018). PXXX indicated the CO_2 of XXX ppm. (a) Non-oscillating simulations obtained with pre-industrial (PI) ice sheets. (b) Oscillating simulations obtained with pre-industrial ice sheets. (c) Non-oscillating simulations obtained with Last Glacial Maximum (LGM) ice sheets. In this case, the LGM ice sheets are the PMIP3 LGM ice sheets of Abe-Ouchi et al. (2015). Taken from Klockmann et al. (2018).

1.1.2.4 Mechanisms of millennial-scale climate variability

To overcome the stable model or potential lack of key physical processes, freshwater forcing was often required to modulate the AMOC (section 1.1.2.2). However, as of recently, general circulation models have appeared to overcome the 'too-stable' phenomenon and multiple groups have successfully simulated Dansgaard-Oeschger-like behaviour in the AMOC without freshwater hosing and with amplitudes and durations matching Greenland variability (Figure 1.6; e.g., Klockmann et al. 2018; Armstrong et al. 2022; Kuniyoshi et al. 2022; Romé et al. 2022; Vettoretti et al. 2022). Using simulations with unforced AMOC oscillations, or 'naturally' occurring abrupt transitions in the AMOC, can help us to understand what conditions encourage more abrupt climate behaviour.

Broecker et al. (1990) added to the multiple equilibria theory by Stommel (1961) by explaining how the AMOC can shift between the different modes without the need for an external trigger.

In this so-called self-sustained *salt oscillator* theory (also known as the salt advection feedback; Drijfhout et al. 2011), strong convection transporting salt out of the North Atlantic and ice sheet melt during the warm AMOC mode causes salinity in the North Atlantic to decrease. The drop in salinity forces the AMOC to shutdown or weaken. Whilst in the cold AMOC mode, meltwater discharge decreases and salinity content in the North Atlantic steadily increases over the next ~1,000 years via evaporation until the AMOC reinvigorates again.

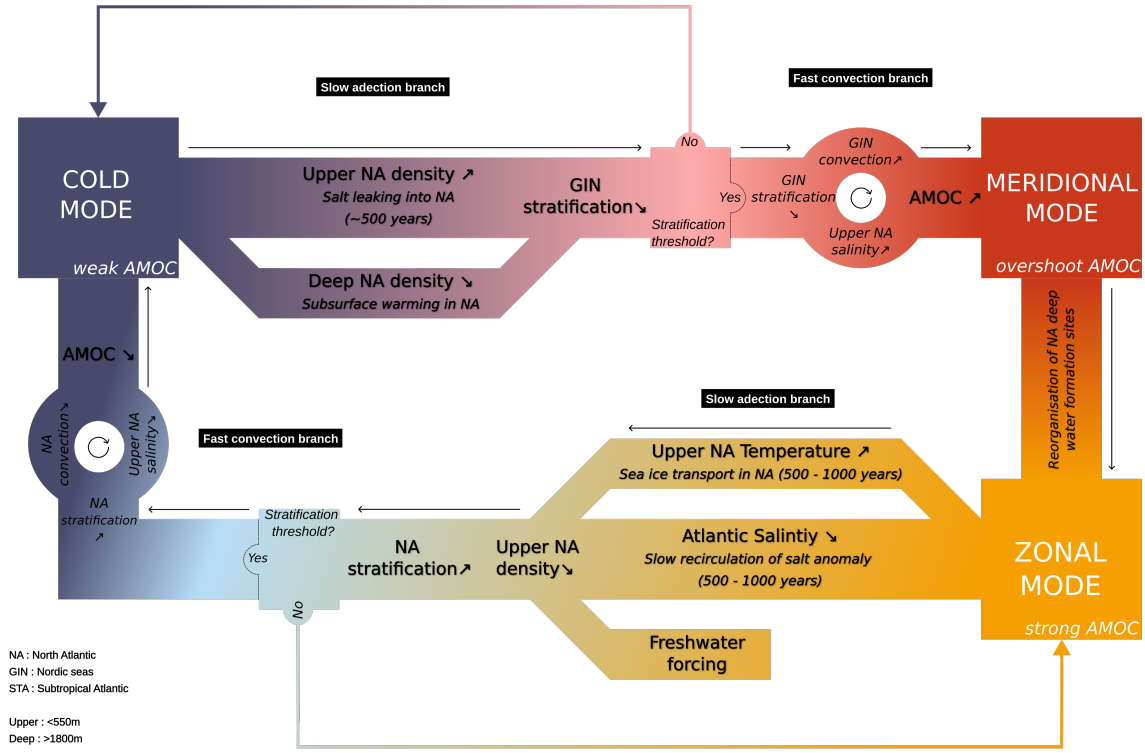

Figure 1.7: Example mechanism for millennial-scale variability, named the *convection-advection* mechanism. Taken from Romé et al. (2025).

The causal mechanisms behind the spontaneous oscillations in the AMOC produced by general circulation models are not always the same, but are compatible with each other and the salt advection feedback. For instance, Armstrong et al. (2022) describe a salt oscillator but with a wind-driven atmospheric feedback in the Nordic Seas as the initiator of the interstadial mode. Vettoretti and Peltier (2018) explained the oscillations of Peltier and Vettoretti (2014) as salt advection driven by North Atlantic sea ice instabilities, initiated by the opening of a large polynya (area of open water surrounded by sea ice) in the Irminger Sea (Vettoretti and Peltier 2016). Romé et al. (2024) present a new mechanism, called the *convection-advection* oscillator, to describe the oscillations of Romé et al. (2022) that is also dependent on salinity transport and North Atlantic stratification (Figure 1.7). The supolar gyre is a prominent feature in multiple mechanistic theories (e.g., Kleppin et al. 2015; Klockmann et al. 2018; Li and Born 2019; Kuniyoshi et al. 2022). Klockmann et al. (2020) combines the concepts of salinity oscillations (Peltier and Vettoretti 2014), with a wind-driven feedback loop (Drijfhout et al. 2013; Kleppin et al. 2015), and a density-driven feedback loop (Montoya et al. 2011) to explain their coupled AMOC-subpolar gyre oscillations. Kuniyoshi et al. (2022) diagnose subpolar

gyre shifts consistent with Li and Born (2019), but the oscillations are heat-driven instead of salt-driven, consistent with Brown and Galbraith (2016). In their case, subsurface ocean temperature change in the North Atlantic plays a significant role in changing the stratification of the vertical water column and shifting the AMOC (compatible with Oka et al. (2012)). Despite attempts by the community to culminate a cohesive mechanistic narrative (Malmierca-Vallet et al. 2023), no mechanisms have so far gained general acceptance.

In addition, these same studies, amongst others, have shown that there is an opportune 'window' in which this oscillatory-like behaviour can occur (Barker and Knorr 2021). The 'window of opportunity is defined as a combination of background conditions that create an optimal environment, or 'sweet spot', for triggering millennial-scale climate variability and affecting their frequency and/or amplitude. The location of the 'sweet spot' is most contingent, in terms of boundary conditions, on ice sheet extent and geometry (Zhang et al. 2014; Brown and Galbraith 2016; Klockmann et al. 2018), background meltwater (Romé et al. 2022), CO_2 concentration (Brown and Galbraith 2016; Zhang et al. 2017; Klockmann et al. 2018; Vettoretti et al. 2022), and orbital configuration (i.e., obliquity, precession, and eccentricity; Brown and Galbraith 2016; Zhang et al. 2021; Kuniyoshi et al. 2022). Although this 'window' can be model-dependent, Malmierca-Vallet et al. (2024) concluded a range of CO_2 concentrations between 185 and 230 ppm that proved to successfully produce AMOC oscillations in three different general circulation models. This CO_2 range also matches the range under which D-O events occurred during Marine Isotope Stage 3. However, it is important to note that often these simulations are performed under a mixture of glacial or even pre-industrial conditions (in regards to the ice sheet topography and orbital configuration) and not those of Marine Isotope Stage 3 (except for Armstrong et al., 2022). Demonstrating that the AMOC can behave significantly differently depending on small changes in the background climate is pertinent to understanding how a transition between a stadial to an interstadial might occur despite a paradoxical freshwater flux, for example.

1.2 Thesis aim

This thesis aims to address the following objective:

To investigate AMOC evolution and its role in abrupt climate change during the Last Glacial Period using different modelling approaches.

To answer this question, I perform and analyse earth system model simulations of the Last Glacial Maximum and last deglaciation as case studies for the Last Glacial Period. Multiple modelling approaches were used, including the first comparison of climate model simulations performed as a part of the Palaeoclimate Modelling Intercomparison Project phase 4 (PMIP4) for the last deglaciation, testing the robustness of millennial-scale variability to changes in atmospheric CO_2 concentration and orbital configuration via new glacial simulations from a general circulation model, and assessing the impact of abrupt sea surface temperature warming on the Northern Hemisphere ice sheets utilising a coupled climate-ice sheet model. The complexity of the thesis aim requires specific questions to make progress on understanding the topic. I,

therefore, adress the thesis aim through these research questions:

- **RQ1**: What is the influence of transient ice sheet meltwater histories on the occurrence of abrupt climate change, such as Heinrich Stadial 1?
- **RQ2**: How do changes in Earth's orbital configuration and atmospheric CO_2 impact abrupt transitions from weak to strong AMOC modes?
- **RQ3**: How sensitive are the Northern Hemisphere ice sheets to the Bølling Warming under transient conditions?

To answer RQ1, I compare multiple transient simulations of the last deglaciation that implemented various meltwater scenarios and determine whether the replication of Heinrich Stadial 1 in the simulations is reliant on the chosen meltwater forcing. After concluding that most models cannot produce an abrupt interstadial-stadial switch with the current reconstructions of ice sheet meltwater, RQ2 aims to investigate these transitions with glacial simulations I know oscillate. Romé et al. (2022) showed the role of freshwater in these AMOC oscillations, so I explore other forcings. Therefore, I know that abrupt, D-O-like AMOC behaviour can be simulated, but it is difficult to do so in transient deglaciation simulations when ice sheets are evolving, an element that could be critical to the meltwater feedback (Romé et al. 2024). Through RQ3, I investigate the impact of an abrupt warming, the Bølling Warming, on the ice sheets and the resulting meltwater discharge into the North Atlantic.

1.3 Research Questions

The thesis is structured so that each research chapter answers one of the research questions in order.

1.3.1 RQ1: What is the influence of transient ice sheet meltwater histories on the occurrence of abrupt climate change, such as Heinrich Stadial 1?

1.3.1.1 Scientific background

The effect of freshwater released from the melting of ice sheets has been clearly identified as the main driver behind AMOC mode shifts (section 1.1.2.2), however there are still many complications impacting our understanding (Bethke et al. 2012). One major point of contention is whether climate models are too sensitive to freshwater fluxes in some instances (He and Clark 2022) or if they, conversely, have too muted of a response to freshwater (Valdes 2011; Liu et al. 2014). In addition, the periods of stronger or weaker AMOC do not always correlate with a weaker or stronger meltwater flux (e.g., the timing of Meltwater Pulse 1a and the Bølling Warming; Deschamps et al. 2012; Ng et al. 2018). The sensitivity of the AMOC in climate models could be dependent on the background climate and the initial climate state, meaning it is important to consider transient forcings. Transient simulations provide the opportunity to better understand multi-millennial-scale processes as well as shorter and more dramatic climate changes whilst taking into account the non-linear interactions that arise between evolving

components of the climate system.

The last deglaciation is a helpful case study for learning about abrupt climate changes and the impact of freshwater fluxes during the Last Glacial Period because it contains abrupt events similar to those we observe deeper in time whilst also being recent enough to have numerous proxy records of the time period. The proxy records allow the research community to not only prescribe their model simulations with more realistic boundary conditions but also to tune or evaluate the model output.

Multiple simulations of the last deglaciation had not previously been collectively analysed, leaving room to take advantage of this model output to build on our understanding of modelling abrupt climate events. The simulations presented as part of answering this research question have applied different meltwater scenarios, creating the opportunity to investigate the impact of different freshwater fluxes on the AMOC and resulting climate. In addition, because they are transient simulations, I can explore the impact of initial climate states as well as the influence of increasing CO_2 concentration and Northern Hemisphere summer insolation on the deglacial progress.

1.3.1.2 Research approach: Multi-model intercomparison project

A multi-model intercomparison project (MIP) provides the opportunity to assess model dependency by comparing results using the same simulation set-up but different models. In this particular case, however, as part of the PMIP4 last deglaciation protocol version 1 (PMIP4 LDv1; Ivanovic et al. 2016), the MIP was designed to be more flexible in effort to incorporate a broad range of models as well as the uncertainty in boundary conditions and forcings of the last deglaciation.

Instead of one specific and rigid configuration for the experimental design, modelling groups were given a choice of recommended forcings and boundary conditions. Thus, analysing model output of multiple simulations of the last deglaciation provides the opportunity to look at differences between experimental designs and their impact on the onset of the deglaciation using different models whilst saving computational resources. However, comparing simulations with different experimental designs is challenging. For example, it is not possible to directly compare results of different models in a strict 'benchmarking' (Braconnot et al. 2012; Harrison et al. 2015) framework, and there may be mismatched performances between variables making it difficult to examine model sensitivities (Harrison et al. 2014). However, this is already the case for transient simulations to some extent, even if a strictly singular protocol is applied, as initial conditions or simulated events can impact later results, such as the starting AMOC condition or whether an abrupt cooling did or did not occur. Furthermore, the technical implementation of boundary conditions/forcings in different models also leads to discrepancies in their configuration, for example the orography calculation of Snoll et al. (2022) or the differences in the meltwater flux calculations between Snoll et al. (2022), Kapsch et al. (2022), and Bouttes et al. (2023) despite deriving from the same ice sheet reconstruction.

The Coupled Model Intercomparison Project (CMIP) has set a precedent for how to analyse

ensembles of simulations with inconsistent experimental designs, such as those testing different Shared Socioeconomic Pathways (SSPs), and the more recent incorporation of PMIP simulations in CMIP has allowed for a better understanding of model biases and therefore, how to better compare the output from different simulations. In addition, past flexible protocols and 'ensembles of opportunity' comprising simulations of contrasting model boundary conditions and forcings (e.g., Schmidt et al. 2012; Lunt et al. 2012; Kageyama et al. 2013) have shown the value of experiment design flexibility for understanding climate change in a multi-model framework without committing all resources to specific paradigms. In short, it can be scientifically advantageous for groups to have the opportunity to determine their own focus whilst still contributing computational expensive and technically challenging simulations towards an overarching, multi-model aim of learning more about physical behaviours in response to different simulated scenarios.

Therefore, although this does provide some complication in drawing conclusions across models, the MIP was also confined enough to be able to draw on similarities between the simulations and categorise them according to commonalities in experimental design. In addition, the choice to focus on the early deglaciation, or pre-Bølling Warming, was beneficial in that the differences between each simulation were minimal in comparison to after 15 ka BP when larger discrepancies transpire between the simulations. The flexibility also facilitated more modelling groups to take part, who otherwise might have not due to conflicting aims. This is of particular concern when discussing the paradoxical nature of the recorded abrupt events of the time period and the meltwater discharge histories derived from ice sheet reconstructions (section 1.1.1.2.3). The PMIP4 LDv1 protocol left room for testing glaciologically consistent meltwater fluxes as well as those 'trained' to produce results consistent with geological reconstructions and their influence on the occurrence of abrupt climate changes in the last deglaciation. I aim to take advantage of the numerous simulations available to better understand the chain of events during the last deglaciation.

1.3.2 RQ2: How do changes in Earth's orbital configuration and atmospheric CO_2 impact abrupt transitions from weak to strong AMOC modes?

1.3.2.1 Scientific background

The causal mechanisms and drivers of abrupt climate change throughout the Last Glacial period have been investigated in climate models, ice sheet models, and proxy records, but no mechanism has so far gained ubiquitous acceptance. Despite there being a large consensus that the AMOC plays a critical role in climate transitions, the sensitivity of the North Atlantic Ocean to freshwater fluxes is poorly constrained and there is even less agreement about how the AMOC responds to atmospheric climate forcings (Toggweiler and Russell 2008; Zhu et al. 2015). Recent studies have shown that climate models are less 'stable' than once thought and that the AMOC can spontaneously oscillate unforced (e.g., Klockmann et al. 2016; Klockmann et al. 2018; Armstrong et al. 2022; Kuniyoshi et al. 2022; Romé et al. 2022; Vettoretti et al. 2022). In Chapter 2, I highlighted the importance of the background climate and initial climate state on the AMOC's ability to spontaneously transition between strong and weak modes, as

seen in the last deglaciation simulation conducted with the MIROC general circulation model (Obase and Abe-Ouchi 2019) modulated by a small, gradually increasing freshwater forcing.

The MIROC simulation prompted me to investigate spontaneous AMOC transitions and their dependence on climate forcings. Simulations showing millennial-scale variability are often idealised to narrow down the combination of background conditions that create optimal environments for triggering climate variability like D-O cycles, (i.e., to capture the 'window of opportunity' Barker and Knorr 2021). Climate parameters that have been shown to impact abrupt climate changes are orbital parameters (i.e., eccentricity, obliquity, and precession), greenhouse gas concentrations, ice sheet topography, and meltwater discharge. Previous studies have demonstrated that the AMOC can more easily transition between strong and weak modes within a specific range of CO_2 concentrations (e.g., Brown and Galbraith 2016; Klockmann et al. 2018; Vettoretti et al. 2022; Sun et al. 2022, and summarised by Malmierca-Vallet et al. (2024)), orbital conditions (Brown and Galbraith 2016; Zhang et al. 2017; Kuniyoshi et al. 2022), as well as meltwater forcings (Romé et al. 2022).

1.3.2.2 Research approach: HadCM3 simulations of Romé et al. (2022)

Using the HadCM3 GCM, I investigate the climatic controls on the AMOC and where the 'window of opportunity' in earth system forcings lies. I focus on the role of CO_2 concentrations and orbital configurations on AMOC oscillations under a glacial background state starting from a previous simulation by Romé et al. (2022) that I know oscillates.

Romé et al. (2022) present multiple simulations of the HadCM3 GCM with an oscillating AMOC, spontaneously transitioning between strong and weak modes. In this study, they test the impact of different melt patterns and amount of melt that represent snapshots from points of time in the GLAC-1D ice sheet reconstruction meltwater history. They determine that if the freshwater forcing was too strong and/or applied in a particularly sensitive part of the ocean, the climate could not recover from a weak AMOC to a strong AMOC. Whereas if the freshwater forcing was too weak, the AMOC could not transition to a weak mode and permanently stayed in a warm state. Romé et al. (2022)'s simulation using a meltwater flux from year 20.7 ka BP of the GLAC-1D ice sheet reconstruction produced fairly consistent AMOC oscillations in periodicity, shape, and magnitude for the entirety of the 10,000-year long simulation. The constant meltwater discharge pattern was also relatively uniform across basins (North America, Arctic, and the Greenland, Iceland, and Norwegian Seas), and the amount of discharge (0.084 Sv) is comparable to the recorded ice sheet melt during the early deglaciation (Carlson and Clark 2012; Lambeck et al. 2014; Peltier et al. 2015; Roy and Peltier 2018; Gorbarenko et al. 2022). The ice sheets were held constant at Last Glacial Maximum conditions, which although are too large for the suggested ice sheets of Marine Isotope Stage 3 (between 60 and 25 ka BP, when D-O cycles more often occur; Martinson et al. 1987), they are not dissimilar from ice sheet conditions we would be interested in testing. For one, ice sheet configurations previous to the Last Glacial Maximum are very uncertain because ice sheet advance up to the Last Glacial Maximum obliterated most traces of previous glacial extent and activity. Nonetheless, temperature and ice volume proxy reconstructions demonstrate that Marine Isotope Stage 3 was a glacial period with extensive

ice sheets relative to modern day, albeit not as cold or with ice sheets as large as the Last Glacial Maximum, so it is a sensible approximation to include LGM ice sheets, even if they are likely too large for the period. Secondly, the constant Last Glacial Maximum ice sheets are also not an unreasonable approximation for the relatively slow and minor North American ice sheet evolution in the early stages of the deglaciation (i.e., before 16 ka BP; Tarasov et al. 2012; Peltier et al. 2015).

The analogous characteristics of Romé et al. (2022)'s *20.7k* oscillating simulation to the last deglaciation and Marine Isotope Stage 3 demonstrates the beneficial opportunity it provides to test the impact of CO_2 and orbital configuration changes on the AMOC's ability to spontaneously transition. Moreover, this particular simulation is unique compared to other studies in that it has a constant meltwater flux, a feature that is often not included in tests of spontaneous AMOC change unless it is to modulate an AMOC response (e.g., Ganopolski and Rahmstorf 2001; Brown and Galbraith 2016). The meltwater flux creates a more representative background climate for testing AMOC sensitivity.

The *20.7k* simulation was performed with the Hadley Centre climate model (HadCM3), a coupled atmosphere-ocean general circulation model. It has shown reliable performance in its appearances in the the third and fourth Intergovernmental Panel on Climate Change (IPCC) Assessment and Coupled Model Intercomparison Project (CMIP) phase 3 and 5 before being superseded by HadGEM, as well as a part of the Palaeoclimate Modelling Intercomparison Project phase 4 models. HadCM3 had been shown to be robust for warm and cold palaeoclimates, with an ideal balance between resolution and speed to perform long simulations over thousands of years (Valdes et al. 2017). The model has been regularly used to simulate abrupt climate changes including those of Marine Isotope Stage 3 (Armstrong et al. 2022), the last deglaciation (Snoll et al. 2022), and the Holocene (Matero et al. 2017).

1.3.3 RQ3: How sensitive are the Northern Hemisphere ice sheets to the Bølling Warming under transient conditions?

1.3.3.1 Scientific background

In most simulations used to explore the casual mechanisms and impacts of abrupt climate change (such as those analysed for RQ1 and RQ2), the ice sheets are prescribed, meaning the atmosphere and ocean can only interact with the ice sheets in one direction, limiting their role in regulating the atmosphere and ocean. The ice sheets can impact the ocean and the atmosphere in the form of wind (e.g., Löfverström and Lora 2017; Sherriff-Tadano et al. 2018), atmospheric blocking (e.g., Häkkinen et al. 2011; Drijfhout et al. 2013; Hanna et al. 2016), the albedo effect (Roberts and Valdes 2017; Booth et al. 2024), and meltwater discharge, but the response of the atmosphere or ocean can not then influence the ice sheets. Higher ice sheet elevations of the North American and Greenland ice sheets correspond to stronger surface wind stress curl over the North Atlantic (Gong et al. 2015; Gregoire et al. 2018; Löfverström and Lora 2017) and have a positive correlation with the strength of the AMOC (Ullman et al. 2014) through the movement of salt into areas of deep water formation, increasing surface salinity (Oka et al. 2012; Muglia and Schmittner 2015; Sherriff-Tadano et al. 2018). Increases in ice sheet height

can cause a strengthening of atmospheric circulation (Löfverström et al. 2014; Gong et al. 2015; Merz et al. 2015) and expansions of ice sheet extent can lead to enhanced surface cooling (Abe-Ouchi et al. 2007). In addition, Romé et al. (2024) propose that ice sheet feedbacks could play a critical role in their convection-advection mechanism for driving AMOC oscillations.

Changes in the atmosphere and ocean, such as from abrupt climate change events, as well as background climate forcings (e.g., insolation and greenhouse gases) also play an important role in surface mass balance feedbacks. Surface mass balance refers to the net gain (amount of snow and ice accumulation on the ice sheet) versus loss (the amount of melt, evaporation, and sublimation that ablate snow and ice from the ice sheet; Lenaerts et al. 2019). During the last deglaciation, orbital forcing is the primary driver of ice sheet retreat followed by CO_2 concentrations (Gregoire et al. 2015; Quiquet and Roche 2024). However, in stadial and interstadial periods, such as Heinrich Stadial 1 and the Bølling Warming during the deglaciation, ice sheets can transition between being in an accumulation zone (positive surface mass balance) or an ablation zone (negative surface mass balance) respectively. This storage and release of freshwater can create a negative feedback that impedes the deglaciation of the ice sheet (Wickert et al. 2023).

Surface mass balance also varies with elevation and mass of the ice sheet (Pelto and Menounos 2021). Temperatures decrease with altitude (i.e., lapse rate), therefore, more accumulation occurs at higher elevations and more ablation occurs at lower elevations, with the highest ablation rates occurring in the summer time. In polar regions, when snow and ice area decreases, the surface albedo of that area decreases, causing more shortwave energy to be absorbed and solar heat to intensify in the region, further melting snow and ice (Schneider and Dickinson 1974). This is part of the ice-albedo feedback which occurs because of the large contrast between water and ice albedo. These surface mass balance feedbacks can only be simulated with a coupled climate-ice sheet model.

1.3.3.2 Research approach: Coupled climate-ice sheet model

To answer RQ3, the climate model, FAst Met Office/UK Universities Simulator (FAMOUS), two-way coupled to the ice sheet model BISICLES, is employed. FAMOUS is a low resolution atmosphere-ocean general circulation model (AOGCM) derived from HadCM3 (Smith et al. 2008). FAMOUS uses roughly half the horizontal resolution of HadCM3 in both the atmosphere and ocean, therefore requiring only about 10% of the computational resources of HadCM3 whilst still retaining the complexity of the processes represented in an AOGCM. This study uses the atmospheric component of FAMOUS, which is a hydrostatic, primitive equation grid point model with a horizontal resolution of 7.5° longitude by 5° latitude and 11 vertical levels (Smith et al. 2008). Land processes are modelled using the MOSES2.2 land surface scheme consisting of a set of sub-grid-scale tiles in each grid box to represent fractions of nine different surface types, including land ice (Smith et al. 2021). Although I prescribe sea surface temperatures and sea ice concentration, FAMOUS can also be utilised fully coupled with a dynamic ocean (e.g., Dentith et al. 2019).

Using the atmosphere-only component of FAMOUS unfortunately limits the interactions between the ocean and the ice sheets. However, not including the ocean component provides the

opportunity to prescribe the behaviour of the ocean and include abrupt events, as it is difficult to simulate abrupt climate changes without forcing or modulating the ocean. Therefore, if the ocean component was included, abrupt climate changes would most likely not be simulated and the research question could not be answered.

When using FAMOUS, resolution is sacrificed for speed, as opposed to using a simpler model like an Earth system model of intermediate complexity (EMIC) as often used in coupled climate-ice sheet simulations (e.g., Quiquet et al. 2021b). EMICs are more complex than box models but are still designed to perform quickly and thus, describe the dynamics of the atmosphere and/or ocean in less detail than conventional general circulation models (Weber 2010). For instance, EMICs rely on simple parameterisations of surface mass balance, whereas in the FAMOUS GCM, surface mass balance is based on energy-mass balance calculations that are performed within the climate model. The coarse resolution of FAMOUS does impact surface mass balance patterns (e.g., precipitation biases), but the more detailed physics provides crucial benefit when investigating atmosphere-ice sheet interactions.

FAMOUS, in the configuration FAMOUS-ice (Smith et al. 2021), is two-way coupled to the ice sheet model BISICLES. BISICLES is a vertically integrated ice flow model based on the L1L2 dynamical scheme (Schoof and Hindmarsh 2010; Cornford et al. 2013). The use of the L1L2 dynamical scheme, as opposed to the Shallow Ice Approximation of other ice sheet models, places it in a better position to simulate the behaviour, configuration, and stability of a marine ice sheet like the Eurasian ice sheet (Stokes and Clark 2001; Hubbard et al. 2009; Pattyn et al. 2012) and the many ice streams within the marine sectors that are vulnerable to processes like Marine Ice Sheet Instability (MISI) that are likely to be important for the deglacial evolution of the ice sheet (Kopp et al. 2017). BISICLES also includes adaptive mesh refinement (AMR) that allows the model to perform quickly and suitably model ice shelves and fast flowing ice streams without the need for approximations, such as the shallow shelf and shallow ice approximations. Where required, the model can simulate at high resolution, whilst the rest of the domain (i.e., the slower moving interior of the ice sheets) remains at lower resolution, thus increasing the efficiency of the model (Cornford et al. 2013). The resolution over the ice sheet is 16 km, but areas of ice streaming over the Barents-Kara ice sheet are refined to 2 km in the model setup used to answer this research question to better represent smaller-scale grounding line processes.

To simulate the abrupt events of the deglacial period and represent the ocean in the atmosphere-only climate model, I prescribe sea surface temperatures and sea ice concentration from two different transient simulations of the last deglaciation that followed the PMIP4 LDv1 protocol. The PMIP4 LDv1 simulations used meltwater fluxes based on the *TraCE-21ka A* deglaciation simulation (Liu et al. 2009) that follows a common interpretation of the AMOC history through this period (e.g., McManus et al. 2004; Ng et al. 2018) with a simulated Heinrich Stadial 1 (weak AMOC) and Bølling Warming (rapid AMOC strengthening).

1.3.4 Thesis workflow

The research questions are addressed in the results chapters 2, 3, and 4 and the discussion chapter, 5. The results chapters have either been published (Snoll et al. 2024), submitted

for review (Chapter 3), or are about to be submitted (Chapter 4) to peer-reviewed journals. They have each been written in the style of an academic publication, including individual abstracts, introductions, methods, and supplementary information for every chapter. Chapter 5 reviews how the three results chapters provide answers to the research questions and tackled the overarching thesis aim.

Chapter 2, *A multi-model assessment of the early last deglaciation (PMIP4 LDv1): a meltwater perspective*, addresses RQ1 and provides critical background for answering RQ3. This chapter presents a new multi-model intercomparison of transient simulations of the last deglaciation following the Palaeoclimate Model Intercomparison Project phase 4 last deglaciation protocol version 1. The content of this chapter was published in Climate of the Past as part of the 'Palaeoclimate Modelling Intercomparison Project phase 4 (PMIP4) (CP/GMD inter-journal SI)' special issue (Snoll et al. 2024). It was replicated with only editorial modifications to the text and figures to fit the formatting of the thesis. It includes contributions from Ruza F. Ivanovic, Lauren J. Gregoire, Sam Sherriff-Tadano, Laurie Menviel, Takashi Obase, Ayako Abe-Ouchi, Nathaelle Bouttes, Chengfei He, Feng He, Marie Kapsch, Uwe Mikolajewicz, Juan Muglia, and Paul Valdes.

Chapter 3, *Competing effects of sea ice change control the pace and amplitude of millennial-scale climate oscillations*, addresses RQ2 by investigating the sensitivity of the AMOC to changes in the background climate. This chapter presents new simulations in which CO_2 concentration or orbital configuration is changed from the original simulation presented by Romé et al. (2022) to determine the impact on the oscillations and the mechanism outlined by Romé et al. (2024). The content of Chapter 3 was submitted for publication to Critical Insights in Climate Change and is awaiting feedback from reviewers. It includes contributions from Ruza F. Ivanovic, Lauren J. Gregoire, Sam Sherriff-Tadano, and Yvan Romé.

Chapter 4, *Impact of the Bølling Warming on the Northern Hemisphere ice sheets: a coupled climate-ice sheet model study*, addresses RQ3 by exploring the effects of an abrupt ocean forcing on the ice sheets. This chapter presents new coupled-climate ice sheet simulations of the last deglaciation forced with abrupt climate changes observed in surface temperature records. The results of Chapter 4 also reflect on the conclusions of RQ1. This chapter will be submitted to The Cryosphere. It includes contributions from Ruza F. Ivanovic, Lauren J. Gregoire, Sam Sherriff-Tadano, and Violet Patterson.

Chapter 5 is the discussion and conclusions chapter that reflects on the novel contributions of this thesis produced in Chapters 2, 3, and 4. I also critically evaluate the thesis work and recommend avenues for future research.

CHAPTER 2

A multi-model assessment of the early last deglaciation (PMIP4 LDv1): a meltwater perspective

Preface

This chapter presents a new multi-model intercomparison of transient simulations of the last deglaciation following the Palaeoclimate Model Intercomparison Project phase 4 last deglaciation protocol version 1. The content of this chapter was published in Climate of the Past as part of the 'Paleoclimate Modelling Intercomparison Project phase 4 (PMIP4) (CP/GMD inter-journal SI)' special issue (Snoll et al. 2024). It was replicated with only editorial modifications to the text and figures to fit the formatting of the thesis. It includes contributions from Ruza F. Ivanovic, Lauren J. Gregoire, Sam Sherriff-Tadano, Laurie Menviel, Takashi Obase, Ayako Abe-Ouchi, Nathaelle Bouttes, Chengfei He, Feng He, Marie Kapsch, Uwe Mikolajewicz, Juan Muglia, and Paul Valdes. The study conception was developed by the PMIP4 Working Group, consisting of RI, LM, TO, AAO, NB, MK, UM, and PV. BS, LG, SST, and RI contributed to the study design, with LM, TO, and AAO providing additional feedback and close communication with BS. The design of the experiments and running of them was performed by RI, LG, LM, TO, AAO, NB, CH, FH, MK, UM, JM, and PV. Material preparation and data collection was performed by BS. The manuscript was prepared by BS with contributions from all co-authors, who read and approved the final manuscript.

Abstract

The last deglaciation (∼20–11 ka BP) is a period of a major, long-term climate transition from a glacial to interglacial state that features multiple centennial- to decadal-scale abrupt climate variations whose root cause is still not fully understood. To better understand this time period, the Palaeoclimate Modelling Intercomparison Project (PMIP) has provided a framework for an internationally coordinated endeavour in simulating the last deglaciation whilst encompassing a broad range of models. Here, we present a multi-model intercomparison of 17 transient

simulations of the early part of the last deglaciation (∼20–15 ka BP) from nine different climate models spanning a range of model complexities and uncertain boundary conditions and forcings. The numerous simulations available provide the opportunity to better understand the chain of events and mechanisms of climate changes between 20 and 15 ka BP and our collective ability to simulate them. We conclude that the amount of freshwater forcing and whether it follows the ice sheet reconstruction or induces an inferred Atlantic meridional overturning circulation (AMOC) history, heavily impacts the deglacial climate evolution for each simulation rather than differences in the model physics. The course of the deglaciation is consistent between simulations except when the freshwater forcing is above 0.1 Sv – at least 70% of the simulations agree that there is warming by 15 ka BP in most places excluding the location of meltwater input. For simulations with freshwater forcings that exceed 0.1 Sv from 18 ka BP, warming is delayed in the North Atlantic and surface air temperature correlations with AMOC strength are much higher. However, we find that the state of the AMOC coming out of the Last Glacial Maximum (LGM) also plays a key role in the AMOC sensitivity to model forcings. In addition, we show that the response of each model to the chosen meltwater scenario depends largely on the sensitivity of the model to the freshwater forcing and other aspects of the experimental design (e.g., CO_2 forcing or ice sheet reconstruction). The results provide insight into the ability of our models to simulate the first part of the deglaciation and how choices between uncertain boundary conditions and forcings, with a focus on freshwater fluxes, can impact model outputs. We can use these findings as helpful insight in the design of future simulations of this time period.

2.1 Introduction

At the onset of the most recent deglaciation, ∼19,000 years before present (ka BP; year 1950 as present), ice sheets that covered the Northern Hemisphere at the Last Glacial Maximum (LGM; Dyke 2004; Lambeck et al. 2014; Hughes et al. 2016) started to melt (Gregoire et al. 2012), Earth began to warm (Jouzel et al. 2007; Buizert et al. 2018), and sea levels rose (Lambeck et al. 2014). Known as the 'last deglaciation', this time period is defined by major, long-term (order of 10,000 years) climate transitions from the most recent cold glacial to the current warm interglacial state, as well as many short-term, decadal- to centennial-scale warmings and coolings of more than 5 °C (Beaulieu and Reille 1992; Severinghaus and Brook 1999; Lea et al. 2003; Buizert et al. 2018). These short-term abrupt temperature changes were often also accompanied by sudden reorganisations of basin-wide ocean circulations (e.g., Roberts et al. 2010; Ng et al. 2018) and jumps in sea level of tens of metres in a few hundred years (e.g., Deschamps et al. 2012; Lambeck et al. 2014).

Abrupt climate changes observed in the early last deglaciation, such as the Greenland cold period known as Heinrich Stadial 1 (between ∼18.5 and 14.7 ka BP; Broecker and Putnam 2012; Huang et al. 2014; Crivellari et al. 2018; Ng et al. 2018) and the Bølling Warming (an abrupt warming that occurs ∼14.7 ka BP in Greenland at the end of Heinrich Stadial 1; Severinghaus and Brook 1999; Lea et al. 2003; Buizert et al. 2018), are often attributed to changes in the Atlantic meridional overturning circulation (AMOC). The strength and structure of the ocean

circulation is a key control on the North Atlantic and Arctic climate and is dependent on the stratification of the water layers in crucial convection sites in the North Atlantic (Lynch-Stieglitz et al. 2007; McCarthy et al. 2017). When the AMOC is strong, more heat is transported towards the North Atlantic, causing regional warming in Greenland and the North Atlantic (Rahmstorf 2002).

Previous studies have shown that the AMOC pattern can be perturbed easily by changes in meltwater input into the North Atlantic. For example, if freshwater is deposited into the critical convection sites in the subpolar North Atlantic, i.e., the Labrador Sea and Nordic Seas, locations of high sensitivity to wind patterns and sea ice formation, the circulation strength can be disrupted (**rahmstorf˙decadal˙1999**). Evidence from several sites report sea level rise, and therefore a freshwater flux, as early in the deglaciation as 19.5 ka BP, attributed to widespread retreat of Northern Hemisphere ice sheets in response to an increase in northern latitude summer insolation (Yokoyama et al. 2000; Clarke et al. 2009). Carlson and Clark (2012) concluded that the LGM was terminated by a rapid 5–10 m sea level rise between 19.5 and 19 ka BP, and sea levels rose a further 8–20 m from ∼19 to 14.5 ka BP with the melting of the Laurentide and Eurasian ice sheets. More recent reconstructions of sea level and ice volume change suggest a similar view with ∼10–15 m of sea level rise between the end of the LGM (∼21–20 ka BP) and 18 ka BP and an additional ∼25 m before 14.5 ka BP (Lambeck et al. 2014; Peltier et al. 2015; Roy and Peltier 2018; Gorbarenko et al. 2022). In some cases where meltwater fluxes are applied to the North Atlantic in model simulations, rapid decreases of up to 10 °C in temperature occur, resembling the transition to Heinrich Stadial 1 (e.g., Ganopolski and Rahmstorf 2001; Knutti et al. 2004; Brown and Galbraith 2016; Menviel et al. 2020).

Transient simulations of the last deglaciation have been increasingly performed to better understand the multi-millennial-scale processes and the shorter and more dramatic climate changes by examining dynamic and threshold behaviours (Braconnot et al. 2012), determining the effects of temporally varying climate forcings, and identifying what mechanisms in the model can cause recorded climate signals (see section 1.2 of Ivanovic et al. 2016, and examples therein). In turn, these simulations also provide us with the opportunity to test the ability of models to simulate climate processes and interactions and different hypotheses for drivers of change (i.e., climate triggers, interactions, and feedbacks).

One particularly challenging aspect in the experimental design of last deglaciation simulations is prescribing ice sheet evolution and the resultant freshwater flux and sea level rise. Notwithstanding the qualitative rationale for why ocean-bound meltwater disrupts ocean circulation and climate (McManus et al. 2004; Clarke et al. 2009; Thornalley et al. 2010), it has been recently argued that climate models are too sensitive to freshwater fluxes under some conditions. For example, data reconstructions suggest only a small change in AMOC ∼11.7 to 6 ka BP, whereas CCSM3 (Community Climate System Model version 3) simulated a greater response to the freshwater forcing associated with the final Northern Hemisphere deglaciation at this time (He and Clark 2022), when sea level rose by 50 m during this interval (Lambeck et al. 2014; Cuzzone et al. 2016; Ullman et al. 2016). This result may be quite model dependent, and we note that others had previously suggested the converse, i.e., that model responses to

freshwater (and other) forcings could be too muted, from what we understand of past climate change (Valdes 2011; Liu et al. 2014). Certainly, to disrupt climate in a Heinrich Stadial-like way, many previous glacial simulations have required quite large meltwater fluxes compared to what may be inferred from geological records (Kageyama et al. 2013). This remains an interesting point of contention (i.e., the meltwater paradox defined below), and certainly some models no longer appear as 'stable' as they once did. Moreover, the sensitivity of the North Atlantic Ocean circulation to glacial melting is poorly constrained.

There are, however, strong indications that the impact of oceanic freshwater fluxes is highly dependent on the location that they enter the ocean (depth and latitude–longitude) and how they are implemented, as it determines the efficiency of convection disruption (e.g., Stocker et al. 2007; Roche et al. 2007; Roche et al. 2010; Smith and Gregory 2009; Otto-Bliesner and Brady 2010; Condron and Winsor 2012; Ivanovic et al. 2017; Romé et al. 2022). Similarly, the background climate and ocean state may also be important for how responsive ocean circulation is to freshwater forcing–e.g., whether AMOC is already strong and deep or weak and shallow (Bitz et al. 2007; Schmittner and Lund 2015; Dome Fuji Ice Core Project Members: et al. 2017; Pöppelmeier et al. 2023b), or specifically where deep water formation occurs (Smith and Gregory 2009; Roche et al. 2010). The choice of a model's boundary conditions in the paleo-setting (e.g., ice sheet geometry) can influence its sensitivity to freshwater perturbation. For example, the Romé et al. (2022) simulations have an oscillating AMOC, whereas the simulations by Ivanovic et al. (2018a) do not, and Kapsch et al. (2022) demonstrated various climate responses in simulations of the last deglaciation with different ice sheets. Ice sheet geometry specifically has been demonstrated to affect AMOC strength due to the impact of ice sheet height on surface winds and wind-driven gyres, which can increase the northward transport of salty waters. Multiple model studies (e.g., Ullman et al. 2014; Löfverström and Lora 2017; Sherriff-Tadano et al. 2018; Kapsch et al. 2022) have shown that a thicker Laurentide ice sheet results in a stronger AMOC. Hence, the influence of deglacial ice sheet meltwater on AMOC is likely to be highly dependent on the model, choice of boundary conditions and forcings, and the initial ocean condition.

Furthermore, CO_2 and orbital forcing are also shown to impact the course of the deglaciation and the occurrence of abrupt climate changes (i.e., results shown by Oka et al. 2012; Klockmann et al. 2016; Klockmann et al. 2018; Zhang et al. 2017; Sherriff-Tadano et al. 2018) and potentially modulate the sensitivity of the AMOC to freshwater fluxes (Obase and Abe-Ouchi 2019; Sun et al. 2022). Liu et al. (2009) demonstrated that the warming in *TraCE-21ka* between 17 and 14.67 ka BP is dominated by the CO_2 forcing (over the orbital forcing; see their Figure 2.16a), which coincides with the first major rise in atmospheric CO_2 in their simulation. Whereas Gregoire et al. (2015) demonstrated that orbital forcing caused 50% of the reduction in North American ice volume, greenhouse gases caused 30%, and the interaction between the two caused the remaining 20% in their coupled climate–ice sheet simulations. Sun et al. (2022) showed the effect that these forcings have on the sensitivity of the AMOC, by demonstrating that a weak AMOC (in a Heinrich Stadial 1-like state, for example) is more likely to recover (like that of the Heinrich Stadial 1 to Bølling Warming transition) with a higher atmospheric CO_2 concentration

and that larger ice sheets result in a stronger AMOC that is less sensitive to meltwater fluxes.

Previous modelling efforts (e.g., Liu et al. 2009; Menviel et al. 2011; Roche et al. 2011; Gregoire et al. 2012; He et al. 2021) performed transient simulations to learn more about the last deglaciation and the interaction between ocean and atmosphere. Liu et al. (2009) were the first to publish a synchronously coupled atmosphere–ocean general circulation model simulation of the last deglaciation, henceforth referred to as *TraCE-21ka*. In this study, a freshwater flux was used to regulate the AMOC to achieve a set of target ocean circulation, surface air temperature, and sea surface temperature conditions as interpreted from a selection of proxy records in multiple locations between the LGM and the onset of the Bølling Warming (see Figure 1 by Liu et al., 2009), followed by a switch to a geologic reconstruction of freshwater forcing (He 2011).

The meltwater inputs used in *TraCE-21ka* and the studies referenced above, however, do not follow ice sheet reconstructions (e.g., Ivanovic et al. 2018a). Instead, the meltwater fluxes are, on occasion over twice as large as suggested by ICE-6G_C VM5a (henceforth 'ICE=6G_C'; Argus et al. 2014; Peltier et al. 2015) and GLAC-1D (Tarasov and Peltier 2002; Tarasov et al. 2012; Briggs et al. 2014; Ivanovic et al. 2016). Furthermore, the freshwater flux must then be shut off to reinvigorate the AMOC and instigate the Bølling Warming, ending Heinrich Stadial 1, but this is at the same time as recorded rise in global sea level of 12–22 m in ∼350 years or less, known as Meltwater Pulse 1a (Deschamps et al. 2012). Meltwater Pulse 1a is a complex event thought to be a culmination of contributions from the North American (Gregoire et al. 2012; Gregoire et al. 2016), Eurasian (Brendryen et al. 2020), and Antarctic (Weber et al. 2014; Golledge et al. 2014) ice sheets. Whilst some studies have suggested that freshwater in the Southern Ocean could have contributed to the temperature changes seen in the North Atlantic during the Bølling Warming, recent studies (e.g., Ivanovic et al. 2018a; Yeung et al. 2019) have demonstrated that the impact of meltwater pulses in the Southern Ocean on the climate are often restricted to the Southern Hemisphere, whereas North Atlantic pulses have much farther-reaching and dominating affects. This creates a meltwater paradox, where the freshwater forcing required by models to produce recorded climate change is broadly in opposition to the meltwater history reconstructed from ice sheet and sea level records.

Simulations performed by Kapsch et al. (2022) and Snoll et al. (2022) add weight to this so-called meltwater paradox. They use meltwater forcing scenarios in accordance with observable ice volume change but have not been able to replicate the AMOC or surface air temperature proxy records. Instead, the AMOC remains stronger than ocean circulation records suggest for Heinrich Stadial 1, and the models simulate an abrupt cooling at ∼14.5 ka BP instead of the Bølling Warming. The picture is further confounded from the ice sheet modelling perspective (e.g., see Figure S2 by Gregoire et al. 2012).

Similar simulations of the last deglaciation (e.g., Roche et al. 2011; Snoll et al. 2022; Bouttes et al. 2023) have been run with no prescribed meltwater or a meltwater forcing that is applied as a global salinity adjustment (i.e., rather than localised surface forcing). Without the use of the freshwater forcing, these simulations do not reproduce any abrupt climate change events during the deglaciation.

The simulation performed by Obase and Abe-Ouchi (2019) is unique in that it is able to simulate a weak AMOC during the onset of the deglaciation and the Bølling Warming without releasing (and then stopping) an unrealistically large amount of freshwater. Instead, they input a gradually increasing amount of meltwater that remains at or below the level of ice volume loss in the reconstruction. This study was able to simulate spontaneous abrupt changes in AMOC thanks to multi-stability in their ocean circulation, as also seen in other modelling studies (Romé et al. 2022; Malmierca-Vallet et al. 2023). This simulation still does not consider Meltwater Pulse 1a and has lower than observed meltwater input before that point, yet it is distinctive in its ability to replicate a weak ocean circulation in the early deglaciation and the Bølling Warming even with a continuous freshwater flux.

Despite the decades of research simulating the last deglaciation and numerous observable records of this time period, uncertainty still remains about the mechanisms that cause the recorded climate signals as well as how to replicate them 'realistically' in model simulations, and therefore how to unravel the meltwater paradox. These findings highlight the importance of solving the convolved issue of model sensitivity to specific forcings and boundary conditions and the initial climate condition and model dependency of simulation results – the crux of the remaining unknowns. To tackle such unknowns, the Palaeoclimate Modelling Intercomparison Project phase 4 last deglaciation protocol version 1 (PMIP LDv1; Ivanovic et al. 2016) was designed to encompass a broad range of models and the uncertainty in boundary conditions and forcings. Instead of one specific and rigid configuration for the experiment design, modelling groups are given a choice of recommended forcings and boundary conditions. Thus, analysing model output of multiple simulations of the last deglaciation provides the opportunity to look at differences between experimental designs and their impact on the onset of the deglaciation using different models.

This study compares 17 simulations of the last deglaciation from nine different climate models with dissimilar experimental designs. Our aim is to take advantage of the numerous simulations available to better understand the chain of events and mechanisms of climate changes in the early last deglaciation (i.e., from 20 to 15 ka BP) and our collective ability to simulate them. We focus on the early deglaciation because although models may start differently from the LGM, the divergence from each other is smaller in comparison to further into the deglaciation. We investigate the similarities and differences between the model results and what aspects of the variations in the model output can be attributed to the experimental design or model biases by analysing the transition from the LGM, when and where the warming starts, and the impact of freshwater forcing. We also address the meltwater paradox by discussing the results of meltwater scenario choices made by the modelling groups.

2.2 Experiment designs across the ensemble

The comparison is based on 17 simulations produced independently by eight different palaeoclimate modelling groups using nine different climate models (Table 2.1). Most groups have followed the most recent PMIP4 last deglaciation protocol for their experimental design, while others use older publications for boundary conditions or a more *bespoke* configuration depend-

ing on their own modelling goals. The simulations from HadCM3, LOVECLIM, iLOVECLIM, iCESM, MIROC, and MPI modelling groups use greenhouse gas configurations on the AICC2012 age model of Veres et al. (2013) (Figure 2.1b). *FAMOUS* and *TraCE-21ka* use an older age model in which the deglacial rise in CO_2 starts a thousand years later. The deglacial CO_2 concentration for these two models is almost identical, with some discrepancies between ∼19.8 and 18.4 ka BP and about 15.7 ka BP. All simulations prescribe insolation following Berger (1978) (Figure 2.1a). The PMIP4 last deglaciation protocol recommends using the GLAC-1D (Ivanovic et al. 2016) and/or ICE-6G_C (Peltier et al. 2015) ice sheet reconstructions. HadCM3, iCESM, MIROC, and UVic modelling groups opted for ICE-6G_C; MPI and iLOVECLIM simulations use both ICE-6G_C and GLAC1-D; and *FAMOUS*, *LOVECLIM*, and *TraCE-21ka* use the older ICE-5G (Peltier 2004).

Freshwater forcing across the ensemble is more complex. The PMIP4 last deglaciation protocol recommends two different meltwater scenarios (*melt-routed* and *melt-uniform*) based on ice volume change as calculated from the ice sheet reconstruction chosen by the modelling group (GLAC-1D and ICE-6G_C are recommended). The *melt-uniform* scenario is a globally uniform freshwater flux or salinity adjustment through time applied throughout the whole ocean to conserve water mass during deglaciation of the ice sheets, whereas the *melt-routed* scenario is a distributed routing that gives the flux of freshwater through time at individual meltwater river outlets along the coast (Ivanovic et al. 2016; Riddick et al. 2018, used by MPI).

Because a large discrepancy between the simulations is the prescribed freshwater flux scenario (Figure 2.1d–f), and ice sheet meltwater fluxes are known to have a major impact on ocean circulation and climate (see above), the simulations have been grouped into four categories based on their meltwater forcing: *melt-routed*, *melt-uniform*, those based on the *TraCE-21ka A* simulation (henceforth referred to as *TraCE-like*; Liu et al. 2009), and *bespoke* scenarios that fall outside of the other three categories. Within these categories, however, there is variation in how the freshwater forcing is derived from the ice sheet reconstruction, as well as in the technical implementation of the chosen meltwater scenario (for example, for the *melt-routed* and *melt-uniform* scenarios, see Wickert, 2016, section 2.2.2 for HadCM3; Kapsch et al., 2022; section 2 for MPI; Bouttes et al., 2023, section 2.4 for iLOVECLIM). For the *melt-routed* simulations, the modelling groups then release the calculated meltwater flux to ocean grid cells according to the distribution calculated by the individual groups' drainage network models (see the respective papers). For the *melt-uniform* simulations, HadCM3 and iLOVECLIM modelling groups apply a globally uniform freshwater flux throughout the entire volume of the ocean, whereas the MPI modelling group applies a freshwater flux at the surface of the ocean or land. Because of this nuance, the MPI *melt-uniform* simulation is instead labelled as a "global surface meltwater flux" but is still placed in the *melt-uniform* category for our analysis.

We somewhat over-simplistically refer to PMIP4 meltwater scenarios as "realistic" because they are based on the chosen ice sheet reconstruction prescribed in the simulation. Nonetheless, it is important to note that the precise history of the meltwater flux (distribution and rates) remains quite uncertain, as hinted at by differences in the reconstructions. Between 20 and 15 ka BP, the realistic freshwater flux according to ICE-6G_C does not exceed 0.1 Sv and according to

GLAC-1D only exceeds 0.1 Sv as it nears Meltwater Pulse 1a. In the *TraCE-like* simulations, the strategy of prescribing freshwater to induce an inferred AMOC history requires the freshwater flux to reach nearly 0.2 Sv or greater – twice the realistic amount based on sea level records (Figure 2.1d; Carlson and Clark 2012; Lambeck et al. 2014).

For the *bespoke*-freshwater cluster of simulations, *MIROC* implements a gradually increasing flux that always remains below the realistic values. *FAMOUS* uses a reconstructed flux based on an earlier estimate from sea level records (produced as part of the ORMEN project; more information provided by Gregoire 2010), which follows the more up-to-date ice sheet reconstructions relatively closely except when a larger freshwater flux is applied at two points during Heinrich Stadial 1 (between 19 and 17 ka BP; corresponding to the acceleration of Northern Hemisphere ice loss, as noted by Carlson and Clark, 2012, and the melt of the Eurasian ice sheet as reconstructed by Hughes et al., 2016). The UVic simulations use a total freshwater flux calculated as 3 times the sea level changes reconstructed by Lambeck et al. (2014); one scenario where the freshwater flux is applied between 19 and 15 ka BP (*Uvic_longhosing*) and one where the flux is only applied between 19 and 17 ka BP (*Uvic_shorthosing*; Table 2.1).

The UVic simulations include a dynamic carbon cycle model with prognostic atmospheric CO_2 aiming to replicate the sedimentary records of deep-ocean carbon. The freshwater flux is therefore tuned to replicate the AMOC structure associated with these sedimentary records, but the location of the meltwater input is based on plume positions like those of the HadCM3 simulations. The UVic simulations are included in the broader comparisons presented here (i.e., Figure 2.3). However, because of their unique experiment design and motivation, the differences between the UVic simulations and the wider multi-model ensemble are too great for a more detailed comparison of results, and they are therefore omitted from parts of the analysis and discussion in this study.

2.3 Analysis method

One of the analyses used in this study was inspired by the year of first significant warming analysis performed by Roche et al. (2011). We define the first significant warming from the LGM using a statistical test. The LGM reference period is selected from the 500-year window between 21 and 20.5 ka BP for each simulation. Each of the simulations are then divided into 65 independent samples of 100 years between 20.5 and 13 ka BP for each grid cell. For each sample, we first performed a Fischer test on the variances in the reference and test samples to assess whether they differed or not. If the variances were equal, we performed a standard one-sided Student's t test with the alternative hypothesis as the sample period being warmer than the reference LGM period. If the variances were not equal, we performed a Welsch's test, or a t test with two unequal variances with the same alternative hypothesis. The samples were tested at 99% confidence. If the sample was significantly warmer than the LGM reference period, then the grid point in Figure 2.5 was assigned the central point of this sample. For example, if the 100-year sample between 16.2 and 16.1 ka BP at a specific grid point was determined to be significantly warmer than the reference period, then that grid point would be assigned the year 16.15 ka BP. This analysis excludes two of the simulations (*HadCM3_TraCE* and *iTraCE*) due

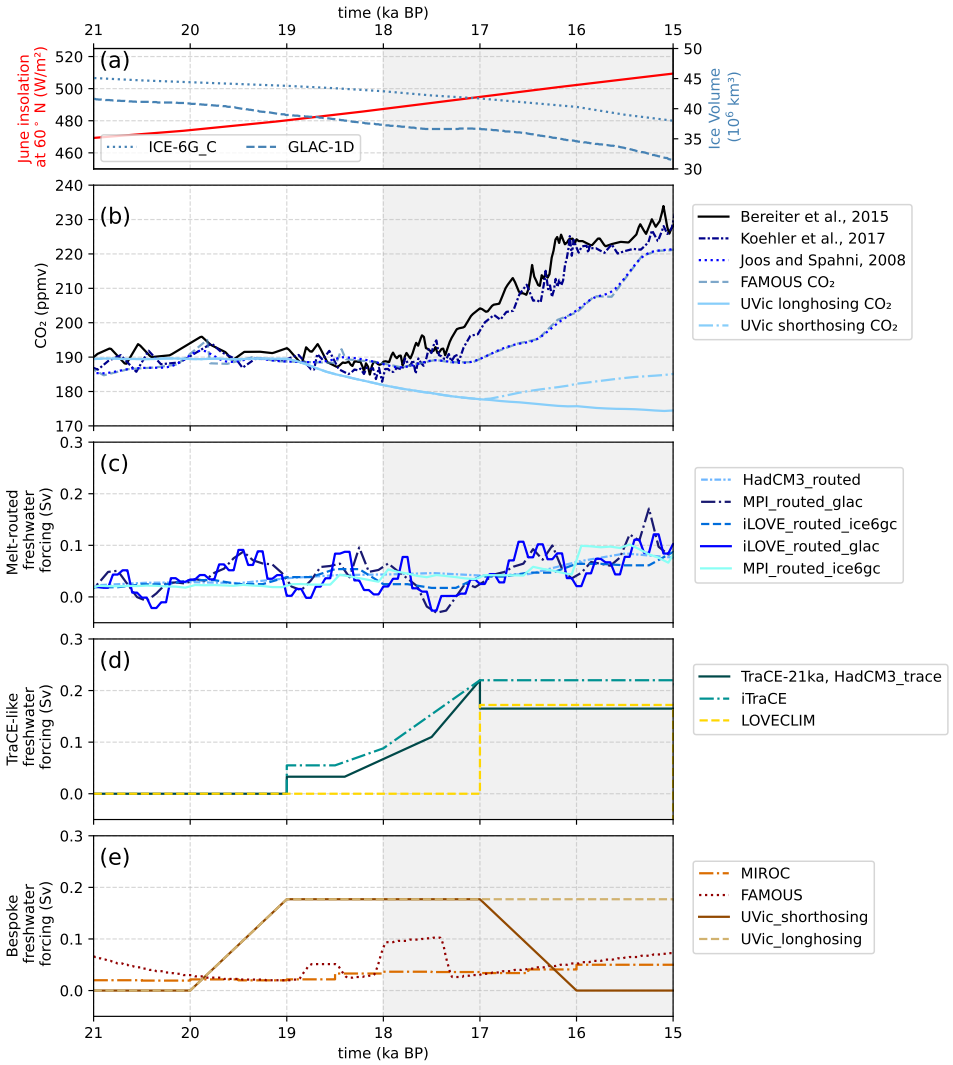

Figure 2.1: Climate forcings for the simulations. (a) Ice volume loss since the Last Glacial Maximum (LGM; 21 ka BP) as part of the ICE6G_C ice sheet reconstruction (Argus et al. 2014; Peltier et al. 2015) and the GLAC-1D ice sheet reconstruction (Tarasov and Peltier 2002; Tarasov et al. 2012; Briggs et al. 2014; Ivanovic et al. 2016) in light blue. June insolation at 60° N (Berger, 1978) is in red. (b) Atmospheric CO_2 concentrations are dependent on the simulation set-up. (c)-(e) Freshwater flux (Sv) for simulations with imposed meltwater. *Melt-uniform* simulations have the same total meltwater flux into the global ocean as *melt-routed* simulations (c), but in *melt-uniform* scenarios, the freshwater is spread through the entire ocean or across the whole ocean surface (see main text), rather than at point sources, and are hence so diluted or uniformly distributed as to have limited direct forcing power.

Model	Resolution	Simulation reference name	Publication (model; simulation)	Simulation duration (ka BP)	Prescribed ice sheet	GHG	Meltwater scenario
CCSM3	Atmosphere: 3.75 ° with 26 levels Ocean: nominal 3 ° with 25 levels	*TraCE-21ka*	Collins et al. (2006); Liu et al. (2009); and further discussed by He and Clark (2022)	22-0	ICE-5G	Joos and Spahni (2008)	*TraCE-21ka*
FAMOUS	Atmosphere: 7.5 °× 5 ° with 11 levels Ocean: 3.75 °× 2.5 ° with 20 levels	*FAMOUS*	Smith et al. (2008); Gregoire et al. (2012)	20-13	ICE-5G	Based on PMIP2; see Harrison et al. (2002)	*Bespoke* (Figure 2.1e)
HadCM3B	Atmosphere: 3.75 °× 2.5 ° with 19 levels Ocean: 1.25 ° with 20 levels	*HadCM3_uniform* *HadCM3_routed* *HadCM3_TraCE*	Valdes et al. (2017); Snoll et al. (2022); and this study	23-2 ka CE 20-13	ICE-6G_C	Loulergue et al. (2008); Schilt et al. (2010); Bereiter et al. (2015)	*Melt-uniform* *Melt-routed* *TraCE-like*
iCESM	Atmosphere: 2.5 °× 1.9 ° with 30 levels Ocean: 1 ° with 60 levels	*iTraCE*	Hurrell et al. (2013); He et al. (2021)	21-11	ICE-6G_C	Lüthi et al. (2008)	*TraCE-like*
iLOVECLIM	Atmosphere: 5.6 ° with 3 levels Ocean: 3 ° with 20 levels	*iLOVE_uniform_ice6gc* *iLOVE_routed_ice6gc* *iLOVE_uniform_glac* *iLOVE_routed_glac*	Goosse et al. (2010); Bouttes et al. (2023)	21-8	ICE-6G_C GLAC-1D	Loulergue et al. (2008); Schilt et al. (2010); Bereiter et al. (2015)	*Melt-uniform* *Melt-routed* *Melt-uniform* *Melt-routed*
LOVECLIM	Atmosphere: 5.6 ° with 3 levels Ocean: 3 ° with 20 levels, dynamic vegetation model	*LOVECLIM*	Goosse et al. (2010); this study, but similar to simulations by Menviel et al. (2011)	21-11	ICE-5G	Köhler et al. (2017)	*TraCE-like*
MIROC	Atmosphere: 2.8 ° with 20 levels Ocean: 1.4 ° with 43 levels	*MIROC*	Hasumi and Emori, 2004; based on Obase and Abe-Ouchi (2019)	21-11	ICE-6G_C	Loulergue et al. (2008); Schilt et al. (2010); Bereiter et al. (2015)	*Bespoke* (gradual increase)
MPI-ESM-CR	Atmosphere: 3.75 ° with 31 levels Ocean: 3 ° with 40 levels	*MPI_global_ice6gc* *MPI_routed_ice6gc* *MPI_routed_glac*	Giorgetta et al. (2013); Kapsch et al. (2022)	26-0	ICE-6G_C GLAC-1D	Köhler et al. (2017)	*Melt-uniform* (global meltwater flux) *Melt-routed* *Melt-routed*
UVic	Atmosphere: 3.6 °× 1.8 ° Ocean: 3.6 °× 1.8 ° with 19 levels	*UVic_shorthosing* *UVic_longhosing*	Weaver et al. (2001); this study but based on LGM simulations by Muglia and Schmittner (2015, 2021)	21-14	ICE-6G_C	dynamic	*Bespoke*

Table 2.1: Detail of simulations referenced in the multi-model intercomparison.

to data availability before 20 ka BP. *LOVECLIM* was also not included due to a small drift between 21 and ∼20.6 ka BP because of an adjustment in the ice sheet. This analysis was performed for all simulations with a later reference period (20–19.5 ka BP) and shown in the Supplement. The remaining analyses in this study use a LGM definition of 20 to 19.5 ka BP to incorporate all simulations.

Two temporal correlations are also performed between AMOC and surface air temperature and CO_2 concentration and surface air temperature. For both relationships, a R^2 value and slope of a linear regression model is calculated at each grid cell for the 5,000-year window from 20 to 15 ka BP.

2.4 Results and discussion

Here, we focus on the course of the deglaciation, how it is impacted by the freshwater forcing, and how this relationship differs on a model-to-model and experimental design-to-experimental design basis. The trajectory of the AMOC in the Northern Hemisphere for each simulation closely follows the meltwater scenario chosen by the modelling group (Figure 2.2). All the *melt-routed*, *melt-uniform*, and bespoke freshwater scenarios display a similar pattern throughout the deglaciation with a gradual warming of surface air temperature in the high latitudes and stronger warming compared to the *TraCE-like* simulations in the Northern Hemisphere (Figure 2.3). The similarity between the simulations increases further into the deglaciation, with warming from the LGM in all regions by 16 ka BP for all the *melt-routed*, *melt-uniform*, and bespoke freshwater scenarios (Figure 2.3 and 2.11 in the Supplement). The *TraCE-like* simulations, however, do not follow the same trajectory, and the Northern Hemisphere, specifically the North Atlantic, remains colder than at the LGM for most of the early deglaciation, with only *LOVECLIM* and *TraCE-21ka* warming beyond the LGM in the North Atlantic by 15 ka BP (Figure 2.12). This colder region in the North Atlantic is evident in a multi-model mean of the ensemble where, on average, the North Atlantic remains the coldest region throughout the early deglaciation (Figure 2.4). Around the onset of Heinrich Stadial 1 (18 ka BP), more discrepancy between simulations arises (as indicated by disagreement even in the sign of change; Figure 2.4) due to differences across the ensemble in when and where the deglaciation begins as well as the freshwater fluxes applied. However, by 15 ka BP, at least 70% of simulations agree with the sign of the mean in most areas. More disagreement remains in the North Atlantic, the region of highest variance across the ensemble and where the different freshwater fluxes used in the simulations have the most direct impact. The ensemble-wide consensus of a warming climate, however, is consistent with the increases in North Hemisphere summer solar insolation and atmospheric CO_2 (Figure 2.1a, b).

2.4.1 Timing of the deglaciation

Between 20 and 15 ka BP, each of the meltwater groups, except for the *TraCE-like* simulations, have relatively constant AMOC strengths. The *melt-uniform* simulations show the least millennial-scale variability in AMOC (Figure 2.2e). The *melt-routed* simulations, in comparison, have more variation, aligned with the respective freshwater fluxes, and show a weakening trend

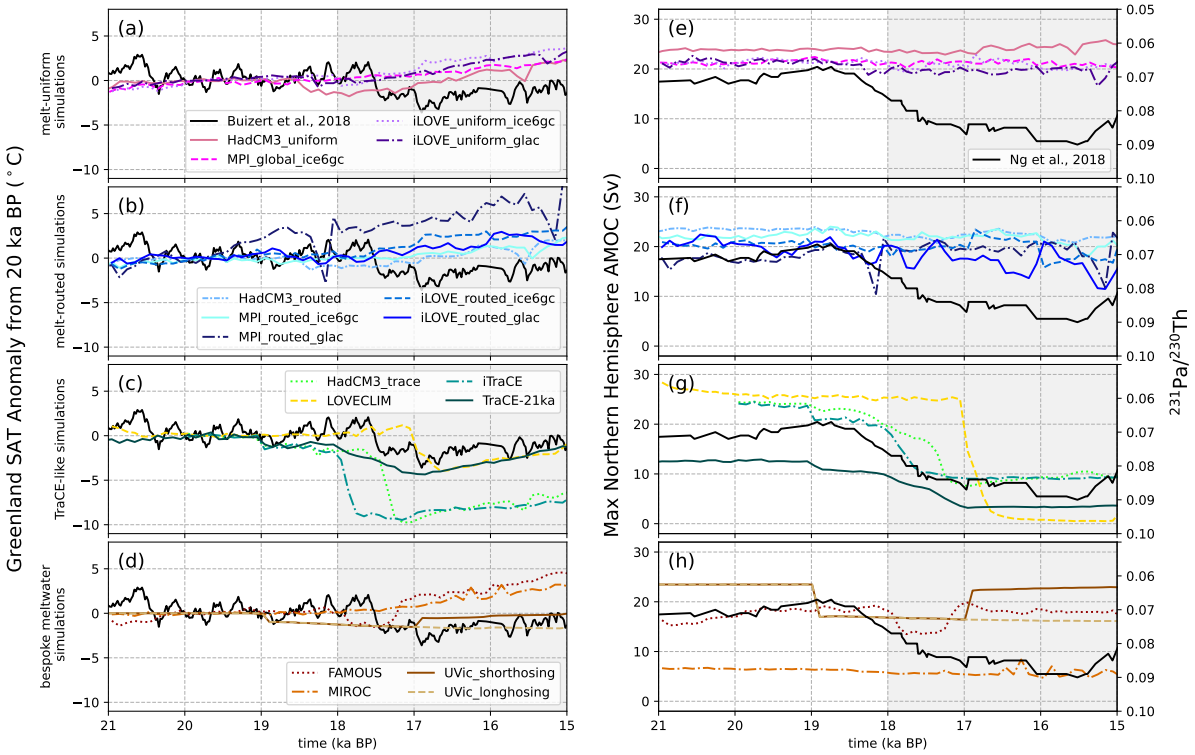

Figure 2.2: Centennial means for (a)-(d) Greenland (between 65 and 82° N and 30 and 55° W) surface air temperature anomaly from approximately the LGM (20–19.5 ka BP) for each simulation. (e)-(h) Maximum AMOC of the Northern Hemisphere at depth between 500 and 3500 m. For comparison, (a)-(d) includes Greenland surface air temperature proxy record from Buizert et al. (2018), plotted as an anomaly from 20 ka BP in black, and (e)-(h) includes the AMOC proxy ^{231}Pa/ ^{230}Th composite record published by Ng et al. (2018), plotted in black (note the arbitrary y-axis scaling). The grey-shaded region denotes the timing of Heinrich Stadial 1.

starting at ∼16.5 ka BP as freshwater input increases towards Meltwater Pulse 1a (Figure 2.2f; Meltwater Pulse 1a at 14.7 ka BP not shown). Like the *melt-routed* simulations, the *bespoke* simulations have more change that is consistent with the freshwater flux, but for all *bespoke* simulations except for *UVic_longhosing*, the AMOC strengths at 21 ka BP and at 15 ka BP are very similar.

The subset of *TraCE-like* simulations, on the other hand, show an abrupt weakening in AMOC strength and an associated decrease in Greenland surface air temperature (anomaly from LGM, calculated as anomalies from the 500-year time window from 20–19.5 ka BP) beginning between 18 and 17 ka BP depending on the simulation (Figure 2.2c, g). The differences in the timing of the decrease in temperature for the *TraCE-like* simulations are likely associated with the differences in timing and magnitude of the freshwater flux. For instance, *iTraCE* shows an earlier and more abrupt cooling than *TraCE-21ka*. Despite both simulations reaching the same magnitude of freshwater at 17 ka BP, the rate of freshwater input into the simulation between 19 ka BP and 17 ka BP differs. At 19 ka BP, there is a larger increase in the freshwater flux in *iTraCE*, which corresponds to a smaller but rapid decrease in the AMOC strength and Greenland surface air temperature at this same time. After 19 ka BP, the freshwater flux in

iTraCE remains higher than in *TraCE-21ka*, and this is consistent with the sharper decrease in surface air temperature in *iTraCE* in comparison to the relatively steady decrease in temperature in *TraCE-21ka*.

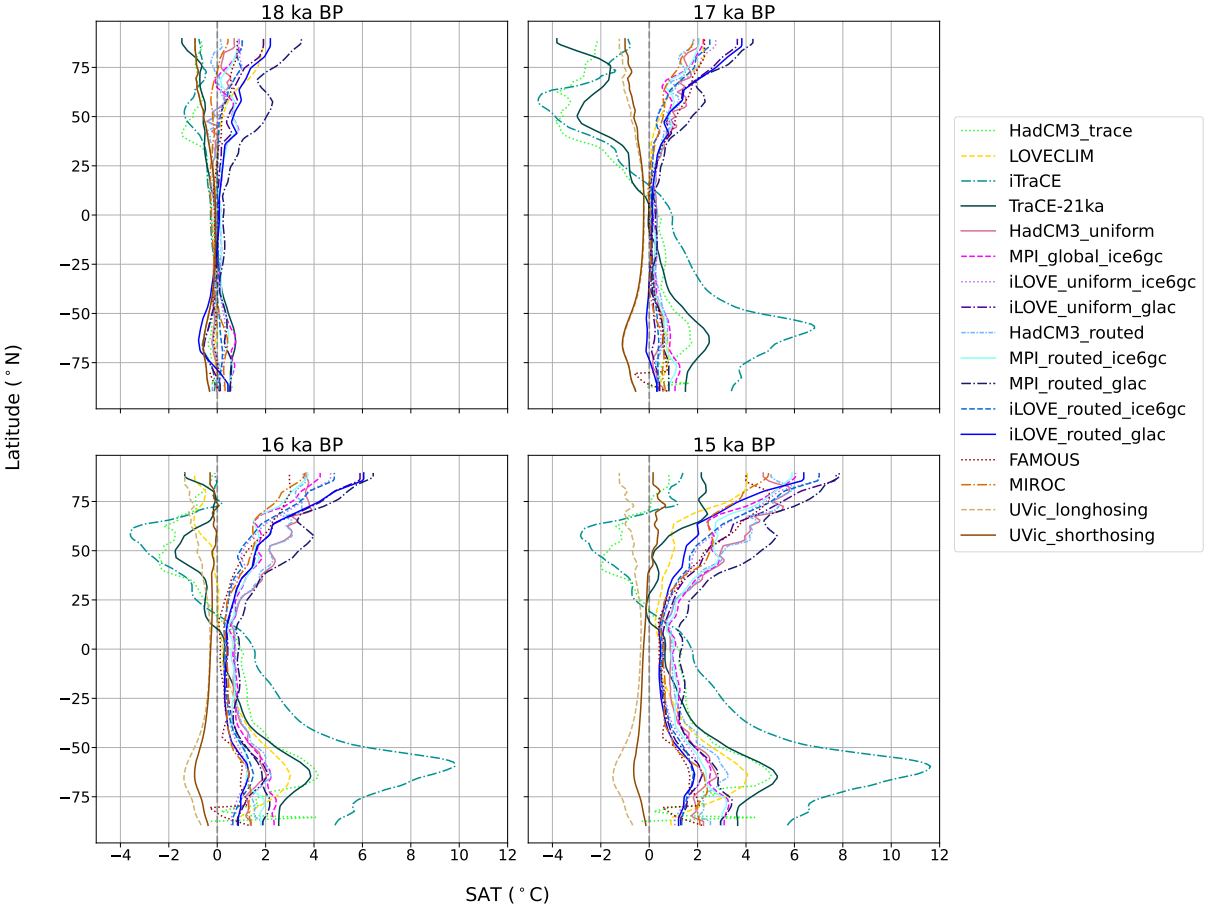

Figure 2.3: Zonal average of decadal mean surface air temperature as anomalies from the LGM (20–19.5 ka BP) for each simulation; 18, 17, 16, and 15 ka BP are calculated as 60-year decadal means centred around the respective time period (e.g., from 17.97 to 18.03 ka BP for 18 ka BP).

HadCM3_TraCE uses the same meltwater scenario as *TraCE-21ka*, but instead of a gradual response, there is a more abrupt decrease in the Greenland surface air temperature at ∼17.5 ka BP and temperatures drop. The drop is as low as in *iTraCE* (with respect to the LGM) and occurs after the freshwater flux has decreased for both *TraCE-21ka* and *HadCM3_TraCE*. However, note that *TraCE-21ka* and *HadCM3_TraCE* are configured with different boundary conditions (i.e., *HadCM3_TraCE* uses greenhouse gas conditions on the AICC2012 timescale and the ICE-6G_C ice sheet reconstruction, whereas the CCSM3 *TraCE-21ka* simulation uses ICE-5G) with the exclusion of the freshwater forcing. Other simulations with similar boundary conditions to *HadCM3_TraCE* (i.e., *HadCM3_routed*) and *TraCE-21ka* (i.e., *FAMOUS*), but different freshwater forcings, do not show the large and abrupt decrease in the Greenland surface air temperature. This suggests that the freshwater forcing is a dominant driver of the abrupt changes displayed in both simulations; however, the differences between them might contribute to the differences in sensitivity to the meltwater flux.

In addition, although the meltwater scenario for *LOVECLIM* is based upon *TraCE-21ka*, the

freshwater flux begins later, at 17 ka BP. Presumably because of this, the decrease in surface air temperature and AMOC strength is also delayed until 17 ka BP. The freshwater input is also much more abrupt in comparison to *TraCE-21ka* and *iTraCE*, corresponding to the rapid transition in the AMOC and surface air temperature at 17 ka BP. The implications of these differences amongst the simulations in the *TraCE-like* meltwater group are further described in section 2.4.4.

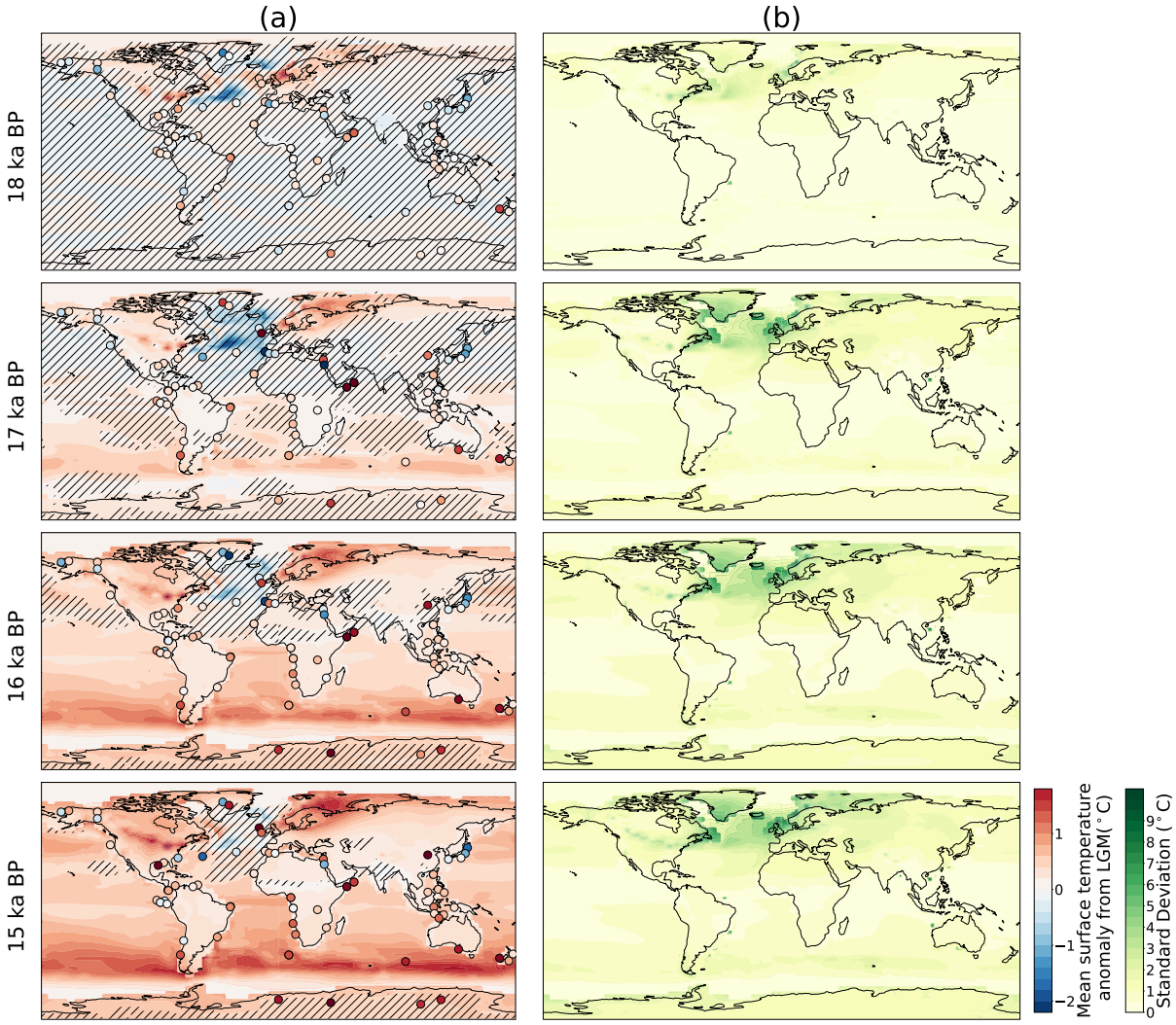

Figure 2.4: (a) Multi-model mean of decadal surface temperature anomaly from the LGM (20–19.5 ka BP) at each time step labelled (not including the UVic simulations). Hatching denotes areas in which less than 70% of the simulations agree with the sign of the mean. The agreement with the sign of the mean was determined using a one sample t test at 95% confidence by testing if the simulation and the mean were both significantly different from zero in the same direction. Column (b) is the same as column (a) but showing the variance. Filled circles show the proxy surface temperature stack from Shakun et al. (2012) on the same colour scale; 18, 17, 16, and 15 ka BP are calculated as 60-year decadal means centred around the respective time period (e.g., from 17.97 to 18.03 ka BP for 18 ka BP).

The GLAC-1D ice sheet reconstruction has more variable meltwater input in comparison to ICE-6G_C, at least partly due to the more frequent updates of the ice sheet geometry and associated boundary conditions (every 100 years compared to every 500 years; Figure 2.1a).

This more variable meltwater forcing is evident in the higher variability of the AMOC strength and Greenland surface air temperature (Figure 2.2b, f; e.g., the sharp decline and subsequent increase in temperature and AMOC strength at ~18.5 ka BP in *MPI_routed_glac* that occurs at the same time as an increase in meltwater release).

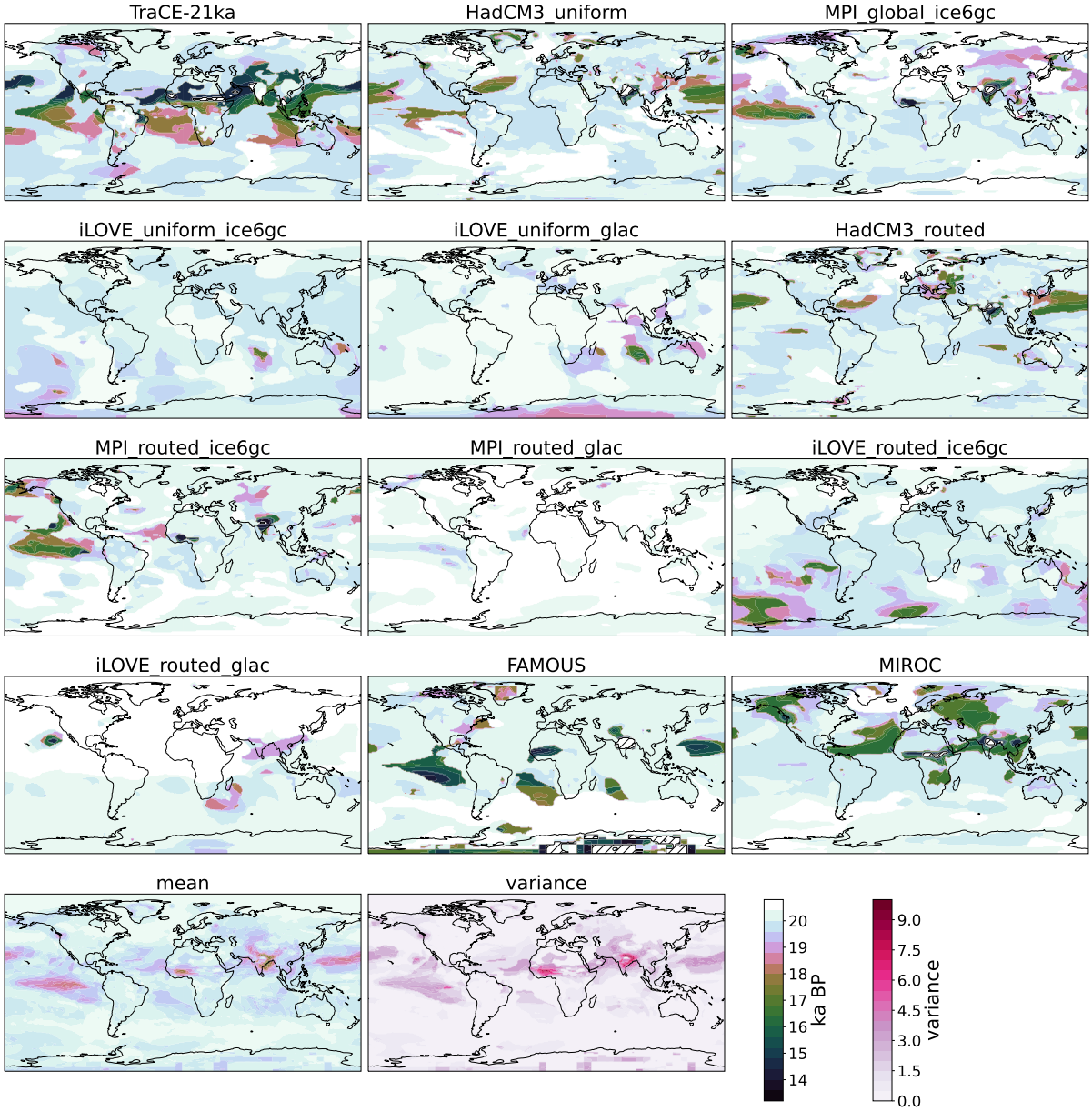

Figure 2.5: Year of first significant warming from 21 ka BP, where 'significant warming' is determined as discussed in section 2.3. Hatching denotes where significant warming did not occur before 13 ka BP

All the simulations that do not follow the *TraCE-like* meltwater forcing follow a similar trajectory throughout the deglaciation with a gradual warming of surface air temperature in Greenland, except for the UVic simulations. The UVic simulations differ presumably because of the bespoke freshwater flux that ends earlier than the end of Heinrich Stadial 1 for the short-hosed simulation and after Meltwater Pulse 1a for the long-hosed simulation. The resultant impacts on the dynamically simulated carbon cycle causes atmospheric CO_2 concentrations to decrease

during AMOC weakening, which contradicts reconstructions of this time period (e.g., Bereiter et al. 2015; Ng et al. 2018). Hence, in *UVic_longhosing*, decadal surface air temperature remains cold throughout the onset of the deglaciation, and *UVic_shorthosing* does not begin to warm in the Northern Hemisphere until the freshwater hosing is turned off at 17 ka BP (Figure 2.2).

In most simulations, significant warming from the LGM (see section 2.3 for how this is defined) occurs in most locations by 19 ka BP except in parts of the tropics where significant warming does not occur until as late as 16–17 ka BP (Figure 2.5). The earlier warming in the high northern latitudes is likely associated with the increase in insolation (Figure 2.1a; Members 2006; Park et al. 2019; Kapsch et al. 2021) and the impact of polar amplification, whereas the warming in the tropics is more delayed and correlates with the timing of CO_2 concentration increase (Figure 2.1b and 2.13a–d). The mean pattern is aligned with the results from Roche et al. (2011) (see Figure 4 by Roche et al., 2011) that similarly show an earlier warming in the northern and southern high latitudes and delayed warming in the tropics. The effect of the freshwater forcing on the global temperature, however, was not incorporated in the no-melt simulations from Roche et al. (2011). Nevertheless, in the *TraCE-like* simulations, the meltwater impact is evident by the strong cold anomalies in the North Atlantic, the region where most of the freshwater forcing is applied or drained into (Figure 2.3 and 2.4). Therefore, warming in this region, despite initially occurring at the onset of the deglaciation, is halted until much later in comparison to the other simulations (as further evident in the discussion around Figure 2.13).

This dissimilarity in the trajectory of warming is also evident in global surface air temperature anomalies from the LGM (Figure 2.4 and 2.11). Early in the deglaciation, at 18 ka BP, there is disagreement between simulations as to the timing and magnitude of the warming as well as to which regions. For instance, *MPI_routed_glac* has warmed ∼4 °C in the North Atlantic by 18 ka BP, whereas *MIROC* still has colder regions throughout the tropics and Pacific with respect to the LGM (20–19.5 ka BP) and has only started to warm in the high latitudes, most likely associated with insolation increases (Figure 2.11).

The iLOVECLIM and MPI simulations have significant warming in most areas from the immediate onset of the deglaciation, with *MPI_routed_glac* displaying the earliest significant warming globally compared to the other simulations (Figure 2.5). Similarities are also evident amongst simulations that use the same model but different meltwater scenarios, e.g., between *HadCM3_uniform* and *HadCM3_routed* and between *MPI_routed_ice6gc* and *MPI_global_ice6gc*. The HadCM3 simulations have a matching cooling region around the Labrador Sea and Gulf Stream, and the MPI simulations have a matching cooling region in the Nordic Seas that each persist until ∼16 ka BP (more detail in section 2.4.3). UVic remains unique amongst the simulations assessed in this study because between 20 and 15 ka BP most regions do not warm from the LGM. The CO_2 increase begins to take precedent in *UVic_shorthosing* after 17 ka BP and the melting ice sheets in North America and Fennoscandia show familiar warming patterns in the Northern Hemisphere for ICE-6G_C. This pattern, warming along the edges of the Northern Hemisphere ice sheets, is also evident in the other simulations using ICE-6G_C.

Despite the disagreements with the timing of the deglaciation on an individual scale, the sign of

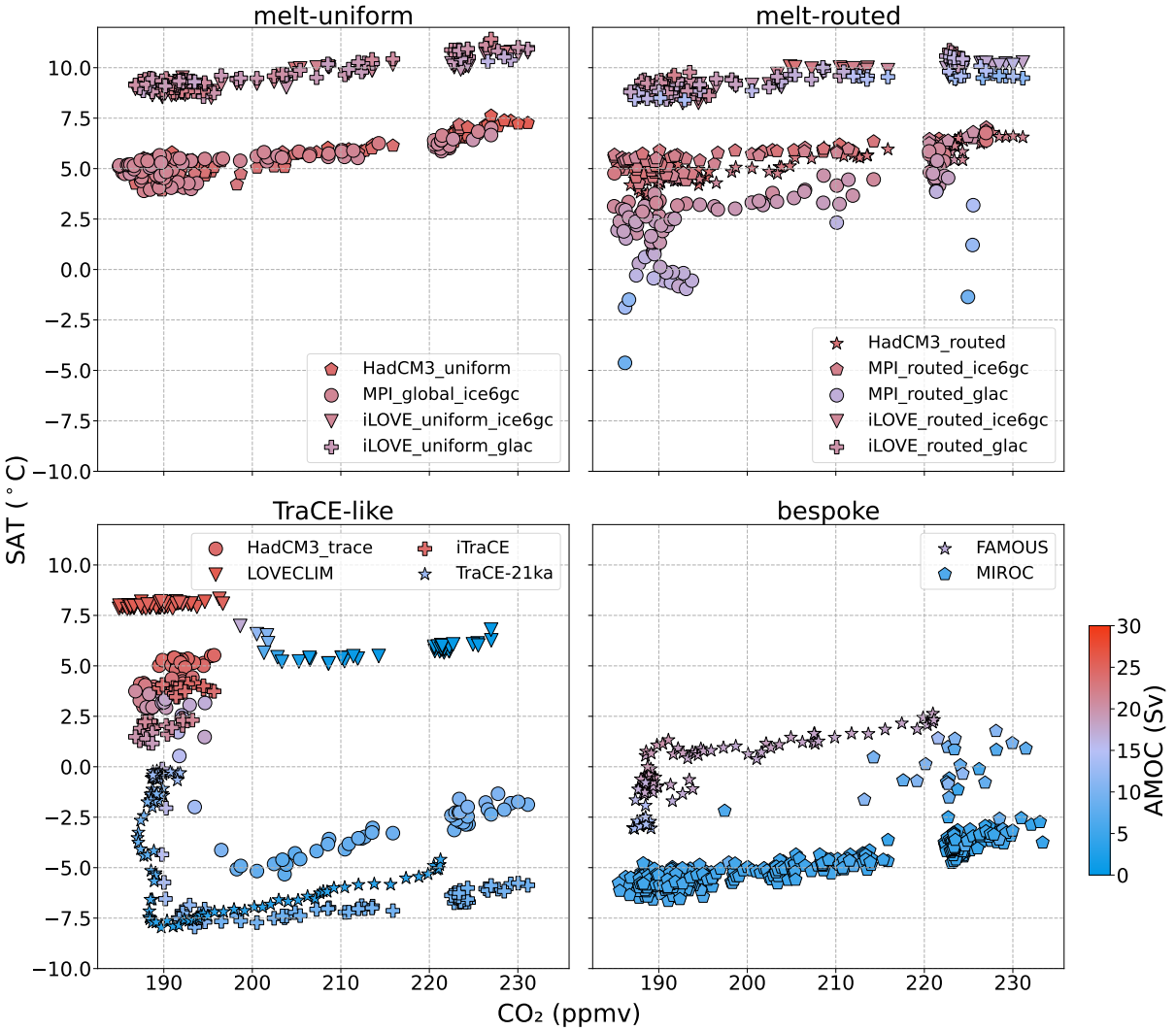

Figure 2.6: Absolute surface air temperature over the North Atlantic (between 35 and 60° N and -60 and 0° E) as a function of CO_2 concentration with symbol shading representing the strength of the AMOC (Sv) split into groups defined by meltwater scenario. The 50-year means are shown for each simulation except for *MIROC*, for which decadal means are shown to capture its temporally finer-scale variability. See Figure 2.16 for the same analysis displayed as anomalies from 20 ka BP.

the multi-model mean of decadal surface temperature shares close agreement with the surface temperature stack produced by Shakun et al. (2012), and this is most significant in the Southern Hemisphere (Figure 2.4). The median point-by-point difference between the multi-model mean and the proxy data is less than 1 °C between 18 and 15 ka BP, with a median of only 0.015 °C at 18 ka BP that increases to 0.993 °C by 15 ka BP, indicating that the multi-model mean of the ensemble replicates the Shakun et al. (2012) proxy stack relatively well but that disagreement with the proxy record grows further into the deglaciation. The largest discrepancies between the model output and reconstruction occur in the North Atlantic and Greenland (after 18 ka BP), which are also areas of more disagreement across the model ensemble (Figure 2.14). This is the region where there are the most proxy records and therefore potentially the location in which the deglacial climate evolution is the best constrained (at least compared to the Pacific sector, for

example). The North Atlantic is also the region where most models would show agreement for similar AMOC change; however, these simulations show various AMOC evolutions. It remains to be thoroughly tested if simulations that fit the constraints of the North Atlantic also fit the constraints of climate records from other locations. The multi-model mean tends to be cooler than the proxy data in the Southern Hemisphere but is warmer in many locations in the Northern Hemisphere (i.e., parts of the North Atlantic, Alaska, and off the coast of Japan). Interestingly, although the *TraCE-like* meltwater group represents the cold areas of the North Atlantic well, those simulations have difficulty replicating the warmer core locations in this same region. Conversely, the other meltwater groups present the opposite difficulty – they are better at replicating the warmer regions of the North Atlantic while failing to represent the cold ones (not shown). This suggests the potential need for subsequent investigations of broader model structure and how we interpret reconstructions (i.e., specific data points).

For the comparison to individual simulations, the surface temperature stack from Shakun et al. (2012) is compared to surface temperature change from the LGM in Figure 2.11. Model–data comparison has also previously been performed by many of the individual modelling groups in their respective studies (see Table 2.1).

2.4.2 Linking surface climate, ocean circulation, and greenhouse gas forcing

In every simulation, there is the expected interrelation between surface air temperature in the North Atlantic, CO_2 concentration, and AMOC. As CO_2 increases, surface air temperature increases, as demonstrated by the increasing trends on each panel of Figure 2.6. Surface air temperature is also higher when the AMOC is stronger, clearly shown by *LOVECLIM*. The simulations with smaller AMOC variation have a clearer relationship with CO_2 concentration (see *melt-uniform* panel and all the *melt-routed* simulations except for *MPI_routed_glac*; Figure 2.6). The *TraCE-like* simulations each have a strong L-shaped curve in the relationship between CO_2 concentration and surface air temperature. This is because the initial large decrease in North Atlantic surface air temperature, representing Heinrich Stadial 1, occurs whilst the CO_2 concentration is relatively constant (Figure 2.1b). However, after ∼18 ka BP (timing dependent on the CO_2 record used by the modelling group), CO_2 concentration begins increasing alongside a slow surface air temperature increase in each simulation.

The relationship between AMOC, CO_2, and surface air temperature is illustrated further by the R^2 values determined by a linear regression model across the entire period between 20 and 15 ka BP on a decadal temporal scale with surface air temperature as the dependent variable (Figure 2.7 and 2.8). The results from the linear regression show that during the period of 20 to 15 ka BP, surface air temperature in the *TraCE-like* simulations has a stronger positive correlation with AMOC, and the other simulations in the ensemble have a stronger positive correlation with CO_2. For instance, the *TraCE-like* simulations have higher R^2 values between AMOC and surface air temperature in the North Atlantic than the other meltwater groups, presumably because changes between AMOC and surface air temperature correspond in the *TraCE-like* simulations between 20 and 15 ka BP, whereas the other simulations have a stable ocean circulation and very little temperature change during this time period (Figure 2.2).

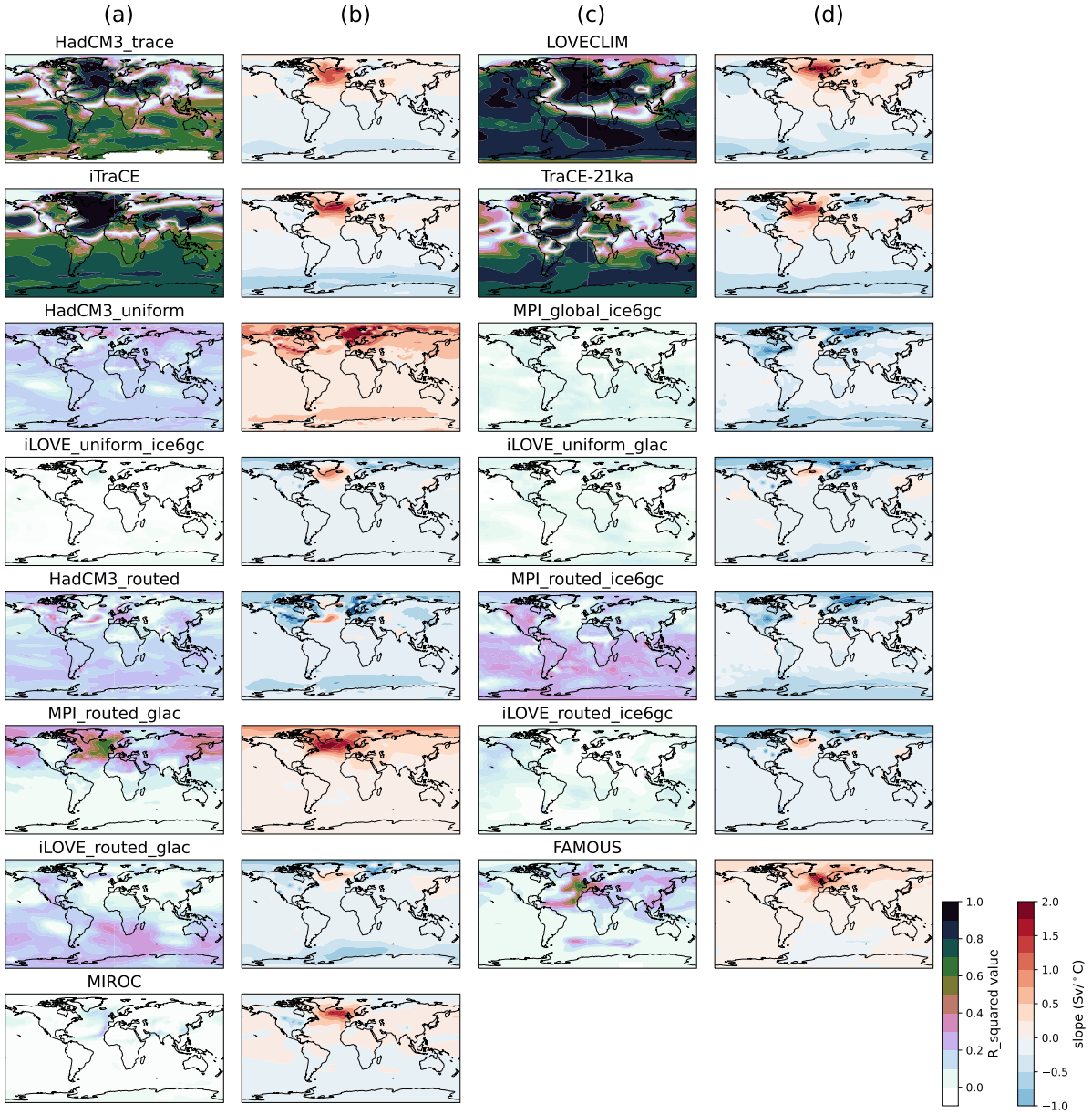

Figure 2.7: Spatial distribution of the temporal correlation of AMOC strength and surface air temperature using a linear regression model for the time period 20–15 ka BP using decadal means. Columns (a) and (c) show R^2 values as a result of the linear regression. Columns (b) and (d) show corresponding slopes to simulations in column (a) or (c) as a result of the linear regression.

FAMOUS, which has a stronger freshwater forcing between 20 and 15 ka BP in comparison to the other non-*TraCE-like* simulations, also has higher R^2 values between AMOC and surface air temperature in the North Atlantic region, though these are dampened relative to those of the *TraCE-like* simulation. The simulations with little AMOC and surface air temperature change show very low correlations between the two variables throughout the globe (e.g., iLOVECLIM simulations, the ICE-6G_C MPI simulations, and *MIROC*). However, the *melt-routed* GLAC-1D simulations, in comparison to their ICE-6G_C same-model counterparts, exhibit higher correlations. The correlation between AMOC and surface air temperature in *MPI_routed_glac*

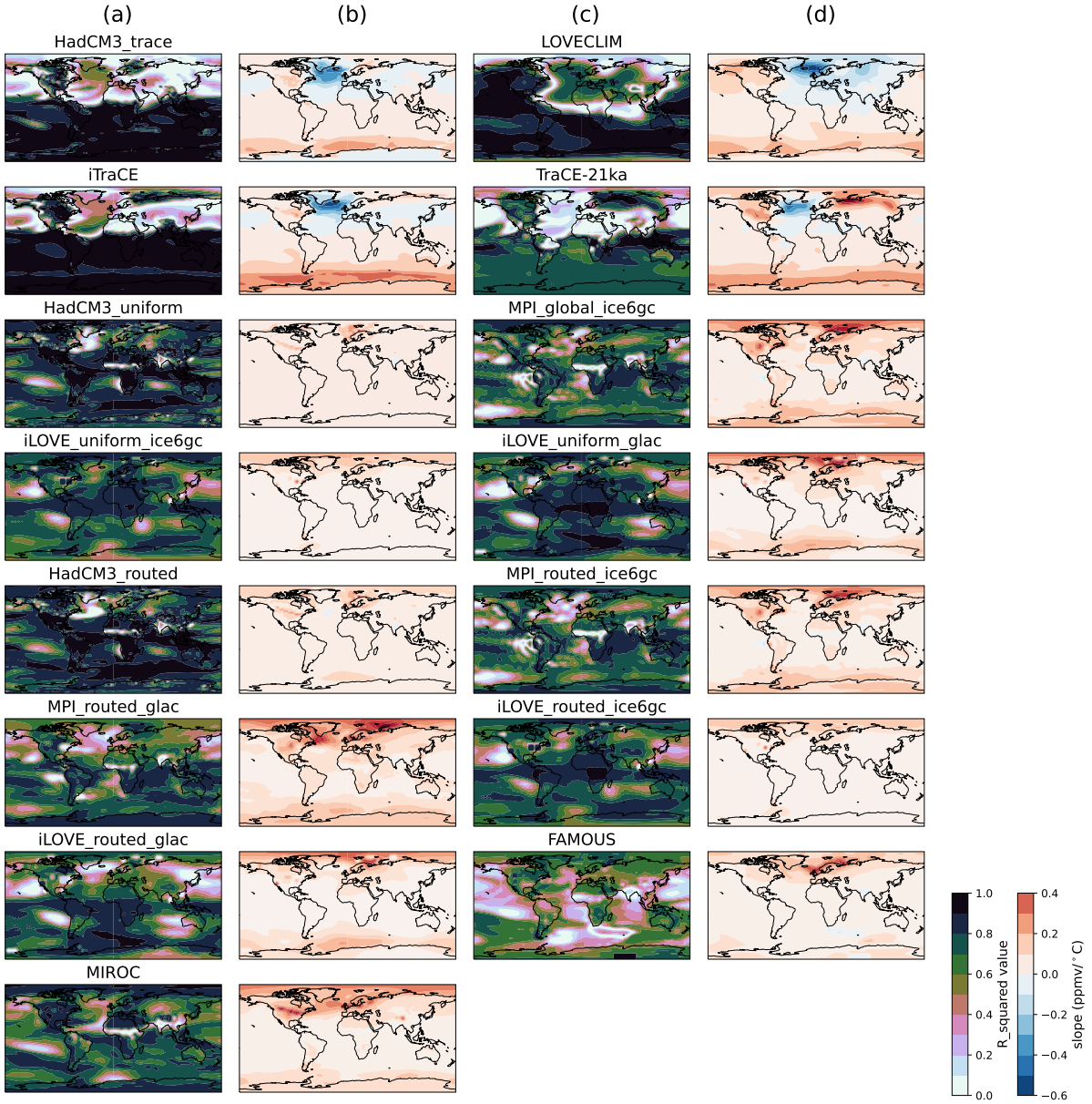

Figure 2.8: Spatial distribution of the temporal correlation of CO_2 concentration and surface air temperature using a linear regression model for the time period 20–15 ka BP using decadal means. Columns (a) and (c) show R^2 values as a result of the linear regression. Columns (b) and (d) show corresponding slopes to simulations in column (a) or (c) as a result of the linear regression.

increases in the Irminger Sea and Nordic Seas from no correlation (R^2 is 0) in *MPI_routed_ice6gc* to an R^2 value of ∼0.6. The slope of the GLAC-1D simulation also changes from negatively correlated in most locations to positively correlated. The differences between the iLOVECLIM GLAC-1D and ICE-6G_C simulations are much smaller. The *iLOVE_routed_glac* simulation does display higher R^2 values in the Southern Hemisphere and some locations in North America and south of Greenland; however, this correlation is still low (below 0.5). The slopes between the simulations are also very similar. The larger differences in the MPI simulations could be due to the higher sensitivity of the simulations to the GLAC-1D freshwater flux, as described in more detail in section 2.4.3.

The positive slope in the North Atlantic region for the *TraCE-like* simulations demonstrates the positive correlation between AMOC and surface air temperature changes, whereas the rest of the globe has a more negative correlation in most simulations, regardless of their meltwater group. This relationship is representative of the bipolar see-saw. The *TraCE-21ka* simulation most clearly exhibits this bipolar connection between the Northern Hemisphere and Southern Hemisphere with a strong positive correlation between AMOC and surface air temperature in the North Atlantic and a strong negative correlation in the Southern Ocean.

The relationship between CO_2 and surface air temperature (Figure 2.8) in the Northern Hemisphere is nearly opposite to the relationship between AMOC strength and surface air temperature (Figure 2.7) for *HadCM3_TraCE*, *iTraCE*, and *TraCE-21ka*, with the areas of strong and positive correlation between AMOC and surface air temperature showing weaker and negative correlation between CO_2 and surface air temperature. This suggests that in the early deglaciation, if the AMOC is weakening or already weak because of the freshwater forcing when CO_2 starts to rise, the impact of CO_2 might be dampened or postponed in the Northern Hemisphere, whereas a strong correlation with surface air temperature remains in the Southern Hemisphere. The relationship between CO_2 and surface air temperature should be positive everywhere, so the negative correlation in the North Atlantic for the *TraCE-like* simulations proposes that the AMOC has a stronger influence than CO_2 during the studied period (20–15 ka BP) and that the regression analysis cannot properly separate the effects of AMOC and CO_2 for this type of experiment. The simulations with weaker correlation between CO_2 and surface air temperature in regions of the tropics (e.g., *FAMOUS* and parts of Sub-Saharan Africa in *MIROC*, *MPI_global_ice6gc*, and *HadCM3_routed*) also display delayed warming in these same locations (Figure 2.5). Increases in obliquity are shown to delay warming in the tropics, specifically in these same parts of Africa as well as India, potentially due to increased cloud coverage and therefore cooling (Erb et al. 2013). In addition, the lag between the start of the CO_2 concentration increase ($\sim$18 ka BP or later depending on the timescale used) and the insolation increase ($\sim$20 ka BP) can disrupt the correlation between CO_2 and surface air temperature and create a localised delay in warming of the tropics (as also demonstrated in Figure 2.5). Note that the analysis in Figure 2.7 and 2.8 only goes until 15 ka BP, whereas the analysis in Figure 2.5 reaches until 13 ka BP. The simulations with the very weak correlations between AMOC and surface air temperature (iLOVECLIM, MPI simulations, and *MIROC*) demonstrate globally high correlations with CO_2 except for a few concentrated regions. These regions of lower correlation are similar between simulations run by the same model and could indicate changes in upwelling strength during this time period.

It is important to note, however, that during the chosen time period only the *TraCE-like* simulations have strong and corresponding changes in the AMOC and surface air temperature. The suggested relationships could be checked by continuing this study through the later parts of the deglaciation to encompass greater amplitudes of change in the non-*TraCE-like* simulations.

2.4.3 Impact of different climate and ice sheet forcings and boundary conditions on model output

In this study, we include multiple simulations from the HadCM3, MPI, and iLOVECLIM modelling groups. These three modelling groups tested different PMIP4 boundary condition and forcing options: for example, implementing the *melt-routed* or *melt-uniform* scenario for the same ice sheet and/or using different ice sheets and associated meltwater scenarios (Table 2.1). Experimenting with the range of options the PMIP4 protocol enables us to review the impact of different climate forcings on the resultant model output.

The AMOC for each of the HadCM3, MPI, and iLOVECLIM simulations is impacted by the chosen meltwater scenario during the deglaciation (see section 2.4.1). However, between 21 and 15 ka BP, the differences between the AMOC trajectory appear to be less affected by the meltwater scenario and are instead more significantly affected by the choice of ice sheet reconstruction (Figure 2.2e–h and 2.9). For instance, when we compare the simulations with the different meltwater scenarios, but with the same ice sheet reconstruction (e.g., ICE-6G_C), i.e., *HadCM3_uniform* and *HadCM3_routed*, *iLOVE_uniform_ice6gc* and *iLOVE_routed_ice6gc*, and *MPI_global_ice6gc* and *MPI_routed_ice6gc*, we notice multiple similarities between the deglaciation trajectory both spatially and temporally. For instance, the HadCM3 simulations begin at a very similar surface air temperature in the North Atlantic at the start of the deglaciation (∼4 °C at 21 ka BP) and follow a comparable warming trajectory until 15 ka BP (reaching ∼7 °C; Figure 2.9) despite the application of different meltwater scenarios, though the *melt-routed* simulation does remain colder in the North Atlantic than the *melt-uniform* simulation throughout the time period. In addition, spatially, as anomalies from the LGM (Figure 2.3 and 2.11), the simulations look almost indistinguishable. Both display surface air temperature cooling along the Gulf Stream, and warming in locations of ice sheet melt, such as the Eurasian ice sheet in Fennoscandia and at the edge of the Laurentide ice sheet in North America. The most evident difference between the simulations is that *HadCM3_uniform* is colder than *HadCM3_routed* in the Labrador Sea and warmer in the Norwegian Sea, corresponding with differences in sea ice concentration – *HadCM3_uniform* has a higher sea ice concentration in the Labrador Sea than *HadCM3_routed* and a lower concentration in the Norwegian Sea (Figure 2.17a, b). This pattern also corresponds to the dissimilarities in the convection sites between the two simulations as the *melt-uniform* simulation has more convection further south, along the sea ice edge, and in the Norwegian Sea, whereas the mixed-layer depth in the *melt-routed* simulation is deeper in the Labrador Sea (Figure 2.17c). *HadCM3_TraCE* has the same dipole pattern as the other HadCM3 simulations, with cooling along the Gulf Stream and into Greenland and the Labrador Sea and warming over Fennoscandia; however, this signal is weak compared to the strong cooling in the North Atlantic due to the larger freshwater forcing applied.

Likewise, *MPI_global_ice6gc* and *MPI_routed_ice6gc* both begin at ∼4 °C at the start of the deglaciation in the North Atlantic and then warm at a comparable rate, but slower than the HadCM3 simulations, warming ∼3 °C by 15 ka BP rather than ∼5 °C. The MPI simulations, like the HadCM3 simulations, also share a similar spatial pattern with an area of strong cooling in the Nordic Seas and stronger warm patches off the coast of north-western North America

and in the North Sea (Figure 2.11). This pattern appears to be independent of the ice sheet reconstruction because *MPI_routed_glac* has the same areas of relative cold and warmth at 18 ka BP, but the signal is weaker, likely because *MPI_routed_glac* is ∼5 °C colder in the North Atlantic at the start of the deglaciation than the ICE-6G_C simulations and warming from the LGM occurs at a faster rate. Temporally, however, *MPI_routed_glac* displays more surface air temperature variability in the North Atlantic with abrupt climate changes as large as 5 °C and AMOC decreases of ∼9 Sv at ∼18.2 and 15.2 ka BP, most likely following the higher-frequency variability in the meltwater input from the GLAC-1D ice sheet reconstruction (Figure 2.1c and 2.2) but also because *MPI_routed_glac* is significantly colder at the LGM compared to its ICE-6G_C counterparts. (Kapsch et al. 2022) showed that the MPI simulations that are colder during the LGM lie closer to a critical threshold of AMOC variability. This aligns with the findings of Oka et al. (2012) and Klockmann et al. (2018) that demonstrate that the AMOC becomes more sensitive to perturbations, such as ice sheet topography and the resultant wind stress and CO_2 concentrations, when it is closer to an existing temperature threshold. Absolute surface air temperatures in the North Atlantic (Figure 2.14e–h) show that multiple simulations in the ensemble are colder than *MPI_routed_glac* at the LGM, but only *MIROC*'s AMOC appears to be close to a critical threshold of variability, as indicated by the changes in maximum AMOC strength towards 15 ka BP.

iLOVE_routed_glac has a similar, but less pronounced, variability of the AMOC and corresponding decreases in Greenland surface air temperature to *MPI_routed_glac* (Figure 2.2b). However, in the North Atlantic, neither the *iLOVE_routed_glac* simulation nor *iLOVE_uniform_glac* exhibit significantly more variability than the ICE-6G_C iLOVECLIM simulations (relative to *MPI_routed_glac* and its ICE-6G_C counterparts). Spatially, the ICE-6G_C and GLAC-1D simulations are also nearly indiscernible (Figure 2.11), except at the beginning of the deglaciation in the Southern Hemisphere, where surface air temperatures remain cooler for longer in the GLAC-1D simulations. This suggests that under these background conditions iLOVECLIM is less sensitive to freshwater perturbations than MPI-ESM-CR. This is dependent, however, on how both modelling groups calculate their freshwater flux, which can vary despite using the same ice sheet reconstruction (see section 2.3), as well as, and potentially more importantly, the fact that these simulations are performed with two very different models. For example, iLOVECLIM is an Earth system model of intermediate complexity (EMIC) with three atmospheric layers (see Table 2.1), whereas MPI-ESM-CR is an Earth system model (ESM) with 31 atmospheric levels and thus can represent topographic feedbacks on the atmosphere with higher complexity and at finer-scale resolution.

Unfortunately, more simulations using a GLAC-1D-derived freshwater flux do not exist to compare to *MPI_routed_glac* and *iLOVE_routed_glac* and to get more robust results. Using GLAC-1D with the MPI model demonstrates more abrupt and higher reactivity to meltwater changes than the ICE-6G_C equivalents; however, this is less clear in the iLOVECLIM GLAC-1D simulations. Further simulations from other model types using both ice sheet reconstructions would be beneficial to understanding whether the systematic differences between the models contribute to the differences in sensitivity to the freshwater forcing. Otherwise, the simulations performed

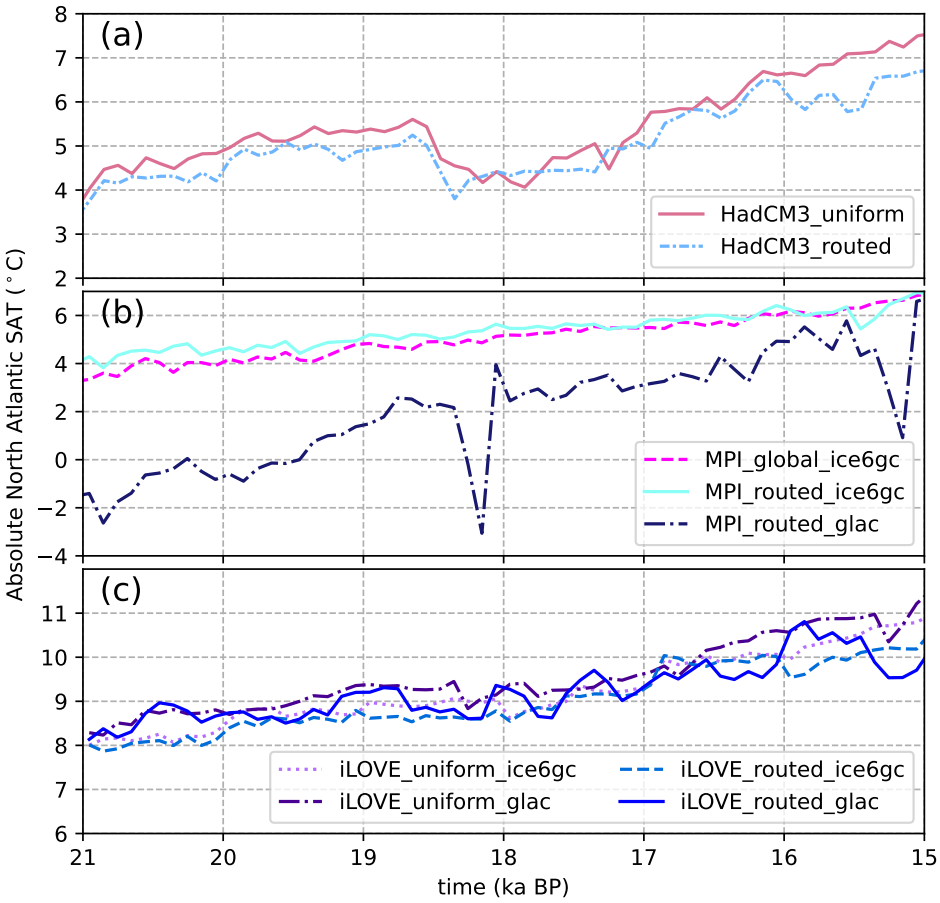

Figure 2.9: Absolute surface air temperature in the North Atlantic (between 35 and 60° N and -60 and 0° E) for the HadCM3, MPI-ESM, and iLOVECLIM simulations. Note that to capture variability, the y-axis limits are not the same for each panel. Absolute surface air temperature in the North Atlantic for the entire ensemble is shown in Figure 2.15e–h.

with the same model and ice sheet reconstruction display many similarities in the deglacial transition between 20 and 15 ka BP despite having different meltwater forcing scenarios.

2.4.4 Sensitivity of climate models to similar forcing(s)

All simulations, with the exclusion of the UVic simulations, *TraCE-21ka*, and *FAMOUS*, use the greenhouse gas forcing on the AICC20212 timescale, with an increase in atmospheric CO_2 concentration at ~17.5 ka BP. In contrast, in *TraCE-21ka* and *FAMOUS*, the CO_2 concentration does not begin increasing until ~17 ka BP. This delayed increase in CO_2 postpones the warming of the deglaciation in these simulations, as is evident in the tropical regions (Figure 2.3, 2.5, and 2.13). *MIROC*, despite not having a delayed CO_2 increase, also displays delayed warming in the tropics, like that of *FAMOUS*. This could be due to the higher sensitivity of MIROC to orbital forcing, causing it to take precedent over the CO_2 forcing earlier in the deglaciation (Obase and Abe-Ouchi 2019).

Contrasting sensitivities of the models used for the *TraCE-like* simulations are evident in the response of the AMOC to the freshwater forcing and corresponding changes in Greenland surface

air temperature in the different models (Figure 2.2). By 17 ka BP, all four simulations have reached a similar and constant freshwater flux (with *iTraCE* ∼0.05 Sv, or 33%, higher). The four simulations, however, begin with a range of different AMOC strengths. *LOVECLIM* has the strongest LGM AMOC at ∼28 Sv, *TraCE-21ka* with the weakest LGM AMOC at ∼12 Sv, and *HadCM3_TraCE* and *iTraCE* are in the middle of the cluster, starting with an AMOC strength of ∼24 Sv (see section 2.6.4; Figure 2.2g). Note that *HadCM3_TraCE* and *iTraCE* start at 20 ka BP, whereas *LOVECLIM* and *TraCE-21ka* start at 21 and 22 ka BP, respectively.

Despite beginning the deglaciation with the strongest AMOC, *LOVECLIM*'s ocean circulation is also the most sensitive to the freshwater perturbation, causing its AMOC to crash to the weakest AMOC state of all the simulations (Figure 2.2g). The temperature change in the *LOVECLIM* simulation, however, is comparable to the temperature change in *TraCE-21ka* despite the very different AMOC responses to the freshwater forcing. The AMOC collapses to nearly 0 Sv, but Greenland surface air temperature only decreases by ∼5 °C.

The Greenland surface air temperature response in *HadCM3_TraCE* and *iTraCE* appears to be impacted similarly by the change in AMOC strength, with both simulations following comparable trajectories throughout the deglaciation despite *iTraCE* having a larger freshwater flux. Both simulations exhibit an AMOC decrease of ∼14 Sv and ∼ -7 °C of temperature change between 19 and 16 ka BP. In addition, although *TraCE-21ka* and *HadCM3_TraCE* use the exact same freshwater flux, the *HadCM3_TraCE* simulation exhibits a decrease in AMOC strength of over ∼14 Sv and a corresponding decrease in surface air temperature of ∼10 °C in Greenland, whereas *TraCE-21ka*'s AMOC strength weakens by only ∼9 Sv and Greenland surface air temperature only decreases by ∼4 °C. This suggests that the HadCM3 simulation is more sensitive to freshwater perturbations than *TraCE-21ka* but also that under the simulated climate conditions Greenland surface air temperature in HadCM3 is also more sensitive to corresponding AMOC changes compared to the other models. Additional exploration would be interesting to determine what different aspects between *HadCM3_TraCE* and *TraCE-21ka* could be contributing to the discrepancies in sensitivity (e.g., whether it could be the initial conditions, other boundary conditions, parameter choices, or simply model structure). The lower sensitivity of CCSM3 to freshwater perturbations is further investigated by He and Clark (2022) by rerunning *TraCE-21ka* but with no freshwater input during the Holocene. This version of the simulation is in better agreement with proxy Holocene AMOC kinematic reconstructions (McManus et al. 2004; Lippold et al. 2019).

The differences in model sensitivity are less observable in the simulations that apply meltwater forcing in accordance with the PMIP4 protocol's ice sheet consistent recommendations, as discussed in section 2.4.3. Whereas the use of very similar freshwater fluxes amongst the *TraCE-like* simulations allows for easier comparison of changes in AMOC strength and corresponding surface air temperature. We determine that *LOVECLIM*'s AMOC is the most sensitive to freshwater perturbations and that Greenland surface air temperature in *HadCM3_TraCE* is most sensitive to corresponding AMOC compared to other simulations in the *TraCE-like* meltwater group. Further simulations from other model types would be beneficial to determine what different aspects between the simulations could be contributing to the sensitivities.

2.4.5 Meltwater paradox

There has been ongoing debate on how much meltwater to input into simulations of the last deglaciation, and these results highlight the impact of the decision. The debate has stemmed from a so-called 'meltwater paradox' that exists between the choice of large and geologically inconsistent meltwater forcings that successfully produce abrupt climate events versus glaciologically realistic meltwater fluxes that do not. This paradox is particularly evident in the last deglaciation during Heinrich Stadial 1 (between ∼18.5 and 14.7 ka BP) and the Bølling Warming (∼14.7 ka BP). Heinrich Stadial 1, for instance, is associated with weak ocean circulation strength (Lynch-Stieglitz 2017; Ng et al. 2018; Pöppelmeier et al. 2023a) and cold climate conditions in multiple regions. There has been difficulty reconciling a weak AMOC in model simulations of the early deglaciation with the small amount of realistic freshwater release, as determined by the ice sheet reconstructions. Because of this, some model experiments (e.g., simulations in the *TraCE-like* meltwater group) have, by design, required overly large quantities of freshwater forcing to collapse their initially strong AMOCs and produce an abrupt cooling event such as that shown by surface air temperature proxy records (e.g., Wang et al., 2001; Ma et al., 2012). Ivanovic et al. (2018) suggested that the AMOC weakening targeted in these simulations is too large and that a smaller meltwater flux inducing more modest North Atlantic change may be sufficient to drive the recorded Heinrich Stadial climate. However, fully transient simulations that include only meltwater that is consistent with the ice sheet reconstructions (i.e., *HadCM3_routed*, *MPI_routed_ice6gc*, *MPI_routed_glac*, *iLOVE_routed_ice6gc*, i*LOVE_routed_glac*, and their corresponding *melt-uniform* simulations) do not achieve either the AMOC change or the surface climate signal of Heinrich Stadial 1.

In this context, the MIROC last deglaciation simulation is unique because it simulates a weak AMOC and cold surface air temperatures of Heinrich Stadial 1 (Figure 2.2h and 2.13h) and the resumption of the AMOC of the Bølling Warming without releasing an unrealistically large amount of freshwater (not shown as this paper only covers until 15 ka BP; see Obase and Abe-Ouchi 2019; Obase et al. 2021). Instead, a cold, weak-AMOC state is achieved with a gradually increasing meltwater flux that remains below the ice volume loss in the reconstruction and is used to regulate the timing of the abrupt resumption of the AMOC. The *MIROC* ocean circulation, therefore, displays a different sensitivity to freshwater input compared to the rest of the last deglaciation ensemble. This is likely in part due to the very weak LGM AMOC state at the start of the simulation, which also plays a role in the surface air temperature response and may make the simulation more susceptible to a small freshwater flux.

There is debate on the strength of the LGM AMOC and how this initial state impacts the subsequent climate change of the deglaciation. Some observations have suggested a weaker and shallower LGM AMOC than present day (e.g., Lynch-Stieglitz et al. 2007; Böhm et al. 2015; Lynch-Stieglitz 2017), with agreement from recent data–model comparison studies(e.g., Menviel et al. 2017; Muglia and Schmittner 2021; Wilmes et al. 2021; Pöppelmeier et al. 2023a). Other ocean circulation proxy studies (e.g., McManus et al. 2004; Gherardi et al. 2005; Gherardi et al. 2009; Ivanovic et al. 2016; Ng et al. 2018) demonstrated a consensus of a vigorous but shallower AMOC coming out of the LGM (relative to the modern day) that subsequently weakened and

shallowed (but remained active; Bradtmiller et al. 2014; Repschläger et al. 2021; Pöppelmeier et al. 2023b) during the abrupt transition to Heinrich Stadial 1. Recent modelling studies have also suggested conditions between a deep and strong ocean circulation at the LGM (e.g., Menviel et al. 2011; He et al. 2021; Sherriff-Tadano et al. 2021; Kapsch et al. 2022; Snoll et al. 2022) due to the presence of thick ice sheets (Oka et al. 2012; Sherriff-Tadano et al. 2018; Galbraith and Lavergne 2019) and a shallow AMOC of similar strength to present day (e.g., Gu et al. 2020; Zhu et al. 2021).

As *MIROC* is the only PMIP4 last deglaciation simulation (LDv1 or previous) to simulate a weak ocean circulation at the onset of the deglaciation and then a later rapid resumption even with a continuous freshwater flux, this simulation may offer important insight to the conditions under which abrupt deglacial climate change may occur. Nonetheless, even this model cannot reproduce the Heinrich Stadial-Bølling Warming transition under Meltwater Pulse 1a-like freshwater forcing. Thus, the meltwater paradox of the last deglaciation remains.

This brings into question whether our models have the right sensitivity to freshwater fluxes. There appears to be a consensus as to the overall climate response to meltwater input in models and proxy records, i.e., the AMOC rapidly weakens, the North Atlantic cools, and sea ice forms, with the converse occurring when meltwater input stops. However, there is still less understanding and less agreement about how the AMOC responds to climate forcings. Because models appear to have AMOCs that are too stable, it is challenging to test both the AMOC response to a climate forcing and the climate response to an AMOC change at the same time. If a modelling group is interested in the response of the global climate to changes in the AMOC, they may be more inclined to adjust the meltwater pattern to trace the AMOC reconstruction, whereas if a modelling group is interested in the response of AMOC to a climate forcing, they may prefer to use the meltwater derived from the ice sheet reconstruction.

2.5 Conclusion

This study presents results from 17 simulations of the early part of the last deglaciation (20–15 ka BP) performed with nine different climate models. Our analyses show the first assessment of these simulations and display the similarities and differences between the model results as shown through the timing of the deglaciation, spatial and temporal surface air temperature changes, the link between the surface climate, ocean circulation, and CO_2 forcing, as well as how the different models respond to different forcings. The impact of the chosen meltwater scenario on the model output is evident in each result of this multi-model intercomparison study. The course of the deglaciation is consistent between simulations except when the freshwater forcing is above 0.1 Sv – at least 70% of the simulations agree that there is warming by 15 ka BP in most places excluding the location of meltwater input. However, for simulations with freshwater forcings that exceed 0.1 Sv from 18 ka BP, warming is delayed in the North Atlantic and surface air temperature correlations with AMOC strength are much higher. The impacts of CO_2 forcing and increasing insolation (i.e., ice sheet melt and surface temperature warming) are reduced by the large freshwater fluxes imposed, delaying the warming in the Northern Hemisphere for these simulations. Nonetheless, the average of the ensemble displays the high latitudes beginning to

deglaciate first in response to insolation and polar amplification and later warming occurring in the tropics in correlation with the rising CO_2 trajectory. The timing of the rise in CO_2 concentration differs between simulations depending on timescale of the CO_2 reconstruction, delaying warming further in the tropics for simulations with a later CO_2 increase.

Simulations run by the same model (such as those from HadCM3, MPI-ESM, and iLOVECLIM) show comparable surface climate patterns despite the use of a different ice sheet reconstruction or the *melt-routed* versus *melt-uniform* freshwater scenarios. The main differences noted during this time period include slower warming in the North Atlantic in the *melt-routed* simulations, additional temporal variability in the GLAC-1D simulations, and faster warming in the GLAC-1D simulations. Simulations run with different models, but similar boundary conditions, provide insight into the sensitivity of the model to a particular forcing. We suggest that LOVECLIM's AMOC is the most sensitive to freshwater perturbation and that CCSM3's is the least sensitive; however, this is not necessarily consistent with the sensitivity of the corresponding surface air temperature changes because of complexity in how surface air temperature is linked to AMOC and other transient climate forcings.

This multi-model intercomparison project compares simulations of different forcings to represent some of the uncertainty of the time period; however, it poses the challenge of drawing direct model-to-model conclusions. It would be ideal to be able to compare more simulations with the same experimental design to learn more about model sensitivities and test additional plausible scenarios of climate changes during the last deglaciation. Hence, this study may guide the design of future protocols for multi-model comparisons of the last deglaciation. One of these protocols could also assist with narrowing down the uncertainties regarding the meltwater paradox; for instance, the simulations that follow the *TraCE-like* meltwater scenario display larger variability in the AMOC and Greenland surface air temperature, following more closely with proxy records of the respective variables. However, to achieve this the *TraCE-like* meltwater scenarios include freshwater fluxes that are much larger than the amount deemed realistic by the ice volume change in ice sheet reconstructions of the time period. In contrast, simulations that follow the ice sheet reconstruction show less agreement with the AMOC and Greenland surface air temperature proxy records but show a more gradual warming throughout the deglaciation that has more agreement with surface temperature proxy records globally. Because meltwater input that is not realistic has such a large impact on the results, dominating over other deglacial forcings, there is difficulty comparing simulations that do and do not choose this *TraCE-like* scenario.

A protocol could assist with the design of additional experiments by outlining the use of different freshwater fluxes than modelling groups used previously. For the modelling groups that followed the PMIP4 meltwater scenarios, for example, it would be interesting to determine what 'trained' freshwater fluxes were required of their respective models to replicate the AMOC and Greenland proxy records as the *TraCE-like* groups and *MIROC* show but also with different ice sheet reconstructions. This would teach us more about the sensitivity of each model to freshwater input and the impact of the ice sheet reconstruction on the AMOC's sensitivity. Similarly, if the *TraCE-like* groups performed simulations with more realistic meltwater input, we would be

able to compare to the previous PMIP4 meltwater experiments and narrow down the impact of different deglacial forcings on the climate trajectory throughout the deglaciation. This protocol would be beneficial to the understanding of the AMOC's sensitivity to freshwater fluxes, as well as other climate forcings, such as CO_2 concentration and ice sheet configuration, and thus assisting with unravelling the current meltwater paradox.

2.6 Supplementary Information

2.6.1 Supplement to timing of the deglaciation

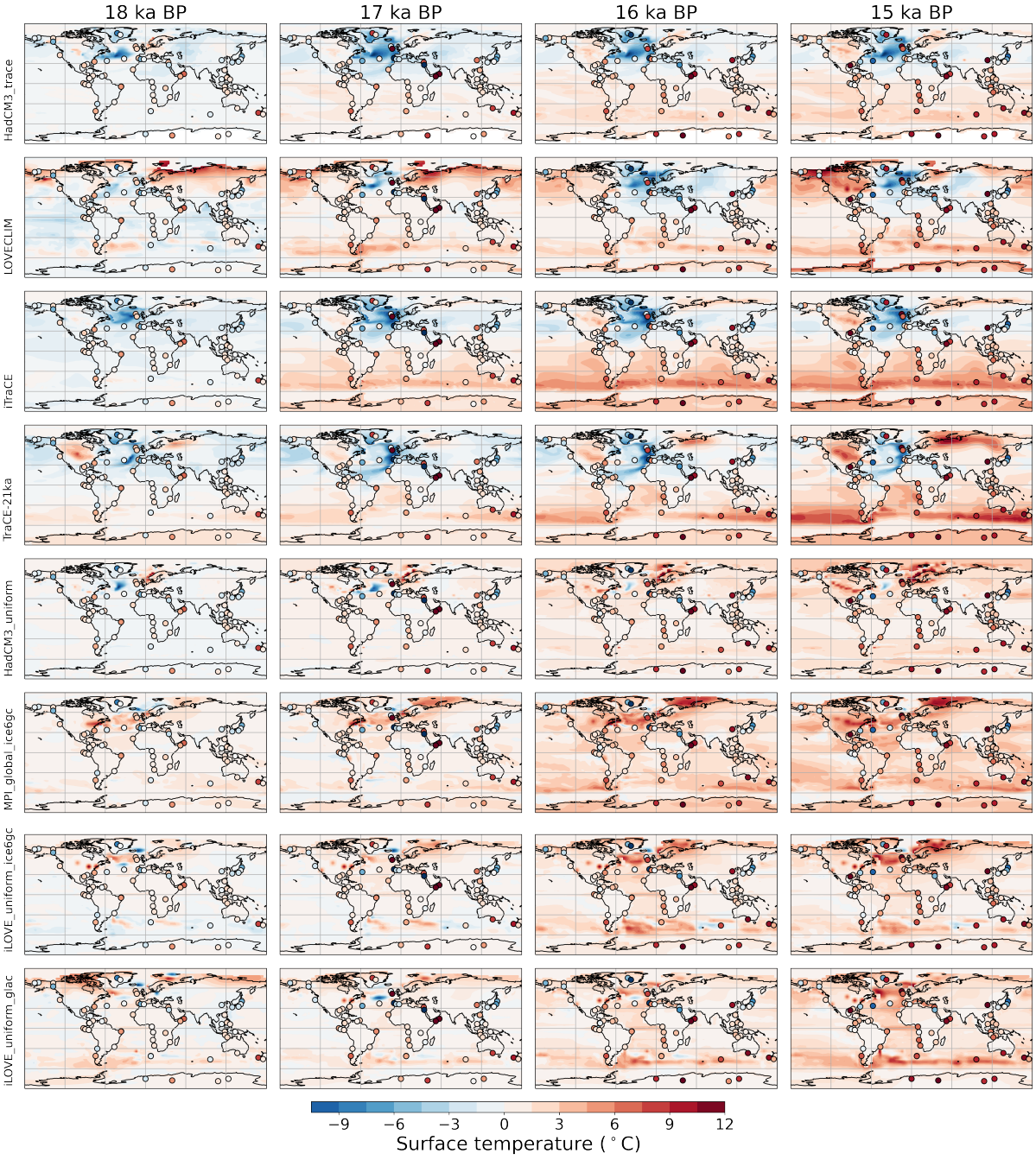

Figure 2.10: Global decadal surface temperature as anomalies from the LGM (average between 20 and 19.5 ka BP) 18, 17, 16, and 15 ka BP are calculated as 60-year decadal means centred around the respective time period (e.g., from 17.97 to 18.03 ka BP for 18 ka BP) for the *TraCE-like* and *melt-uniform* groups. The surface temperature stack by Shakun et al. (2012) as anomalies from the LGM is overlayed.

The main text shows the year of first significant warming from the LGM defined as 21 – 20.5 ka BP. For three of the simulations, *LOVECLIM*, *HadCM3_TraCE*, and *iTraCE*, we did not have the data to do this analysis. We have repeated the analysis here but with a later reference

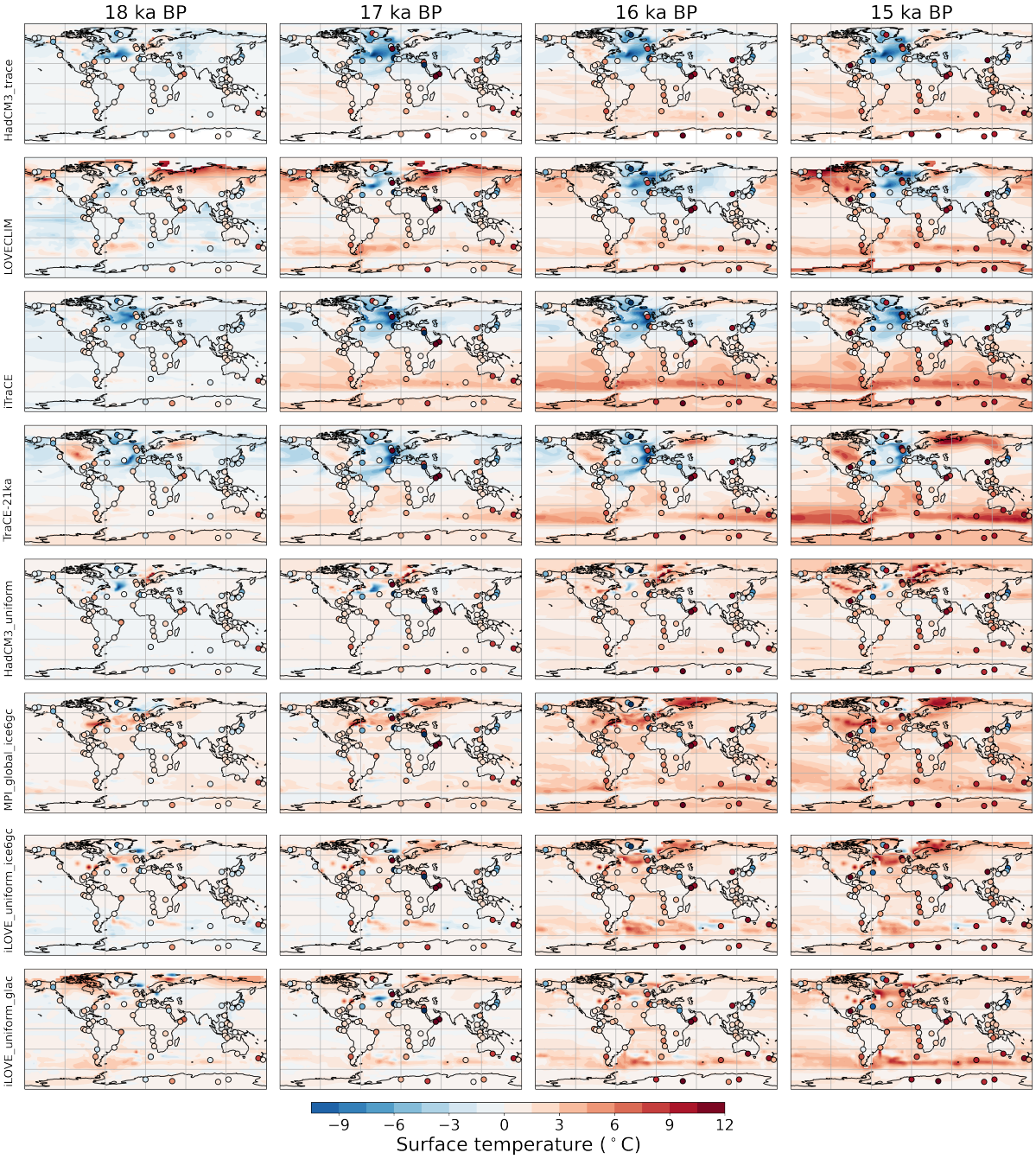

Figure 2.11: Same as Figure 2.10, but for the *melt-routed* and *bespoke* groups. Global decadal surface temperature as anomalies from the LGM (average between 20 and 19.5 ka BP). 18, 17, 16, and 15 ka BP are calculated as 60-year decadal means centred around the respective time period (e.g., from 17.97 to 18.03 ka BP for 18 ka BP). The surface temperature stack by Shakun et al. (2012) as anomalies from the LGM is overlayed.

period (20 – 19.7 ka BP). The year of first significant warming from the reference perspective of 19.7 ka BP opposed to 21 ka BP (as Figure 2.13 shows) demonstrates the impact of the large freshwater forcing the *TraCE-like* simulations use on the speed of warming during the deglaciation. Immediately coming out of the LGM, *TraCE-21ka* does warm in the north and south high latitudes (Figure 2.5). However, in the North Atlantic, the meltwater flux induces a cooling that pauses significant warming until $\tilde{1}5$ ka BP when temperatures would have increased

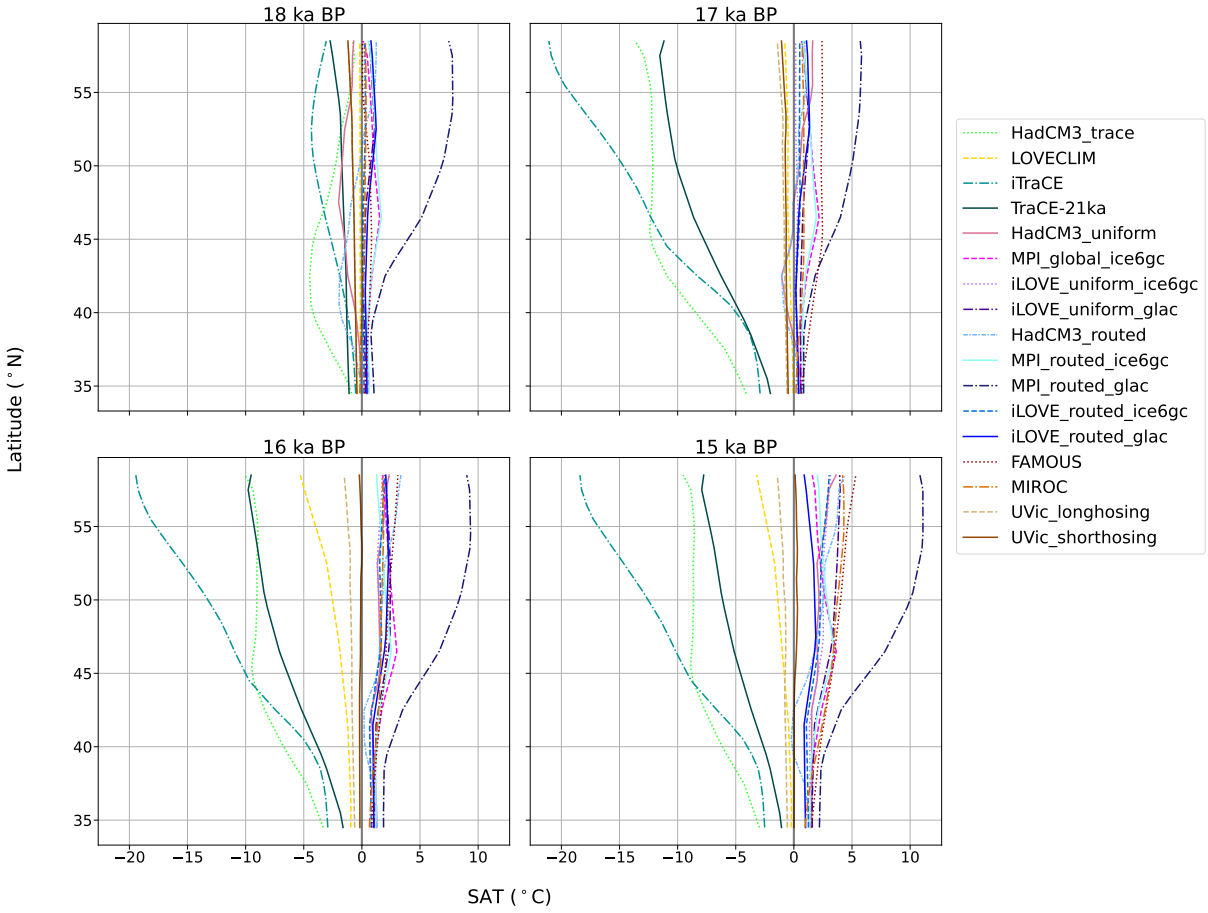

Figure 2.12: Zonal average of decadal surface air temperature across the ensemble for the North Atlantic (between 35 and 60° N and -60 and 0° E) as anomalies from the LGM (20 – 19.5 ka BP) for each simulation. 18, 17, 16, and 15 ka BP are calculated as 60-year decadal means centred around the respective time period (e.g., from 17.97 to 18.03 ka BP for 18 ka BP).

towards the Bølling Warming. This same pattern is also evident in *HadCM3_TraCE*, *LOVECLIM*, and *iTraCE* except *LOVECLIM* warms earlier in Fennoscandia and Russia than the other *TraCE-like* simulations. By 16 ka BP, the non-*TraCE-like* simulations show significant warming throughout the globe with respect to 20 – 19.5 ka BP, whereas the *TraCE-like* simulations still have the strong cooling in the North Atlantic associated with the freshwater input (Figure 2.11 and 2.13). FAMOUS also has more delayed warming in the tropics which could correspond with the later increase in CO_2 concentration. In the *TraCE-like* simulations (most evident in *HadCM3_TraCE* and T*raCE-21ka*), the earlier deglacial warming in the Southern Hemisphere and the delayed warming in the Northern Hemisphere are due to the bipolar seesaw (Broecker 1998; Stocker 1998) associated with the simulated slowdown of AMOC within Heinrich Stadial 1 (He et al. 2013). This is less evident in *LOVECLIM*, potentially because the cooling from the freshwater flux occurs later, at 17 ka BP, and therefore, significant warming has already occurred beforehand (as also evident by the zonal surface air temperature means; Figure 2.3).

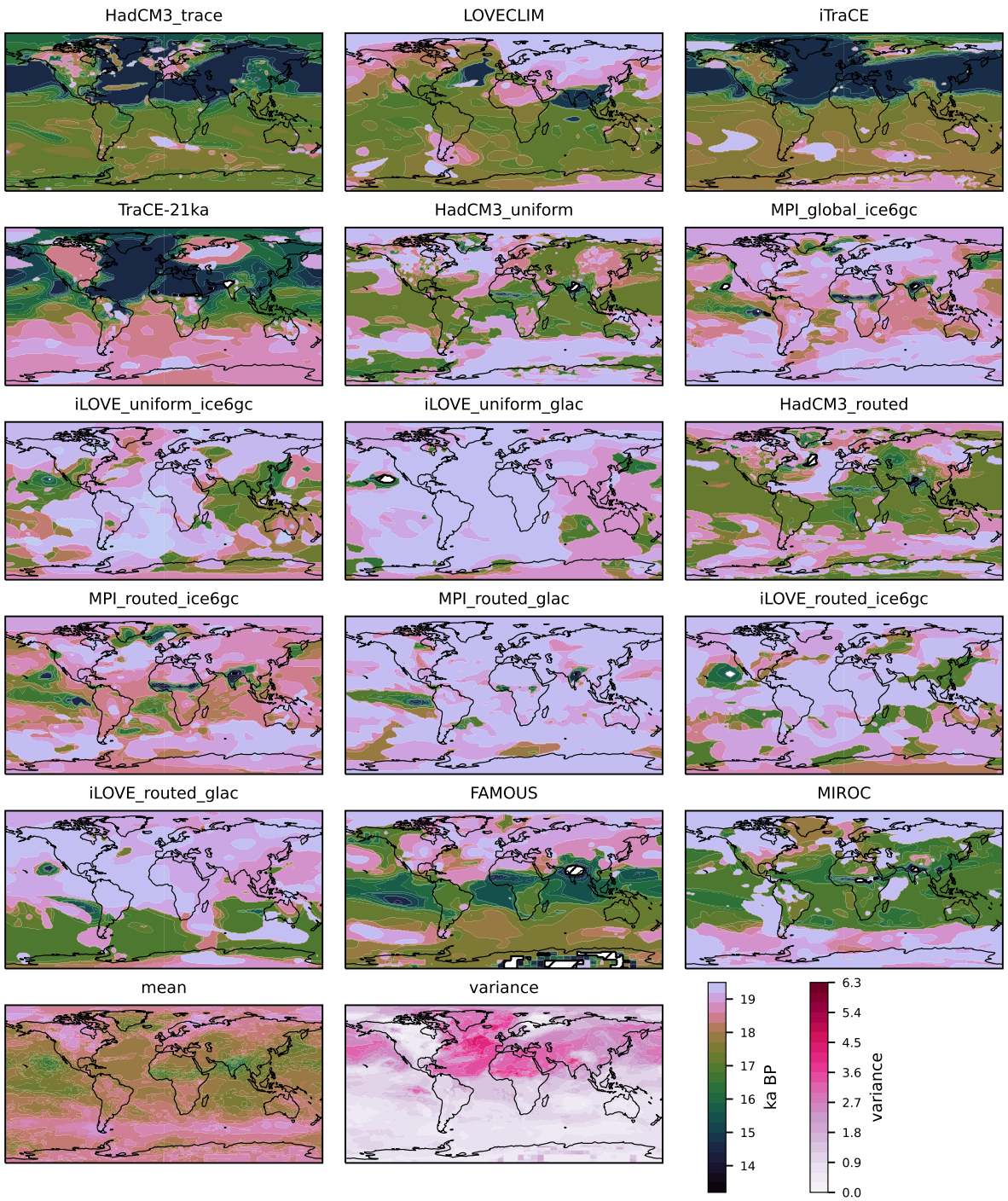

Figure 2.13: Year of first significant warming from 20 ka BP, where 'significant warming' is determined as discussed in section 2.3 but the reference period is between 20 and 19.5 ka BP instead of between 21 and 20.5 ka BP. Hatching denotes where significant warming did not occur before 13 ka BP.

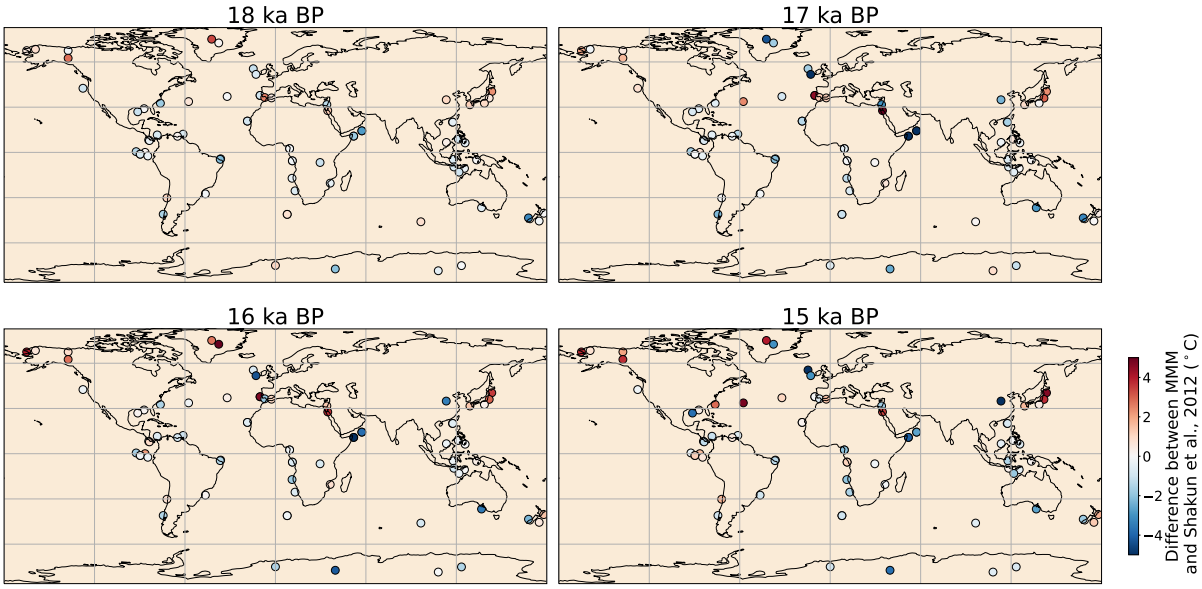

Figure 2.14: Point-by-point difference between multi-model ensemble mean surface temperature (Figure 2.4) and the surface temperature stack by (Shakun et al. 2012).

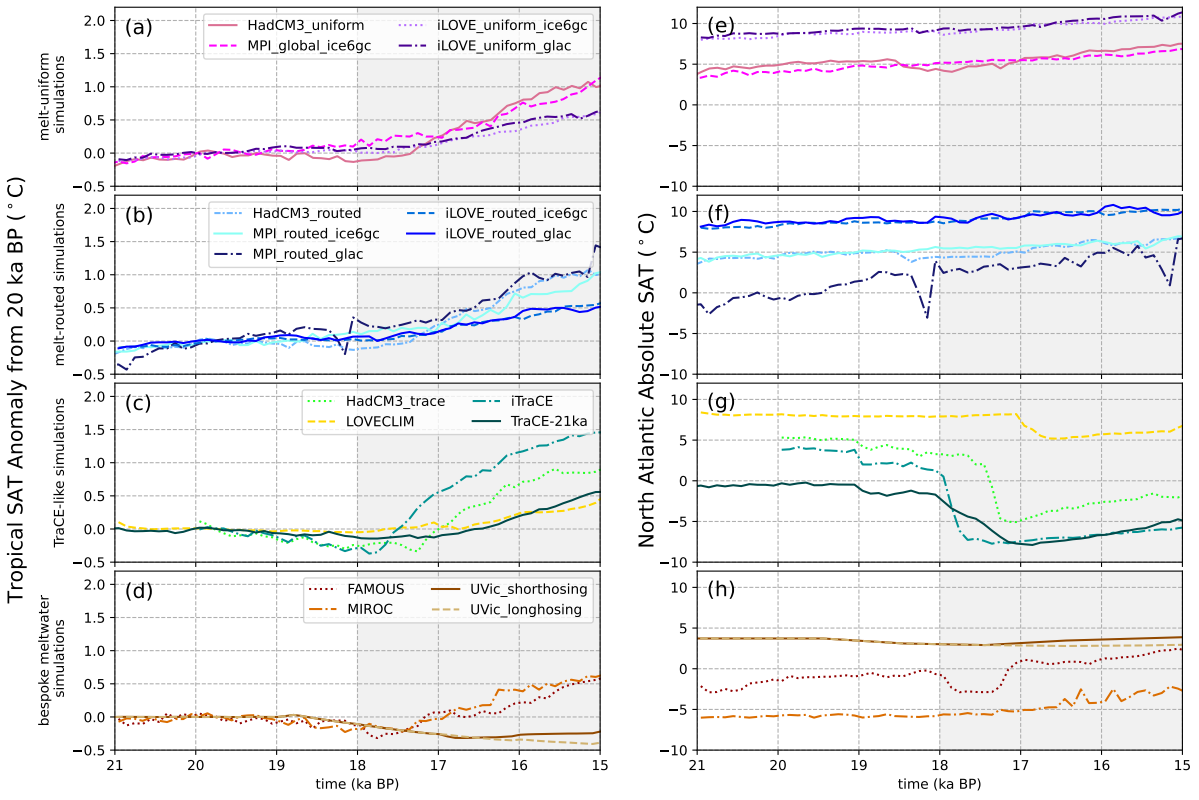

Figure 2.15: (a) – (d) Surface air temperature of the tropics (30° N to 30° S) anomaly from the LGM (20 to 19 ka BP). (e) – (h) Absolute surface air temperature of the North Atlantic region (between 35 and 60° N and -60 and 0° E) for each simulation grouped by meltwater scenario.

2.6.2 Supplement to linking surface climate, ocean circulation, and greenhouse gas forcing

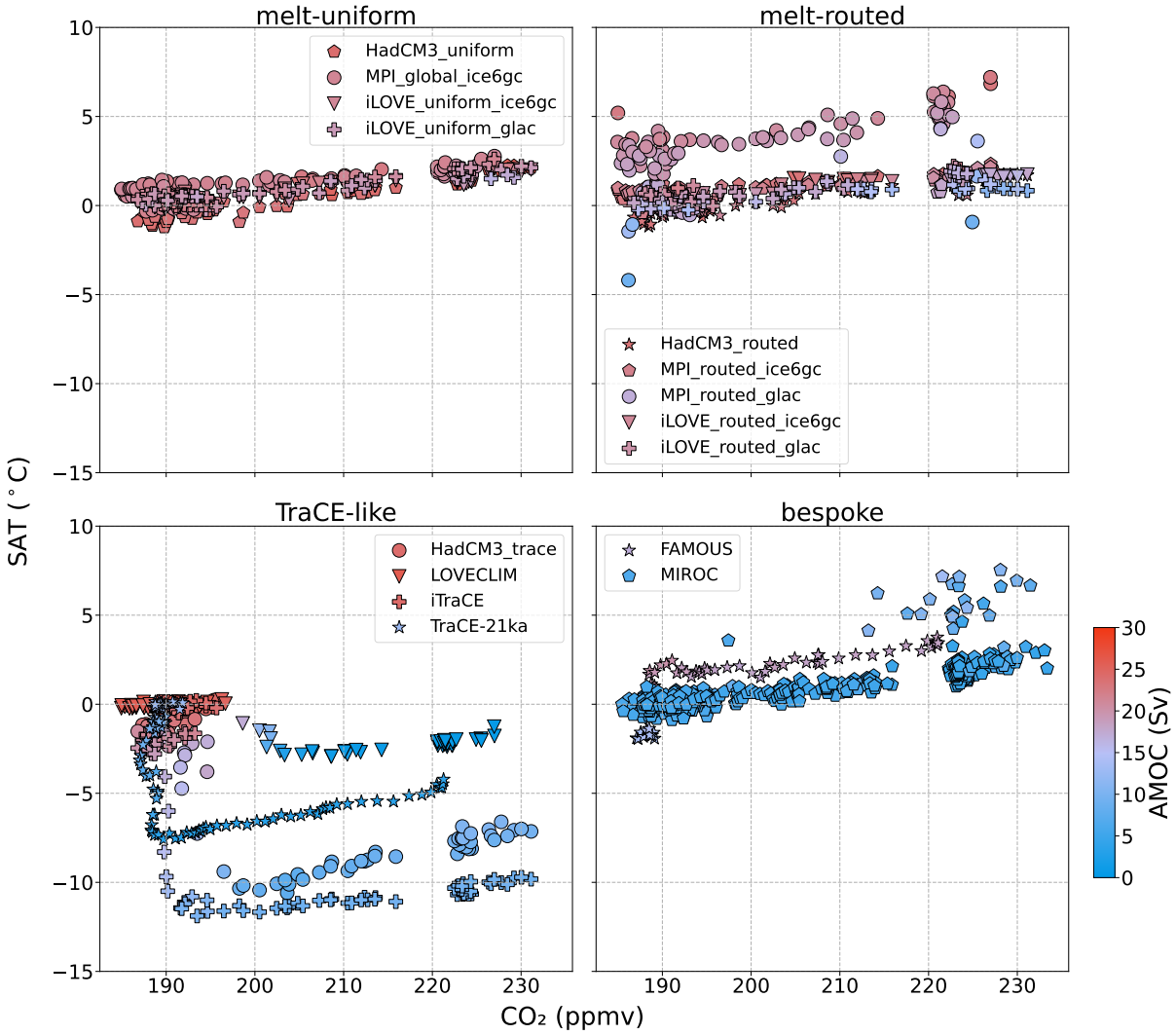

Figure 2.16: Anomalous surface air temperature from the LGM (20 – 19.5 ka BP) over the North Atlantic (between 35 and 60° N and -60 and 0° E) as a function of CO_2 concentration with symbols' shading representing the strength of the AMOC (Sv) split into groups defined by meltwater scenario. Each simulation is represented as 50-year means except for *MIROC* which is shown as decadal means to capture the smaller-scale variability.

2.6.3 Supplement to impact of different climate and ice sheet forcings and boundary conditions on model output

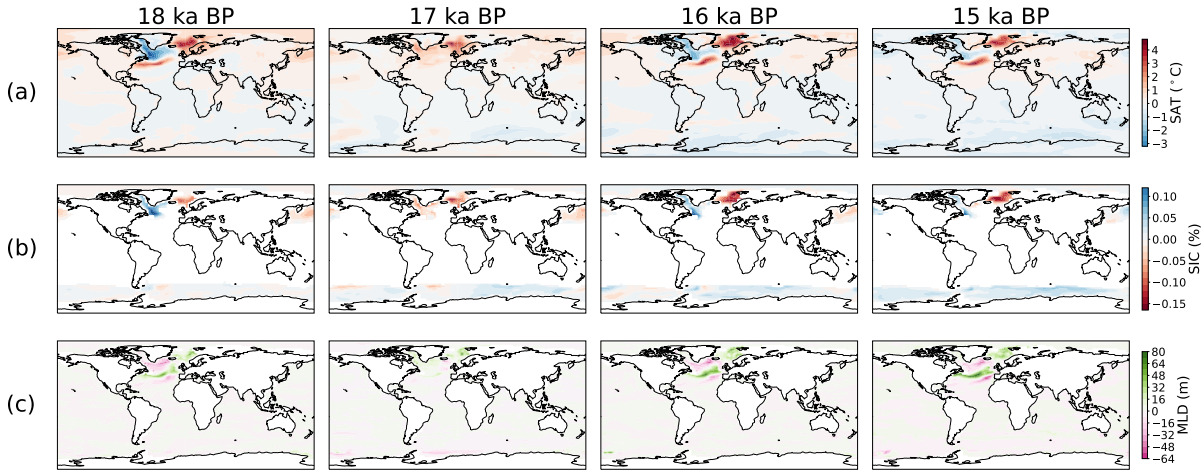

Figure 2.17: Anomaly of *HadCM3_uniform* and *HadCM3_routed* for (a) surface air temperature, (b) sea ice concentration, and (c) Mixed-layer depth (MLD). 18, 17, 16, and 15 ka BP are calculated as 60-year decadal means centred around the respective time period (e.g., from 17.97 to 18.03 ka BP for 18 ka BP).

1892

2.6.4 Supplement to sensitivity of climate models to similar forcing(s)

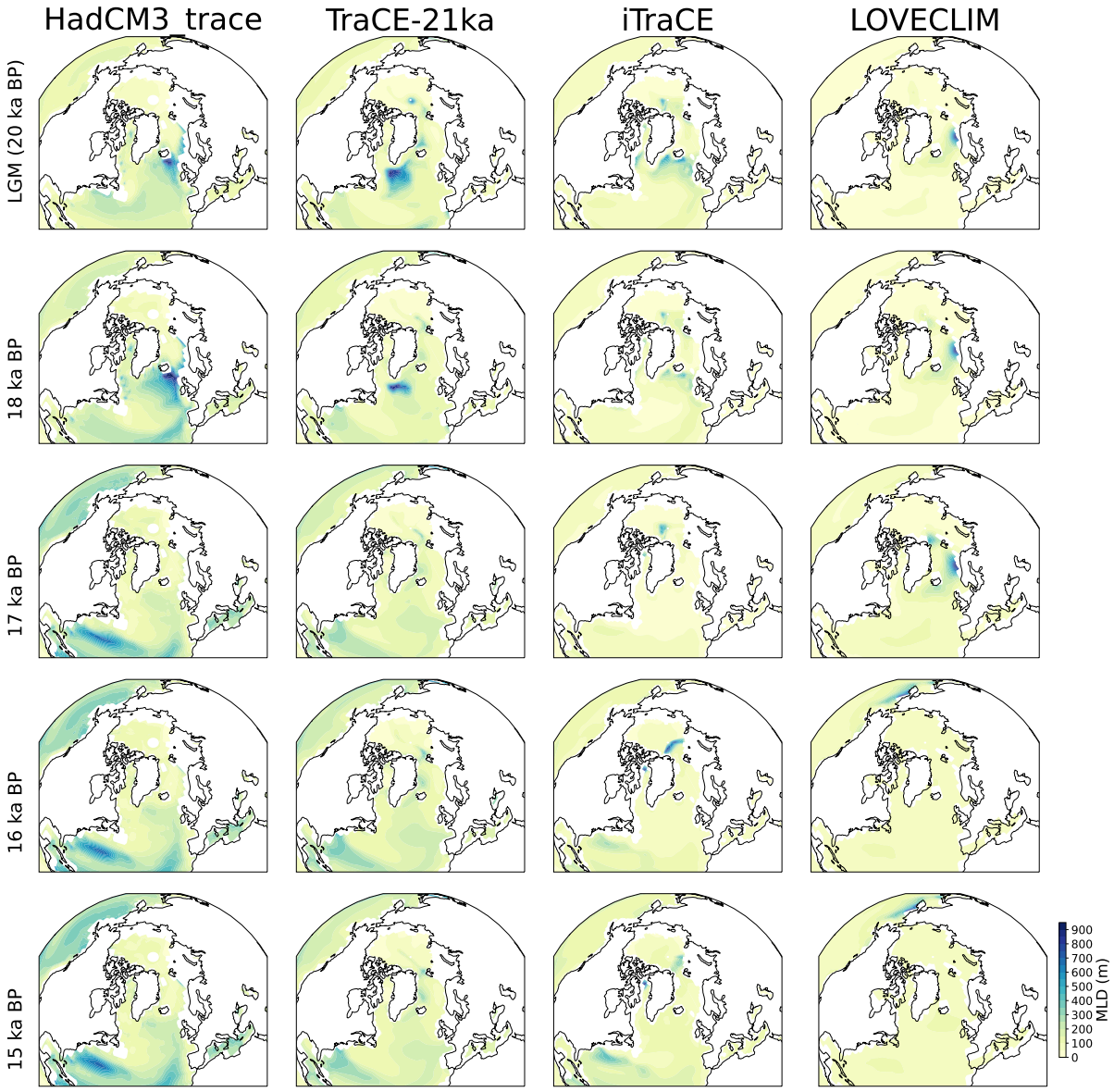

Figure 2.18: Evolution of mixed-layer depth for the *TraCE-like* simulations. 18, 17, 16, and 15 ka BP are calculated as 100-year decadal means centred around the respective time period (e.g., from 17.95 to 18.05 ka BP for 18 ka BP). The LGM is calculated as a 500-year mean between 20 and 19.5 ka BP.

Simulation Reference Name	Average depth at 19 ka BP (m)	Average depth at 16 ka BP (m)	Level of max AMOC at 19 ka BP at 26.6° N (m)	Level of max AMOC at 16 ka BP at 26.6° N (m)	Max strength in NH 19 ka BP (Sv)	Max strength in NH 16 ka BP (Sv)	Max strength at 26.6° N at 19 ka BP (Sv)	Max strength at 26.6° N at 16 ka BP (Sv)	NADW formation sites at 19 ka BP	NADW formation sites at 16 ka BP
HadCM3_TraCE	2586.5	1995.7	800.0	800.0	24.6	9.8	18.4	7.9	Southeast of Iceland/Norwegian Sea	Weak convection in Irminger Sea
TraCE-21ka	2017.9	1606.6	600.0	600.0	12.6	3.4	12.6	3.4	Irminger Sea/Labrador Sea	Weak convection in Greenland Sea
iTraCE	2500.0	2691.2	800.0	600.0	23.9	9.3	16.8	5.0	Irminger Sea	Weak convection[1]
LOVECLIM	5000.0[2]	AMOC shutdown[3]	1750.0	600.0	26.8	1.0	22.5	0.0	Norwegian Sea	NADW shut down

Table 2.2: Corresponding AMOC changes from before the abrupt decrease in Greenland surface air temperature (19 ka BP) and after the abrupt increase in meltwater (16 ka BP) for the *TraCE-like* simulations. Average depth is calculated as the average vertical reach of the upper cell of the AMOC in the water column between 25° S and 25° N (as Muglia and Schmittner (2021)). The level of max AMOC is the depth of the maximum stream function at 26.6° N (as Sigmond et al. (2020)). Max strength of the Northern Hemisphere (NH) is calculated as the maximum stream function between 500 and 3500 metres depth above 0° N. Maximum strength at 26.6° N is calculated at the same depth range, but only at 26.6° N.

[1]Convection site appears to be in Arctic Ocean (Figure 2.18) where sea ice is located, however, this is not affecting the global climate or the AMOC (Figure 2.19).
[2]Upper cell reaches the seabed (Figure 2.19).
[3]At 16.8 ka BP, depth has raised to an average of 2650.0 metres before AMOC collapses (see Figure 2.19).

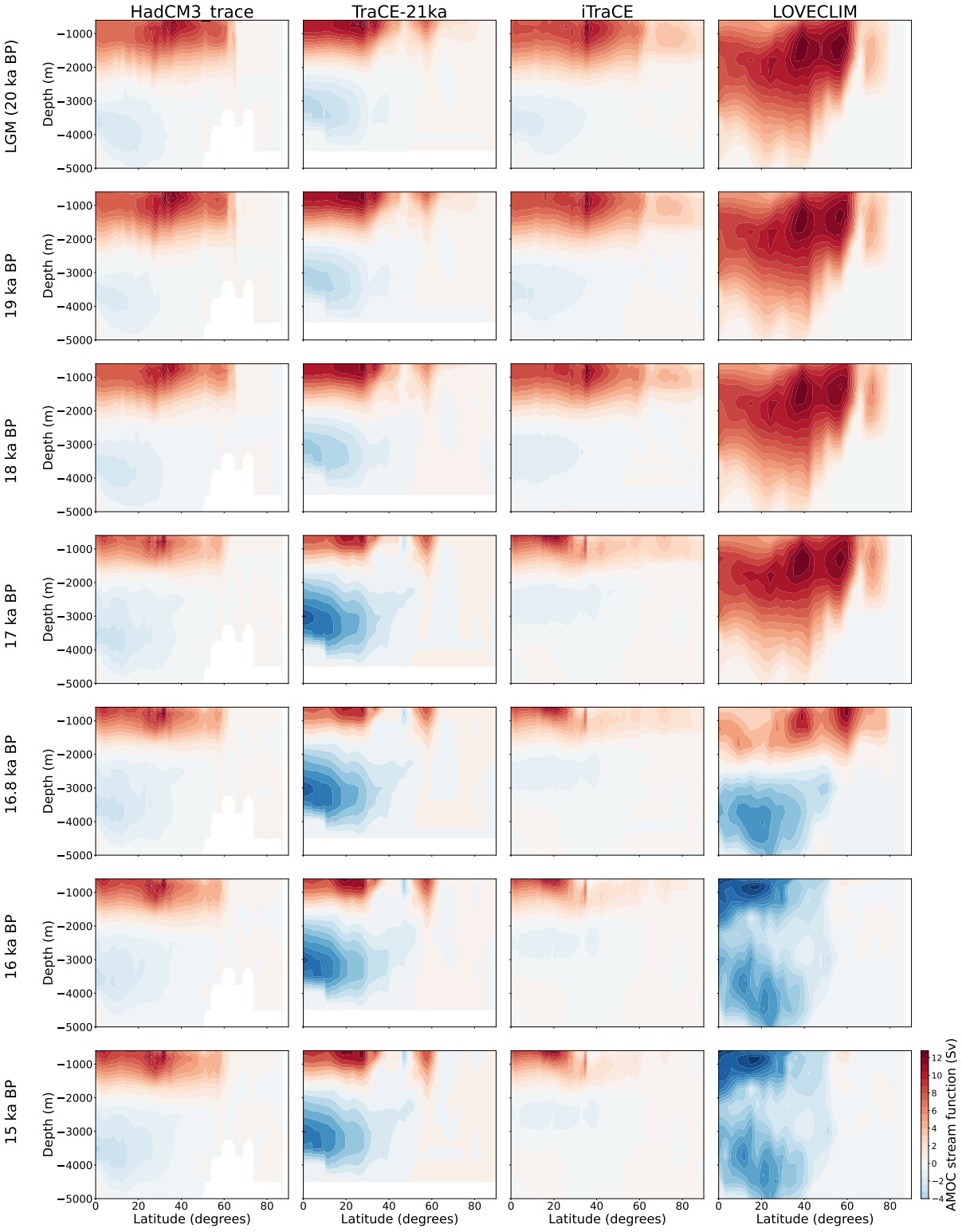

Figure 2.19: AMOC stream function evolution for the *TraCE-like* simulations in the Northern Hemisphere. 19, 18, 17, 16, 16.8, and 15 ka BP are calculated as 100-year decadal means centred around the respective time period (e.g., from 17.95 to 18.05 ka BP for 18 ka BP). The LGM is calculated as a 500-year mean between 20 and 19.5 ka BP.

CHAPTER 3

Competing effects of sea ice change control the pace and amplitude of millennial-scale climate oscillations

Preface

This chapter presents new Hadley Centre general circulation model simulations used to test the robustness of oscillations in the AMOC and contribute a new pathway to the convection-advection mechanism (Romé 2024). The content of this chapter was submitted for publication to Critical Insights in Climate Change and is in revision. Any differences are due to the editorial and examination processes of each (article and thesis respectively). It includes contributions from Ruza F. Ivanovic, Lauren J. Gregoire, Sam Sherriff-Tadano, and Yvan Romé. The study conception was developed by BS, RI, LG, and SST. BS, RI, LG, and SST contributed to the study design with YR providing additional feedback and close communication with BS. BS, RI, and LG designed the experiments, and BS performed them. Material preparation and data analysis was performed by BS. The manuscript was prepared by BS with contributions from all co-authors, who read and approved the submitted manuscript.

Abstract

Modelling groups have increasingly focused on simulating oscillatory climate behaviour, like Dansgaard-Oeschger events, observed over the last 60,000 years. Previous experiments of the Last Glacial Maximum showed unforced millennial-scale oscillations between cold and warm regimes triggered by varying ice-sheet meltwater scenarios from the early deglaciation. To understand the conditions sustaining these oscillations and triggering AMOC tipping points, we test the robustness of them under different climate forcings, such as changes in CO_2 concentration and orbital configuration. Our results show that a small CO_2 decrease weakens ocean circulation and reduces the warm-mode duration, shortening periodicity. In contrast, CO_2 increases warm the North Atlantic and suppress oscillations. Orbital changes influence seasonality and localized sea ice dynamics, shortening or lengthening glacial periods based on obliquity

variations. Sea ice plays a key role as a pacer, regulating AMOC transitions between strong (interstadial) and weak (stadial) modes. These simulations show that small climate changes can impact the shape and existence of oscillations in glacial climates, potentially explaining the variability in the periodicity and amplitude of Dansgaard-Oeschger events and transitions from glacial to interglacial states. The findings emphasize the sensitivity of the climate system to seemingly minor perturbations, offering insights into past and future climate variability.

3.1 Introduction

Modern climate change is occurring rapidly due to an unprecedented rate of atmospheric carbon dioxide rise, but abrupt climate changes, such as the warming we are currently observing, have happened before. During the Last Glacial period (∼115 to 11.7 thousand years ago; ka BP), millennial-scale variability in the form of rapid climate transitions between warm and cold regimes was observed in surface air temperature proxy records worldwide (e.g., Fletcher et al. 2010; Fritz et al. 2010; Wolff et al. 2010). The most commonly referred to example of these abrupt climate changes are Dansgaard-Oeschger (D-O) events, which were transitions of up to 10-15 °C in Greenland (Huber et al. 2006; Kindler et al. 2014; Andersen et al. 2006). D-O events are best documented during Marine Isotope Stage 3 (MIS3; between 60 and 25 ka BP; Sanchez Goñi and Harrison 2010), as observed in Greenland ice cores and more globally, including the Tropics (Deplazes et al. 2013; Adolphi et al. 2018), North and South America (Wang et al. 2004; Asmerom et al. 2010; Deplazes et al. 2013; Vanneste et al. 2015), and Eurasia (Wang et al. 2008; Rousseau et al. 2017). There were ∼25 occurrences of D-O events during the Last Glacial Period, with a periodicity of ∼1500 years (Schulz 2002; Rahmstorf 2002).

Despite decades of research on D-O events, uncertainty remains as to the underpinning mechanisms and drivers of these transitions. There is, however, a large consensus that the Atlantic Meridional Overturning Circulation (AMOC) plays a critical role in the climate transitions. The strength and structure of the AMOC is a key control on the North Atlantic and Arctic climate. When the AMOC is strong[weak], more [less] Atlantic heat is transported northwards, causing regional warming in the North Atlantic and surrounding land masses (Rahmstorf 2002). AMOC strength is dependent on the stratification of the water layer in the main convection sites in the North Atlantic (i.e., the Labrador Sea, Irminger Sea, and the Greenland, Iceland, and Norwegian Seas (or GIN Seas); Lynch-Stieglitz et al. 2007; McCarthy et al. 2017).

Previous studies have shown that the AMOC responds to freshwater input into the North Atlantic from melting icebergs and ice sheets; for example, if freshwater is discharged into the critical sites of ocean convection, the circulation strength can be disrupted (Rahmstorf 1999; Smith and Gregory 2009; Roche et al. 2010). D-O events were originally thought to be driven by the melting of armadas of icebergs released during Heinrich events (Hemming 2004; Heinrich 1988). Although this has since been refuted, at least in some cases (Barker et al. 2015), there may at least have been an iceberg-meltwater feedback to the stadial mode (Ivanovic et al. 2018a). In any case, significant meltwater was also released from the long-term melt of ice sheets during the Last Glacial period (Gregoire et al. 2012), and may be a contender for the triggering of at least some AMOC tipping points.

The impact of 'background' ice sheet melt on the climate has been investigated by multiple studies (e.g., Snoll et al. 2022; Kapsch et al. 2022; Ivanovic et al. 2018a; Matero et al. 2017). However, the sensitivity of the North Atlantic Ocean to freshwater fluxes is poorly constrained, and there is even less agreement about how the AMOC responds to atmospheric climate forcings (Toggweiler and Russell 2008; Zhu et al. 2015). Modelling groups have begun to investigate what conditions are required for oscillatory behaviour in the AMOC in their respective models. This has become more and more successful in recent years (e.g., Sherriff-Tadano and Abe-Ouchi 2020; Romé et al. 2022, and experiments referenced by Malmierca-Vallet et al., 2023) under a wide range of parameter values, boundary conditions, and forcings, including pre-industrial or present-day conditions (e.g., Klockmann et al. 2018; Drijfhout et al. 2013; Martin et al. 2015), glacial (Last Glacial Maximum) conditions (e.g., Peltier and Vettoretti 2014; Kuniyoshi et al. 2022; Romé et al. 2022) and MIS3 conditions (e.g., Armstrong et al. 2022; Zhang et al. 2021). Background climate and initial ocean state are thought to be important for how responsive ocean circulation is to a meltwater flux (e.g., whether AMOC is already strong and deep or weak and shallow; Bitz et al. 2007; Schmittner and Lund 2014; Dome Fuji Ice Core Project Members: et al. 2017; Pöppelmeier et al. 2023b); therefore, the choice of a model's boundary conditions in the palaeo setting (e.g., ice sheet geometry, atmospheric trace gas concentrations, or orbital parametres) can influence the ocean's sensitivity to freshwater perturbation.

Barker and Knorr (2021) infer from geological records that some combinations of background conditions (trace gases, orbital forcing, ice sheet geometries, ocean gateways, etc.) create optimal environments for triggering millennial-scale climate variability, affecting their frequency and/or amplitude. More specifically, such 'windows of opportunity' are thought to exist when both ice volume and atmospheric CO_2 concentrations are at levels mid-way between full glacial and warm interglacial. For instance, when the background climate is mid-glacial, CO_2 concentrations are not high enough to make the AMOC monostable and strong (Zhang et al. 2017; Klockmann et al. 2018), and the ice sheets are not so large that they make the AMOC monostable and weak (Zhang et al. 2017). Thus, the climate may exist in a 'window of opportunity' during D-O events, which occur during glacial periods with ice sheets are smaller than at glacial maxima, or may move through a 'window of opportunity' during periods of deglaciation, when ice sheets are melting away and atmospheric CO_2 is rising. This is consistent with the proposition that the AMOC can remain 'bistable'. This 'window of bistability' can also move with respect to one variable–e.g., CO_2–with dependence on another–e.g., ice sheet meltwater–(Obase and Abe-Ouchi 2019). Climate models are useful for validating the 'window of opportunity' hypothesis, although the simulated windows may be model dependent. Most helpfully, models can be used to understand the underlying mechanisms that explain why a specific climate state is more or less susceptible to abrupt change, which may have broader significance beyond the specific model structure and inputs.

Multiple modelling groups have tested the impact of atmospheric CO_2 and orbital forcings over the course of the deglaciation and the occurrence of abrupt climate changes (i.e., results shown by Oka et al. (2012), Brown and Galbraith (2016), Klockmann et al. (2016), Klockmann et al. (2018), Zhang et al. (2017), Zhang et al. (2021), and Sherriff-Tadano et al. (2018)), as

well as potentially modulating the sensitivity of the AMOC to freshwater fluxes (Obase and Abe-Ouchi 2019; Sun et al. 2022; Sherriff-Tadano et al. 2021). Sun et al. (2022) demonstrated that a weak AMOC is more likely to recover (such as a transition from a stadial D-O-like state to an interstadial state) with a higher atmospheric CO_2 concentration. This coincides with the findings of Brown and Galbraith (2016), Klockmann et al. (2018), and Vettoretti et al. (2022), who only successfully produced oscillatory behaviour under a specific range of CO_2 concentrations. Using a general circulation model (MPI-ESM), Klockmann et al. (2018) achieve oscillations with pre-industrial ice sheets and a range of CO_2 concentrations between 195 and 217 ppm. Interestingly, Malmierca-Vallet et al. (2024) show that three general circulation models (HadCM3, MPI-ESM, and CCSM4) produce oscillations within the atmospheric CO_2 window between 185 and 230 ppm, matching the range under which D-O events occurred during MIS3.

In addition, changes in Earth's orbit are known to drive glacial terminations throughout at least the last 800,000 years (Jouzel et al. 2007; Gregoire et al. 2015). Multiple studies have demonstrated that changes in orbital configuration (more specifically obliquity and precession) can impact millennial-scale climate variability (Yin et al. 2021; Kuniyoshi et al. 2022; Zhang et al. 2021; Erb et al. 2013) and the periodicity of oscillations (Brown and Galbraith 2016; Kuniyoshi et al. 2022). Brown and Galbraith (2016) display simulations with pre-industrial ice sheets and lower obliquity that achieve oscillations between two AMOC modes. An experiment with precession at 90°(representing weak boreal seasonality) resolved to longer oscillations with a periodicity of ∼1200 years, whereas the experiment with precession at 270°(representing strong boreal seasonality) remained with very quick oscillations between the AMOC states. These oscillations did not occur under higher obliquity regardless of the precession. Similarly, Kuniyoshi et al. (2022) use a coupled atmosphere-ocean general circulation model, MIROC, to find that stronger boreal seasonality, shortens periodicity in AMOC oscillations. Unlike Brown and Galbraith (2016), however, Kuniyoshi et al. (2022) were able to achieve self-sustained oscillations with glacial ice sheets (based on the ICE-5G ice sheet reconstruction; Peltier 2004).

The results from the studies with stadial-interstadial-like climate oscillations show how model-dependent the 'window of opportunity' is. For example, where Klockmann et al. (2018) cannot produce climate oscillations under glacial conditions, Peltier and Vettoretti (2014) can. The oscillations presented by Romé et al. (2022) are triggered by meltwater fluxes, whereas Kuniyoshi et al. (2022) do not use freshwater forcing to obtain their oscillations. There are instances of quasi-consistency between models, for example, where oscillatory behaviour occurs within a similar range of atmospheric CO_2 concentration, although other boundary and background climate conditions are significantly different (Malmierca-Vallet et al. 2024). However, across models and climate experiments, the characteristics of stadial-interstadial climate oscillations vary considerably (see simulations listed by Malmierca-Vallet et al. (2023)). Not only do simulated oscillations not always have comparable amplitudes and periodicities, is it also uncertain whether they are even governed by the same mechanism; as highlighted by Malmierca-Vallet et al. (2023), the precise controls on the oscillations are hard to identify.

Previous mechanistic studies have focused on the role of the AMOC and the impact of temperature and salinity have on stratification in deep water formation sites. Li et al. (2010), Dokken

et al. (2013), Li and Born (2019), and Vettoretti and Peltier (2018), e.g., demonstrate the control of sea ice in the GIN seas on the transition between cold and warm phases. Vettoretti et al. (2022) show with Last Glacial Maximum simulations that Arctic and North Atlantic sea ice governs the duration of the warm and cold regimes. Advection of sea ice into AMOC convection sites in the North Atlantic increases stratification and forces the end to the warm regime, whereas the cold regime is terminated by ocean heat loss in the same region. When in a cold regime, sea ice concentration increases, insulating the surface ocean. Eventually, this leads to the warmer waters melting the sea ice above it, starting the transition to interstadial conditions (Dokken et al. 2013). Other research groups have looked deeper into the control of sea ice on salinity in oscillations (e.g., Cheng et al. 2018; Armstrong et al. 2022; Peltier and Vettoretti 2014). Armstrong et al. (2022) demonstrate how the seasonal nature of sea ice can impact the salinity content of the subpolar gyre. During the warm regime, freshening is reduced in the subpolar gyre increasing salinity, whereas during the cold regime, sea ice freshening dominates in the region, weakening convection. While hypotheses are emerging on the mechanisms causing AMOC oscillations and abrupt changes, there is not yet an understanding of how D-O mechanisms are influenced by orbital and CO_2 forcings.

In this study, we investigate how and why the characteristics of oscillations simulated by Romé et al. (2022) (henceforth referred to as *Romé22*) are affected by different greenhouse gas concentrations and orbital configurations. These simulations come from one of four studies, to our knowledge, that have successfully modelled AMOC oscillations under glacial climate conditions (Peltier and Vettoretti 2014; Kuniyoshi et al. 2022; Romé et al. 2022; Vettoretti et al. 2022). Specifically, *Romé22* follow the PMIP4 Last Glacial Maximum experiment (including 21 ka BP orbit, 190 ppm atmospheric pCO_2; Kageyama et al. 2017) with the GLAC-1D ice sheet reconstruction (Ivanovic et al. 2016; Tarasov et al. 2012; Tarasov and Peltier 2002; Briggs et al. 2014) and associated boundary conditions. Crucially, on top of the PMIP4 protocol, the simulations include fixed patterns and amplitudes of meltwater inputs, derived from the early deglacial GLAC-1D meltwater history. Some of those meltwater scenarios, which are constant in time, cause millennial scale oscillations between strong and shallow glacial AMOC modes, and a near-to or completely collapsed AMOC. Greenland surface temperatures cool and warm ∼10 °C with a periodicity of about 1,500 years. Romé et al. (2025) identify a precise explanation for the *Romé22* oscillatory behaviour. The so-called convection-advection oscillator mechanism incorporates fast North Atlantic ocean buoyancy changes as the convection component and slow reorganisation of global salinity as the advection component. The detailed description facilitates easier comparison to previous studies, allowing us to explore how changes in climate forcings affect the dynamics of D-O events.

We test how the convection-advection mechanism is affected by perturbations in the background CO_2 and orbit, by selecting one of the oscillating simulations from *Romé22* and altering atmospheric CO_2 concentration and orbital configuration. We present the results of the CO_2 and orbit changes (section 3.3.2 and 3.3.3) and discuss the corresponding impact on the convection-advection mechanism (section 3.4.1). We further explore the implications on AMOC stability (section 3.4.3) and relevance to glacial termination (section 3.4.4).

3.2 Methods

3.2.1 Model description

We used the Hadley Centre Coupled Model version 3 (HadCM3), a coupled ocean-atmosphere-vegetation general circulation model (Gordon et al. 2000; Pope et al. 2000) with minor modifications described by Valdes et al. (2017). HadCM3 has an atmospheric resolution of 2.5° latitude by 3.75° longitude with 19 vertical levels starting at the surface and ending at 10 hPa. The ocean's horizontal resolution is 1.25° by 1.25° with 20 vertical layers from the surface of the ocean to ∼5500 m deep with maximum resolution at the surface. The ocean volume stays constant throughout the simulations. Vegetation is represented by the dynamic vegetation model TRIFFID (Top-down Representation of Interactive Foliage and Flora Including Dynamics) coupled to the atmospheric general circulation model and linked to the land surface with MOSES 2.1 (or the Met Office Surface Exchange Scheme). See 3.6.1 for a discussion of how HadCM3 performs for sea ice and convection sites compared to modern observations.

3.2.2 Experimental design

Glacial simulations were run with Last Glacial Maximum boundary conditions following the PMIP4 protocol for 21 ka BP (Kageyama et al. 2017) using the GLAC-1D ice sheet reconstruction (Ivanovic et al. 2016; Tarasov et al. 2012; Tarasov and Peltier 2002; Briggs et al. 2014). All simulations were initialised from *Romé22*'s Last Glacial Maximum control simulation, which has no meltwater. The Last Glacial Maximum control simulation was initiated from a previous set of HadCM3 Last Glacial Maximum simulations with PMIP3 conditions (i.e., 190 ppm atmospheric pCO_2, 21 ka BP orbital configuration, and a Last Glacial Maximum ice sheet; Davies-Barnard et al. 2017). It was then spun-up for 3,500 years with the PMIP4 Last Glacial Maximum conditions, and then run for an additional 4,000 years for comparison to the other simulations run by *Romé22*. We began our simulations from year 1,000 of the additional 4,000 years.

Romé22 derived a transient meltwater history from GLAC-1D's reconstruction of the last deglaciation global ice sheet evolution, and then selected six different meltwater 'snapshots' from fixed points in time along this transient meltwater history. The total amount of salt is content is also fixed throughout the simulation by salt correction. We have selected their 20.7 ka BP snapshot simulation to further investigate. This simulation has consistent oscillations and a relatively uniform distribution of meltwater forcing in the Arctic, GIN seas, and Western North America. We refer to *Romé22*'s simulation as *20.7k_Rome22*.

The *REF* simulation in this study was performed with the same boundary conditions as *20.7k_Rome22* (see Table 3.1) and was used to test the consistency of our results with those of *Romé22*. We then performed six further simulations with the same meltwater forcing and palaeogeography (including ice sheets) to assess how sensitive our oscillations are to small and large changes in atmospheric CO_2 and orbital parametres (Table 3.1). Three simulations test changes in atmospheric CO_2 concentration–specifically a 10 ppm decrease (180 ppm), a 10 ppm increase (200 ppm), and a 20 ppm increase (210 ppm)–keeping the orbital configuration con-

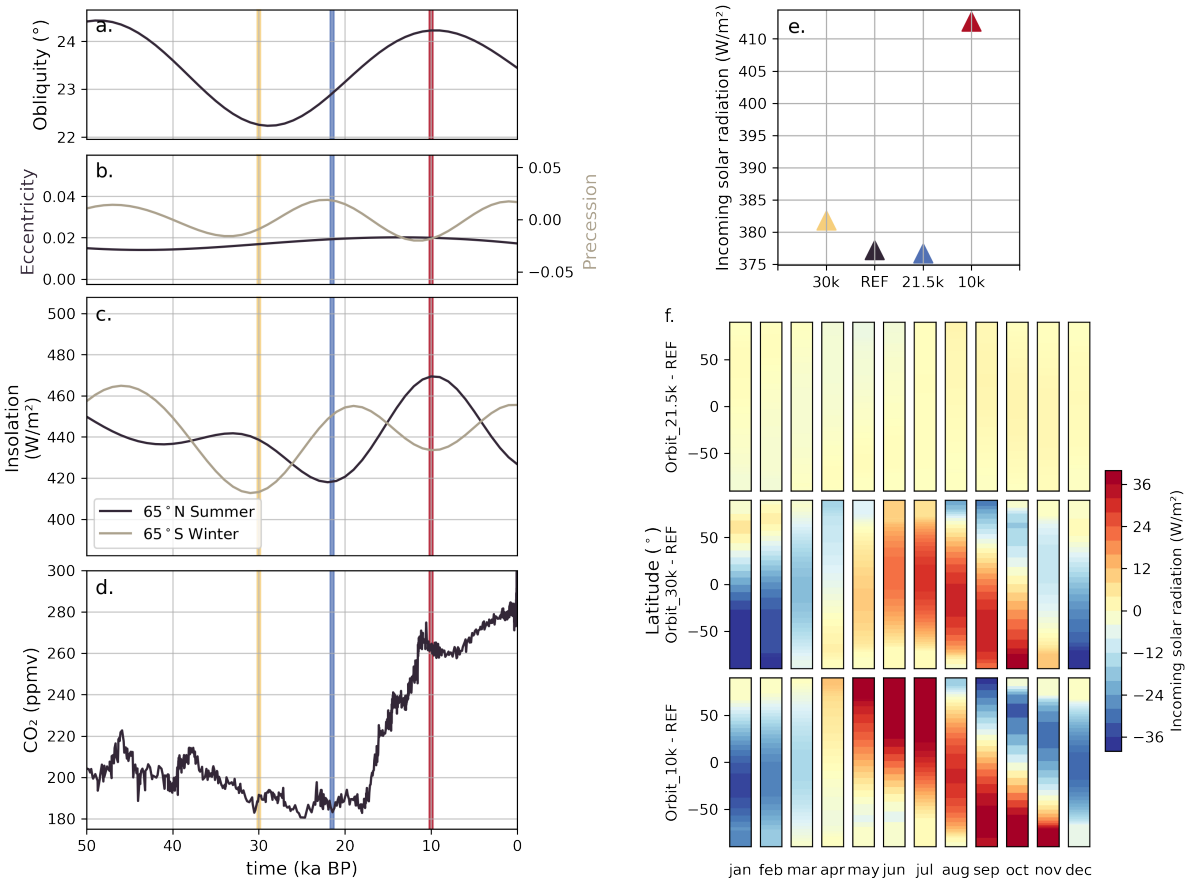

Figure 3.1: (a) - (b) Earth's orbital variation and (c) the impact on incoming solar radiation at the top of the atmosphere throughout the last 50 thousand years (Berger 1978). The last 150 thousand years is in the supplementary information (Figure 3.14). (d) Atmospheric CO_2 concentration throughout the last 50 thousand years (Köhler et al. 2017). (e) Quantification of boreal seasonality strength, calculated as the anomaly between median June-July-August incoming solar radiation and median December-January-February solar radiation, for the experiments testing orbital parameter changes and *REF*. (f) Incoming solar radiation anomalies from *REF* for each latitude in each month of the year.

sistent with *REF*. These CO_2 concentrations represent high and low concentrations between 50 and 20 ka BP (Figure 3.1d), and happen to fall roughly within the 'window of opportunity' for climate oscillations identified by Malmierca-Vallet et al. (2024) in a different set of simulations performed with HadCM3, CCSM4, and MPI-ESM. The other three simulations test the influence of changes in Earth's orbit, using triads of obliquity, precession, and eccentricity parametres corresponding to 30, 21.5, and 10 ka BP, but keeping atmospheric CO_2 concentration consistent with *REF*. Conditions at 30 ka BP are closest to MIS3, when D-O events were prevalent. We use 21.5 ka BP to investigate the impact of a small 500-year shift in time from the 21.0 ka orbit of *REF*. The 10 ka BP period was selected to explore how a high boreal seasonality and higher level of summer insolation at 65° N, the latitude of much Northern Hemisphere ice, would impact our oscillations. Thus, in each simulation, all initial and boundary conditions remained the same as in *REF* and *20.7k_Rome22* except for the condition tested (i.e., either atmospheric CO_2 concentration or orbital configuration year; Table 3.1). To test the impact of stochastic

variability on the oscillations, two simulations were repeated without making any changes–the *REF* simulation and *Orbit_21.5k*. They are labelled *REF2* and *Orbit_21.5k2* respectively (see Table 3.1). An analysis of their differences are described in section 3.4.2.

Simulation	Atmospheric CO_2 (ppm)	Orbital configuration year (ka BP)	Integration length (years)
20.7k_Rome22	190	21	10,000
REF	190	21	6,000
CO_2_180ppm	180	21	6,000
CO_2_200ppm	200	21	6,000
CO_2_210ppm	210	21	6,000
Orbit_10k	190	10	6,000
Orbit_21.5k	190	21.5	6,000
Orbit_30k	190	30	6,000
REF2	190	21	6,000
Orbit_21.5k2	190	21.5	6,000

Table 3.1: Table of simulations, showing the differences in boundary conditions and integration length. All other aspects of model configuration are identical across the experiments. See the supplementary information for a timeline of the experiments included in this study and who generated them (Figure 3.13)

3.2.3 Defining AMOC modes

For this analysis, we describe the simulations in terms of their AMOC modes (as described by *Romé22*). We prefer the use of warm and cold regimes to the stadial and interstadial terminology following the justification given by Romé et al. (2022). AMOC is defined as the maximum of the Atlantic-basin meridional streamfunction at 26.5° N. The definition of specific geographical regions is demonstrated by the maps in Figure 3.4e and 3.6f.

In our oscillatory cycles, there is one *cold* mode, where ocean convection in the high latitudes is weak, and two *warm* modes, a *meridional* and a *zonal* mode. In the *meridional* mode, the Greenland, Iceland, and Norwegian Seas (GIN) seas are the dominant location for convection (Figure 3.2), whilst the Irminger Sea shows weaker convection. During the *zonal* mode, the opposite occurs, with the strongest convection in the Irminger Sea and weak convection occurs in the GIN seas. After the initial descent into a *cold* mode during an oscillatory cycle, the AMOC recovers, moving the cycle into its first warm mode, the *meridional* mode. The ocean circulation strength then slightly decreases and, moving into its second warm phase, AMOC switches to the *zonal* mode, before transitioning back towards its *cold* mode and restarting the cold phase of the cycle. This oscillatory cycle takes about 1,540 years (see *Romé22* for more detail).

Simulations *CO_2_180ppm*, *Orbit_21.5k*, and *Orbit_30k* follow the full oscillatory cycle, moving AMOC through all three of its modes, and we thus use the *cold-meridional-zonal* terminology when referring to these simulations. The *CO_2_200ppm*, *CO_2_210ppm*, and *Orbit_10k* simulations do not pass through all three AMOC modes, and thus the different phases of those simulations are categorised more simply as having a 'strong' or *relatively* 'weak', or 'moderate', AMOC

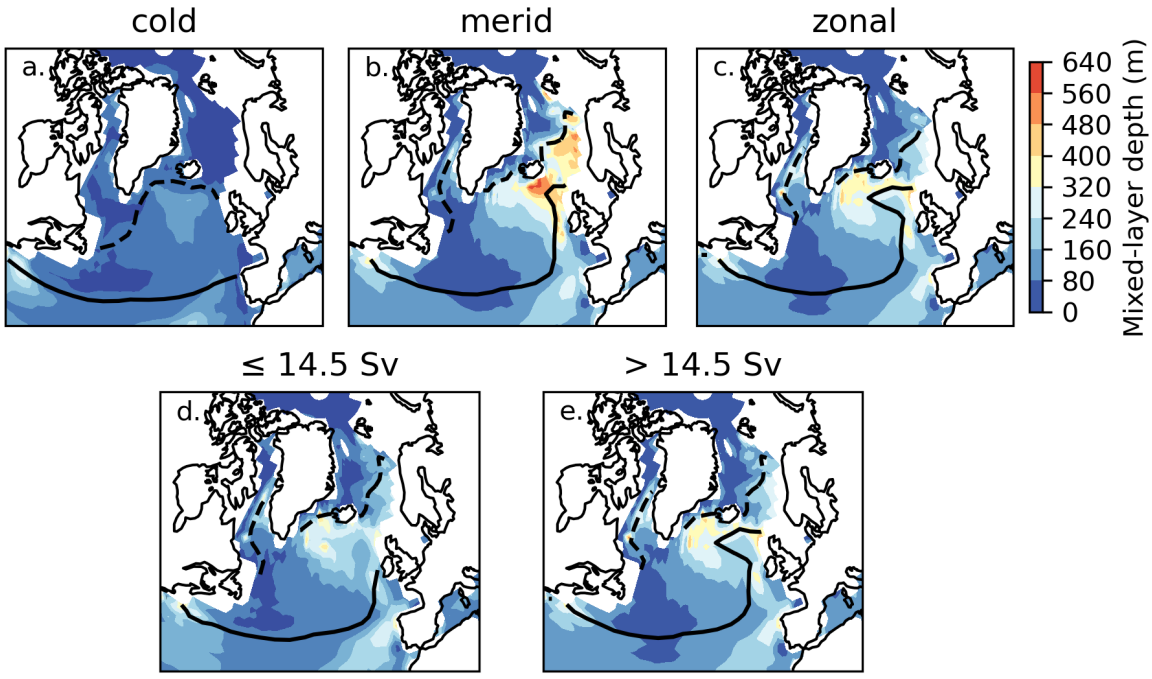

Figure 3.2: [Mixed-layer depth during each convection mode] (a-c) December-January-February mixed-layer depth for *REF* averaged over each of the convection modes – *cold*, *meridional* (*merid*), and *zonal*. (d-e) As (a-c), but with *Orbit_10k* representing the state of convection when the AMOC is less than or equal to 14.5 Sv or in the 'moderate' mode (d) and when the AMOC is greater than 14.5 Sv or in the 'strong' mode (e).

mode. In these instances, the *strong* AMOC mode is identified when maximum AMOC strength exceeds 14.5 Sverdrup (Sv; 1 Sv is equal to 1 million cubic metres per second), and the *moderate* mode has an AMOC strength equal to or weaker than 14.5 Sv. Note, however, that we use the term *moderate* because the AMOC never drops below 10 Sv for *CO_2_200ppm*, *CO_2_210ppm*, and *Orbit_10k*. When the simulations are compared to *REF*, *REF* is defined by the corresponding definition. For example, when *REF* is compared to *CO_2_180ppm* the *cold*, *meridional*, and *zonal* definitions are used. Whereas if *REF* is compared to *Orbit_10k* the *strong* (greater than 14.5 Sv) and the *moderate* (less than or equal to 14.5 Sv) definitions are used.

To create composite descriptions of the different modes in a simulation, the initial 1,000 years are excluded to remove the early spin-up period when the AMOC is adjusting to changes in climate forcing. Periodicity is defined by the average sum of the duration of each mode. We use the term 'state' when referring to a time window in the evolution of a simulation and use the term 'phase' when that time window is part of a cycle.

3.3 Results

Six new sensitivity experiments are presented here to understand the impact of CO_2 and orbital configuration on oscillatory-like behaviour in our simulations (Figure 3.3). In all simulations, there is an initial spin-up period where the climate system adjusts to the updated climate forcings. This is evident in the sharp decrease in AMOC strength and Greenland surface air

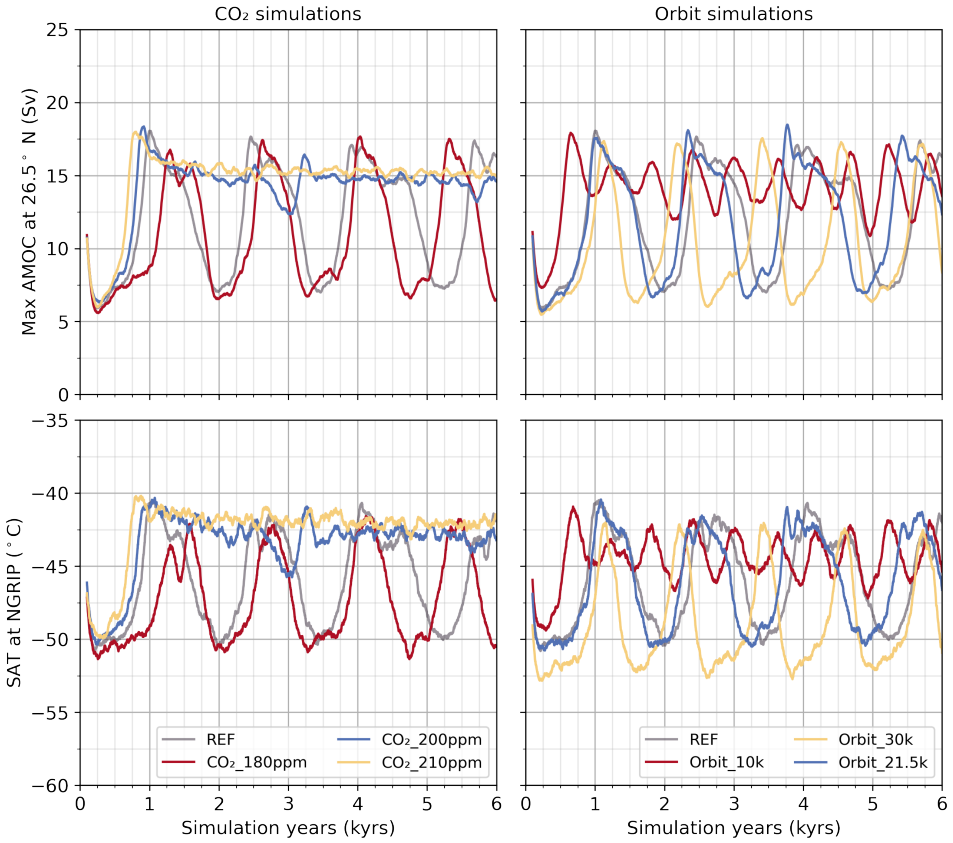

Figure 3.3: Top row: Maximum Atlantic meridional overturning circulation (AMOC) strength at 26.5° N. Bottom row: Surface air temperature (SAT) at NGRIP (North Greenland Ice Core Project; 42.32° W, 75.01° N). Data are shown as 100-year rolling means.

temperature, followed by an abrupt increase in ocean circulation strength of ∼10-15 Sv in all simulations. All of the simulations are characterised by oscillatory behaviour except for the higher CO_2 simulations (*CO_2_200pm* and *CO_2_210ppm*).

3.3.1 The reference simulation

The *REF* simulation is used as a benchmark for comparison between the new simulations presented here and the work of *Romé22*. In the *REF* experiment, oscillations have a periodicity close to 1,500 years with an maximum AMOC strength spanning from ∼6 to 17 Sv. The AMOC moves through the modes described in section 3.2.3 (*cold*, *meridional*, *zonal*) along with two transitionary modes (a *warming* mode between the *cold* and *meridional* modes, and a *cooling* mode between the *zonal* and *cold* modes). Because the circulation modes are defined by mixed-layer depth and AMOC strength, we can determine when the circulation is in a particular mode with a diagram of mixed-layer depth in the Irminger Sea as a function of mixed-layer depth in the GIN Seas (Figure 3.4a). Through this diagram, we observe that some simulations follow a shortened cycle without the *cold* phase. Changes in atmospheric CO_2 concentration or the orbital configuration are shown to impact the oscillatory pattern shown in *REF* by increasing the speed of the oscillations, disrupting the shape and amplitude, or ceasing oscillations all together.

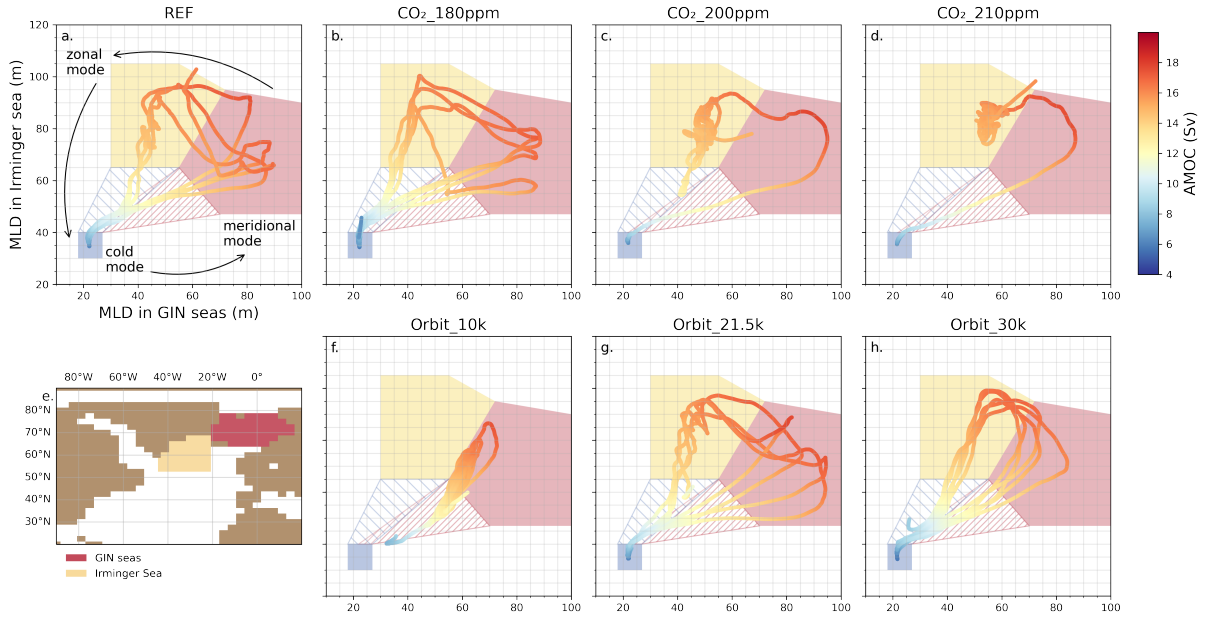

Figure 3.4: (a) - (d) and (f) - (h) Mixed-layer depth (MLD) in the Irminger Sea as a function of mixed-layer depth in the GIN Seas with the colours representing maximum strength of the AMOC at 26.5° N. Red shading represents the *meridional* phase, yellow shading is the *zonal* phase, and blue shading represents the *cold* phase. Red hatched region is the transition between the *cold* and *meridional* phase (or the *warming* phase), and blue hatched region is the transition between the *zonal* and *cold* phase (or the *cooling* phase). (e) The map of the North Atlantic illustrates what locations are used to represent the GIN seas and the Irminger Sea. The colour of the location corresponds to the colour of the mode in which convection is strongest in the region.

3.3.2 Impact of CO_2 on the oscillatory regime

Three sensitivity experiments were run to test the effect of CO_2 concentrations (180, 200, and 210 ppm). The higher CO_2 concentration simulations reach a *strong* AMOC mode after the initial spin-up period and remain in the *strong* mode for the rest of the simulation. The lower *CO₂_180ppm* simulation, on the other hand, oscillates at a quicker pace than *REF*, with an overall weaker AMOC that remains in a warm mode for a shorter period of time. From these simulations, we determine that CO_2 concentration controls the strength of the AMOC and how long the climate remains in a warm and cold state.

3.3.2.1 Low atmospheric CO_2 concentration

The *CO₂_180ppm* simulation represents the lowest end of atmospheric CO_2 concentration during the last 50 thousand years (Figure 3.1d). According to Bereiter et al. (2015), atmospheric CO_2 concentration dips to approximately 180 ppm around 25 ka BP, when ice sheets were at their largest extent. This simulation, despite the lower CO_2 conditions, oscillates; with a periodicity ~200 years shorter than *REF* (Figure 3.3). In comparison to *REF* in each oscillatory phase, *CO₂_180ppm* has colder surface temperatures throughout the Northern Hemisphere, due to the overall lower atmospheric CO_2 concentration (Figure 3.5a-c). The thicker and more expansive sea ice in *CO₂_180ppm* (compared to *REF*) traps heat from the surface ocean (Figure 3.15a-c),

preventing it from being released to the atmosphere and inducing subsurface ocean warming. The cycling between the *meridional*, *zonal*, and *cold* modes still occurs in this simulation, as it does in *REF* (Figure 3.4b), but the transitions between the *meridional* and *zonal* modes are more abrupt and less consistent between cycles. The length of the warm mode decreases (by ∼300 years, on average) and although the length of the *cold* mode increases (by ∼100 years, on average), overall, the periodicity of the simulation is shorter. This suggests that the lower CO_2 concentration produces a larger response in the warm phases of the oscillation than in the cold phase, in accord with the results of Zhang et al. (2021) and Gao et al. (2024).

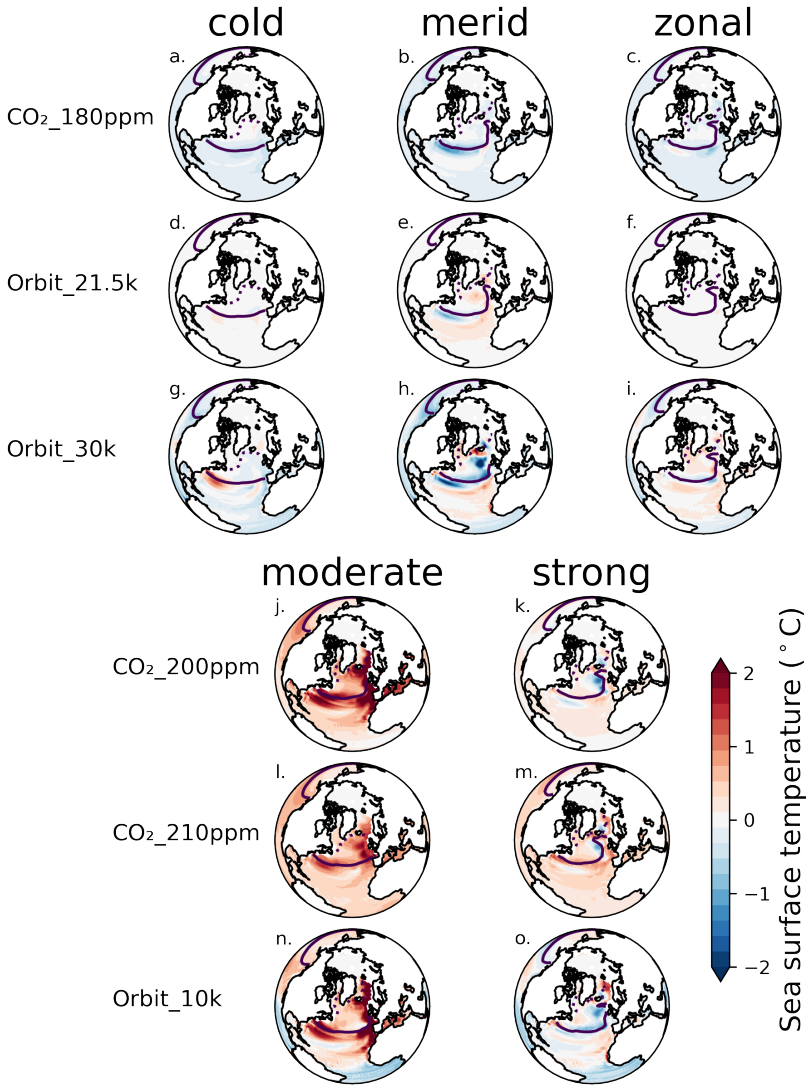

Figure 3.5: (a) - (i) Annual sea surface temperature anomaly from *REF* averaged for each AMOC mode (*cold*, *meridional*, and *zonal*). (j) - (o) Same as (a) - (i) but AMOC modes are defined by '*strong*' (greater than 14.5 Sv) and '*moderate*' (10-14.5 Sv) for *CO_2_200ppm*, *CO_2_210ppm*, and *Orbit_10k* and *REF* is defined by '*strong*' (greater than 14.5 Sv) and '*moderate*' (less than or equal to 14.5 Sv). For all, the solid line depicts March sea ice extent (15% cover) and the dashed line depicts September sea ice extent.

3.3.2.2 High atmospheric CO_2 concentration

In contrast to *CO_2_180ppm* and *REF*, the *CO_2_200ppm* simulation does not oscillate. During the spin-up period (the first 1,000 years of simulation), the AMOC in *CO_2_200ppm* travels through the initial stages of the *cold-meridional-zonal* cycle, first dropping into the *cold* mode, then rapidly transitioning through the warm *meridional* mode and onto the *zonal* mode (Figure 3.4c). Thereafter, *CO_2_200ppm* mainly remains in the *zonal* mode, with a maximum AMOC strength of $\tilde{1}5$ Sv. Nonetheless, the *CO_2_200ppm* simulation does show signs of instability. Around ∼2,500 years into the run, AMOC weakens by ∼2.5 Sv, instigating a transition to the *cold* mode (temporary excursion into the *cooling* phase, Figure 3.4c), but AMOC quickly recovers back to the *zonal* mode after ∼700 years. This sequence occurs again on a smaller scale ∼5,750 years into the run. During the first period of instability and reduced AMOC strength, the surface air temperature in the North Atlantic and Greenland decreases by ∼4 °C. This temporary excursion is reminiscent of the 8.2 kyr event (an abrupt cooling of 1-3 °C that lasted ∼160 years in the Northern Hemisphere; Thomas et al. 2007; Morrill et al. 2013), raising the question of whether some century-long AMOC perturbations could be intrinsic rather than forced by a meltwater pulse.

Adding an additional 10 ppm of CO_2 to the atmosphere appears to safely stabilise the AMOC in a warm mode for the entirety of the *CO_2_210ppm* simulation, after the spin-up period. The AMOC remains at ∼15 Sv from year 1,500 to the end of the simulation, surface air temperature stays warmer than *REF* at most locations (Figure 3.5l, m), and there is the least Northern Hemisphere sea ice cover in the *strong* mode compared to the other CO_2 sensitivity simulations and *REF* (Figure3.9e).

3.3.3 Impact of orbital configuration on the oscillatory regime

We performed three sensitivity experiments to test the impact of orbital configurations throughout the last 50 thousand years (*Orbit_30k*, *Orbit_21.5k*, and *Orbit_10k*). In these simulations, the year of the orbital configuration is changed from *REF*, and therefore includes differences in the obliquity, eccentricity, and precession of the Earth (Figure 3.1a, b). The main result from these orbital changes is that the impact of altered boreal seasonality is modulated by the complete orbital configuration. For instance, whether the Earth is in a state of high or low obliquity, regardless of the impact on seasonality, leads to different localised effects from the perturbed insolation, resulting in very different patterns of oscillation.

3.3.3.1 Low boreal seasonality (*Orbit_21.5k*)

Insolation at 21.5 ka BP is most similar to the *REF* experiment. Northern Hemisphere insolation at 21.5 ka BP is only ∼0.31 W m^{-2} less than the 21 ka BP orbit. Precession is slightly closer to 90°, and obliquity has decreased (Figure 3.1a,b). This orbital configuration results in a weak boreal seasonality, also slightly weaker than in *REF* (Figure 3.1e). Oscillations in the *Orbit_21.5k* simulation have a similar amplitude to *REF*, but a difference in shape that shortens the periodicity by an additional ∼100 years with each oscillation (Figure 3.3 and 3.4g). Surface temperatures are very comparable to *REF* especially in the *cold* and *zonal* (Figure 3.5d-f). In

the *meridional* mode, the North Atlantic in *Orbit_21.5k* is ∼1°C warmer.

3.3.3.2 Strong boreal seasonality (*Orbit_30k* and *Orbit_10k*)

The *Orbit_30k* simulation demonstrates the effect of an orbital configuration from the end of Marine Isotope Stage 3, a period when cycles between weak and strong AMOC (D-O events) were common, on simulated millennial-scale variability. The insolation is 20 W m^{-2} higher than at 21 ka BP, but obliquity has decreased from a median degree to a low point (from 23 to 22°). Precession is at ∼220° and eccentricity has decreased a small amount from *REF* (Figure 3.1a-c). As precession nears 270°, the boreal seasonality increases in strength. As shown in Figure 3.1e,f, *Orbit_30k* has the second strongest boreal seasonality of the ensemble, after the *Orbit_10k* simulation.

The oscillations in *Orbit_30k* have a shorter periodicity and faster transition time from warm to cold modes compared to *REF* (Figure 3.3). The AMOC briefly passes through the *meridional* and *zonal* modes (in a warm mode for ∼300 years on average compared to ∼700 years for *REF*) before transitioning back into the *cold* mode (Figure 3.4h) which lasts on average ∼60 years longer than in *REF*. Despite the increase in Northern Hemisphere insolation, North Atlantic sea surface temperatures (Figure 3.5g-i) in the *cold* and *meridional* modes and surface air temperature at NGRIP in Greenland (Figure 3.3) are ∼1-2°C colder than *REF* (Figure 3.5g-i).

In the *Orbit_10k* simulation, summer Northern Hemisphere insolation further increases to ∼469.5 W m^{-2}, another 30 W m^{-2} greater than the *Orbit_30k* simulation. Obliquity is close to the highest value ∼24°, and precession is very close to 270°. The *Orbit_10k* simulation has the strongest boreal seasonality of our sensitivity experiments (Figure 3.1e). The periodicity of the oscillations decreases significantly to ∼500 years. After the initial spin-up, maximum AMOC strength rapidly oscillates between ∼12 (*moderate* mode) and 18 Sv (*strong* mode) and Greenland temperature transitions between ∼ -37 and -43°C, respectively, but note that each oscillatory cycle varies in amplitude (Figure 3.3). During these quick oscillations, the AMOC never reaches the *meridional* mode, neither does it return to the initial *cold* mode (Figure 3.4f). Compared to *REF*, in the *strong* mode, sea surface temperatures are colder (∼1°C) in the North Atlantic and along the March sea ice edge but ∼1 °C warmer in the GIN Seas (Figure 3.5o).

Orbit_30k and *Orbit_10k* have obliquity values at opposite ends of the spectrum. Because of this, the pattern of incoming solar radiation is different, impacting the seasonality distribution. For instance, *Orbit_10k* has stronger incoming solar radiation in the Northern Hemisphere in the boreal summer months, as well as in the Southern Hemisphere during the boreal winter months (Figure 3.16). *Orbit_10k* has the weakest incoming solar radiation compared to *Orbit_30k* in the mid- to high Northern latitudes during the boreal winter months. These differences demonstrate the stronger boreal seasonality that *Orbit_10k* has over *Orbit_30k*.

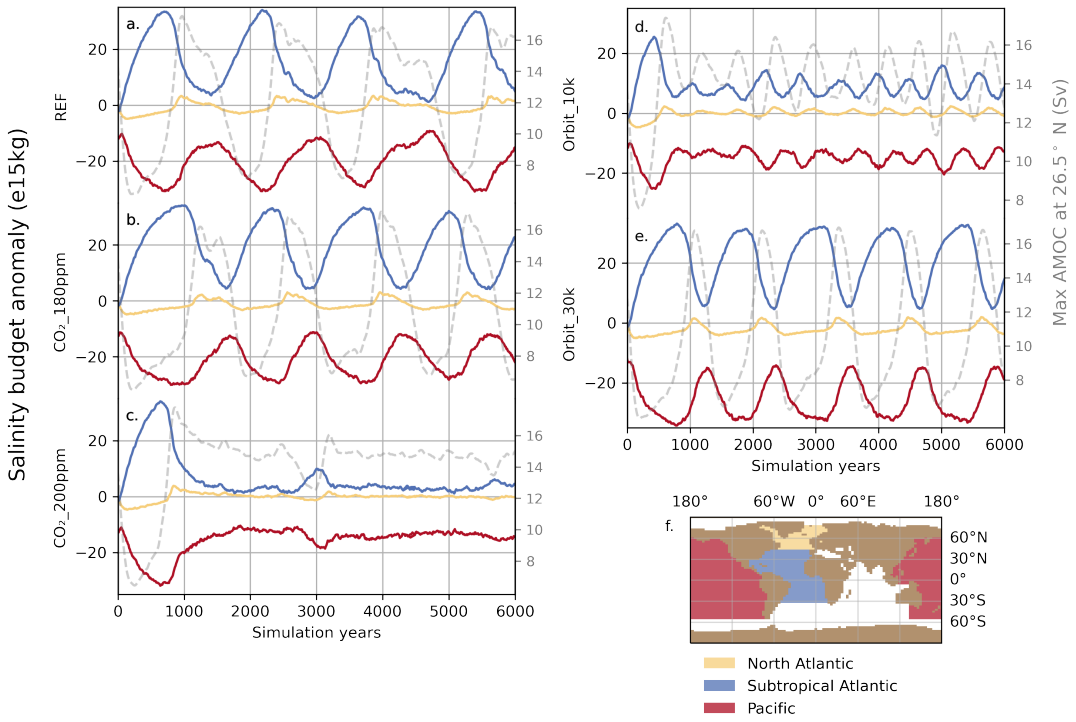

Figure 3.6: (a) - (e) Salinity budget anomaly from Last Glacial Maximum conditions in three different ocean basins; North Atlantic, Subtropical Atlantic, and Pacific Ocean. Maximum AMOC strength at 26.5° N is also shown (grey dashed line) to easily identify when the simulation is in a warm or cold regime. (f) Map illustrating the extent of how each region is defined. *CO_2_210ppm* and *Orbit_21.5k* are similar to *CO_2_200ppm* and *REF* respectively so are left out of this figure for simplicity.

3.4 Discussion

3.4.1 Impact of atmospheric CO_2 and orbital configuration changes on the convection-advection mechanism

3.4.1.1 Following the convection-advection mechanism

Romé et al. (2025) introduced the convection-advection oscillator mechanism to explain the millennial-scale variability simulated in the HadCM3 *Romé22* set of simulations. This simulation relies on the coupling between the fast changes of stratification in the North Atlantic and the slow global reorganisation of salt content through abrupt changes of the AMOC. In this paper, we explore the different roles of North Atlantic sea ice processes and their implication for the convection-advection mechanism. By looking at the movement of salt in the Atlantic Ocean, we can first establish whether the simulations here follow the same mechanism as the simulations in *Romé22*.

Figure 3.6 shows the salt content budget of the six sensitivity experiments and *REF*. Whilst in the *cold* mode, salinity accumulates in the subtropical Atlantic. Eventually, this high con-

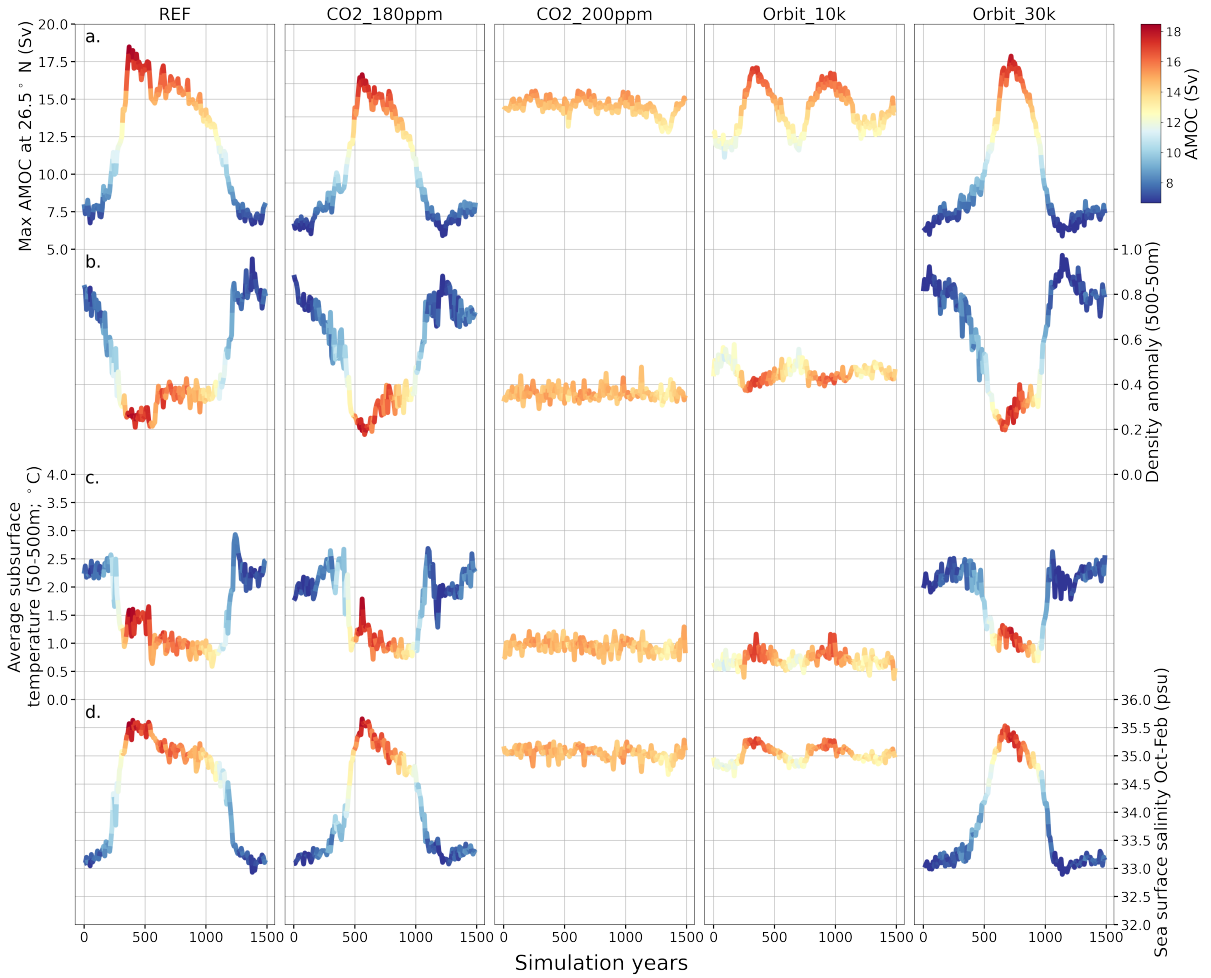

Figure 3.7: (a) Maximum AMOC strength at 26.5° N, (b) density anomaly between 500 and 50 metres for the GIN seas, (c) mean ocean temperature between 50 metres depth and 500 metres depth in the GIN seas, (d) sea surface salinity in the sea ice formation months (October to February) in the GIN seas for one oscillation of each of the sensitivity experiments. The colour map is normalised to the max AMOC strength in *REF* (a) as shown in the colour bar. All data are shown as decadal means. *CO_2_210ppm* and *Orbit_21.5k* are like *CO_2_200ppm* and *REF* respectively so are left out of this figure for simplicity.

centration of salt leaks into the upper North Atlantic due to gyre circulation, reaching high latitude regions like the GIN seas. The leakage into the GIN seas causes salinity and density of the surface ocean to increase. Stratification then decreases, allowing deep convection to restart, passing a threshold and re-invigorating the AMOC into the overshoot, *meridional* mode. We assume a threshold is represented by the density anomaly between 500 and 50 metres (Figure 3.7b). Whilst convection is strong, salinity is transported around the globe to ocean basins that lost salt to the subtropics during the *cold* mode (e.g., the Pacific Ocean; Figure 3.6). As the subtropical Atlantic becomes depleted in salt, salinity in the GIN seas begins to decrease alongside surface density, causing stratification to increase again until a threshold is crossed, whereby the AMOC weakens abruptly. This circulation of salinity throughout the ocean basins is a key control in the change of stratification in the sea basins and vice versa, oscillating with the same periodicity as the AMOC (Figure 3.7a,b). We also observe salinity changes in the

Southern Ocean due to the strengthening and weakening of the Antarctic bottom water during the warm and cold regimes (Figure 3.17) which may have an impact on the AMOC. However, these changes are too weak to drive significant changes in North Atlantic convection (Romé et al. 2025). In other simulations with higher sensitivity to Antarctic bottom water, these salinity changes could be more effective (Sherriff-Tadano et al. 2023).

The transport of salt from the subtropical Atlantic to the North Atlantic and Pacific is evident in the spin-up period of each simulation and continues in the experiments that oscillate fully from cold to warm regimes. However, this mechanism alone cannot explain the changes in the periodicity of simulated AMOC oscillations relative to *REF*. We hypothesise that sea ice impacts the pace of the convection-advection mechanism, as the growth and retreat of sea ice controls the ability of the transported salt to reach sites of deep water formation in the GIN seas. The changes in CO_2 concentration and boreal seasonality provide new insight into the role of sea ice, including the part it plays in controlling the speed at which the AMOC can switch between warm and cold regimes.

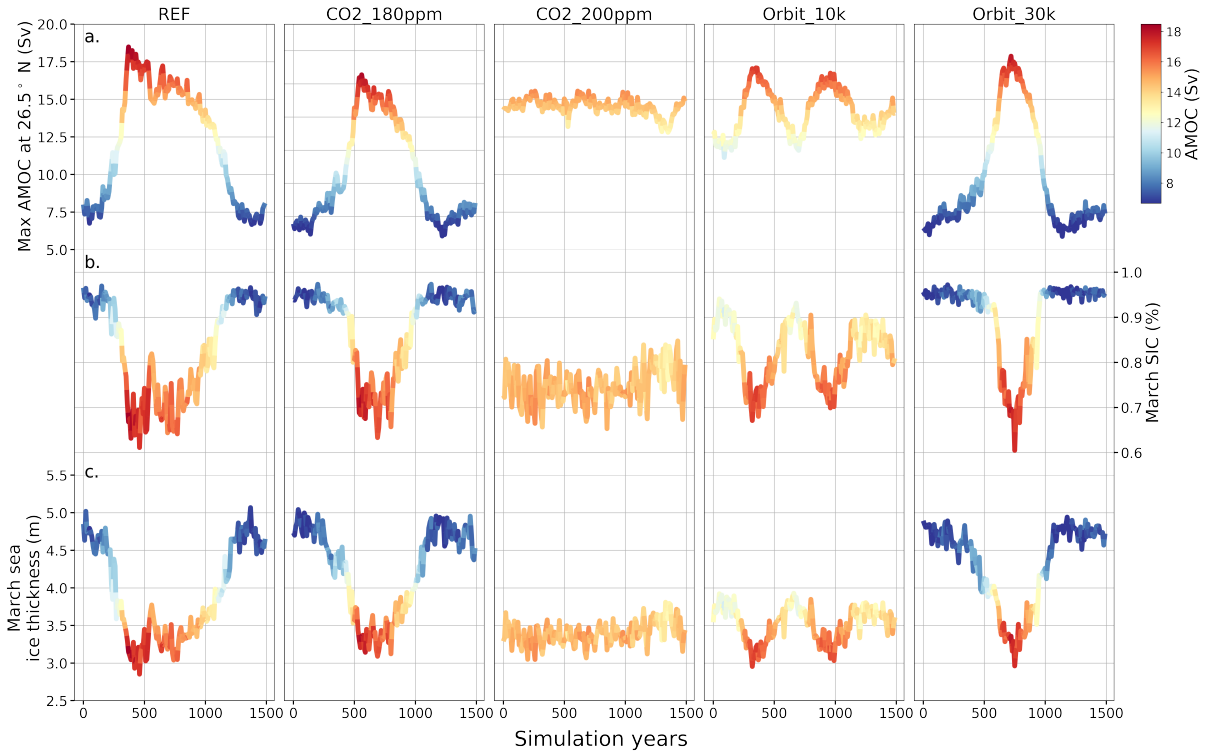

Figure 3.8: (a) Maximum AMOC strength at 26.5° N, (b) March sea ice concentration (SIC) calculated between 50° N and 70° N, and (f) sea ice thickness in March between 50° N and 70° N for one oscillation of each of the sensitivity experiments. The colour map is normalised to the max AMOC strength in *REF* (a) as shown in the colour bar. All data are shown as decadal means. *CO_2_210ppm* and *Orbit_21.5k* are like *CO_2_200ppm* and *REF* respectively so are left out of this figure for simplicity.

3.4.1.2 Impact of CO_2 on the convection-advection oscillator mechanism

Lower surface temperatures in the *CO_2_180ppm* simulation lead to increased Northern Hemisphere sea ice area in every AMOC mode compared to *REF* (~2.7 x 10^5 km^2 on average; Figure

3.9). When CO_2 is lower, the sea surface remains colder relative to the warmer and higher CO_2 climates (Figure 3.5a-c), allowing sea ice to return quicker from the warm modes (Figure 3.8b,c). In addition, the colder surface temperatures promote thicker sea ice in the Arctic and northern North Atlantic (Figure 3.18). As the AMOC strengthens, enhanced convection in the GIN and Irminger Seas warms the surface ocean, causing proximal sea ice to melt. However, because the sea ice is thicker, it contributes ∼104% more freshwater than *REF* (faster decrease of sea surface salinity in Figure 3.7d) to sites of deep water formation during the warm modes. The decrease in salinity concentration paired with the warmer subsurface temperatures increases stratification, hindering the AMOC's ability to sustain its strength in the strong mode moving the climate out of the *zonal* mode and into the *cold* mode again (following Path (b) and (c); Figure 3.10). Thus, greater sea ice cover is linked to an extended *cold* mode as sea ice builds up for a longer period of time sustaining a higher stratification, before the warming transition begins to force its retreat.

When CO_2 is higher as in *CO₂_200ppm* and *CO₂_210ppm*, surface temperatures increase, while deeper ocean temperatures are less impacted (Figure 3.5j-m). Sea ice is also naturally thinner and sparser (Figure 3.9 and 3.8b,c) compared to *REF*. Stratification in the North Atlantic, therefore, is lower, salinity concentration is consistently higher, and subsurface temperatures in the convection sites are cooler (Figure 3.7b,c). Because of these factors, it is more difficult to pass the stratification threshold that forces AMOC to weaken.

The two temporary excursions present in *CO₂_200pm* resemble the oscillations in *Orbit_10k*. We describe the mechanistic behaviour behind these particular excursions and shorter oscillations in the next section.

3.4.1.3 Impact of orbital configuration on convection-advection oscillator mechanism

Our simulations bring to the fore a further extension to the convection-advection oscillator proposed by Romé et al. (2025), relating to the influence of boreal seasonality on sea ice. Moreover, we find that weaker boreal seasonality (such as in *REF* and *Orbit_21.5k*) drives a tendency towards thicker sea ice. With weaker summer insolation, less melt occurs in the summer, allowing for the sea ice to build up in the winter. Thicker sea ice is less vulnerable to melting and creates a barrier between the ocean's upper waters and the atmosphere. The ocean's upper waters are better insulated and thus retain more heat, causing the surface North Atlantic density to decrease and deep water formation to slow. Eventually, the accumulation of subsurface heat melts overlying sea ice. After the initial impact of surface freshening is overcome, the thermal reconnection between atmosphere and ocean leads to surface cooling. Combined with elevated ocean salinity along the newly retreated sea ice edge, the drop in surface temperature drives a rise in surface density, kick-starting the transition to warm conditions as deep ocean convection resumes (a process described in detail by Dokken et al. (2013)). Nonetheless, since thicker sea ice takes longer to melt, the climate is able to remain in a *cold* state for longer than is possible under strong boreal seasonality with otherwise equivalent forcings (as seen between *REF* and *Orbit_21.5k* with an increase in the duration of the *cold* mode by

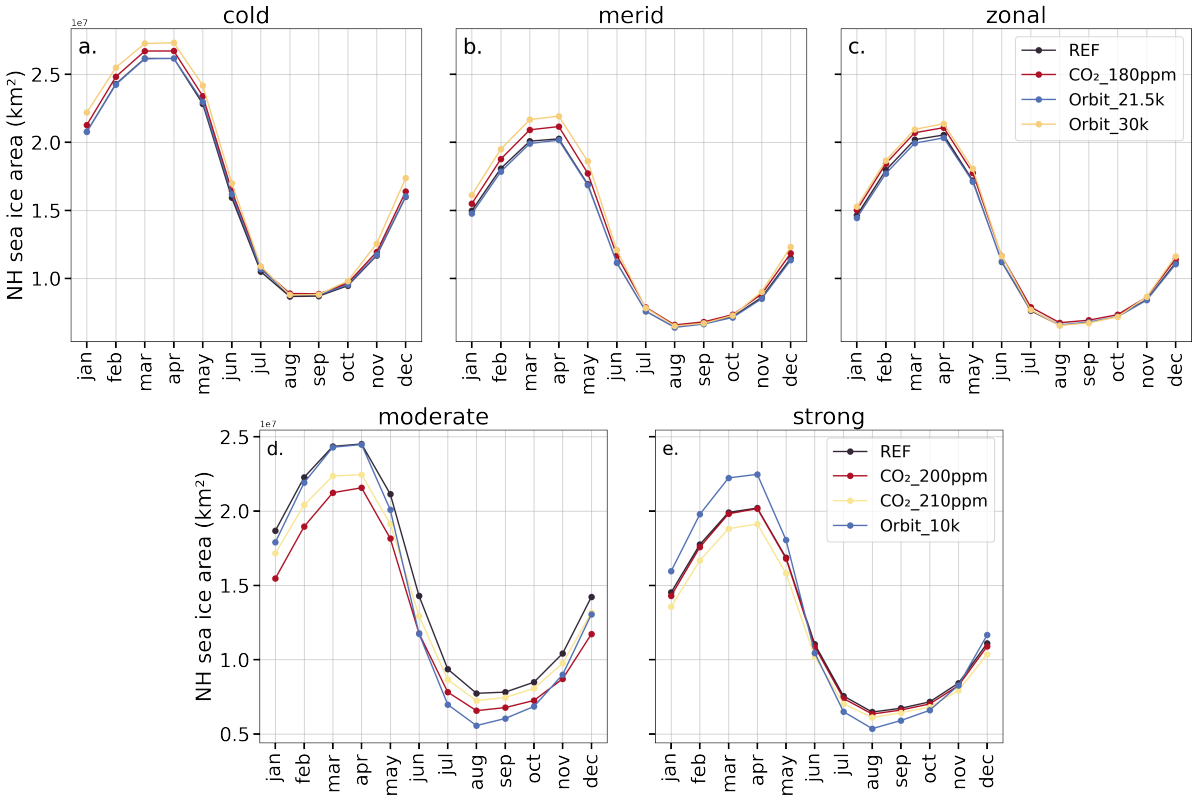

Figure 3.9: Monthly mean Northern Hemisphere sea ice area for each AMOC mode (different panels) in all simulations (different colours). *REF* is behind *Orbit_21.5k* in panels (a) - (c) and behind *CO_2_200ppm* in panel (d).

~20 years on average and also shown by Kuniyoshi et al. (2022)).

In contrast, the climate produced under stronger boreal seasonality tends to have thinner sea ice because the summers are warmer. However, the winters are also colder, allowing for faster surface expansion of the albeit thinner sea ice during these months. This transition between warmer summers and cooler winters, compared to a climate with weaker seasonal shifts, can impact the speed at which deep convection sites become sea ice covered or sea ice free, allowing the AMOC to quickly weaken or strengthen.

Strong seasonality plays a crucial role in generating the *Orbit_10k* oscillations, noting that despite having a relatively similar AMOC strength, the *CO_2_200ppm* and *CO_2_210ppm* simulations show less signs of instability. The strong seasonality allows for a substantial increase in sea ice concentration each winter as well as substantial melt each summer. This is evident in the large seasonal sea ice variability in the GIN and Irminger seas (e.g., sea ice concentration increases from 25% in boreal autumn to 95% concentration in spring in the GIN seas during the *moderate* mode). During the *strong* mode, our *Orbit_10k* simulation has the greatest sea ice coverage in boreal spring and the least sea ice coverage in boreal autumn out of all of the simulations (Figure 3.9e).

Unlike the other oscillating simulations, the AMOC never returns to a weak regime after the initial spin-up period (Figure 3.3), and the ocean basins have a smaller amplitude of salt content

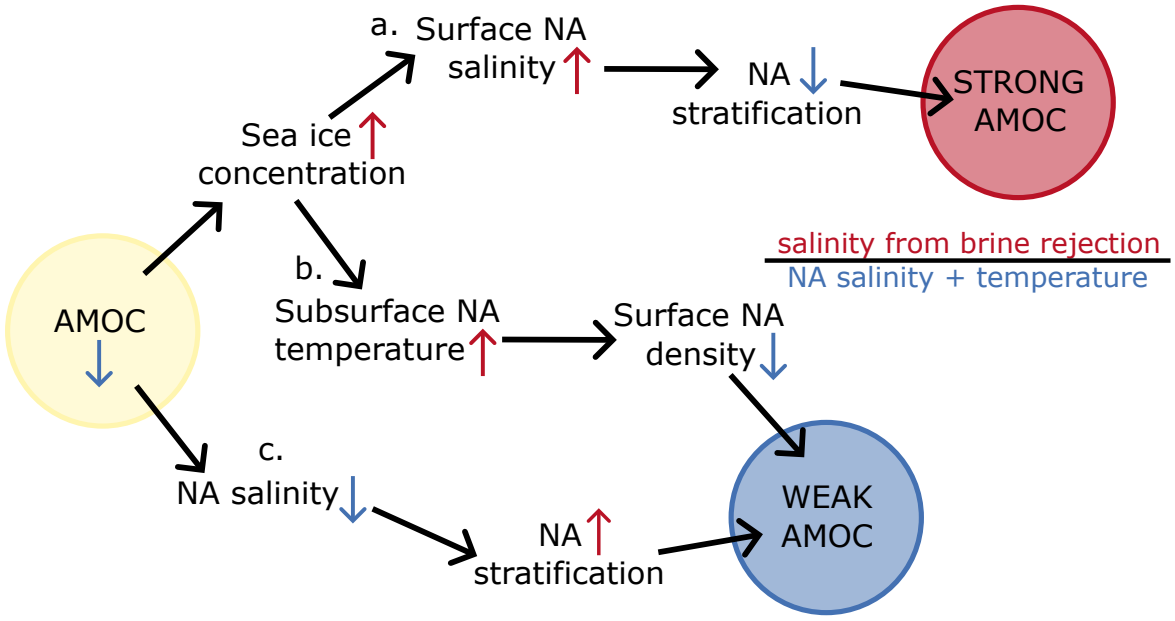

Figure 3.10: Update to the convection-advection mechanism when transitioning out of a warm AMOC regime. A possible pathway (a) whereby brine rejection from increases in sea ice concentration overpowers the decrease in North Atlantic (NA) salinity and the surface NA temperature increase, leading to an AMOC strengthening. Possible pathways whereby (b) an increase in surface North Atlantic temperature or (c) a decrease in North Atlantic salinity promotes AMOC weakening. Paths (b) and (c) are already incorporated into the original convection-advection mechanism by Romé et al. (2025), whereas Path (a) is new to this study.

change (Figure 3.6d). Instead, the AMOC in *Orbit_10k* oscillates around 15 Sv, remaining in a warmer regime for the entirety of the simulation after the spin-up period. Following the convection-advection mechanism, when the AMOC begins to weaken as the *zonal* mode ends, North Atlantic salinity is at a low point. Stratification begins to increase towards the *cold* mode as salt continues to be depleted from the subtropics, eventually leading to an AMOC shut down (as described in section 3.4.1.1 and Figure 3.10c). However, we demonstrate that the salinity increase from brine rejection during sea ice formation competes with the salinity removal and temperature increases in the North Atlantic during a strong AMOC regime; the dominant effects determine whether or not AMOC strength will decline.

In *Orbit_10k*, sea ice extent reaches nearly the same maximum and minimum aerial cover as for the other simulations, despite not reaching the same maximum and minimum high latitude surface air temperatures or AMOC strengths (Figure 3.8). We suggest that the rapid increase of March sea ice concentration would substantially increase the surface salinity in the North Atlantic through brine rejection, counter-balancing the depletion of salinity in the same region. This can be seen in Figure 3.7d, where the amplitude of surface salinity changes are muted relative to the other simulations. This increase in surface salinity would also impact ocean stratification, reducing the stability of the North Atlantic water column (Figure 3.7b), leading to AMOC resumption (Figure 3.10a). Unlike the other oscillating simulations in this study, stratification in the convection sites is nearly constant throughout the simulation, potentially because of the counter-balance of salinity changes from the sea ice formation. Subsurface tem-

perature changes in the GIN Seas are also very minimal, with only temperature in the Irminger Sea showing variability akin to the maximum AMOC strength (Figure 3.7c and 3.19c). We suggest the *CO_2_200ppm* simulation also follows Path (a) during the temporary excursions. The first period of cooling (~2,500 years in to the run), there is an increase in sea ice concentration on the same scale as the *Orbit_10k* simulation when moving from the *strong* to the *moderate* mode.

On the other hand, *Orbit_30k* moves through the full oscillatory cycle similar to *REF*, just ~350 years faster. On average, the time spent in the *cold* mode is actually longer (by ~60 years) than for *REF*, but this is more than compensated for by the shortening (by ~400 years) of the time spent in a warm AMOC regime, very similar to *CO_2_180ppm*. As mentioned in section 3.4.1.3, despite the higher summer insolation, surface temperatures are actually colder in this simulation (see Greenland temperature in Figure 3.3 and sea surface temperatures compared to *REF* in Figure 3.5g-i). Because of these colder surface temperatures as well as the low obliquity at 30 ka BP (consistent with previous studies; e.g., Turney et al. 2015), sea ice accumulates in the Arctic and northern North Atlantic, to become even thicker than in *CO_2_180ppm* and *Orbit_10k* (Figure 3.9 and 3.18). This contributes an even larger amount of freshwater to sites of deep water formation when sea ice melts during the warm modes and subsequently, sea surface salinity decreases faster for *Orbit_30k* than *CO_2_180ppm*, producing a more rapid shift from the *zonal* to *cold* mode.

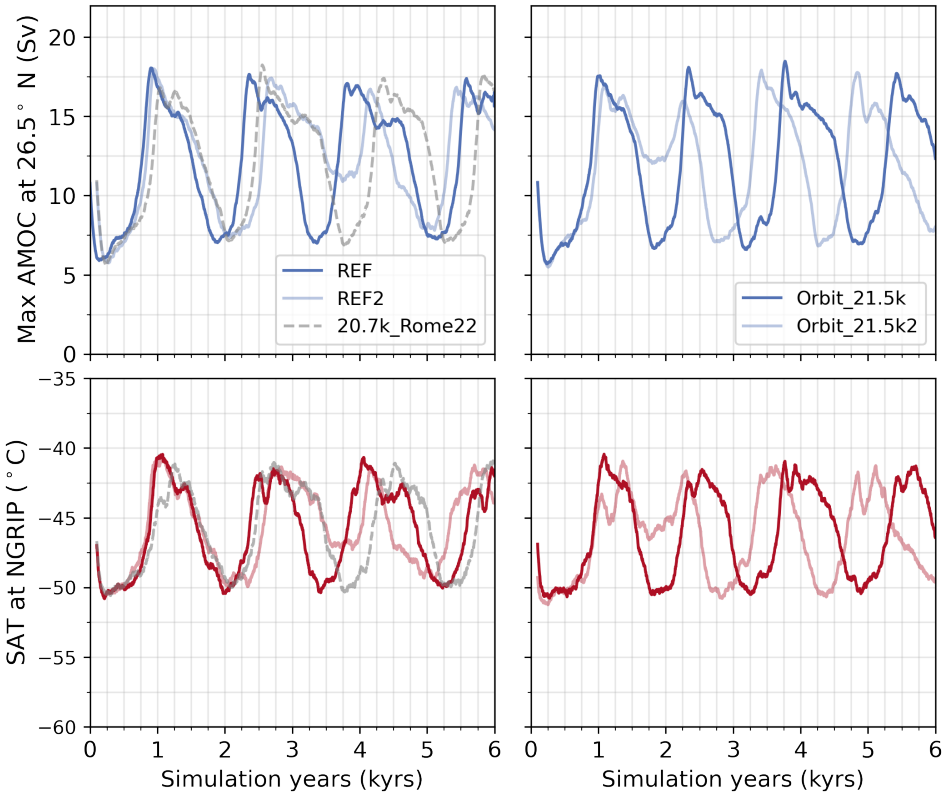

Figure 3.11: Top row: Maximum AMOC strength at 26.5° N. Bottom row: Surface air temperature at NGRIP (North Greenland Ice Core Project; 42.32° W, 75.01° N). The original *REF* and *Orbit_21.5k* simulations are shown in bolder colours, and the corresponding repeat simulations are shown in the paler colours.

3.4.2 Variation between simulations of the same boundary conditions

Although the evolution of the oscillating simulations is mostly deterministic, stochasticity influences the precise shape and duration of the oscillations in our multi-millennial simulation ensembles. Small differences can be seen in the amplitude of AMOC changes, the duration of each phase, and the strength of deepwater formation. To investigate this further, we repeated a subsection of simulations using exactly the same boundary conditions/forcings, but introducing some slight noise to the initial condition. Thus, *REF*, *REF2*, and *20.7k_Rome22* are triplets and *Orbit_21.5k* and *Orbit_21.5k2* are twins.

The most remarkable difference between these simulations is that *REF2* and *Orbit_21.5k2* skip an oscillation compared to *REF* and *Orbit_21.5k*. In *REF2*, the second oscillation does not contain a *cold* phase (Figure 3.11). Similarly, in *Orbit_21.5k2* the first oscillation does not contain a *cold* phase (Figure 3.20). Romé et al. (2025) argue that *20.7k_Rome22* is close to reaching equilibrium in the salt budget at the end of the *zonal* phase, suggesting that this could, in rare cases, prevent the system to enter a positive feedback leading to the abrupt deactivation of the North Atlantic deep water formation. Instead, the AMOC stalls in an extended warm phase, switching from a *meridional* phase to a *zonal* phase, before a slight weakening comparable to *CO_2_200ppm* and a recovery into a *meridional* mode. At the end of the meridional phase, the positive feedback is activated and the system switches to a *cold* phase. The skip of the cold transition results in a 500-year offset between the *Orbit_21.5k* and *Orbit_21.5k2* cycles. There is less of an offset between the *REF* and *REF2* cycles by the end of the simulations due to the longer warm regime in the second oscillation followed by an oscillation with a warm regime 700 years shorter.

We propose that the differences in the evolution of the twin and triplet experiments are caused by the competing influences on ocean density of sea ice growth (which increases both North Atlantic salinity, Figure 3.10a, and surface temperatures, Figure 3.10b) and the depletion of salinity through ocean transport (Figure 3.10c). Because *20.7k_Rome22* and its siblings (*REF* and *REF2*) are close to reaching an equilibrium in the salt budget, the sea ice effect can dominate the salinity effect and the oscillating pattern can temporarily shift to a shorter brine rejection-driven oscillation similar to *Orbit_10k*. During these oscillations, there is minimal change in the stratification in the GIN Seas compared to a full *cold-meridional-zonal-cold* cycle, but sea ice concentration still reaches a similar minimum and maximum as the other cycles and sea surface salinity remains high (Figure 3.21). Because sea ice is a stochastic and highly sensitive system, its feedbacks do not always dominate the climate trajectory, hence the salinity and temperature threshold is sometimes crossed first, before the sea ice threshold is reached, allowing the AMOC to return to the *cold* mode.

3.4.3 Controls on AMOC stability

Fully understanding earth system changes induced by climate forcings in complex models is difficult due to the wide variety of initial climate conditions and the potential non-linearity of responses when comparing across different models and different model experiments. Although multiple abrupt climate change events are positively correlated with transitions in the AMOC,

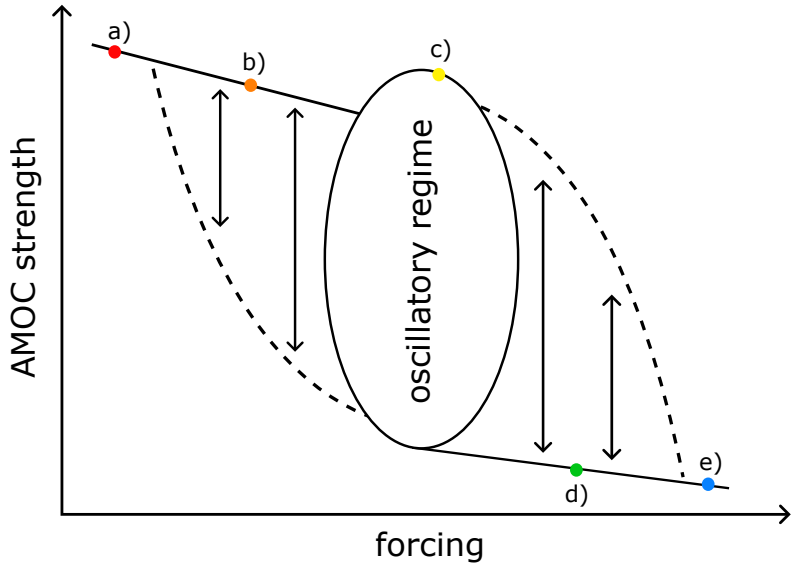

Figure 3.12: Bistability curve of AMOC stability modes according to strength of forcing (e.g. ice meltwater flux or atmospheric pCO_2); a schematical view. (a) A monostable and strong AMOC (e.g., *CO_2_210ppm*), (b) an excitable or chaotic, strong AMOC that occasionally gets pulled into a weaker mode (e.g., *CO_2_200ppm*), (c) an oscillating AMOC (e.g., *REF*, *CO_2_180ppm*, and the orbit simulations), (d) an excitable or chaotic, weak AMOC that occasionally gets pulled into a stronger mode (e.g. *Romé22*'s *18.2k* simulation), and (e) a monostable and weak AMOC (e.g., *P185* and *P149* from Klockmann et al. (2018)).

how the AMOC is impacted by external forcings and the resultant response of the climate is still largely unknown. In this section, we have tried to capture and understand the impact of glacial-period changes in orbit and CO_2 on the ability of the AMOC to remain in or transfer between different modes of stability.

Previous studies (Rahmstorf 2000; Berk et al. 2021; Barker and Knorr 2021) have demonstrated the impact of freshwater forcing on AMOC stability in the form of a bifurcation diagram. From our results, we can conceive an illustration of something similar, positioning our simulations, and those of *Romé22*, along the curve (Figure 3.12). For example, examining *Romé22*'s simulations with different meltwater forcings, we determine that as meltwater increases, the AMOC moves from a monostable, strong regime (e.g., *Romé22*'s *21.5k* simulation) to an oscillating regime (e.g., *Romé22*'s *20.7k* and *19.4k* simulations) to an excitable/chaotic, weak AMOC (e.g., *Romé22*'s *18.2k* simulation). A monostable, weak AMOC is not found by *Romé22*. However, other previous studies have demonstrated collapsed and unrecoverable AMOCs with high freshwater fluxes (e.g., Bouttes et al. 2023). In this study, and previous studies such as Klockmann et al. (2018), lowering atmospheric CO_2 concentration forces the AMOC along the bistability curve in the same direction as elevated freshwater (e.g., ice sheet meltwater) discharge to the oceans. Our *CO_2_210ppm* simulation represents the monostable, strong AMOC; the *CO_2_200ppm* simulation fits the profile of an excitable/chaotic, strong AMOC; *REF* moves the AMOC fully into an oscillatory regime and *CO_2_180ppm* remains there. This study does not

include simulations with an atmospheric CO_2 concentration lower than 180 ppm, so it is uncertain whether the AMOC would move further on, eventually to a monostable, weak AMOC. However, Klockmann et al. (2018) do demonstrate this behaviour with low CO_2 simulations under pre-industrial conditions.

How the forcing of boreal seasonality (e.g., through insolation changes) moves AMOC through this bistability curve is more complex. As the strength of boreal seasonality changes, the AMOC does not move in or out of the oscillatory regime. Instead, as the boreal seasonality strength increases, the oscillations decrease in periodicity and as the *Orbit_10k* simulation demonstrates, begin to oscillate in a *warm* (i.e. interstadial) mode. However, how the periodicity is impacted (i.e., the length of time spent in a *warm*/strong AMOC mode and a *cold*/weak AMOC mode, relative to *REF*) is not purely dependent on boreal seasonality alone, but controlled by the combination of the independent orbital parametres. For instance, despite both simulations having stronger boreal seasonality, *Orbit_30k* has a longer *cold* mode than *REF* whereas *Orbit_10k* does not re-enter the *cold* mode. We put this down to the differences in obliquity, which impact how the insolation is distributed across the globe, creating contrasting localised effects (e.g., sea ice thickness distribution; Figure 3.18) and leading to different patterns of oscillatory behaviour.

3.4.4 Glacial terminations and the 'window of opportunity'

Barker and Knorr (2021) suggest four possible scenarios for how the AMOC could recover during a glacial termination: an increase in North American ice sheet height (producing stronger winds and thus a stronger AMOC Ullman et al. 2014; Löfverström and Lora 2017; Sherriff-Tadano et al. 2018; Kapsch et al. 2022), an AMOC recovery during a bistable window from an external forcing like a negative freshwater event, an increase in CO_2 concentration that outpaces the rate of ice sheet decline, or a CO_2 increase that reaches the needed interglacial threshold. Our high CO_2 simulations demonstrate from a mechanistic perspective the credibility of the latter two situations.

Because no other variables have been changed, from the *CO_2_200ppm* and *CO_2_210ppm* simulations we are able to isolate the impact of an increase in CO_2 similar to the 10 ppm rise in atmospheric CO_2 that occurs between Heinrich Stadial 1 (a cold period between ∼18.5 and 14.7 ka BP characterised by weak ocean circulation; Broecker and Putnam 2012; Ng et al. 2018; Crivellari et al. 2018; Huang et al. 2014; Huang et al. 2019) and the Bølling-Allerød Warming (an abrupt warming ∼14.7 ka BP in Greenland; Severinghaus and Brook 1999; Lea et al. 2003; Buizert et al. 2018). The constant ice sheet geometry in our experiments, however, is not an unreasonable approximation for the relatively slow and minor North American ice sheet evolution reconstructed between 21 and 17 ka BP (Tarasov et al. 2012; Peltier et al. 2015). Thus, our simulations demonstrate that an addition of only 10 ppm of CO_2 can be enough to move the AMOC from a bistable to a monostable interstadial regime, reaching the needed interglacial threshold. Reversing the direction of CO_2 change, our atmospheric CO_2 experiments also show how only a small change in CO_2 concentration, could move the climate from a more stable regime to within the 'window of opportunity'.

Moreover, we have demonstrated one way in which the background climate state can condition

the ocean to be more vulnerable to tipping across density thresholds, triggering and controlling the nature of unforced AMOC oscillations, but the nuances of this relationship between background climate and AMOC oscillation become clearer when we compare our results to previous work. For example, Malmierca-Vallet et al. (2024) empirically identified a similar atmospheric CO_2 'window of opportunity' for AMOC oscillation in three different models under different background climates and boundary conditions; ∼185 to 230 ppm. Notably, 230 ppm, the top end of their window, is higher than ours (< 200 ppm). Additionally, 185 ppm, the bottom end of their window, is higher than our lowest CO_2 simulation (180 ppm), though we do not have enough simulations to identify a comprehensive range. Notwithstanding the differences in trigger for the oscillations (Armstrong et al. 2022; Romé et al. 2022), the contextual differences in the experimental designs–i.e., differences in initial and boundary conditions, such as the meltwater flux existent in ours–are likely key for explaining this difference between the CO_2 threshold for oscillation in our results and the earlier work.

The impact of boundary and initial conditions on a 'window of opportunity' for AMOC oscillation are clearest when comparing simulations run with the same model. For example, although our *Orbit_30k* simulation and the HadCM3 simulations presented by Malmierca-Vallet et al. (2024) share the same orbital forcing (from 30 ka BP), our glacial maximum ice sheets are much larger than the mid-glacial sized ice sheets (Peltier 2004) implemented by Malmierca-Vallet et al. 2024. In our simulations, the larger glacial maximum ice sheets produce stronger winds and thus a stronger AMOC, suppressing oscillations from being triggered at higher atmospheric pCO_2.

The important role of the background climate state in influencing the characteristics of triggered oscillations is further confirmed when comparing our *Orbit_30k* simulation with the full 30 ka BP experiment of Armstrong et al. (2022), which includes 30 ka BP orbit, 200 ppm atmospheric CO_2 and the mid-glacial 'ICE-5G' ice sheet of Peltier (2004). The previously published oscillations are of similar periodicity to our *Orbit_30k* simulation, both ∼1200 years. However, the amplitudes differ between the two studies. The AMOC in the simulation presented by Armstrong et al. (2022) ranges in maximum strength from 6 Sv to 12 Sv, whereas the AMOC oscillations in our *Orbit_30k* run span a larger amplitude from 6 to 18 Sv. Considering that in our other simulations, as well as previous studies (e.g., Klockmann et al. 2018), AMOC strengthening correlates with higher atmospheric CO_2, it is interesting that Armstrong et al. (2022)'s maximum AMOC strength is lower than ours even though their atmospheric CO_2 concentration is 10 ppm higher, suggesting that in this case, the afore described influence of ice sheet size/geometry on the AMOC overrides the smaller impact of atmospheric CO_2. The similarity in the shape and periodicity of the oscillations, despite the impact of differences in ice sheet size and CO_2 concentration on the amplitude, hints at the importance of the orbital control on insolation patterns compared to other forcings during this time period.

In our other orbit simulations, the *Orbit_10k* simulation has the strongest boreal seasonality and the *Orbit_21.5k* simulation has the weakest boreal seasonality (with *REF* only stronger by less than 1 W m^{-2} difference in seasonal insolation). The change in periodicity of our simulations is consistent with the findings of both Brown and Galbraith (2016) and Kuniyoshi et al. (2022), and

for our simulations, we explain this with the changes in sea ice relative to *REF*. The *Orbit_10k* simulation displays oscillations of the shortest periodicity (only ∼500 years). The *Orbit_30k* simulation, which has the second strongest boreal seasonality, has oscillations ∼1200 years in length. The *warm-cold* cycles in *REF* and *Orbit_21.5k* are ∼1500 years in length. However, dissimilar to Brown and Galbraith (2016), who did not observe oscillations under high obliquity, we do find oscillations in *Orbit_10k*, the simulation with the highest obliquity–but as a reminder, these oscillations are much shorter in amplitude and less D-O-like than the other oscillatory behaviour in our results.

Previous studies, including Barker and Knorr (2021) and Zhang et al. (2021), demonstrate that the combination of changes between atmospheric CO_2 and ice volume control the sensitivity of AMOC to other climate perturbations, such as orbitally-induced changes in insolation. These studies have not found any AMOC mode changes under peak glacial or interglacial conditions, but they have produced AMOC oscillations under intermediate conditions (i.e. between glacial and interglacial states) with changes in orbit, atmospheric CO_2 concentration, and ice volume. Although we observe very different variations in the oscillatory behaviour in our simulations, they are only tested under one background climate. It would be interesting to further test our results against other background climates.

3.5 Conclusion

In this study, we present six new simulations from the Hadley Centre general circulation model version 3 (HadCM3), with four of the simulations oscillating under glacial climate conditions. These simulations are sensitivity experiments branching from *Romé22*'s *20.7k* simulation with Last Glacial Maximum conditions and a constant meltwater flux derived from the GLAC-1D ice sheet reconstruction of the early deglaciation. We tested the impact of different atmospheric CO_2 concentrations and orbital forcing on the oscillations and their respective mechanisms of AMOC tipping (Romé et al. 2025).

Our results showed that raising CO_2 concentrations from 190 ppm to 200 and 210 ppm prevents the periodic AMOC oscillations from occurring, whereas decreasing atmospheric CO_2 to 180 ppm shortened the duration of the *warm* (or interstadial) phase, by ∼200 years, and led to an overall shorter periodicity of the oscillation. In addition, we observe that when boreal seasonality increases (equivalent to conditions at 30 ka BP), the duration of the *warm*, interstadial state decreases. However, the simulation with the strongest boreal seasonality (equivalent to conditions at 10 ka BP) robustly remains in a *warm*, interstadial state. We conclude that this contrasting response to a boreal seasonality increase is due to the differences in obliquity (with obliquity low at 30 ka BP and high at 10 ka BP).

We show that the sensitivity of AMOC tipping to changes in climate forcings (atmospheric CO_2 and orbital configuration) is controlled by sea ice conditions, which play an important role in maintaining ocean circulation and pushing AMOC into different modes. While our AMOC oscillations are controlled by the convection-advection mechanism described by Romé et al. (2025), we show that their periodicity is further governed by Northern Hemisphere sea

ice concentration and thickness. We add a new branch to the convection-advection mechanism to explain the new AMOC behaviour demonstrated in this study, where the AMOC skips the weak mode in some cycles. The impacts of changes in CO_2 concentration and orbital insolation forcing on our AMOC oscillations demonstrate the importance of the role of sea ice in controlling the speed at which the AMOC can switch between warm and cold regimes. Furthermore, these impacts demonstrate how even small changes to the background climate condition can significantly impact the AMOC's ability to oscillate.

3.6 Supplementary Figures

3.6.1 HadCM3's performance compared to modern day observations

In studies by Gordon et al. (2000) and Turner et al. (2013), the sea ice performance in HadCM3 is deemed to be realistic in the Arctic and the Antarctic. Gordon et al. (2000) compare a modern-day 400-year long simulation of sea ice to satellite observations and the annual mean sea ice area consistently falls within the recorded seasonal extents for both the Northern and Southern Hemispheres. However, Arctic sea ice extents are overestimated at the maxima (boreal winter-spring), whereas the seasonal minimum is simulated reasonably well. The overestimation is due to more modelled sea ice in the GIN seas and in the North Pacific and Barents Sea than in satellite observations.

Convection normally occurs in the Irminger and GIN seas in HadCM3. Convection in the Labrador Sea is weak. Similar results are found in modern day simulations of HadCM3, but convection is more prominent in the Labrador Sea than at the Last Glacial Maximum (Grist et al. 2007). In previous years, the hypothesis was that more convection took place in the Labrador Sea than modelled by HadCM3, however, in more recent years, observations suggest that convection in the Labrador Sea is weaker and more deep-water formation occurs in the Nordic and Irminger seas, more attuned to the HadCM3 simulations shown in this chapter (Lozier et al. 2019; Petit et al. 2020).

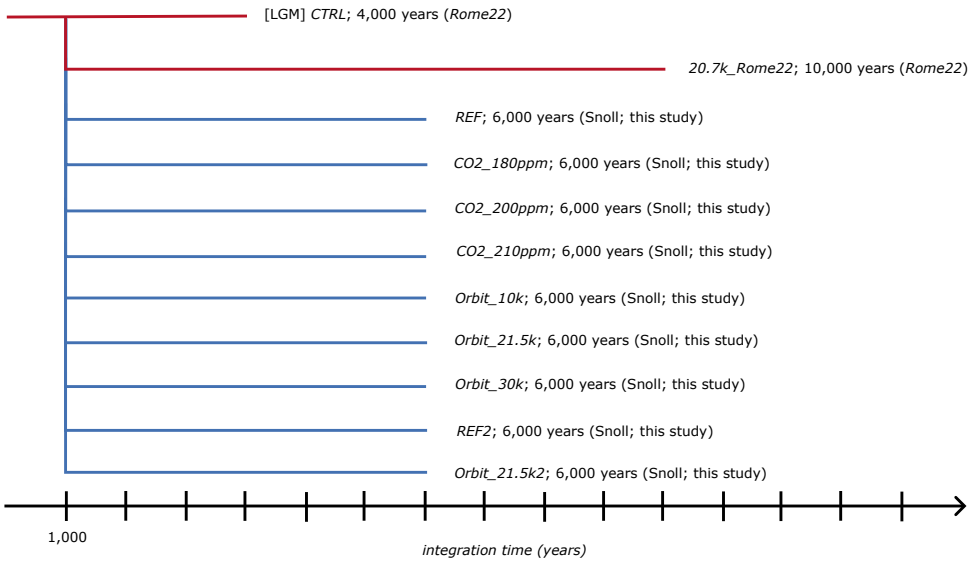

Figure 3.13: Timeline of the experiments included in this study and who generated them.

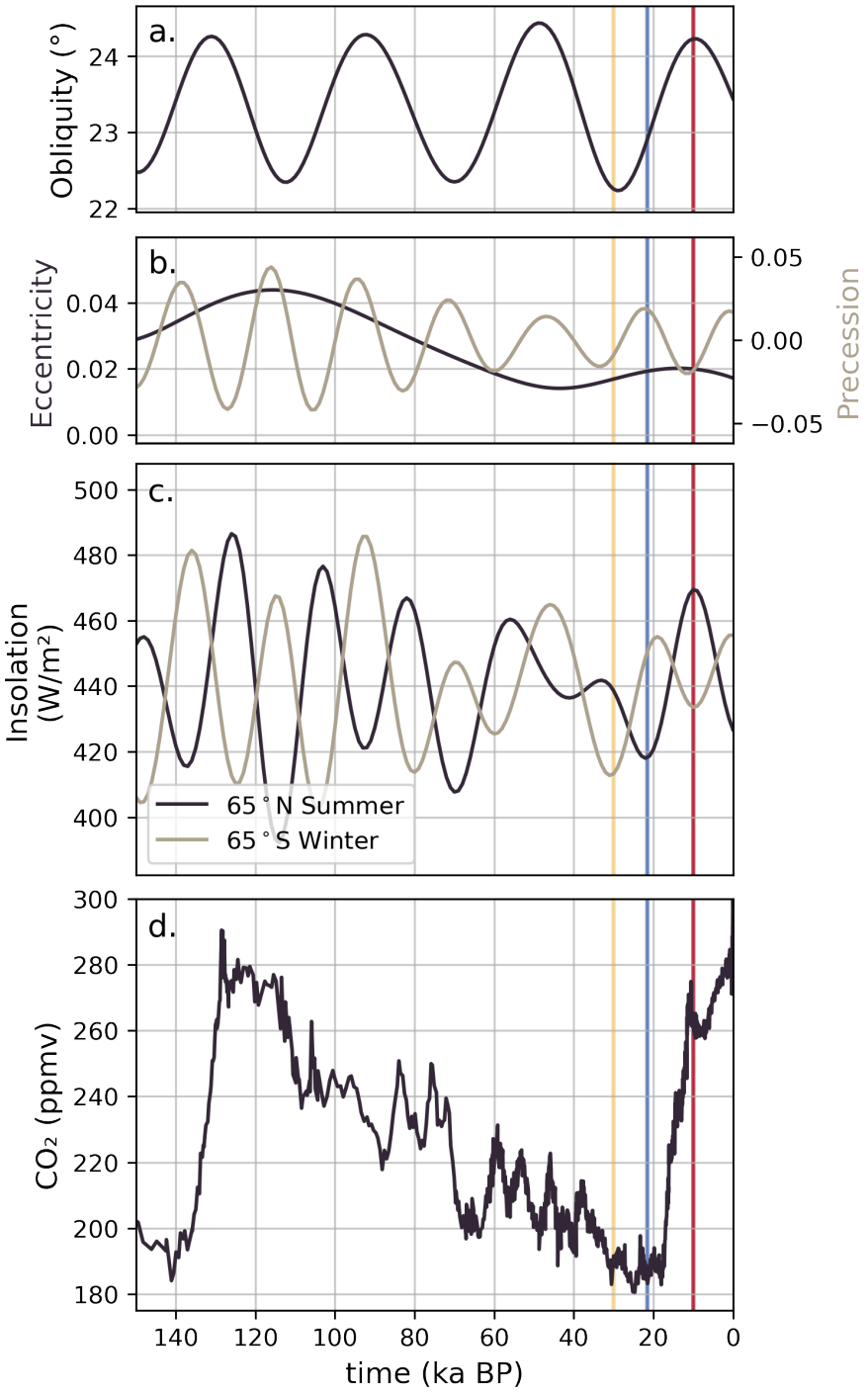

Figure 3.14: (a) - (b) Earth's orbital variation, (c) the impact on incoming solar radiation at the top of the atmosphere (Berger 1978), and (d) atmospheric CO_2 concentration throughout the last 150 thousand years (Köhler et al. 2017).

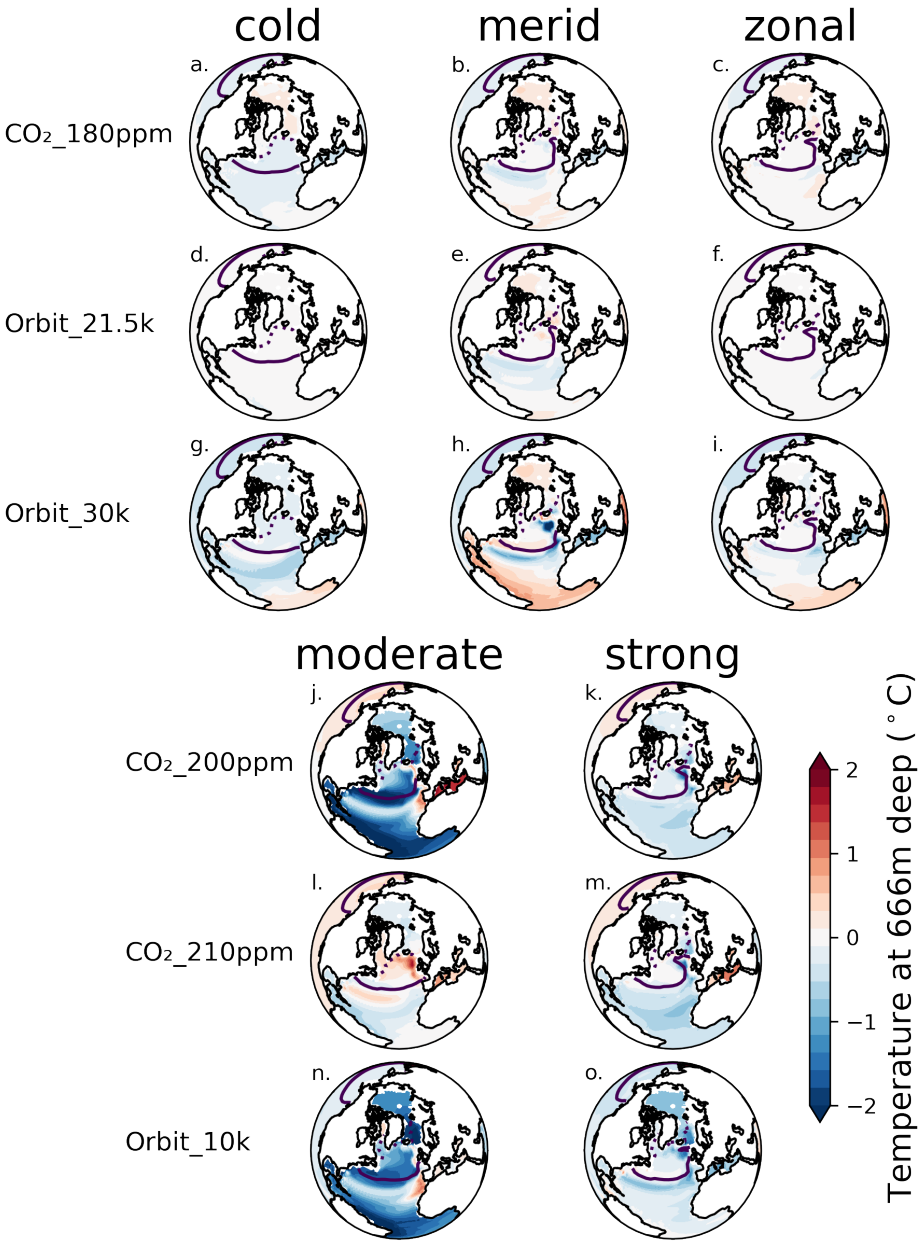

Figure 3.15: (a) - (i) Annual subsurface temperature (666 metres deep) anomaly from *REF* averaged for each AMOC mode (*cold*, *meridional*, and *zonal*). (j) - (o) Same as (a) - (i) but AMOC modes are defined by '*strong*' (greater than 14.5 Sv) and '*moderate*' (10-14.5 Sv) for *CO2_200ppm*, *CO2_210ppm*, and *Orbit_10k* and *REF* is defined by '*strong*' (greater than 14.5 Sv) and '*moderate*' (less than or equal to 14.5 Sv). For all, the solid line depicts March sea ice extent (15% cover) and the dashed line depicts September sea ice extent.

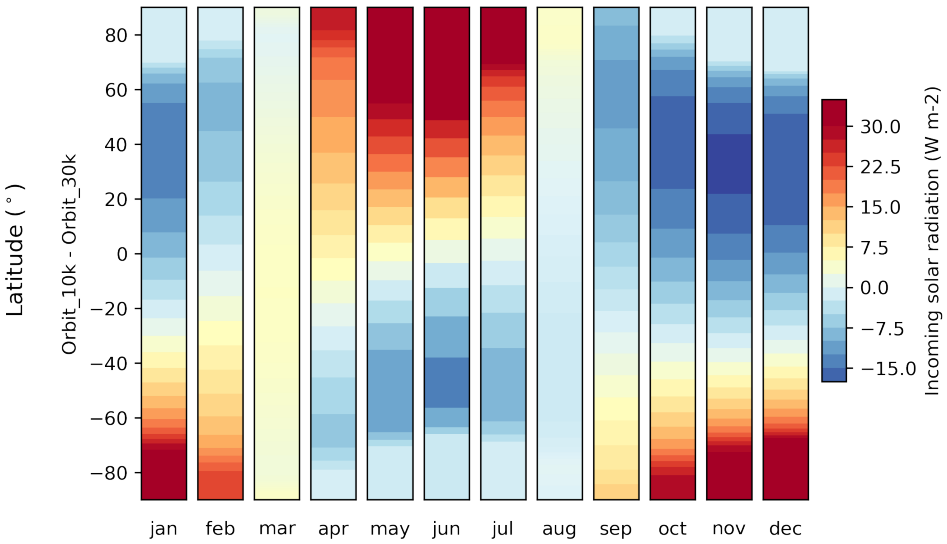

Figure 3.16: Incoming solar radiation anomalies between *Orbit_10k* and *Obrit_30k* for each latitude in each month of the year.

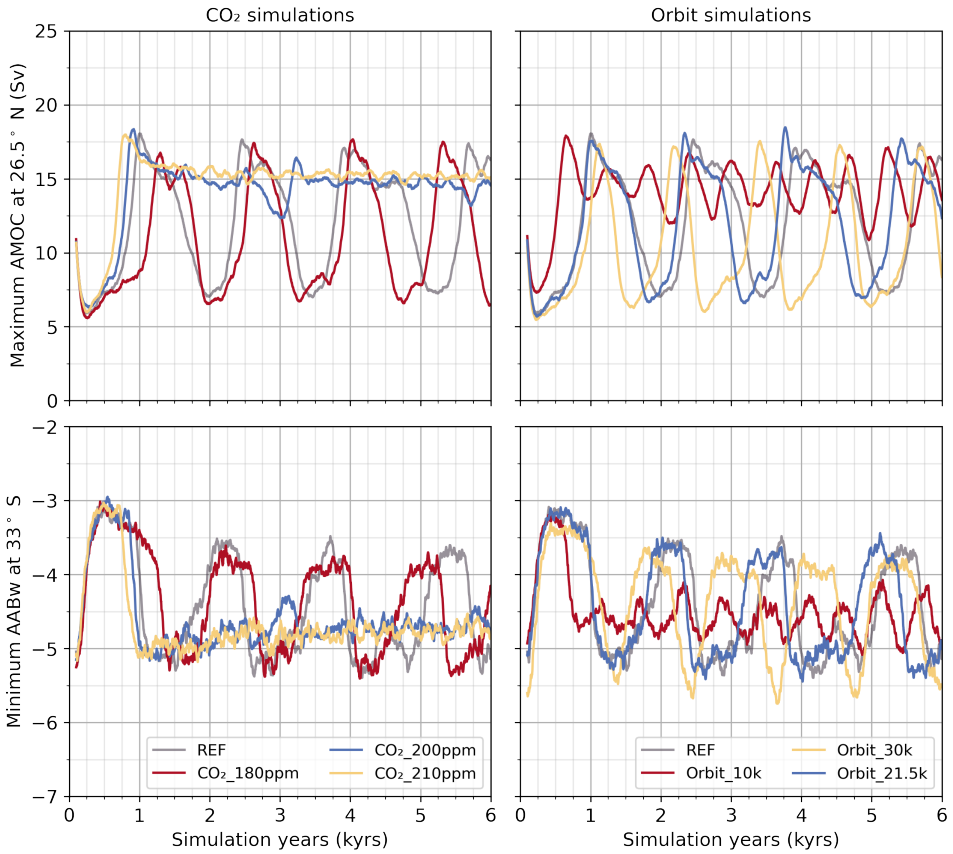

Figure 3.17: Top row: Maximum Atlantic meridional overturning circulation (AMOC) strength at 26.5° N. Bottom row: Minimum Antarctic bottom water strength at 33° S. Data are shown as 100-year rolling means.

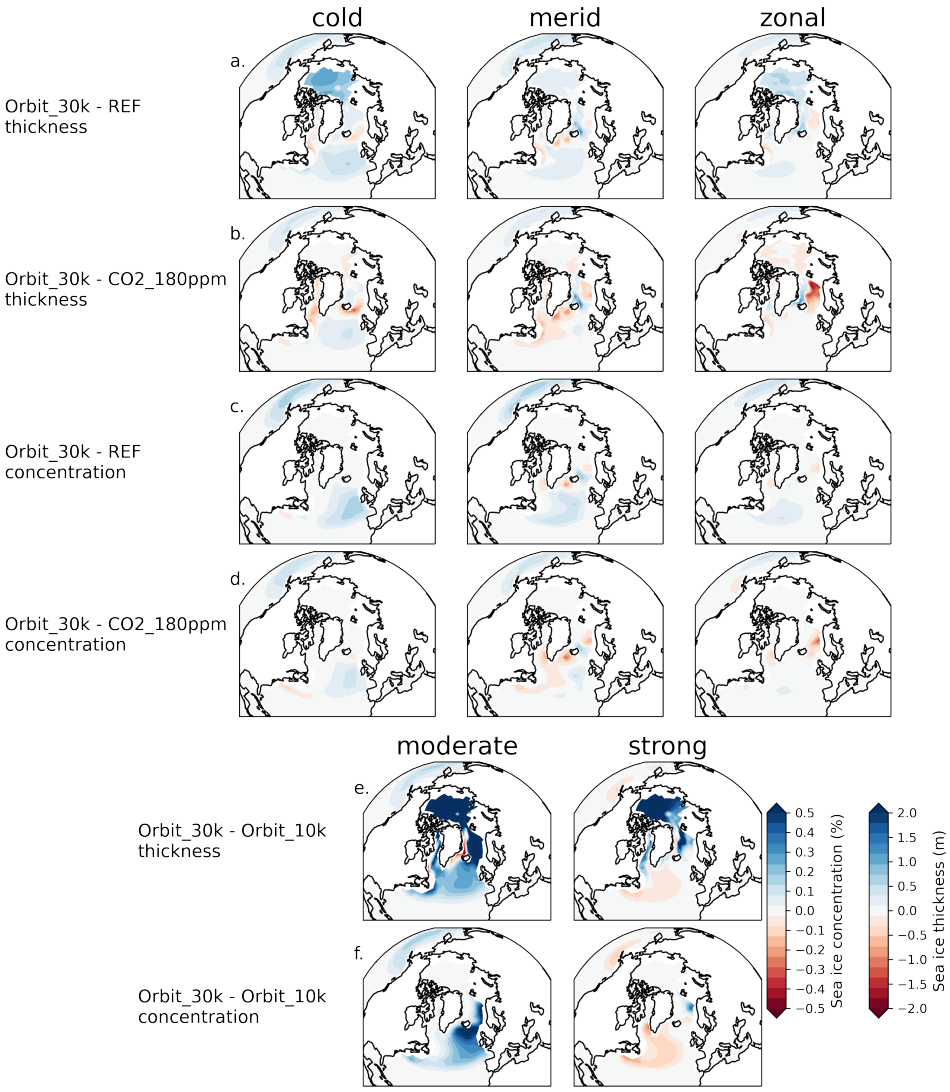

Figure 3.18: (a) - (d) December-January-February sea ice concentration and sea ice thickness anomalies averaged for each AMOC mode (cold, meridional, and zonal). (e) - (f) December-January-February sea ice concentration and sea ice thickness anomalies averaged for each AMOC mode–moderate (<14.5 Sv) and strong (>14.5 Sv).

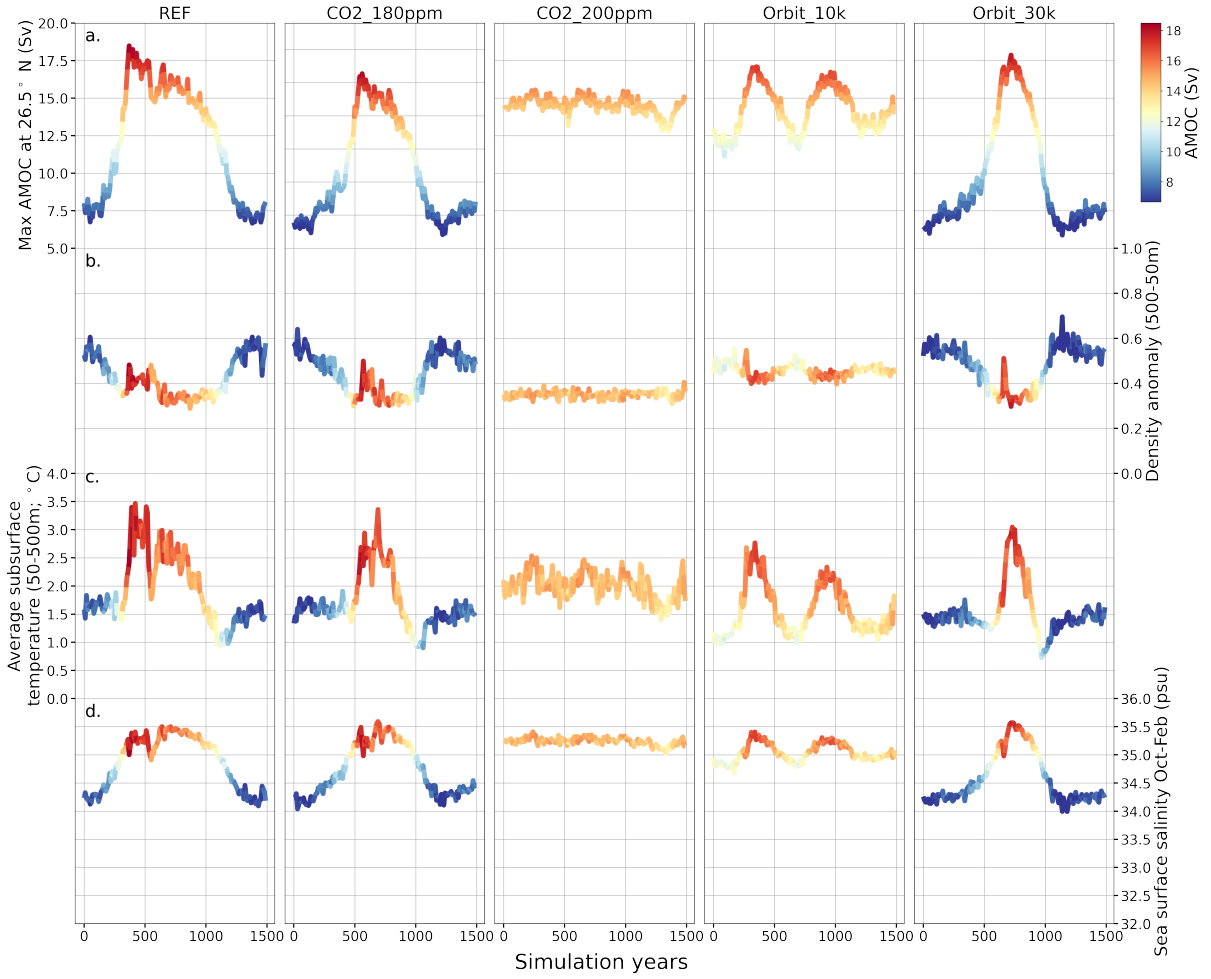

Figure 3.19: (a) Maximum AMOC strength at 26.5° N, (b) density anomaly between 500 and 50 metres for the Irminger Sea, (c) mean ocean temperature between 50 metres depth and 500 metres depth in the Irminger Sea, (d) sea surface salinity in the sea ice formation months (October to February) in the Irminger Sea for one oscillation of each of the sensitivity experiments. The colour map is normalised to the max AMOC strength in REF (a) as shown in the colour bar. All data are shown as decadal means. *CO2_210ppm* and *Orbit_21.5k* are like *CO2_200ppm* and *REF* respectively so are left out of this figure for simplicity.

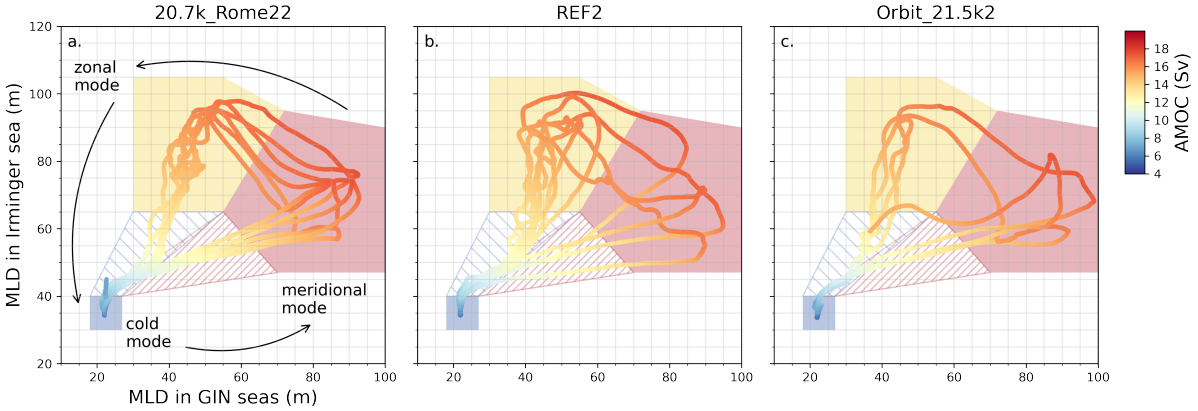

Figure 3.20: (a) - (c) Mixed-layer depth (MLD) in the Irminger Sea as a function of mixed-layer depth in the GIN Seas with the colours representing maximum strength of the AMOC at 26.5° N. Red shading represents the *meridional* phase, yellow shading is the *zonal* phase, and blue shading represents the *cold* phase. Red hatched region is the transition between the cold and *meridional* phase (or the *warming* phase), and blue hatched region is the transition between the *zonal* and *cold* phase (or the *cooling* phase). The map in Figure 3.4 in the main text illustrates what locations are used to represent the GIN seas and the Irminger Sea.

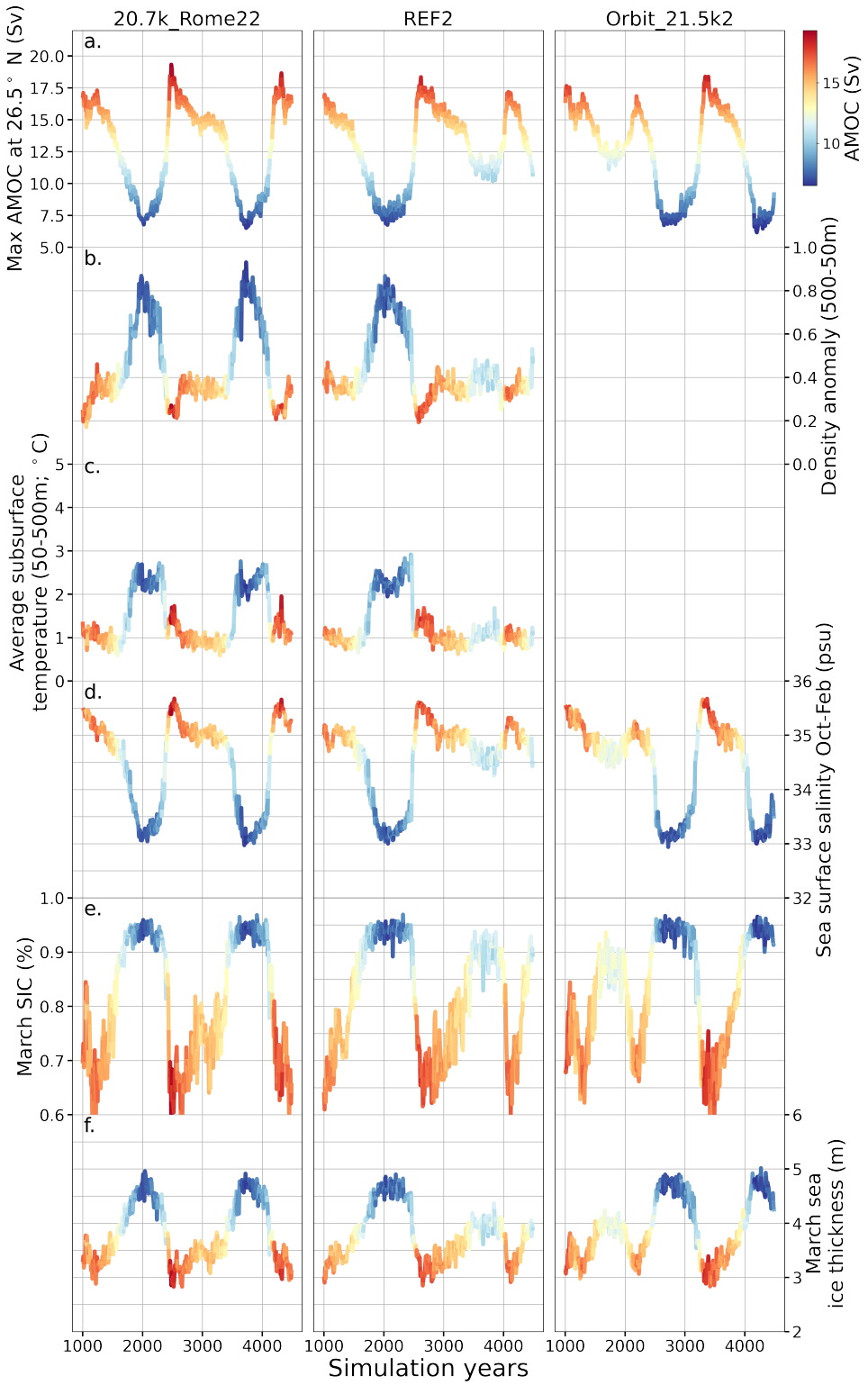

Figure 3.21: (a) Maximum AMOC strength at 26.5° N, (b) Density anomaly between 500 and 50 metres for the GIN seas, (c) Average ocean temperature between 50 metres depth and 500 metres depth in the GIN seas, (d) sea surface salinity in the sea ice formation months (October to February) in the GIN seas, (e) average sea ice concentration in March between 50° N and 70° N, and (f) sea ice thickness in March between 50° N and 70° N for one oscillation of each of the sensitivity experiments. The colour map is normalised to the max AMOC strength in *20.7k_Romé22* (a) as shown in the colour bar. All data are shown as decadal means. Deep ocean level data was unavailable for experiment *Orbit_21.5k2*.

CHAPTER 4

Impact of the Bølling Warming on the Northern Hemisphere ice sheets: a coupled climate-ice sheet model study

Preface

This chapter presents new transient last deglaciation coupled climate-ice sheet simulations used to evaluate the impact of the Bølling Warming on the Northern Hemisphere ice sheets and their respective contribution to Meltwater Pulse 1a. The content of this chapter will be submitted to The Cryosphere. It includes contributions from Ruza F. Ivanovic, Lauren J. Gregoire, Sam Sherriff-Tadano, and Violet Patterson. The study conception was developed by BS, RI, and LG. BS, RI, LG, and SST contributed to the study design. BS, RI, and LG designed the experiments, and BS performed them with assistance from VP. Material preparation and data analysis was performed by BS. The manuscript was prepared by BS with contributions from RI, LG, and SST, who read and approved a previous version of this manuscript.

Abstract

Studies have suggested the Bølling Warming caused accelerated melt from the Northern Hemisphere ice sheets that could explain Meltwater Pulse 1a. However, many of these modelling studies do not represent climate-ice sheet feedbacks, only use simple surface mass balance calculations, and/or have not used more complex climate models. Here we present coupled-climate ice sheet model simulations prescribed with surface ocean forcings that include the abrupt climate changes, Heinrich Stadial 1 and the Bøling Warming, we observe during the last deglaciation. We examine the impact of the Bølling Warming on the surface mass balance of the Northern Hemisphere ice sheets and the resulting ice sheet melt and meltwater flux. We conclude that the ice sheets deglaciate faster with the additional warming from the Bølling Warming than without, but that this is dependent on the choice of starting ice sheet topography and prescribed ocean forcing. The prescribed ocean forcing is most influential with marine-based ice sheets, like the Barents-Kara ice sheet. Regardless of the starting ice topography and choice of

ocean forcing, we simulate an abrupt shift in the surface mass balance of the North American ice sheet coincident with the Bølling Warming and a meltwater pulse, but these responses are small compared to previous ice sheet simulations and observation of Meltwater Pulse 1a.

4.1 Introduction

The most recent deglaciation, the *last deglaciation*, marks the transition from the Last Glacial Maximum (LGM; ∼21 thousand years ago, ka BP)–when ice sheets were at their largest extent in North America, Greenland, Eurasia, and Antarctica (Figure 4.1; Dyke 2004; Lambeck et al. 2014; Hughes et al. 2016) and surface temperatures were 4 to 7 °C cooler than present-day (Annan et al. 2022; Liu et al. 2023)–to the Holocene (interglacial period beginning ∼11.7 ka BP). The deglaciation was driven by gradual changes in the orbital configuration and increasing atmospheric greenhouse gases (Loulergue et al. 2008; Schilt et al. 2010; Bereiter et al. 2015), causing the Earth to warm (Jouzel et al. 2007; Buizert et al. 2018), the ice sheets to melt (Gregoire et al. 2012), and sea level to rise (Lambeck et al. 2014).

Sea level and temperature, however, did not rise at a consistent rate. Alongside the major, long-term climate transition from cold glacial to the current warm interglacial state, the last deglaciation is defined by many short-term, decadal- to centennial-scale warmings and coolings (Beaulieu and Reille 1992; Severinghaus and Brook 1999; Lea et al. 2003; Kindler et al. 2014; Buizert et al. 2018). One of these key climate events is the Bølling Warming, which is characterised by abrupt Greenland warming between ∼14.7 and 14.2 ka BP (Severinghaus and Brook 1999; Lea et al. 2003; Buizert et al. 2018), as well as other sites in Europe (e.g. Grafenstein et al. 1999; Hoek 2009; García-Alix et al. 2014; Druzhinina et al. 2023), at the end of a cold period known as Heinrich Stadial 1 (Shakun et al. 2012; Martin et al. 2023; Naughton et al. 2023). At around the same time (∼14.7 to 14.3 ka BP), a notably large abrupt sea level rise event occurs, known as Meltwater Pulse 1a (MWP1a; Fairbanks 1989; Deschamps et al. 2012; Lambeck et al. 2014). During MWP1a, records show global sea level rose by 8-22 meters in ∼350 years or less (Deschamps et al. 2012; Liu et al. 2016), but the origin MWP1a has long been debated and is further confounded by the occurrence of the Bølling Warming at the same time. It is reasonable that warming would cause ice sheet melt (e.g., Gregoire et al. 2016), but an Atlantic-bound meltwater pulse, such as MWP1a, would weaken the Atlantic Meridional Overturning Circulation (AMOC; Rahmstorf 1999; Brown and Galbraith 2016) and cause a cooling effect in the Northern Hemisphere (Ivanovic et al. 2017).

In attempt to reconcile this paradox through the theory of the bipolar see-saw effect, or the concept that meridional heat transport leads to asynchronous temperature changes in the hemispheres (Stocker 1998; Weaver 2003), older studies have focussed on contributions to MWP1a from Antarctica (Clark et al. 1996; Golledge et al. 2014; Weber et al. 2014). However, this has since been refuted, with the balance of evidence suggesting that (a) a meltwater pulse draining into the Southern Ocean would only induce non-linear responses dependent on the magnitude of the freshwater discharge and speed at which it is dispersed from the Southern Ocean (Swingedouw et al. 2009; Menviel et al. 2010) or climate changes that were restricted to the Southern Hemisphere (Ivanovic et al. 2018a; Yeung et al. 2019), and (b) that the Northern Hemisphere ice

sheets most likely released the majority if not all of the meltwater pulse (Peltier 2004; Tarasov et al. 2012; Lambeck et al. 2014; Peltier et al. 2015; Lambeck et al. 2017; Lin et al. 2021).

There is also some disagreement over the total contribution from the Eurasian ice sheet; some studies suggest that the marine sectors of the ice sheet deglaciated well before Meltwater Pulse 1a and the Bølling Warming (Clark et al. 1996; Hormes et al. 2013; Hughes et al. 2015), whilst others have argued that the ice sheet was a source of ∼3-8 metres sea level equivalent (m SLE) volume loss towards MWP1a based on a revised Eurasian chronology (Brendryen et al. 2020; Lin et al. 2021; Coonin et al. 2025). Multiple studies have pointed to the Laurentide-Cordilleran ice saddle collapse ∼14.9-13.6 ka BP as a major contributor (Gregoire et al. 2012; Lin et al. 2021), providing a compelling link between the abrupt warming and a large meltwater event (Gregoire et al. 2016). However, there is a large temporal uncertainty over precisely when such a saddle collapse occurred, undermining this hypothesis (Menounos et al. 2017; Reyes et al. 2024).

To learn more about the chain of events of the deglaciation and how warming can impact ice sheets, modelling groups have begun to more frequently utilise ice sheet models to investigate atmosphere-ocean-ice interactions (e.g., Abe-Ouchi et al. 2007; Gregoire et al. 2012; Carlson et al. 2012; Gregoire et al. 2016; Obase et al. 2021). Surface temperature warming, such as from the Bølling Warming, causes the surface mass balance (the sum of rainfall and snowfall minus sublimation, run-off, and eroded snow) of the ice sheets to become significantly more negative, leading to increased melting on ice sheets and glaciers and thus more run-off and reduced snow accumulation (Nowicki et al. 2016; Favier et al. 2017; Seroussi et al. 2020). The significant climate changes and variability associated with changes in Northern Hemisphere ice sheets during the last deglaciation highlight the need for realistic representation of surface mass balance (Fyke et al. 2018).

Gregoire et al. (2016) use an ice sheet model, GLIMMER-CISM, and input from the *TraCE-21ka* simulation (Liu et al. 2009) to determine the impact of the Bølling Warming on the Northern Hemisphere ice sheets. In their simulations, the Bølling Warming leads to the Cordilleran-Laurentide saddle collapse and a respective 5-6 m SLE contribution to MWP1a from the North American ice sheet in 340 years, corroborating the results of Carlson et al. (2012) who simulate a 5.8-8 metre contribution of the Laurentide ice sheet with an energy-mass balance model. Petrini et al. (2020) also prescribe their ice sheet model with *TraCE-21ka* conditions but focus on the Barents Sea ice sheet (Figure 4.1), simulating a ∼2 m SLE contribution to MWP1a between 15 and 14 ka BP. However, each of these studies utilise stand-alone representations of surface mass balance and therefore cannot consider atmosphere-ocean-ice interactions.

To do this, interactive ice sheet models can be coupled to climate models as carried out in transient simulations of the last deglaciation with Earth system models of intermediate complexity (EMIC; e.g., Charbit et al. 2005; Roche et al. 2014; Heinemann et al. 2014; Ganopolski and Brovkin 2017; Quiquet et al. 2021b). EMICs, compared to general circulation models (GCMs), are often used as they are less computationally expensive to run. Whereas studies with more complex climate models have been focused on shorter timescales (e.g., Ridley et al. 2005; Ziemen et al. 2014; Vizcaino et al. 2015; Muntjewerf et al. 2020) or equilibrium tests

of model parameters (e.g., Patterson et al. 2024; Sherriff-Tadano et al. 2024; Patterson et al. 2025). The transient simulations of the last deglaciation highlight the difficulty in simulating abrupt climate changes, as they often only simulate a gradual warming during the deglaciation, and therefore cannot determine the impact of the events on the ice sheets.

Only a recent study from Mikolajewicz et al. (2024) successfully models the last deglaciation with spontaneous abrupt climate change events utilising an atmosphere-ocean general circulation model fully coupled to an ice sheet model. The abrupt events are either caused by melt from massive iceberg discharges or freshwater input into the Arctic from the Laurentide ice sheet, both of which lead to a weakening the AMOC and surface cooling in the North Atlantic. After each rapid cooling event, there is an immediate respective increase in AMOC strength and temperature, but there are no abrupt climate changes simulated that can directly correspond to the timing or magnitude of the events recorded in the deglaciation (e.g., Mikolajewicz et al. (2024) simulate abrupt sea surface temperature changes of less than or approximately equal to 4°C–less than half the recorded magnitude of the Bølling Warming).

In this study, we aim to investigate the impact of the Bølling Warming on the Northern Hemisphere ice sheets with the atmosphere component of a GCM (FAMOUS) coupled to an ice sheet model (BISICLES). Utilising a GCM incorporates the more complex physical processes to simulate abrupt climate change, whilst prescribing sea surface temperatures and sea ice concentration from previously preformed transient simulations of the last deglaciation (similar to *TraCE-21ka*) ensures that we include abrupt events like those recorded in the Greenland temperature record (Buizert et al. 2018). We experiment with different surface ocean forcings and starting ice sheet conditions to determine the impact on the patterns of ablation and accumulation of the Northern Hemisphere ice sheets and conclude on the resulting potential sea level rise and how it corresponds to the timing of MWP1a.

4.2 Methods

4.2.1 Model descriptions

The FAst Met Office/UK Universities Simulator (FAMOUS) is a low resolution atmosphere-ocean general circulation model (AOGCM) derived from the Hadley Centre general circulation model (HadCM3; Smith et al. 2008). FAMOUS uses roughly half the horizontal resolution of HadCM3 in both the atmosphere and ocean, therefore requiring only about 10% of the computational resources of HadCM3 whilst still retaining the complexity of the processes represented in an AOGCM. This study uses the atmospheric component of FAMOUS, which is a hydrostatic, primitive equation grid point model with a horizontal resolution of 7.5 °longitude by 5 °latitude and 11 vertical levels (Smith et al. 2008). Land processes are modelled using the MOSES2.2 land surface scheme consisting of a set of sub-grid-scale tiles in each grid box to represent fractions of nine different surface types, including land ice (Smith et al. 2021). Although we prescribe sea surface temperatures and sea ice concentration, FAMOUS can also be utilised fully coupled with a dynamic ocean (e.g., Dentith et al. 2019).

FAMOUS, in the configuration FAMOUS-ice (Smith et al. 2021), is two-way coupled to the ice

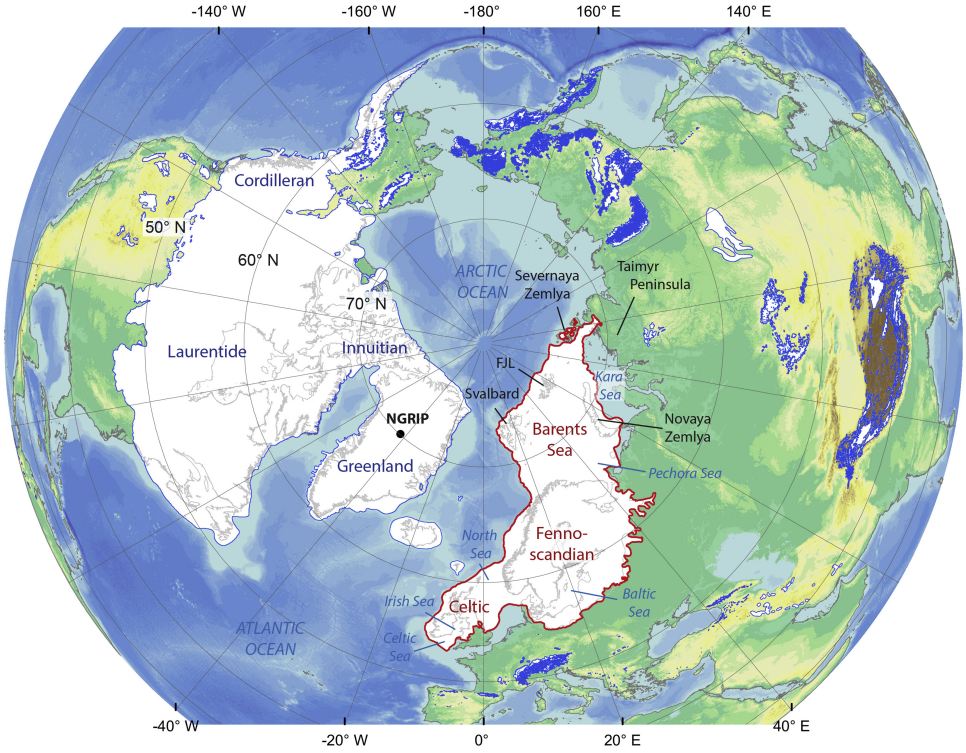

Figure 4.1: Map of Northern Hemisphere ice sheets. Taken from Patton et al. (2016).

sheet model BISICLES. BISICLES is a vertically integrated ice flow model based on the L1L2 dynamical scheme (Schoof and Hindmarsh 2010; Cornford et al. 2013). The L1L2 approximation is a variant of Glen's flow law that includes longitudinal and lateral stresses and approximates vertical shear strains in vertically integrated models (Schoof and Hindmarsh 2010). BISICLES also includes adaptive mesh refinement (AMR) that allows the model to perform quickly and suitably models ice shelves and fast flowing ice streams without the need for approximations, such as the shallow shelf and shallow ice approximations. Where required, the model can simulate at high resolution, whilst the rest of the domain (i.e., the slower moving interior of the ice sheets) remains at lower resolution, thus increasing the efficiency of the model (Cornford et al. 2013). BISICLES has previously been used to successfully simulate the ice streams and retreat of the marine based British-Irish ice sheet at the last deglaciation (Gandy et al. 2018; Gandy et al. 2019; Gandy et al. 2021), the final retreat of the North American ice sheet during the early Holocene (Matero et al. 2020), produce an initial condition of the present-day Greenland ice sheet (Lee et al. 2015), and model the future evolution of the Antarctic ice sheet (Cornford et al. 2015; Siahaan et al. 2022). Additionally, FAMOUS-BISICLES has been used to explore the sensitivity of the North American and Greenland ice sheets at the Last Glacial Maximum to model parameter values through large ensemble analysis (Sherriff-Tadano et al. 2024).

We use the updated version of BISICLES developed by Gandy et al. (2019), which implements a pressure limited basal sliding law that is sensitive to the presence of till water. This is mostly found to be applicable near the grounding line, and the inclusion of the Coulomb sliding law has been shown to have an effect on ice sheet stability in models, with greater grounding line retreat occurring in simulations that include this law than those without (Schoof 2006; Tsai

et al. 2015; Nias et al. 2018). The upper surface temperature boundary condition in the ice sheet model (surface heat flux) is determined by the climate model and the basal boundary condition (basal heat flux) is set as a constant flux (3 x 10^6 J a^{-1} m^{-2}). The effective pressure, and therefore the basal sliding, depends on the basal water pressure and thus the depth of the till water layer. Once the englacial drainage water fraction *(w)* grows beyond a certain value (0.01) it is drained to a till layer at a rate proportional to the water fraction, up until a maximum water fraction (0.05). The till water is then transported elsewhere by the basal hydrology model (Pelt and Oerlemans 2012). It is lost vertically at a rate proportional to the till water depth which is determined by the specified till water drain factor (*drain*). The implementation of this basal sliding scheme coupled with this hydrology parameterisation allows the simulation of spontaneous ice stream generation and evolution (Gandy et al. 2019; Gandy et al. 2021).

Sub-shelf melt rate is calculated with prescribed subsurface ocean temperatures (as shown in equation below, where *ssm* is the subshelf melt rate in metres per year; m/yr, c is a constant, T_{ocn} is prescribed subsurface temperature, and T_f is the freezing point of sea water). The freezing point of water is calculated using the parameterisation of Beckmann and Goosse (2003), which takes into account the salinity of the water at the particular depth of the subsurface temperature. In this study, we use -2.27 °C as the freezing point of water.

$$ssm(m/yr) = c(T_{\mathrm{ocn}} - T_{\mathrm{f}})$$

Glacial isostatic adjustment (GIA) of bedrock topography due to changes in the ice sheet load is included through coupling BISICLES to a simple Elastic Lithosphere Relaxing Asthenosphere (ELRA) model, which approximates this response by assuming a fully elastic lithosphere above a uniformly viscous asthenosphere (Kachuck et al. 2020). A relaxation time of 3000 years is applied in this model based on previous studies (Pollard and DeConto 2012). This method does not account for changes in the gravitational pull that ice sheets exert on sea level or adjustments in Eustatic sea level caused by changing global ice sheet volume (e.g., Gomez et al. 2010).

Sherriff-Tadano et al. (2024) found that some of the FAMOUS-BISICLES simulations of the North American ice sheet at the LGM exhibit a strong local melting of the ice sheet from parts of the interior. This phenomenon is caused by warm temperature biases over the ice sheet interior in the atmospheric model, which are amplified by the downscaling method and a positive height-mass balance feedback. The warm temperature bias is due to the low resolution of FAMOUS. In reality, a very cold atmospheric layer often forms at the surface of the ice sheet, especially in the interior, which induces a stable boundary layer and isolates the cold surface from the ambient warm air. However, a global climate model cannot resolve the effect of the stable boundary layer and overestimates the exchange of heat between the surrounding atmosphere and the ice sheet surface. As a result, FAMOUS overestimates the temperature in the ice sheet interior and causes a high equilibrium line altitude (ELA) bias, which results in surface melt.

Name	Value	Unit	Definition
daice	-0.34546	K^{-1}	Darkening effect of warm surface air temperature on bare ice in the albedo scheme, mimicking water collecting at the surface (Smith et al. 2021)
fsnow	725.274	kgm^{-3}	Density threshold for snow in the albedo scheme beyond which the surface starts to be regarded as bare ice (Smith et al. 2021)
avgr	0.000176	μm^{-3}	Dependence of snow albedo on increasing grain size (Smith et al. 2021)
rhcrit	0.671611	no units	Threshold of relative humidity to form large-scale clouds (Smith 1990)
Vf1	1.212316	ms^{-1}	Speed of ice sedimentation (Heymsfield 1977)
ct	0.00026	s^{-1}	Conversion rate of cloud liquid water droplets to precipitation (Smith 1990)
cw_sea	0.0004213	kgm^{-3}	Threshold value of cloud liquid water for formation of precipitation (Smith 1990); over sea only
cw_land	0.001128	kgm^{-3}	Threshold value of cloud liquid water for formation of precipitation (Smith 1990); over land only
tgrad	-0.00203	Km^{-1}	Air temperature lapse rate used during the downscaling to ice sheet surfaces (Smith et al. 2021)
elevcon	1.278856	no units	Height correction; scaling factor for the height of the vertical levels read by the ice sheet model
beta	35590.47831	$Pam^{-1/3}a^{1/3}$	Coefficient in Weertman friction law (Gandy et al. 2019)
coef	0.5	no units	Coefficient in Coulomb friction law (Gandy et al. 2019)
drain	0.023486381	myr^{-1}	Magnitude of drainage removing water from the till (Gandy et al. 2019)
n	3.0	no units	Coefficient in Glen's flow law

Table 4.1: Summary of parameter values chosen for this version of FAMOUS-BISICLES.

We mitigate the effect of the warm temperature bias by modifying the height adjustment of atmospheric surface temperature to the ice tiles across the entire ice sheet through the introduction of a new parameter in the model, called *elevcon* (see the impact of *elevcon* in Figure 4.17). The *elevcon* parameter affects the surface temperature and surface mass balance during the height adjustment to the ice sheet tiles by multiplying the effective elevation by the value of *elevcon*. For example, a value of 1.10 means that the elevation of an 1,800 metre tile has been increased by 10%, or to 1,980 metres. Surface air temperatures and longwave radiation are then downscaled to each increased elevation tile, and surface fluxes and surface mass balance are calculated based on the downscaled variables and other variables from the original FAMOUS grid. The surface mass balance and surface fluxes are passed to the ice sheet and atmospheric but are taken to represent the original tile elevation, not the increased elevation to which the surface temperature was downscaled to. For example, the surface air temperature and surface mass balance could be calculated on a 1980 metre elevation tile, but they will be passed to the ice sheet and atmospheric models as outputs from an 1800 metre elevation tile. In this way, additional cooling is applied over the ice sheet interior by *elevcon*, which can be regarded as elevation-dependent height adjustment over ice sheets. This crudely mimics the effect of the

stable boundary layer in maintaining the cold surface condition in that area.

BISICLES has 10 vertical layers, which increase in thickness from 2% of ice thickness near the base to 15% of ice thickness near the surface. The resolution over the ice sheet is 16 km, but areas of ice streaming over the Barents-Kara ice sheet are refined to 2 km in our model setup to better represent smaller scale grounding line processes.

The parameter values tested by Patterson et al. (2025) and used for this version of FAMOUS-BISICLES are shown in Table 4.1. The parameter, *tgrad*, is the air temperature lapse rate used for calculations of surface air temperature (as in Figure 4.11). The average elevation of the particular area of interest is calculated, multiplied by the lapse rate (-0.00203 per kilometre), and added to the surface air temperature over the region.

4.2.2 Experimental design

4.2.2.1 *HadCM3_TraCE* versus *iTraCE* ocean forcing

To represent the effect of abrupt climate changes in the atmosphere-only climate model, we prescribe sea surface temperatures and sea ice concentration from two different simulations of the last deglaciation: *HadCM3_TraCE* (Snoll et al. 2024) and *iTraCE* (He et al. 2021), providing two ocean forcing scenarios. Both of these original simulations followed the Palaeoclimate Modelling Intercomparison Project version 4 (PMIP4) protocol for modelling the last deglaciation (Ivanovic et al. 2016). The ICE-6G_C ice sheet reconstruction is prescribed and updated every 500 years in *HadCM3_TraCE* and every 1,000 years in *iTraCE*. *iTraCE* uses the carbon dioxide record by Lüthi et al. (2008) whereas *HadCM3_TraCE* uses the record suggested by the PMIP4 protocol by Bereiter et al. (2015) (Figure 4.2b), however they both match the AICC2012 age model with carbon dioxide concentration starting to increase at ∼18 ka BP (Veres et al. 2013). Both simulations prescribe a meltwater flux based on the *TraCE-21ka A* last deglaciation simulation (Figure 4.2f; Liu et al. 2009) that follows a common interpretation of the AMOC history through this period (e.g., Ng et al. 2018; McManus et al. 2004) with a simulated Heinrich Stadial 1 (weak AMOC) and Bølling Warming (rapid AMOC strengthening).

During the last deglaciation, the sea surface temperature evolution in the North Atlantic is relatively similar in *HadCM3_TraCE* and *iTraCE* (Figure 4.2c). Sea surface temperatures start between 7 and 10 °C and decrease ∼5 °C between 18 and 17.5 ka BP for Heinrich Stadial 1 in the North Atlantic. Sea surface temperatures then remain cold until 14.7 ka BP, when the Bølling Warming occurs and a rapid warming of 7 to 10 °C occurs.

Nevertheless, during much of the early deglaciation *HadCM3_TraCE* sea surface temperatures are at least 1-2 °C higher than those in *iTraCE*. The greatest difference between sea surface temperatures occurs between ∼18 and 17.3 ka BP, when temperatures in the *HadCM3_TraCE* simulation are almost 5 °C warmer, attributed to a lag in cooling. The start of the abrupt cooling into Heinrich Stadial 1 for *iTraCE* is at 18 ka BP, whereas this strong cooling does not occur until ∼17.5 ka BP in *HadCM3_TraCE*, therefore allowing the North Atlantic to remain warmer for a longer period of time. Whilst the simulations are both in the Heinrich stadial, the sea surface temperatures return to only about a degree apart, with *HadCM3_TraCE* warmer.

Simulation reference name	Timing of forcing (ka BP)	BISICLES integration length (yrs)	Accelerated	LSM change	Initial ice sheet condition	Ocean forcing
Acc_H21-15	21-15	6000	yes	no	End of LGM equilibrium run (Patterson et al. 2025)	*HadCM3_TraCE*
H15-13	15-13	2000	no	no	*Acc_H21-15* at 15 ka BP	*HadCM3_TraCE*
Acc_H15-13	15-13	2000	yes	no	*Acc_H21-15* at 15 ka BP	*HadCM3_TraCE*
H15-13_LSM	15-13	2000	no	yes	*Acc_H21-15* at 15 ka BP	*HadCM3_TraCE*
Acc_H15_SST	SSTs and SIC at 15 ka BP; Orbit and GHGs 15-13 ka BP	2000	yes	no	*Acc_H21-15* at 15 ka BP	*HadCM3_TraCE*
Acc_H15-13_Orb	SSTs, SIC, and GHGs at 15 ka BP; Orbit 15-13 ka BP	2000	yes	no	*Acc_H21-15* at 15 ka BP	*HadCM3_TraCE*
Acc_H15	15	2000	yes	no	*Acc_H21-15* at 15 ka BP	*HadCM3_TraCE*
H15-13_GLAC	15-13	2000	no	no	GLAC-1D at 15 ka BP	*HadCM3_TraCE*
Acc_H15_GLAC_SST	SSTs and SIC at 15 ka BP; Orbit and GHGs 15-13 ka BP	2000	yes	no	GLAC-1D at 15 ka BP	*HadCM3_TraCE*
Acc_iT21-15	21-15	6000	yes	no	End of LGM equilibrium run (Patterson et al. 2025)	*iTraCE*
iT15-13	15-13	2000	no	no	*Acc_iT21-15* at 15 ka BP	*iTraCE*
iT15-13_LSM	15-13	2000	no	yes	*Acc_iT21-15* at 15 ka BP	*iTraCE*
Acc_iT15_SST	SSTs and SIC at 15 ka BP; Orbit and GHGs 15-13 ka BP	2000	yes	no	*Acc_iT21-15* at 15 ka BP	*iTraCE*
Acc_iT15	15	2000	yes	no	*Acc_iT21-15* at 15 ka BP	*iTraCE*

Table 4.2: Detail of simulations referenced in this study. See Figure 4.16 for the timeline of the experiments included in this study and who generated them.

At the Bølling Warming, *iTraCE* warms at a faster rate and to a higher level (∼3 °C warmer). While *HadCM3_TraCE* reaches similar temperatures (∼13 °C about 200 years later), sea surface temperatures quickly drop back down by a few degrees, showing an 'overshoot'-like behaviour, leaving *iTraCE* sea surface temperatures to be warmer for most of the period following the Bølling Warming, except for between ∼14.2 to 13.9 ka BP, where *iTraCE* has an Older Dryas-type event.

When comparing Greenland surface air temperature between the simulations and Buizert et al. (2018), both *HadCM3_TraCE* and *iTraCE* are warmer than the temperature proxy record suggests (Figure 4.2g). At 20 ka BP, the simulations and Greenland proxy record differ by over 10 °C. This discrepancy decreases during Heinrich Stadial 1 as *HadCM3_TraCE* and *iTraCE* cool by 7-10 °C, whereas Buizert et al. (2018) observe only a 4 °C cooling. Greenland surface air temperature in the climate simulations and proxy record are most comparable during the warm period after the abrupt warming. Because the temperature evolution in the two simulations is different, and both are warmer than the Greenland ice core record suggests throughout the whole simulation, it is difficult to identify which simulation performs 'best'. We judge that both are reasonable approximations for how sea surface conditions may have evolved and therefore for this study, we explore both scenarios.

The largest differences between the simulations are present in the Northern Hemisphere sea ice concentration and subsurface temperatures in the Barents-Kara Seas (Figure 4.2). Previous studies have used subsurface temperatures at ∼400 metres deep as that is approximately the Barents Sea grounding line depth (Petrini et al. 2018; Clark et al. 2020). However, due to data availability, subsurface temperatures are represented by different depths (666 metres deep is used for *HadCM3_TraCE*, whereas for *iTraCE* 400 metres deep is used). The similarity in subsurface temperature between the ocean at 400 m and 666 m deep is dependent on the depth of the mixed layer. If the mixed layer does not reach as deep as 666 m, as common when convection is weak, it is expected that the subsurface temperatures at 400 m would be warmer than those at 666 m. In this case, the opposite is true, and subsurface temperatures in *iTraCE* are colder than the deeper ocean temperatures of *HadCM3_TraCE* at all times except for between 14.7 and 14 ka BP when there is an abrupt ∼4°C increase at the time of the Bølling Warming.

The discrepancy between the expected differences in subsurface temperature between *HadCM3_TraCE* and *iTraCE* could be due to the concentration of sea ice in the North Atlantic. *HadCM3_TraCE* has significantly more sea ice, potentially contributing to more insolation of the subsurface ocean, whereas *iTraCE* ocean temperatures are more susceptible to the atmospheric temperatures (Figure 4.2e).

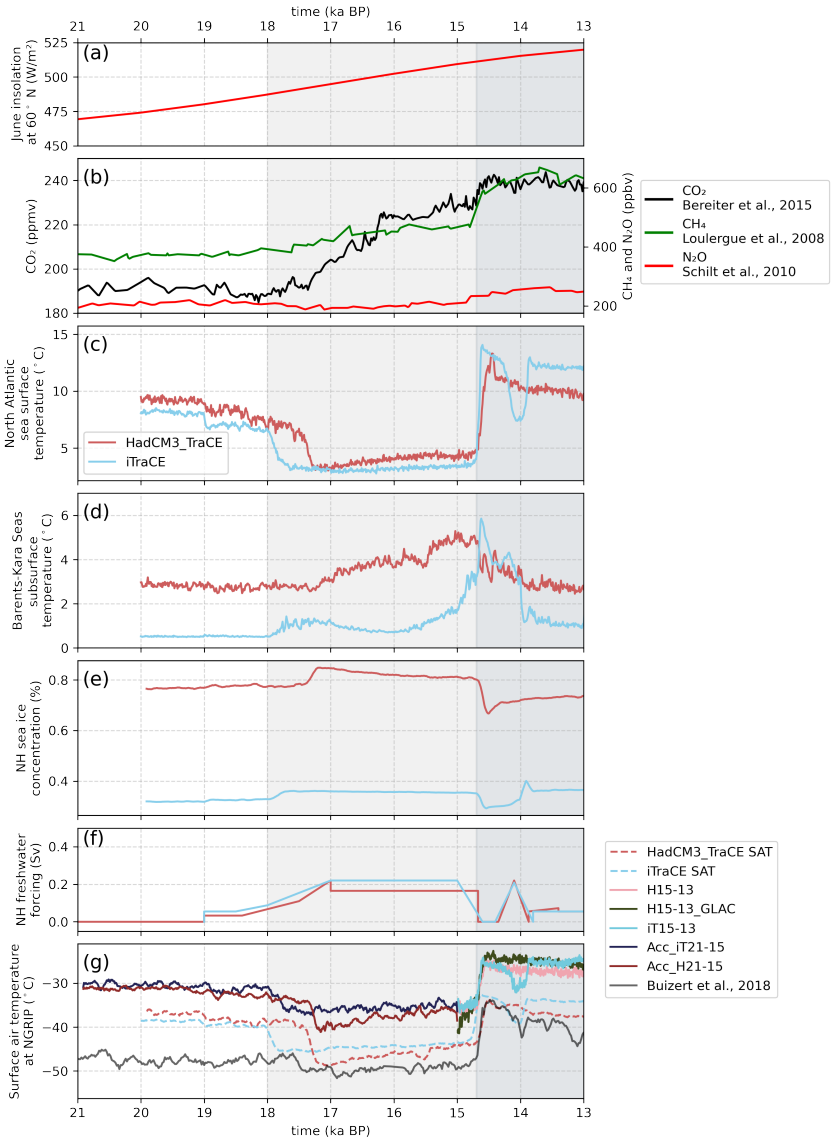

Figure 4.2: (a) Insolation (combined impact of the respective orbital parameters of Berger (1978)) prescribed for all simulations in this study. (b) Greenhouse gas concentrations prescribed in simulations and used in initial *iTraCE* and *HadCM3_TraCE* simulations. (*iTraCE* actually uses Lüthi et al. (2008), but this is on the same timescale as Bereiter et al. (2015) and hence is comparable). (c) North Atlantic (between 40 and 70° N and 60 and 115° E) sea surface temperature forcing (from *HadCM3_TraCE* and *iTraCE*). (d) Sub-surface temperature forcing in the Barents and Kara Seas (between 70 and 85° N and 10 and 60° E and at 666 m deep for *HadCM3_ TraCE*, 400 m deep for *iTraCE*) with the freezing point of water subtracted (-2.27 °C). (e) Sea ice concentration north of 50° N forcing (from *HadCM3_TraCE* and *iTraCE*) (f) Northern Hemisphere freshwater forcing used in *HadCM3_TraCE* and *iTraCE*. (g) Surface air temperature at Greenland Summit from *HadCM3_TraCE* and *iTraCE* compared to the output from the simulations performed as part of this study as well as the Greenland temperature proxy record from Buizert et al. (2018).

2934

4.2.2.2 Initialising the ice sheet: 21-15 ka BP

To reach 15 ka BP boundary conditions in the climate and ice sheet models, we performed transient coupled climate-ice sheet simulations from 21 to 15 ka BP. The model parameter values in Table 4.1 were chosen based on the 'not ruled out yet' LGM simulations from Patterson et al. (2024). We found that the parameter set-ups that matched with the two best performing LGM model configurations (in terms of both ice sheet volume and extent criteria) were too stable and did not adequately deglaciate, potentially as a result of several factors (independently, or in combination). The simulated maximum extent ice sheets may have been spun-up to equilibrium under constant glacial conditions for too long, when in reality it is likely that the glacial maxima climates were never in equilibrium, or the simulated maximum extents may be too big, however, Patterson et al. (2025) show that the ice volume and extents were at the lower end of palaeo-constraints so this is unlikely, or, finally, the model may be unable to deglaciate from a plausible glacial maximum ice sheet due to some model bias. A single model configuration may not be sufficiently flexible to be applied across all time periods, as also demonstrated by Gandy et al. (2023). To overcome this, we selected a 'not ruled out yet' simulation that, after 5,000 years of ice sheet integration, met the extent constraint, but fell short on the volume criteria. The resulting LGM ice sheet volume is approximately 10 m SLE less than the total ice volume in the GLAC-1D ice sheet reconstruction at 21 ka BP mostly originating from the Greenland (∼2 m SLE shortfall) and Eurasian (∼6 m SLE shortfall) ice sheets (Figure 4.5). The ICE-6G_C ice sheet reconstruction has an additional ∼5 m SLE in total ice sheet volume (attributed to thicker Greenland and North American ice sheets). Despite the differences in ice sheet volume, ice sheet extent is similar to reconstructions in most areas (Figure 4.3), with the largest discrepancies in the smaller size of the Eurasian ice sheet and the less extensive southern margin of the North American ice sheet.

To start the deglaciation, we initialised our model with the smaller LGM ice sheet, which proved to be more susceptible to early deglacial climate forcing and match reconstructions of the deglaciation relatively well (Figure 4.6; also discussed in later sections).

HadCM3_TraCE and *iTraCE* sea surface temperatures and sea ice concentration data is available only from 20 to 13 ka BP. To alleviate the gap between the 21 ka BP starting ice sheet conditions and the start of the available sea surface temperatures and sea ice concentration, an equilibrium/transient hybrid simulation was performed between 21 and 20 ka BP for each ocean forcing scenario (*HadCM3_TraCE* and *iTraCE*) in an accelerated coupling format. The accelerated coupling means that the ice sheet model and climate model are coupled, in our case, every 10 years, or there are 10 ice sheet years for every 1 climate year. For each of these respective runs, monthly climatologies for sea surface temperatures, sub-shelf melt rate (i.e., subsurface temperatures), and sea ice concentration were fixed at 20 ka BP conditions from the associated last deglaciation simulation (*HadCM3_TraCE* or *iTraCE*), whilst the other FAMOUS-BISICLES climatological boundary conditions were transient (i.e., orbital configuration and greenhouse gases) and updated every 10 years during the coupling to the climate model. This first 1,000 ice sheet years (100 climate years) of the two simulations were then continued from 20 to 15 ka BP with the respective fully transient forcings (orbital parameters

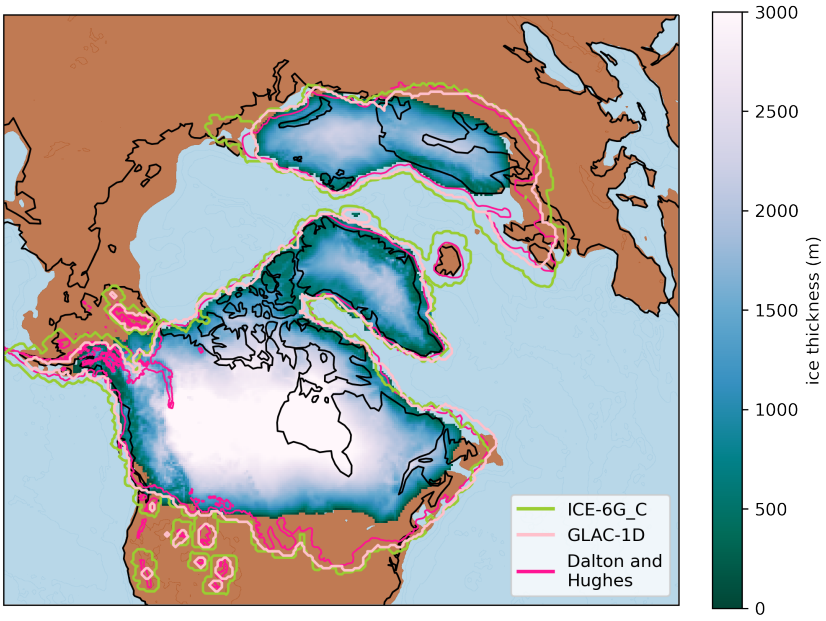

Figure 4.3: Initial 21 ka BP ice sheet geometry compared to reconstructions of ice extent (ICE-6G_C in green, GLAC-1D in pale pink, Dalton et al. (2023) for the North American and Greenland ice sheets and Hughes et al. (2015) for the Eurasian ice sheet in deep pink).

and atmospheric trace gases; plus ocean surface forcing from *HadCM3_TraCE* and *iTraCE*).

From 20-15 ka BP, the accelerated format was also used. To account for this, sea surface temperatures and sea ice concentration were selected monthly every 10 years from *HadCM3_TraCE* or *iTraCE* output and then prescribed in the climate model. The sub-shelf melt rate calculation in BISICLES uses subsurface temperatures from the respective simulations, and as with the surface ocean forcings, they are transient and updated every 10 years. The 20-15 ka BP segment of the simulations follows seamlessly on from the 21-20 ka BP segment to produce our two simulations of the LGM-mid deglaciation transition; *Acc_H21-15* (*HadCM3_TraCE* ocean forcing) and *Acc_iT21-15* (*iTraCE* ocean forcing) simulations.

4.2.2.3 The abrupt event: 15-13 ka BP

After 15 ka BP conditions are achieved with the *HadCM3_TraCE* and *iTraCE* ocean forcings, we performed two not accelerated simulations (with synchronous years between the climate and ice sheet models) from 15-13 ka BP; *H15-13* (*HadCM3_TraCE* ocean forcing) and *iT15-13* (*iTraCE* ocean forcing). During this 2,000-year window, we aim to capture the response of the ice sheets to the Bølling Warming event induced by prescribed sea surface temperature and sea ice concentration. The experiments are not accelerated to utilise the full temporal resolution of the abrupt climate warming.

4.2.2.4 Sensitivity experiments

We also performed multiple sensitivity experiments to test various research questions (Table 4.2) such as, the impact of the Bølling Warming as prescribed in the surface ocean forcing and

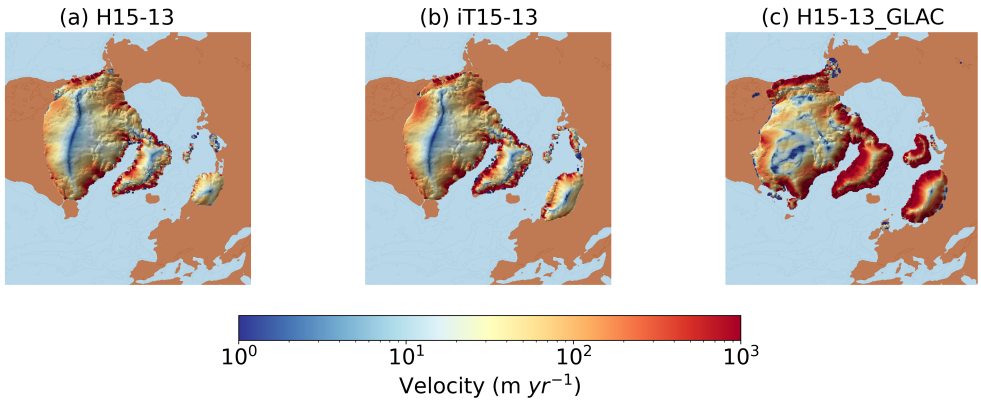

Figure 4.4: Initial 15 ka BP ice sheet thickness and velocity for (a) the *H15-13* simulation (also for *H15-13_LSM*, *Acc_H15_SST*, and *Acc_H15-13*), (b) the *iT15-13* simulation (also for *iT15-13_LSM* and *Acc_iT15_SST*), and (c) the *H15-13_GLAC* simulation (and *Acc_H15_GLAC_SST*). (a) and (b) are from the first ice sheet year of the simulation, whereas (c) is from ice sheet year 50 to account for the equilibrating ice sheet.

the comparative response to greenhouse gases or orbital configuration, the importance of the starting ice sheet conditions, the affect of the accelerated coupling format, and the influence of updating land-sea mask after a Barents-Kara ice sheet collapse.

To evaluate the impact of the Bølling Warming on the Northern Hemisphere ice sheets, we performed the *Acc_H15_SST* (with *HadCM3_TraCE* forcing) and *Acc_iT15_SST* (with *iTraCE* forcing) simulations with constant ocean forcings at 15 ka BP conditions (i.e., sea surface temperatures, subsurface temperatures, and sea ice concentration) but with transient orbit and greenhouse gas concentrations. Both simulations are integrated for 2,000 ice sheet years in the accelerated format. This simulations serves as a 'control' experiment to determine the impact of the sea surface temperature and sea ice concentration changes during 15-13 ka BP when compared to *H15-13*. However, because the greenhouse gas concentrations still show a Bølling Warming signal, we investigated experiments with complete constant forcings (i.e., including orbit and greenhouse gases; *Acc_H15* and *Acc_iT15*) and as well as a simulation with exclusively transient orbit (only for *HadCM3_TraCE*; *Acc_H15-13_Orb*).

For each of the *HadCM3_TraCE*-based sensitivity tests, we start from the 15 ka BP ice sheet produced in *Acc_H21-15* (Figure 4.4a), and for each of the *iTraCE*-based sensitivity tests, we start from the 15 ka BP ice sheet produced in *Acc_iT21-15* (Figure 4.4b). Both starting ice sheets have a total ice sheet volume of ∼10 meters sea level equivalent (m SLE) less than the GLAC-1D ice sheet reconstruction due to smaller Eurasian and Greenland ice sheets (∼4-6 m SLE less ice in each; Figure 4.4c), meaning that large parts of Eurasian ice sheet have already melted before 15 ka BP. Surface mass balance depends not only on the climate, but also on the geometry of the ice sheet (extent and elevation) primarily because of ice albedo and elevation controls. We, therefore, test the impact of a different starting ice sheet topography on the response of the ice sheets to the Bølling Warming with *H15-13_GLAC* and a respective constant forcing run, *Acc_H15_GLAC_SST*. The results of these simulations are mostly contained to the

supplementary figures.

To test the impact of climate-ice acceleration, *Acc_H15-13* is the same as *H15-13* but with an accelerated climate forcing (i.e., 2,000 ice sheet year integration, but only 200 climate year integration). Often ice sheet models are utilised with an accelerated set-up due to the long response time of ice sheets to the climate changes; however, these simulations often also do not contain abrupt and rapid changes. We use this sensitivity experiment to test the impact of the acceleration setting when there is an abrupt warming as opposed to a gradual climate forcing.

We test the impact of a land-sea mask update with the *HadCM3_TraCE* and *iTraCE* forcings. *H15-13_LSM* corresponds with *H15-13* and *iT15-13_LSM* corresponds with *iT15-13* except that at 15 ka BP (i.e., at the start of the simulation), we update the land-sea mask from an LGM land-sea mask to one that resembles the ice sheet changes that have occurred between 21 and 15 ka BP, that is, to conditions at 15 ka BP in *Acc_H21-15* or *Acc_iT21-15* respectively. The difference between the LGM land-sea mask and that of 15 ka BP ice sheet conditions is shown in the supplementary information and differs slightly for *HadCM3_TraCE* and *iTraCE* (Figure 4.18). The most significant change between the LGM and 15 ka BP is the melting of the marine-based sector of the Eurasian ice sheet, opening up part of the Barents Sea. Thus, this is the area of focus when updating the land-sea mask. Often land-sea mask is not updated in ice sheet model simulations; however, we hypothesised that especially around the Eurasian ice sheet, this could make a significant difference in the deglaciation and timing of melting events (Alvarez-Solas et al. 2019; Petrini et al. 2020). The results of *Acc_H15-13*, *H15-13_LSM*, and *iT15-13_LSM* are mostly contained in the supplementary information.

All of the simulations conducted in the not accelerated format unexpectedly failed after ∼1000 years. The simulations with a land-sea mask update crashed only once 1005 years in, whereas the simulations without a land-sea mask update failed twice, 955 years in and 1955 years in. At the point of the failure, the last climate year was corrupted. We still aren't certain as to the source of the malfunction, but we suspect based on previous work in the research group that it was due to unrealistically high values of snow fall resulting in abnormally high accumulation in one grid cell. To resolve these failures and continue with the run, we started a new simulation from the year before the crash and cleared the start dump of high snow fall values by starting all snow fall values at zero. These simulations were then concatenated together. Note that the transition between simulation phases across these points of concatenation are seamless; we do not observe any jumps in the climate or ice sheet model output.

4.3 Results and discussion

4.3.1 Pattern of deglaciation: 21-13 ka BP

During the early part of the last deglaciation (i.e., in our case, before the Bølling Warming), there is cooling throughout the six thousand year period in the North Atlantic (Figure 4.2c, g). Despite this, there is ∼18-20 m SLE of total ice volume melt in *Acc_H21-15* and *Acc_iT21-15* (Figure 4.5). Half of the ice sheet melt comes from the Eurasian ice sheet, specifically the marine-based sector over the Barents and Kara seas. About a third of the ice volume loss is

from the margins of the North American ice sheet, and the rest is attributed to the Greenland ice sheet.

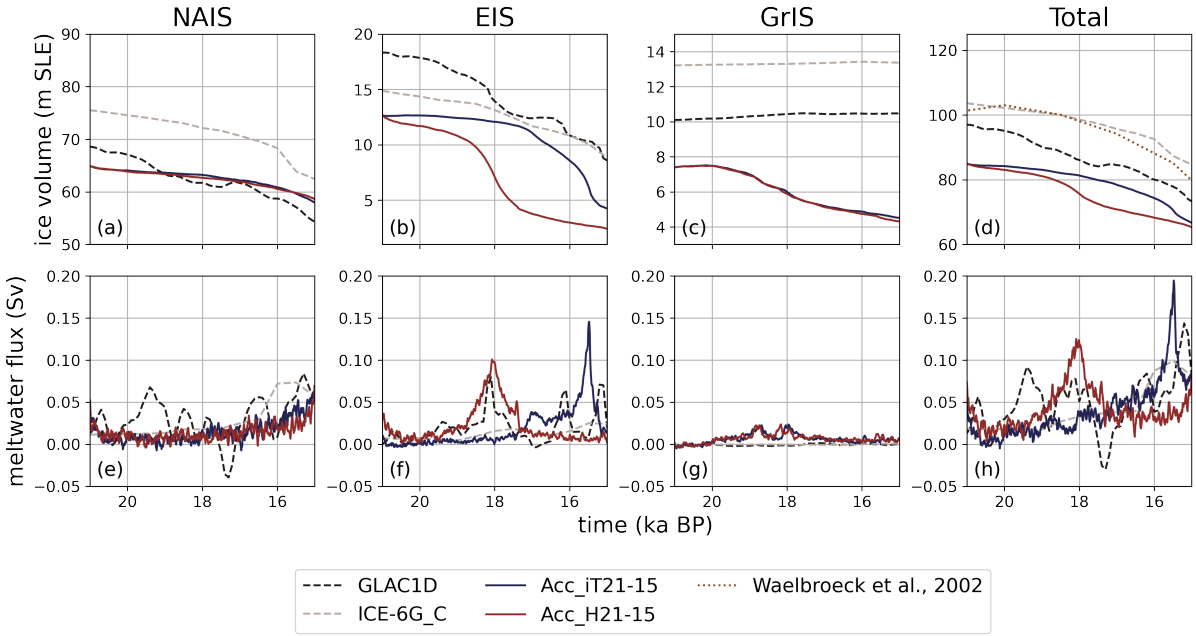

Figure 4.5: (a)-(d) Ice volume from the early deglaciation experiments compared to ice sheet reconstructions GLAC-1D and ICE-6G_C averaged over the North American ice sheet (NAIS), Eurasian ice sheet (EIS), the Greenland ice sheet (GrIS), and all three ice sheets in total compared to the global relative sea level reconstruction by Waelbroeck et al. (2002) with 14 m SLE subtracted to represent Antarctica (Huybrechts 2002; Briggs et al. 2014). (e)-(h) Meltwater flux as derived from the ice volume curve compared to ice sheet reconstructions. See Figure 4.21a for defined area of ice sheet.

Very early in the deglaciation, beginning ∼19 ka BP, an ice stream south of Svalbard in the Barents Sea begins to widen in *Acc_H21-15* (Figure 4.6b). By 18.5 ka BP, a large sector of the Eurasian ice sheet has melted, and by 18 ka BP half of the marine-based ice sheet is gone, completely melting by 17 ka BP and releasing a relatively large meltwater pulse of ∼0.1 Sv (Figure 4.5f and 4.7). The GLAC-1D ice sheet reconstruction also has a meltwater pulse peaking at the same time (18 ka BP) and of a similar magnitude. The rapid melting and collapse of the northern Barents-Kara ice sheet in *Acc_H21-15* corresponds to a period of gradual cooling in the *HadCM3_TraCE* sea surface temperatures (Figure 4.2c), as well as a period of stable subsurface temperature in the Barents and Kara Seas (Figure 4.2d). However, warmer waters infiltrate from lower latitudes into the Arctic after 18 ka BP (Figure 4.22), and by 15 ka BP, the southern sector of the Eurasian ice sheet has also melted, leaving only about a third of the ice sheet left from the LGM. The melting of the marine-based sector of the Eurasian ice sheet occurs more gradually in the ice sheet reconstructions (Figure 4.5).

When the ice stream begins to widen in *Acc_H21-15*, at 19 ka BP, the Eurasian ice sheet in *Acc_iT21-15* is still relatively stable and maintains a consistent ice volume, potentially coincident with the colder subsurface temperatures in the Arctic than in *Acc_H21-15* (Figure 4.22). The anomaly between Eurasian ice sheet volume for the two simulations rapidly increases to nearly 8 m SLE by 17.5 ka BP (Figure 4.5b). However, at ∼17 ka BP, an ice stream be-

gins to widen north of Franz Josef Land (FJL; Figure 4.1), similar to that of *Acc_H21-15* but in a different location and 2,000 years later (Figure 4.6j). Between 17 and 15 ka BP, the marine-based sector of the Eurasian ice sheet rapidly retreats and collapses, leaving only the land-based Fennoscandian ice sheet. During this time, the accelerated ice volume loss catches up to *Acc_H21-15*, and by 15 ka BP, there is a 2 m SLE difference in the Eurasian ice sheet volume between the two simulations (Figure 4.5). The difference in timing of the Barents-Kara ice sheet collapse between *Acc_H21-15* and *Acc_iT21-15* is most likely due to the subsurface temperature differences (section 4.2.2.1) as the Eurasian ice sheet is particularly sensitive to ocean changes (Figure 4.7).

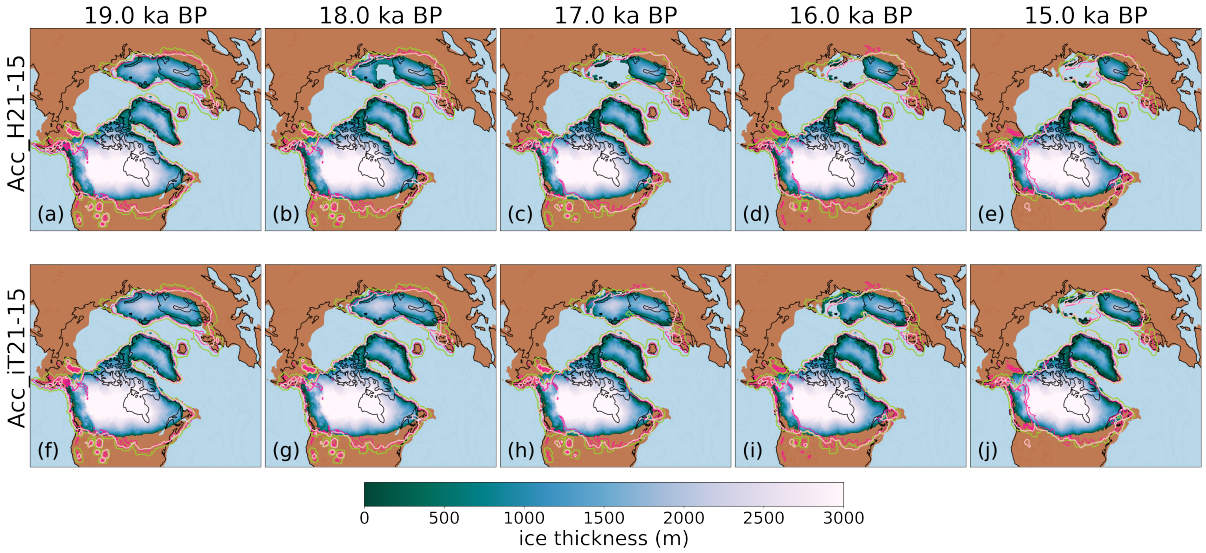

Figure 4.6: Ice sheet thickness during the early deglaciation compared to extent reconstructions and observations. As in Figure 4.3, the yellow-green contour is ICE-6G_C, the pale pink contour is GLAC-1D, and the deep-pink contour is by Dalton et al. (2023) for the North American and Greenland ice sheets and Hughes et al. (2015) for the Eurasian ice sheet.

Ice volume loss originating from the Greenland ice sheet in both simulations is fairly consistent throughout the ice sheet with some higher concentrations of melt on the coasts due to warmer temperatures at lower elevations. The Greenland ice sheet begins ~3-6 m SLE smaller than ice sheet reconstructions suggest and loses ~3 m SLE. This contrasts with our best estimates from reconstructions (GLAC-1D and ICE-6G_C), which show that the Greenland ice sheet is relatively stable during the early deglaciation (Figure 4.5c). There is negligible difference in melt in the North American and Greenland ice sheets, emphasising that most of the difference in total volume loss between the two simulations originates from the Eurasian ice sheet.

Despite starting with smaller ice sheets than GLAC-1D and ICE-6G_C, the simulated ice sheets in both *Acc_H21-15* and *Acc_iT21-15* melt slower and reach 15 ka BP with a total ice volume loss comparable to that of the reconstructions, each with ~20 m SLE of ice volume loss for all Northern Hemisphere ice sheets. The Eurasian and Greenland ice sheets are smaller than observations suggest by ~4-6 m SLE and ~6-9 m SLE respectively, depending on the ocean forcing, but the North American ice sheet reaches a relatively ideal 15 ka BP ice sheet in volume and extent for both simulations (Figure 4.5 and 4.6). At 15 ka BP, North American ice volume

sits directly in the middle of the GLAC-1D and ICE-6G_C estimates. In addition, ending surface temperatures match proxy records in most locations at 15 ka BP (Figure 4.23), both providing a decent starting point for the next 2,000 years.

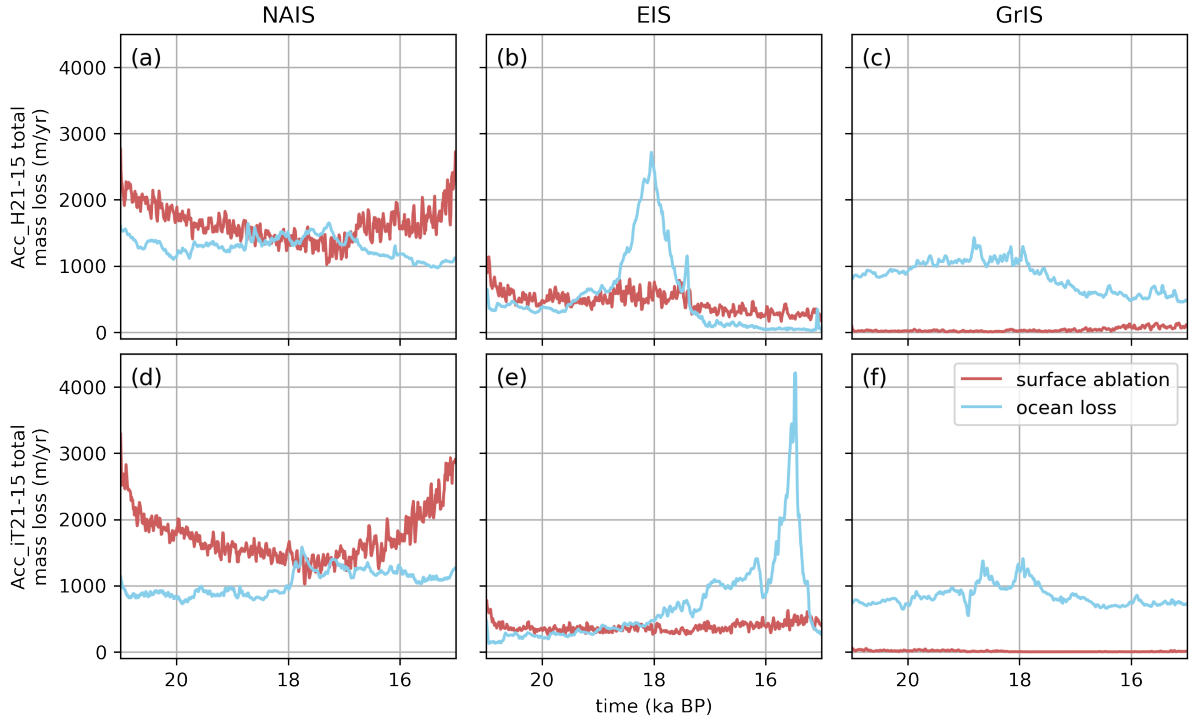

Figure 4.7: Total mass loss separated into surface ablation (red) and ocean loss (or mass loss from calving, ice shelf breakage, etc.; blue) for *Acc_H21-15* (a-c) and *Acc_iT21-15* (d-f) averaged over each ice sheet: North American (NAIS), Eurasian (EIS) and Greenland (GrIS). See Figure 4.21b for the area used to define each ice sheet.

Simulations *H15-13* and *H15-13_GLAC* are forced with *HadCM3_TraCE* sea surface temperatures, and *iT15-13* is forced with *iTraCE* sea surface temperatures between 15 and 13 ka BP. The Bølling Warming begins at 14.7 ka BP with an abrupt increase in North Hemisphere surface air temperature, e.g., 5 °C increase at the NGRIP core site in Greenland (Figure 4.2f) as well as warming in the North Atlantic in the boreal summer months (June-July-August; Figure 4.24). After the abrupt warming, surface air temperatures in Greenland remain warm.

Between 15 and 13 ka BP, *H15-13* loses ~17 m SLE of ice volume, *iT15-13* loses ~14 m SLE, and *H15-13_GLAC* loses ~46 m SLE. Most of this ice loss is attributed to the North American ice sheet with ~15.5 m SLE, ~12 m SLE, and ~31 m SLE of ice mass loss from the respective simulations, followed by just over 1 m SLE, ~2 m SLE, and ~9 m SLE from the Eurasian ice sheet, and the remaining <0.5 m SLE, <0.5 m SLE, and ~6.5 m SLE mass loss from the Greenland ice sheet (Figure 4.9 and 4.20).

For *H15-13_GLAC*, the Eurasian ice sheet is prematurely gone except for a small sector in northern Scandinavia by 13 ka BP (Figure 4.19 and 4.27), whereas a small (a volume of 1.5-2 m SLE) Fennoscandian ice sheet remains for *H15-13* and *iT15-13* (Figure 4.10). The Greenland ice sheet melts over 6 m SLE more than reconstructions suggest (Figure 4.20c) in *H15-13_GLAC*, whereas the ice sheet remains relatively stable in *H15-13* and *iT15-13* betwen 15 and 13 ka BP

but begins ∼6-8 m SLE smaller than in GLAC-1D and ICE6-G_C (Figure 4.9).

The *H15-13*, *iT15-13*, and *H15-13_GLAC* simulations are not able to replicate the specific patterns of ice extent observed in proxy records and reconstructions (Figure 4.27). We do not successfully simulate the timing and pattern of separation between the Laurentide and Cordilleran ice sheets seen in the reconstruction of Dalton et al. (2023), however the simulated southern extent of the North American ice sheet matches the reconstruction well until ∼14 ka BP for *H15-13* and *H15-13_GLAC* and through to 13 ka BP for *iT15-13* (Figure 4.27).

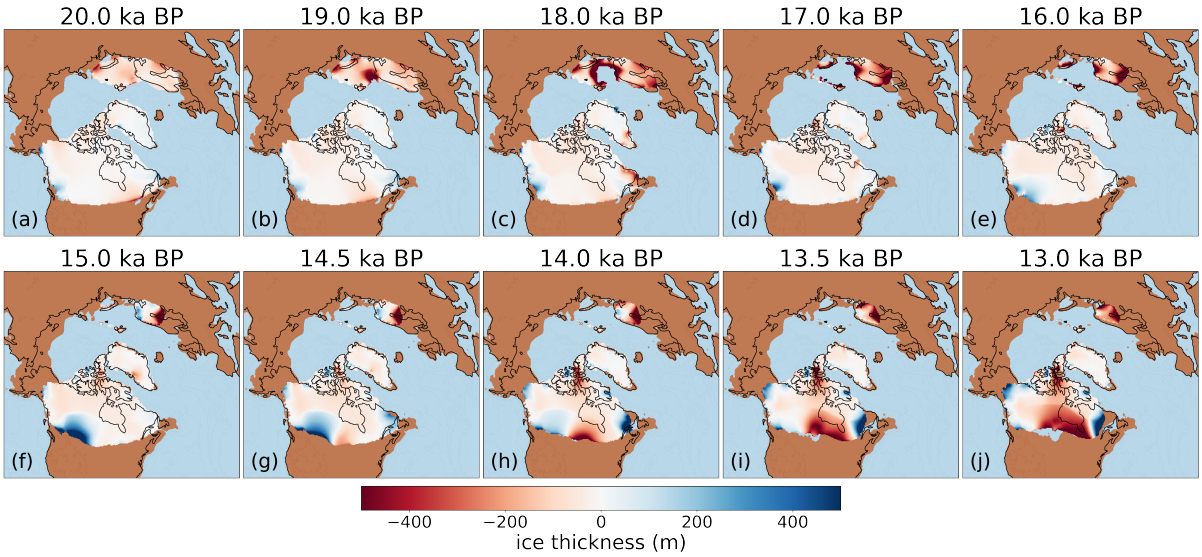

Figure 4.8: (a)-(e) Ice thickness anomaly between *Acc_H21-15* and *Acc_iT21-15* at each timestep. (f)-(j) Ice thickness anomaly between *H15-13* and *iT15-13* at each time step.

Accordingly, in each of these simulations, most of the melt from the North American ice sheet originates from the southern margin (Figure 4.10), the region nearest the warmest surface air temperatures of the lower latitudes (Figure 4.24), rather than from the saddle region. The central southern margin ice loss occurs faster in *H15-13* and *H15-13_GLAC* than with the *iTraCE* ocean forcing, potentially due to the consistently warmer surface temperatures, but notably, the *iT15-13* southern margin is not more extensive everywhere. For instance, the south western margin of the North American ice sheet (or the southern portion of the Cordilleran ice sheet) extends *further* in *H15-13* (Figure 4.8). The thicker ice sheet at southeastern margin in *H15-13* is related to the colder sea surface temperatures with the *HadCM3_TraCE* ocean forcing in the North Pacific along the Cordilleran ice sheet's coastline (Figure 4.28). Comparatively, in the *iT15-13* simulation, more melt occurs at the eastern tip of the Laurentide ice sheet (i.e., over the Gulf of St. Lawrence), a region more impacted by North Atlantic surface temperatures which are warmer for longer in *iTraCE* than *HadCM3_TraCE* between 15 and 13 ka BP. Both simulations produce a small increase in ice thickness around the Hudson Bay region (Figure 4.10), possibly due to the *elevcon* parameter (Figure 4.17).

The significantly larger-scale melt of *H15-13_GLAC* (Figure 4.20) and therefore potential disequilibrium with the climate might suggest that the climate is too warm at 15 ka BP in our simulations compared to our knowledge of this time period. However, there is a lot of consistency

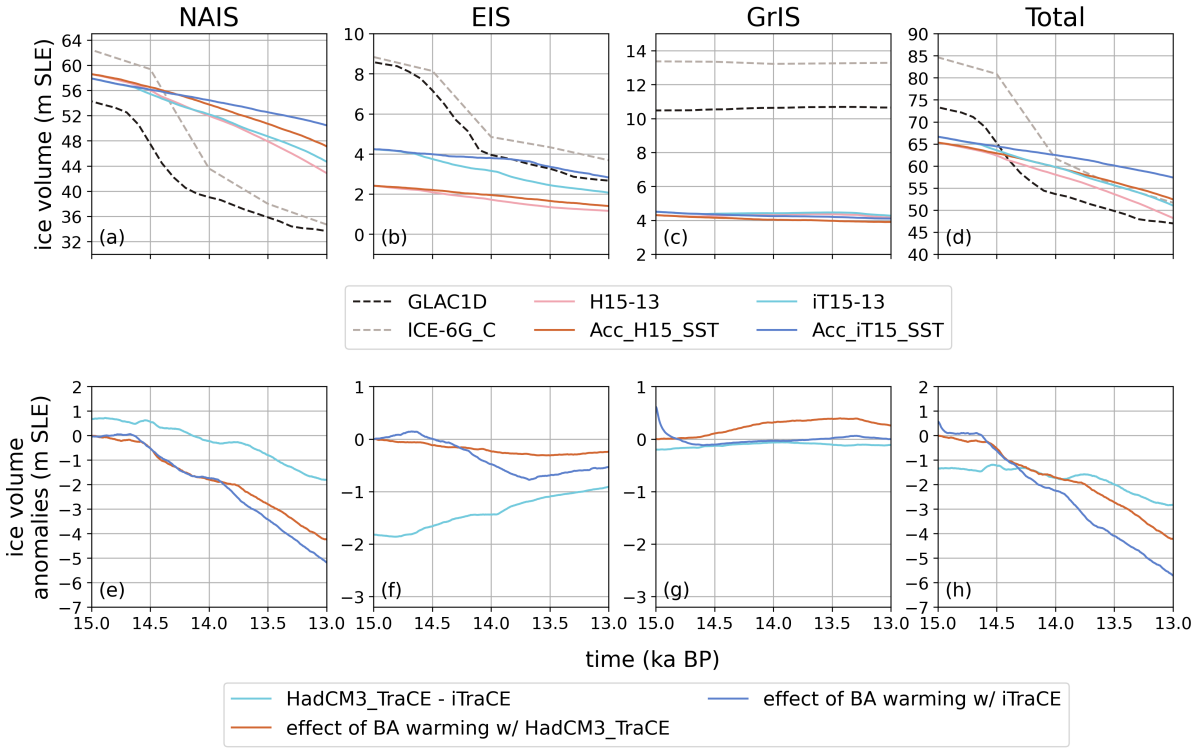

Figure 4.9: (a)-(d) Absolute ice volume for each simulation compared to ice sheet reconstructions GLAC-1D and ICE-6G_C and averaged over the North American ice sheet (NAIS), the Eurasian ice sheet (EIS), the Greenland ice sheet (GrIS) and the three ice sheets in total. (e)-(h) Ice volume anomalies between simulations in this study (see Table 4.3 for how each curve is calculated) for the same locations as (a)-(d). See Figure 4.21b for the area used to define each ice sheet.

Curve label in Figure 4.9	**Anomaly calculation**
HadCM3-iTraCE without LSM update	H15-13 - iT15-13
Effect of BA warming with HadCM3_TraCE	H15-13 - Acc_H15_SST
Effect of BA warming with iTraCE	iT15-13 - Acc_iT15_SST

Table 4.3: Label key for Figure 4.9

between the our starting 15 ka BP surface temperature with the Shakun et al. (2012) temperature stack throughout the Northern Hemisphere (with the caveat that there are not many data points over the ice sheets we are focussed on; Figure 4.23). The largest contrast between the Shakun et al. stack and our surface temperatures is in Greenland, with Greenland significantly warmer in our simulations than in the observations (as also true for the *HadCM3_TraCE* and *iTraCE* climate simulations used to provide the surface ocean forcing; Figure 4.2g). This could be due to the differences in the Greenland ice sheet elevation (i.e., Figure 4.23 is not lapse rate corrected) or biases in surface albedo or clouds, or it could signal that temperature is not cold enough over the ice sheets in general. Notwithstanding, the warmer Greenland in our simulations also potentially provides an explanation for why the Greenland ice sheet is melting in our early deglaciation simulations, despite it being more stable or growing in the reconstructions. As GLAC-1D is also a thinner ice sheet–the North American ice sheet starts thinner than the simulated starting ice sheets for *H15-13* and *iT15-13* particularly in the saddle region as well

as the area over the Hudson Bay, thought to also collapse and contribute to the 8.2 kyr cold event (Matero et al. 2017; Ji et al. 2021)–it is more sensitive to smaller scale changes in surface temperature. These particular regions (the saddle between the Cordilleran and Laurentide ice sheets and Hudson Bay) are impacted by the *elevcon* parameter (section 4.2.1), and as a result, ice sheet thickness actually increases in these regions between 15 and 13 ka BP in the *H15-13_GLAC* simulation (Figure 4.10). Increases in ice sheet thickness over the Hudson Bay also occurs in *H15-13* and *iT15-13* (Figure 4.10). Whereas, the rest of the North American ice sheet melts and leads to the smallest resultant North American ice sheet out of all of the experiments. By 13 ka BP, the southern margin of the North American ice sheet reaches the Hudson Bay, significantly farther north than reconstructions suggest and farther north than *H15-13* and *iT15-13*.

If we compare absolute ice volume from our experiments to the GLAC-1D and ICE-6G_C ice sheet reconstructions (Figure 4.9 and 4.20), and assuming that the two reconstructions represent reasonable targets, our simulations perform best over the total Northern Hemisphere and perform worst in Greenland. For the North American ice sheet, *H15-13_GLAC* and *Acc_H15_GLAC_SST* unsurprisingly (since the ice sheet was reset at 15 ka BP to match GLAC-1D) match the closest to the reconstruction, albeit the simulations having different rates of ice volume loss to the reconstructions. The *Acc_H15_GLAC_SST* simulation with constant ocean forcing replicates the reconstruction the closest, as the additional warming in *H15_GLAC* causes the North American ice sheet to melt too much. For the Eurasian ice sheet, the GLAC-1D simulations are able to capture the abrupt melting of 5 m SLE demonstrated in both ICE-6G_C and GLAC-1D between 15 and 14 ka BP, but by 13 ka BP the constant ocean forcing from the *iTraCE* forced runs (*iT15-13* and *Acc_iT15_SST*) end more aligned with the reconstructions. All simulations fail to capture the size of Greenland between 15 and 13 ka BP. Nevertheless, all the simulations with the abrupt warming included, disregarding those with the GLAC-1D ice sheet, reach a total ice volume that falls between what is suggested by ICE-6G_C and GLAC-1D (Figure 4.9). Our simulations have a total ice volume at 13 ka BP of between ∼48 (*H15-13*) and 52 (*iT15-13*) m SLE and the total ice volume for the reconstructions is between 47 (GLAC-1D) and 53 (ICE-6G_C) m SLE.

Additional sensitivity tests have allowed us to diagnose the impact of orbit and greenhouse gases on the Northern Hemisphere ice sheets between 15 and 13 ka BP (Figure 4.20). Approximately 12 m SLE of the 17 m SLE ice loss from the ice sheets in *H15-13* can be attributed to orbital forcing (70%) and ∼1 m SLE to the effect of greenhouse gases. There is slightly more ice lost (∼0.5 m SLE) with an accelerated climate forcing (*Acc_H15-13*; Figure 4.20), which we would expect since the climate remains in certain states, in this case warm, for a longer period of time as an artifact of acceleration. Updating the land-sea mask at 15 ka BP (*H15-13_LSM*) forces a small jump in the Eurasian ice sheet that results in ∼1 m SLE more melt in Eurasia and therefore overall total volume loss (Figure 4.20).

4.3.2 Response of each ice sheet to the 14.7 ka BP abrupt climate change

Between 14.7 and 14.1 ka BP, *H15-13* demonstrates about 5.7 m SLE of total melt from the Northern Hemisphere ice sheets, of which ∼5.3 m SLE originates from the North American ice sheet (mostly from the southern Laurentide margin) and ∼0.5 m SLE from the Fennoscandian ice sheet. The Greenland ice sheet increases in size by <0.15 m SLE (Figure 4.10), most likely due to an increase in precipitation by ∼50% corresponding to the increase in temperature. The Greenland ice sheet is more impacted by atmospheric surface mass balance processes than ocean forcing.

With the *iTraCE* ocean forcing, as in *iT15-13*, the ice sheets melt ∼0.3 m SLE less than *H15-13* over the total Northern Hemisphere between 14.7 and 14.1 ka BP. This is due to a combination of increased melt in Eurasia (∼0.9 m SLE in *iT15-13*) and decreased melt in North America (∼4.5 m SLE) relative to *H15-13* (Figure 4.9 and 4.10), potentially caused by the simulated Older Dryas in *iT15-13* that is not present in *H15-13* (section 4.2.2.1).

The Eurasian ice sheet is the region most impacted by the change in ocean forcing (Figure 4.9f), presumably due to the large marine-based Barents-Kara ice sheet and the marine terminating boundaries of the Fennoscandian ice sheet (Figure 4.1). The difference in melt that is also diagnosed in the early deglaciation results in the size of the 15 ka BP Eurasian ice sheet initial condition differing between *H15-13* and *iT15-13* by ∼2 m SLE. As the *H15-13* simulation runs through the Bølling Warming period, the Eurasian ice sheet, which had already lost its southern sectors, remains more stable than in *iT15-13* which shows ∼1 m SLE more ice loss in this region, as the southern margin melts (Figure 4.10 and 4.9). This not only demonstrates the importance of the starting ice sheet topography, a topic further explored by *H15-13_GLAC*, but also the significance of the ocean forcing on the Eurasian ice sheet (see supplementary information for the main results of *H15-13_GLAC*).

There is ∼2 m SLE less ice volume loss over the total Northern Hemisphere in *Acc_iT15_SST* than with transient ocean forcings (as in *iT15-13*), suggesting that the Bølling Warming had a ∼2 m SLE impact on the ice sheets between 14.7 and 14.1 ka BP. For the *HadCM3_TraCE* forced simulations, there is 1.5 m SLE of additional melt from *H15-13* compared to *Acc_H15_SST*. In both simulations, the impact of the Bølling Warming is most significant in North America, as more than 70% of the additional ice volume loss can be attributed to the North American ice sheet.

4.3.2.1 Abrupt warming and ice sheet melting

Although we do not observe any sudden changes in ice volume as a result of the abrupt warming event, we do see an immediate deviation in the rate of ice volume changes (Figure 4.9) coincident with rapid changes in the surface mass balance (Figure 4.11). Directly in time with the surface air temperature increase, surface mass balance becomes more negative on all three ice sheets, with the largest response on the North American ice sheet (Figure 4.11). The magnitude of the post-warming rapid decrease in surface mass balance is largest for *iT15-13* and *H15-13_GLAC* (Figure 4.25) on the North American ice sheet with peaks at different times. For the *H15-13*,

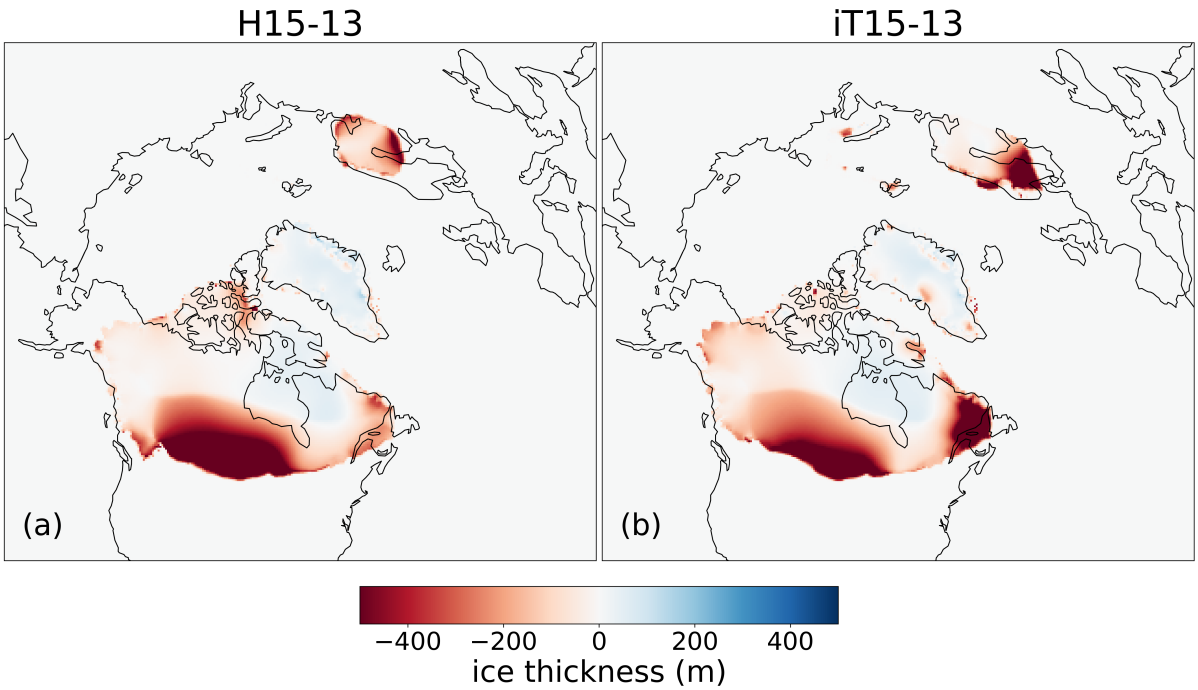

Figure 4.10: Ice thickness anomaly from between 14.7 ka BP and 14.1 ka BP for (a) *H15-13* and (b) *iT15-13*.

surface mass balance rapidly becomes more negative starting from 14.7 ka BP, peaks with a value of ∼2.2 m/yr at 14.4 ka BP, and then rapidly becomes less negative again (Figure 4.11). Surface mass balance is most negative (∼ -2.8 m/yr) at ∼14.6 ka BP for *iT15-13*, whereas *H15-13* peaks at 14.4 ka BP (Figure 4.12). After the abrupt decrease in surface mass balance, there is a respective increase, that is similarly most evident on the North American ice sheet (Figure 4.11). There are no peaks in surface mass balance in the constant ocean forcing simulations. The *Acc_iT15_SST* simulation has a relatively constant surface mass balance on each ice sheet between 14.7 and 14.1 ka BP and until the end of the simulation at 13 ka BP. The simulations driven by *HadCM3_TraCE* ocean forcing show more changes in the surface mass balance of the North American ice sheet (the *H15-13* surface mass balance becomes more negative and the *H15-13_GLAC* becomes more positive), but no abrupt shifts are evident.

The decrease in surface mass balance starting at 14.7 ka BP and the coincident abrupt warming event, corresponds with a meltwater pulse peaking at 14.4 ka BP with *H15-13* and at 14.6 ka BP for *iT15-13* (Figure 4.13). Each of the meltwater pulses align in time with Meltwater Pulse 1a as described by Deschamps et al. (2012). *H15-13_GLAC* has the largest total meltwater pulse at 0.3 Sv (though still only two-thirds the size of the pulse depicted in GLAC-1D; Figure 4.29), potentially with contributions from the disequilibrium offset. The meltwater pulse in *H15-13* is half of the size, peaking at 0.15 Sv and then quickly transitioning to 0.1 Sv where it remains (Figure 4.13d). Whereas the 0.1 Sv flux starts sharply, but lasts ∼300 years in *iT15-13* before decreasing to 0.05 Sv during the Older Dryas (Figure 4.13h). The longer length of the meltwater pulse in the *iT15-13* simulation (∼300 years) more closely aligns with the reconstructions of Meltwater Pulsa 1a (∼350-500 years).

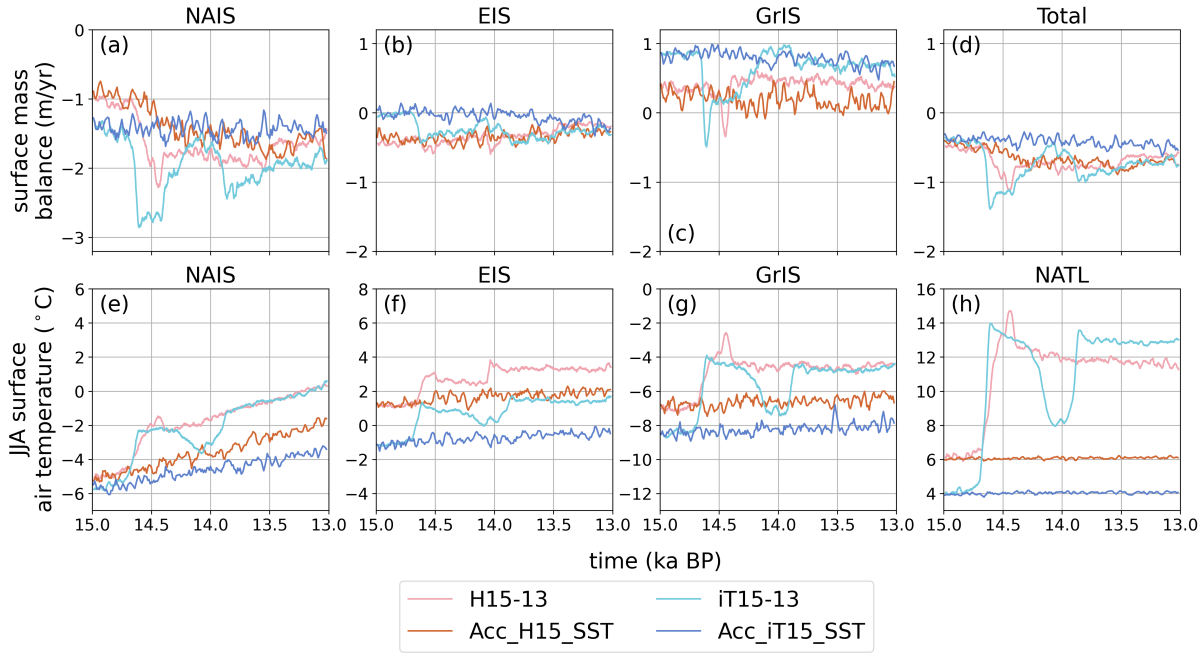

Figure 4.11: (a)-(d) Surface mass balance averaged over the North American ice sheet (NAIS), Eurasian ice sheet (EIS), Greenland ice sheet (GrIS), and all three ice sheets for each simulation. (e)-(h) Boreal summer (June-July-August; JJA) and lapse rate corrected (see section 4.2.1) surface air temperature for each simulation averaged over the NAIS, EIS and GrIS for panels (e), (f), and (g) and the North Atlantic (NATL) region in panel (h). All data are shown as the 30-year running mean. See Figure 4.21 for the area used to define each region.

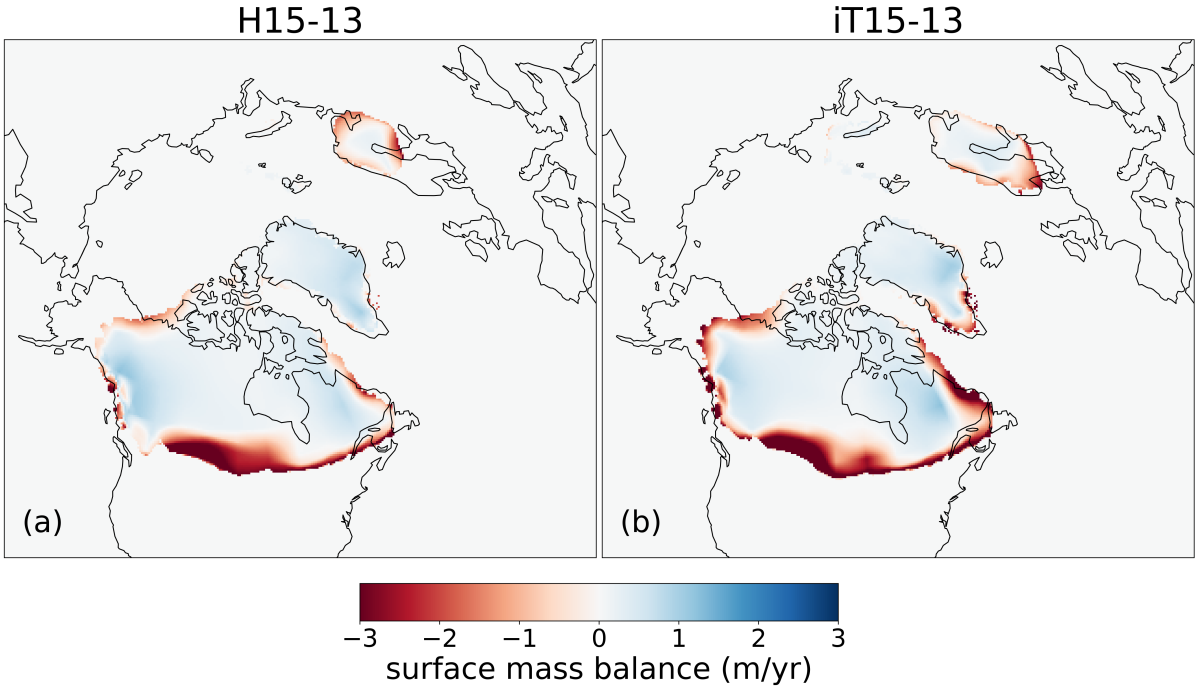

Figure 4.12: Surface mass balance at the time of peak surface mass balance (Figure 4.11) on the Northern Hemisphere ice sheets for each simulation. (a) Surface mass balance for *H15-13* at 14.4 ka BP. (b) Surface mass balance for *iT15-13* at 14.6 ka BP.

For both *H15-13* and *iT15-13*, this accelerated meltwater flux originates from ice mass loss along the southern margin of the North American ice sheet; this is the region with the largest difference between the ice sheet and its respective ice sheet under constant ocean forcing (Figure 4.10 and 4.26). For *H15-13_GLAC*, the freshwater flux originates mainly from the Innuitian ice sheet, with smaller contributions also from the southern and eastern margin of the North American ice sheet.

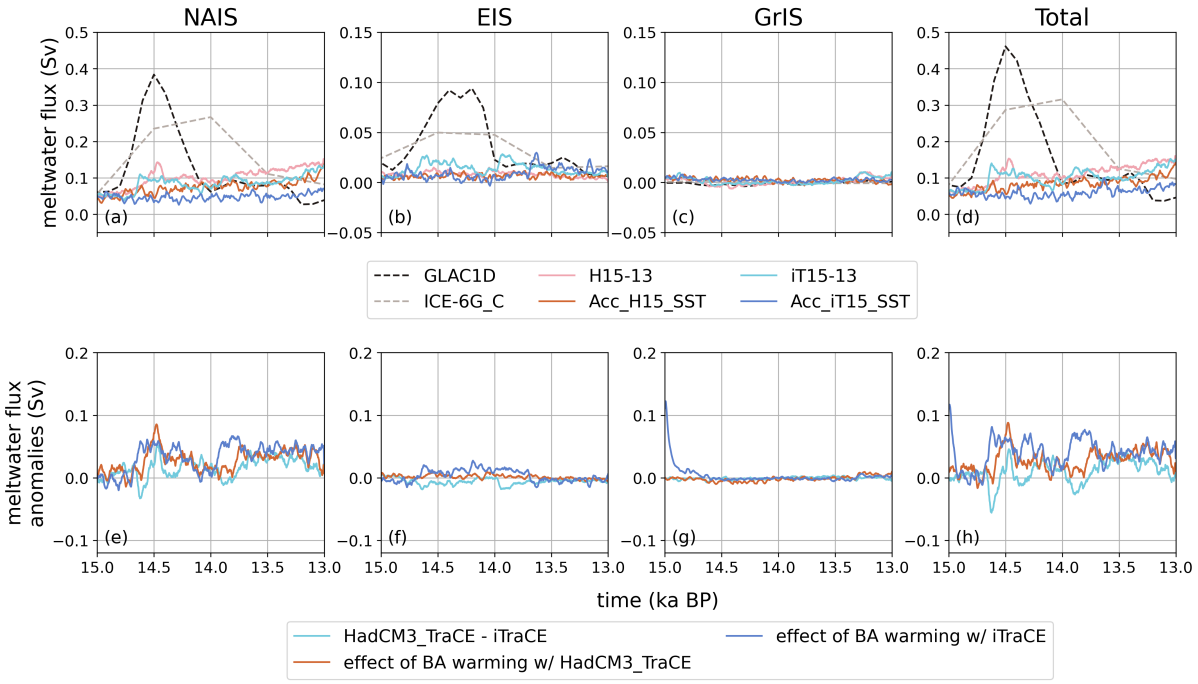

Figure 4.13: (a)-(d) Meltwater flux as derived from the ice sheet volume curve for each ice sheet (North American ice sheet; NAIS, Eurasian ice sheet; EIS, and Greenland ice sheet; GrIS) and all ice sheets in total for each simulation. (e)-(h) Meltwater flux anomalies between simulations in this study (see Table 4.3 for how each curve is calculated) for the same locations as (a)-(d). See Figure 4.21b for the area used to define each ice sheet.

For all simulations, the North American ice sheet remains in an ablation zone and therefore has a continuous meltwater flux between 15 and 13 ka BP (Figure 4.11). Even after 2,000 ice sheet years, the ice sheets with constant ocean forcing do not reach a surface mass balance equilibrium except for the Eurasian ice sheet in *Acc_H15_GLAC_SST* (Figure 4.25) and the Greenland ice sheet in *Acc_H15_SST*, corroborating that not only sea surface temperatures impact surface mass balance but also greenhouse gas and orbital forcing. Each of the other ice sheets under constant ocean forcing still undergo ablation (especially the North American ice sheet) except for the Greenland ice sheet, which is accumulating mass. Ablation even *increases* in the North American ice sheet for *Acc_H15_SST* (Figure 4.11a). Nevertheless, abrupt changes in surface mass balance do not occur under constant forcing, suggesting that the rapid changes in surface mass balance and meltwater discharge are attributed to the sudden shifts in surface air temperature.

4.3.2.2 Timescale of ice sheet response to abrupt ocean change

Previous work suggests that the ocean has had critical influence in ice sheet growth or retreat in the past (e.g., Solas et al. 2011; Snow et al. 2017; Tabone et al. 2018) due to ocean temperatures modulating melt of outlet glaciers and grounding-line retreat. In recent years, an increasing number of studies have demonstrated how ice sheets can be impacted by millennial-scale variability in ocean circulation, such as Dansgaard-Oeschger events during Marine Isotope Stage 3 or Heinrich Stadial 1 and the Bølling Warming in the last deglaciation (Alvarez-Solas et al. 2019; Wickert et al. 2023), or how ice sheets can potentially drive the abrupt events themselves (Gregoire et al. 2012; Ivanovic et al. 2017; Menviel et al. 2020). The timescale of ice sheet response to abrupt ocean changes is a crucial piece of information for our understanding of ice-ocean interactions with the broader climate. Wickert et al. (2023) describe a mechanism that links Laurentide ice sheet response time to changes in the Atlantic Meridional Overturning Circulation (AMOC) strength, a negative feedback loop in which meltwater from the Laurentide, weakens the AMOC, and then hinders further deglaciation of the ice sheet (see their Figure 4). This feedback is dependent on an ice sheet response time of ∼1,000 years, agreeing with the previous estimate from Jóhannesson et al. (1989), stating that the southern Laurentide takes approximately 500-2000 years to react to a significant mass-balance perturbation.

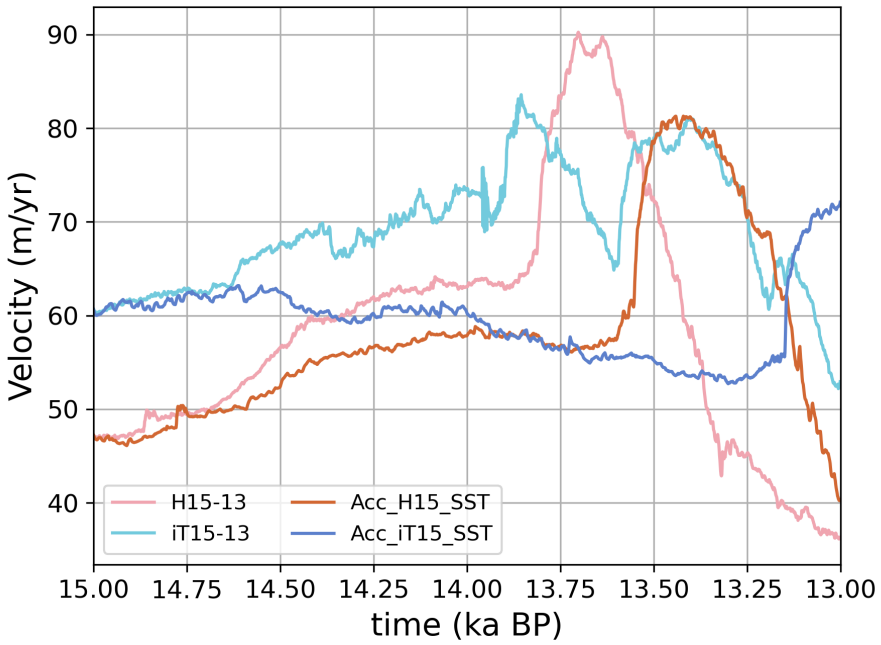

Figure 4.14: Ice velocity at the southern margin of the North American ice sheet for each simulation. The southern margin area averaged over is between 45 and 55° N and 65 and 120°E.

In our simulations, there is an immediate mass-balance response to the abrupt increase in sea surface temperature at 14.7 ka BP (as discussed in section 4.3.2.1), and we notice the impact of this rapid decrease in surface mass balance in other aspects of the ice sheet, such as velocity and ice loss, shortly after. For example, around the time of the Bølling Warming,

there is a divergence in average velocity at the southern margin of the North American ice sheet between the simulations with the abrupt warming, (i.e., *H15-13* and *iT15-13*) and their respective constant ocean forcing runs (i.e., *Acc_H15_SST* and*Acc_iT15_SST*; Figure 4.14). The additional warming at 14.7 ka BP induces an acceleration at the southern margin compared to the trends induced by the background deglaciation. For both *H15-13* and *Acc_H15_SST*, there is a large acceleration later in the deglaciation (beginning at ∼13.8 ka BP for *H15-13* and at ∼13.6 ka BP for *Acc_H15_SST*), lasting ∼200 years before a corresponding deceleration as the southern margin retreats (Figure 4.9). This event of accelerated discharge occurs 200 years earlier for *H15-13* compared to *Acc_H15_SST* because of the additional ocean warming, implying that the Bølling Warming has implications for the timing of melt even much later on in the deglaciation. With the *iTraCE* ocean forcing, a similar pattern of acceleration in velocity unfolds and the *iT15-13* ice sheet shows early signs of acceleration beginning at ∼13.9 ka BP although, in this case, *Acc_iT15_SST* has a relatively constant velocity at the southern margin throughout the simulation and does not exhibit accelerated discharge until ∼13.1 ka BP. This is consistent with the North American ice sheet in *Acc_iT15_SST* also melting the least out of all of the simulations (Figure 4.27). Simulation *iT15-13* additionally does not reach the same ice velocity at the North American southern margin as *H15-13* and oscillates between an acceleration and deceleration in ice velocity.

As discussed in section 4.3.2.1, there is also a meltwater pulse that starts at the time of divergence in ice velocity, and more importantly at the time of the Bølling Warming. The pulse lasts for ∼300 years before levelling out in both *H15-13* and *iT15-13*. The peak of the *H15-13* pulse, occurs ∼250 years after the start of the Bølling Warming and the start of the increased meltwater discharge, whereas the more plateau-shaped meltwater pulse from *iT15-13* peaks only ∼60 years after the initial rapid warming and then decreases throughout the ensuing 300-year length of the meltwater flux.

The differences between the *HadCM3_TraCE* and *iTraCE* simulations highlight that shape and pattern of an abrupt warming in sea surface and subsurface temperatures are very important for the velocity and overall response of an ice sheet.

4.3.2.3 Contributions to Meltwater Pulse 1a

Between 14.7 and 14 ka BP, when the Bølling Warming, Meltwater Pulse 1a, and the saddle collapse are all thought to occur, the total ice volume loss in our simulations is comparable to best estimates from geological archives (Table 4.4). *H15-13* and *iT15-13* demonstrate ∼5.5-6 m SLE of total melt between 14.7 and 14.1 ka BP (section 4.3.2), which is about 2 metres less than the low end of sea level rise assessed by Liu et al. (2016) who use a glacial isostatic adjustment model to reinterpret tropical sea-level reconstructions from this time period. In our simulations, the North American ice sheet is the largest source of meltwater (∼5 m SLE), followed by the Eurasian ice sheet (∼1 m SLE). The North American ice sheet values are on a similar scale to those determined by other modelling studies (Gregoire et al. 2012; Gregoire et al. 2016; Yeung et al. 2019), but over a longer period of time. They are also below estimates based on geological constraints on sea level rise (e.g., Carlson and Clark 2012; Lin et al. 2021)

and ice sheet reconstructions like GLAC-1D (Tarasov et al. 2012). The small contribution of the Eurasian ice sheet is consistent with previous studies (Hormes et al. 2013; Lambeck et al. 2014; Hughes et al. 2015; Petrini et al. 2020) showing the earlier melt of the marine-based sectors of the ice sheet, aligning well with our early deglaciation simulations (*Acc_H21-15* and *Acc_iT21-15*), but significantly lower than recent reinterpretations of the Eurasian ice sheet chronology (Brendryen et al. 2020; Lin et al. 2021; Coonin et al. 2025).

In Gregoire et al. (2016)'s similar study forcing an ice sheet model, GLIMMER, with a deglacial temperature forcing including abrupt events, the *TraCE-21ka* simulation (Liu et al. 2009), the Cordilleran-Laurentide separation tends to occur later than in GLAC1-D and ICE6G_C–between 12.9 and 10.9 ka BP, more around the time of the Younger Dryas (similar to Gregoire et al. 2012). Interestingly, however, the simulations that successfully reproduce the ice saddle collapse at the time of the Bølling Warming produce the best match with geological constraints (Dyke 2004; Gregoire et al. 2012). The ice saddle collapse produces a maximum meltwater flux of 0.25 to 0.43 Sv from the North American ice sheet, which is equivalent to a 5-6 m SLE contribution to MWP1a in 340 years. Only *H15-13_GLAC* is able to produce a meltwater pulse on this scale of magnitude (a 0.3 Sv pulse or a 13.7 m SLE contribution in 600 years; equivalent to 8 m SLE in 340 years). If we continued our simulations, we could potentially achieve a late saddle collapse, but, more importantly, if we were able to simulate the Cordilleran-Laurentide saddle collapse at the time of the Bølling Warming, *H15-13* and *iT15-13* would most likely exhibit more melting on the scale of other studies (Table 4.4).

4.3.3 Gradual forcing versus abrupt events

There are very few previous studies that used coupled-climate ice sheet simulations to investigate the pattern of ice sheet retreat during the last deglaciation. Additionally, even fewer have investigated the impact of abrupt climate changes on ice sheets.

We can make the most direct comparison to Patterson et al., (Thesis) who also simulate the last deglaciation using FAMOUS-BISICLES. The results from the simulation are shown in Figure 4.15 and labelled as *Acc_HSm21-9*. This simulation uses the same greenhouse gas forcing and transient orbital conditions as our study, but a different ocean forcing. Specifically, *Acc_HSm21-9* has prescribed sea surface temperatures, subsurface temperatures, and sea ice concentration interpolated between last deglaciation snapshot HadCM3 runs (Armstrong et al. 2019; Huntley et al. 2023) that do not include abrupt climate change events (Figure 4.15e-f). There is ∼5 m SLE more melt with the abrupt events than with the smooth deglacial forcing by 13 ka BP (Figure 4.15). The evolution of the North American ice sheet volume of *Acc_HSm21-9* is most similar to the simulations in this study, with the ice volume for *H15-13*, *iT15-13*, and *Acc_HSm21-9* all reaching ∼45 m SLE by 13 ka BP. However, larger differences are present for the other ice sheets. The *Acc_HSm21-9* Greenland ice sheet melts only a very small amount (∼3 m SLE less than the simulations presented in this study), and the Eurasian ice sheet melts more gradually leaving it ∼2 m SLE larger by 13 ka BP than in our study.

Patterson et al., (Thesis) also identify an instability in their simulated Barents-Kara ice sheet. They determine that the ice sheet could be overly sensitive in their model set-up (which is the

Ice sheet	Method	Duration (years)	MWP1a Contribution (m)	Reference
NAIS	Ocean driven climate-ice sheet modelling	600	4.5-5.3, or ∼9.8 w/ GLAC-1D (SLE)	this study
NAIS	Data-driven inversion with GIA modelling	400	∼3	Coonin et al. (2025)
NAIS	Saddle collapse with ice sheet model	340	≥5-6	Gregoire et al., (2012, 2016)
NAIS	Data-driven inversion with GIA modelling	500	5.6-15.4	Lin et al. (2021)
NAIS	Ice area-volume transition	800	6.7-8.7 (SLE)	Carlson and Clark (2012)
NAIS	Glacial systems model with Bayesian style calibration	500	9.4-13.2	Tarasov et al. (2012)
NAIS	Saddle collapse with ice sheet model	500	10.5	Gomez et al. (2015)
NAIS	GIA analysis (ICE-6G_C)	500	16.5-18	Peltier et al. (2015)
NAIS	GIA and tilting of glacial lake shoreline analysis	600	∼18.7	Lambeck et al. (2017)
EIS	Ocean driven climate-ice sheet modelling	600	0.5-0.9, or ∼3 w/ GLAC-1D (SLE)	this study
EIS	GIA analysis	500	0.8-1	Lambeck et al. (2014)
EIS	Compilation of large geomorphological dataset	500	1.7-2	Hughes et al. (2016)
EIS	Ice sheet modelling	1,000	1.96	Petrini et al. (2020)
EIS	Thermomechanical ice modelling	340	2.5 (SLE)	Patton et al. (2016)
EIS	Data driven inversion with GIA modelling	500	3.2-6.4	Lin et al. (2021)
EIS	GIA analysis (ICE-6G_C)	500	3.5-4	Peltier et al. (2015)
EIS	Ice area-volume transition	1,000	4.1-5.7 (SLE)	Carlson and Clark (2012)
EIS	Chronological reinterpretation of Eurasian ice sheet margin	500	4.5-7.9 (SLE)	Brendryen et al. (2020)
EIS	Data driven inversion with GIA modelling	150	∼7	Coonin et al. (2025)

Table 4.4: Estimates of the contribution of the North American ice sheet (NAIS) and Eurasian ice sheet (EIS) to Meltwater Pulse 1a (MWP1a).

same as ours) when the resolution in this region is refined but the bedrock topography is left at a coarse resolution. Petrini et al. (2020) also show that the instability and retreat of the grounding line is driven by an increase in the sub-surface ocean forcing (section 4.3.1).

Interestingly, prescribed subsurface temperatures are warmer in the Barents and Kara seas in *Acc_HSm21-9* than those prescribed from *HadCM3_TraCE* and *iTraCE*, and prescribed sea surface temperatures are consistently colder except during Heinrich Stadial 1 (Figure 4.15e,f). This suggests that sea surface temperatures could be a stronger driver than the subsurface temperatures in keeping melting at bay for Greenland and Eurasia in *Acc_HSm21-9*, further highlighted by the smaller concentration of sea ice in the Northern Hemisphere (Figure 4.15g). The similarity in the total and North American ice sheet volume at 13 ka BP also indicates that Heinrich Stadial 1 has less of an impact on ice evolution than the warming, potentially because the cooling mostly occurs in the boreal winter time without an increase in snow accumulation, which is less impactful than if it had a stronger signal during the summer melt season.

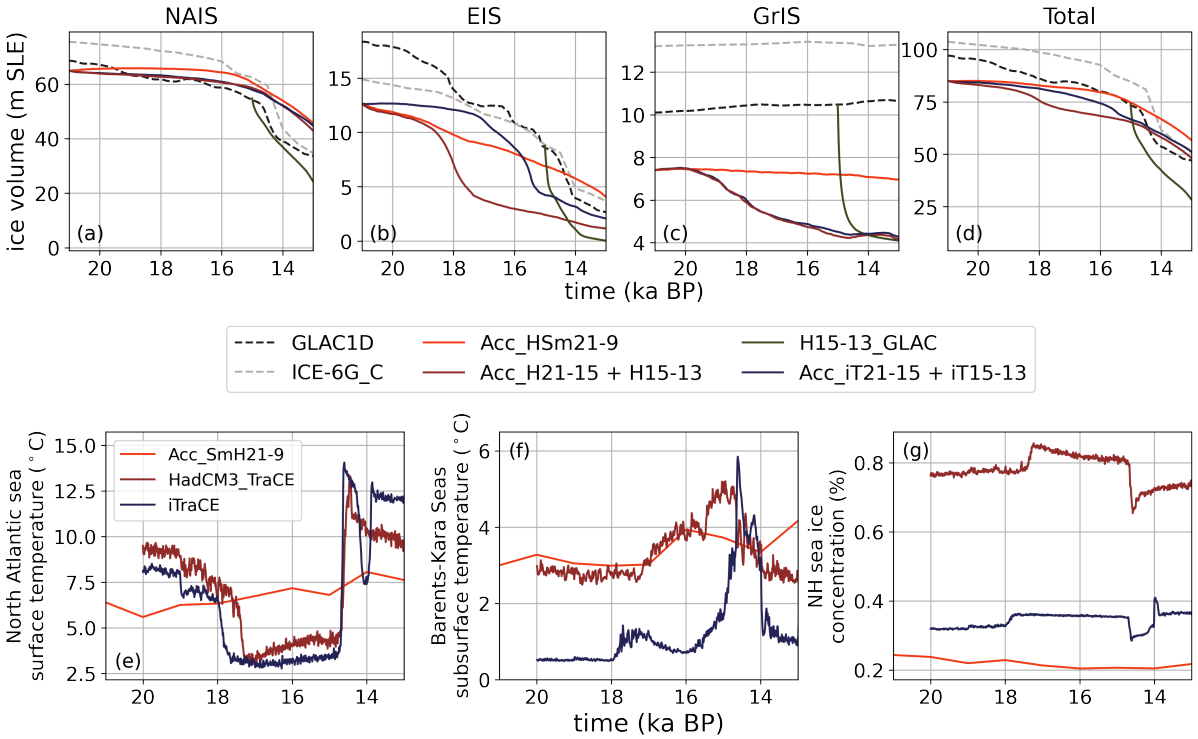

Figure 4.15: (a)-(d) Ice sheet volume from 21-13 ka BP averaged over each ice sheet (North American ice sheet; NAIS, Eurasian ice sheet; EIS, and Greenland ice sheet; GrIS) and all Northern Hemisphere ice sheets in total for the simulations performed in this study, GLAC-1D and ICE-6G_C ice sheet reconstructions, and the *Acc_HSm21-9* simulations performed by Patterson et al. (Thesis). (e) North Atlantic (between 40 and 70° N and 60 and 115° E) sea surface temperature forcing (from *HadCM3_TraCE*, *iTraCE*, and *Acc_HSm21-9*). (f) Subsurface temperature forcing in the Barents and Kara Seas (between 70 and 85° N and 10 and 60° E and at 666 m deep for *HadCM3_ TraCE*, 400 m deep for *iTraCE*, and 450 m deep for *Acc_HSm21-9*) with the freezing point of water subtracted (-2.27 °C). (g) Sea ice concentration north of 50° N forcing (from *HadCM3_TraCE*, *iTraCE*, and *Acc_HSm21-9*).

Quiquet et al. (2021b) also simulates the last deglaciation, but using an Earth System Model of Intermediate Complexity (EMIC; called iLOVECLIM; Goosse et al. 2010) coupled to an ice

sheet model. In the case of Quiquet et al. (2021b), the inclusion of an ocean model allows them to simulate the impact of meltwater fluxes derived from ice sheet melting on the Atlantic Meridional Overturning Circulation (AMOC). They simulate a freshwater flux that increases to ∼0.2 Sv between 15 and 10 ka BP as a result of the accelerated ice sheet retreat (as do Mikolajewicz et al. (2024)), but they do not simulate any abrupt AMOC changes. However, despite the differences between studies (e.g., our simulations do not include a dynamic ocean, and theirs does not include abrupt climate changes such as Heinrich Stadial 1 or the Bolling Warming), the deglacial pattern of the North American ice sheet follows closely with what is simulated by Quiquet et al. (2021b) (see their Figure 10). Without a saddle collapse in our study and Quiquet et al. (2021b)'s, the majority of ice loss originates from the southern margin of the North American ice sheet, and the Eurasian ice sheet retreats faster than proxy records suggest. Quiquet et al. (2021b) also simulate an enlarged surface elevation of the North American ice sheet thought to be caused by an overestimation of precipitation. We hypothesise that likewise, due to the low resolution of FAMOUS, we get precipitation biases near the Cordilleran ice sheet, which in combination with our *elevcon* parameterisation, creates a saddle region that is too thick to collapse during our simulation (Figure 4.17). In addition, Quiquet et al. (2021b) also test the impact of using an accelerated or asynchronous ice sheet, and similar to our results, they determine that the acceleration factor only weakly affects the pattern of retreat.

Mikolajewicz et al. (2024) is the only study to successfully produce spontaneous, unforced abrupt climate events with a coupled climate-ice sheet model. They simulate sharp increases in meltwater discharge of up to 0.4 Sv in the early deglaciation, with some pulses on a similar scale as those identified in this study. They are often associated with iceberg melt in the North Atlantic, like we see in the early deglaciation from the Barents-Kara ice sheet (section 4.3.1), whereas the freshwater pulses in the later deglaciation in our simulations are caused by surface ablation. The Northern Hemisphere ice volume evolution of Mikolajewicz et al. (2024) matches closely with the GLAC-1D and ICE-6G_C, however between 15 and 13 ka BP the rate of ice volume loss is too slow compared to reconstructions of MWP1a (e.g., Deschamps et al. 2012). Nevertheless, this work provides critical insight into the casual mechanisms of abrupt climate changes and how they can be driven by changes in the ice sheets. We do not observe corresponding surface air temperature changes associated with the meltwater pulses (e.g., there is no abrupt decrease in temperature at 18 ka BP associated with the collapse of the Barents-Kara ice sheet in *Acc_H21-15*; Figure 4.2g), suggesting that not only is an interactive ocean critical to demonstrate the impact of meltwater discharge on the climate, but also that the collapse of the Barents-Kara ice sheet in *Acc_H21-15* and *Acc_iT21-15*, as well as any other ice sheet changes, did not induce an atmospheric shift large enough to invoke a temperature change.

It would be interesting for our next steps to account for model uncertainty and test whether a different selection of model parameter values could produce the saddle collapse between the Laurentide and Cordilleran ice sheets. For instance, Patterson et al. (Thesis) test the sensitivity of the simulated ice evolution to key model parameters values (i.e., increased sub-shelf melt parameter, reduced removal of drainage water from the till, and increased dependence of snow

albedo on increasing albedo, resulting in lower albedo) on their deglaciation runs. Each of these tests led to increased melt and smaller ice sheets compared to the original simulation (*Acc_HSm21-15*), suggesting a combination of other parameters might be more helpful for simulating the deglaciation. Furthermore, the inclusion of a three-dimensional ocean model would be beneficial to investigate the impact of the meltwater feedback to ocean circulation.

The differences in ice evolution and resulting rate of ice volume loss between simulations with gradual compared to abrupt climate forcing highlights the need for careful consideration of experiment purpose when designing simulations. The 13 ka BP ice volume is relatively similar between simulations irrespective of whether gradual or abrupt climate forcing is applied. Thus, if the experiment purpose is to arrive at a suitable starting condition for a later period (e.g., the interglacial climate/ice-sheet state), a gradual forcing would suffice and would enable the use of a dynamic, interactive ocean. On the other hand, the inclusion of abrupt climate changes is evidently critical for evaluating the detailed temporal and spatial history of deglaciation for individual ice sheets, including the response to rapid forcing, which may necessitate the means to impose abrupt climate change (e.g., by controlling surface ocean forcing). Both approaches hold value for reaching a better understanding of the role ice sheets play in atmosphere-ocean-ice interactions and our broader understanding of noteworthy climate change.

4.4 Conclusion

With 14 coupled climate-ice sheet model simulations running at times between 21 and 13 ka BP, we have demonstrated the impact of an abrupt warming event, the Bølling Warming, on the Northern Hemisphere ice sheets. Through these experiments, we conclude that the impact of the Bølling Warming is dependent on the ocean forcing and starting ice sheet topography. Approximately 5.7 m SLE of ice volume loss over the total Northern Hemisphere ice sheets occurs after the abrupt warming event (between 14.7 and 14.1 ka BP) with the *HadCM3_TraCE* ocean forcing, whereas ∼5.3 m SLE of ice volume loss occurs with the *iTraCE* ocean forcing, both of which correspond with previous ice sheet modelling studies but are small compared to reconstructions of MWP1a. The source of the ice volume loss varies depending on the ocean forcing (i.e., more ice loss originates from the North American ice sheet with *HadCM3_TraCE* than with *iTraCE* forcing, whilst the simulation with *iTraCE* forcing has more loss from the Eurasian ice sheet compared to when forced by *HadCM3_TraCE*). However, simulations with constant ocean forcing (i.e., constant prescribed sea surface temperature and sea ice concentration) demonstrate that the simulation forced with *iTraCE* output exuded *more* ice volume loss specifically attributed to the inclusion of the Bølling Warming compared to the simulation forced with *HadCM3_TraCE* output. We suggest that the larger impact of the abrupt warming in *iTraCE* is caused by surface mass balance becoming more negative for longer than in *HadCM3_TraCE* simulations. The most amount of melt occurs when the starting ice sheet topography is changed to that of the GLAC-1D ice sheet reconstruction at 15 ka BP. There is an additional ∼8 m SLE of absolute ice volume loss over the Northern Hemisphere ice sheets, with ∼3 m SLE attributed to the impact of the Bølling Warming. The larger amount of ice volume loss with the GLAC-1D ice sheet topography is potentially due to the disequilibrium of

the thinner ice sheet with the 15 ka BP simulated climate, causing both the GLAC-1D simulations with and without the transient sea surface temperatures to demonstrate large immediate decreases in ice volume on each ice sheet.

We simulate a sharp change in surface mass balance and an acceleration of ice loss after the Bølling Warming, but it is small compared to the results of previous studies. The detailed response to the surface mass balance change varies dependent on the ocean forcing and starting ice sheet topography, but in all cases the Bølling Warming prompts an acceleration in deglaciation that is absent without it.

We determine from our simulations of the early deglaciation as well as those between 15 and 13 ka BP, that changing the ocean forcing is most impactful on the Eurasian ice sheet due to the marine-based sector over the Barents and Kara Seas (i.e., during the early deglaciation we see a collapse of the Eurasian ice at 18 ka BP with *HadCM3_TraCE* forcing and at 15.5 ka BP with *iTraCE* forcing, occurring later with *iTraCE* forcing because of colder subsurface temperatures in the Barents and Kara Seas). Total volume by 13 ka BP for both *HadCM3_TraCE* and *iTraCE* simulations fall in the middle of what is suggested by the GLAC-1D and ICE-6G_C ice sheet reconstructions (i.e., between 55 and 45 m SLE), suggesting that ice melt occurs slower in our simulations, as the ice sheets reach reasonable 13 ka BP conditions despite starting with smaller LGM ice sheets. We do not successfully simulate the saddle collapse between the Cordilleran and Laurentide ice sheets, but this melt is compensated for by ice volume loss at the southern margin of the North American ice sheet in all simulations.

Altogether, we demonstrate the importance of the starting ice sheet topography and the ocean forcing on the deglaciation of the ice sheets. Future tests would also seek to evaluate model uncertainty with a perturbed parameter ensemble alongside abrupt forcings.

4.5 Supplementary Figures

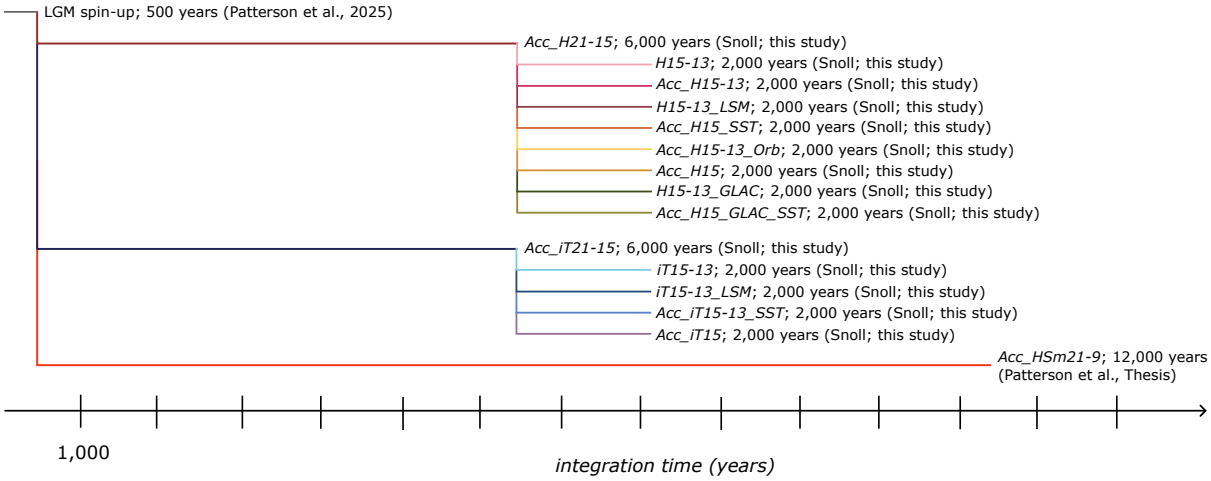

Figure 4.16: Timeline of the experiments included in this study and who generated them.

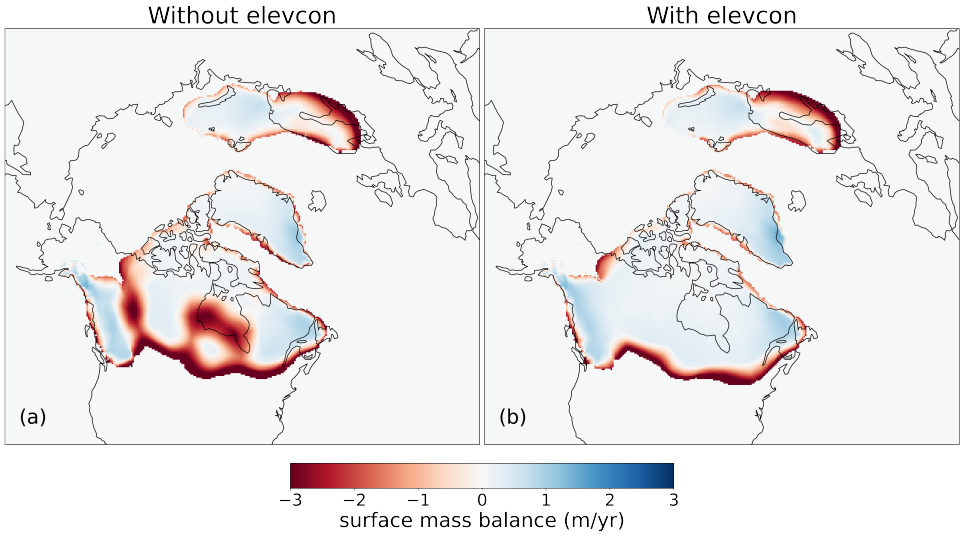

Figure 4.17: Surface mass balance without the *elevcon* parameter (a) versus with (b) after 80 ice sheet integration years. Significant melt would occur prematurely in the Hudson Bay region before the use of *elevcon*, but this also impacts other thinner areas of ice like the saddle region between the Laurentide and Cordilleran ice sheets. The simulation with *elevcon* uses a value of 1.2.

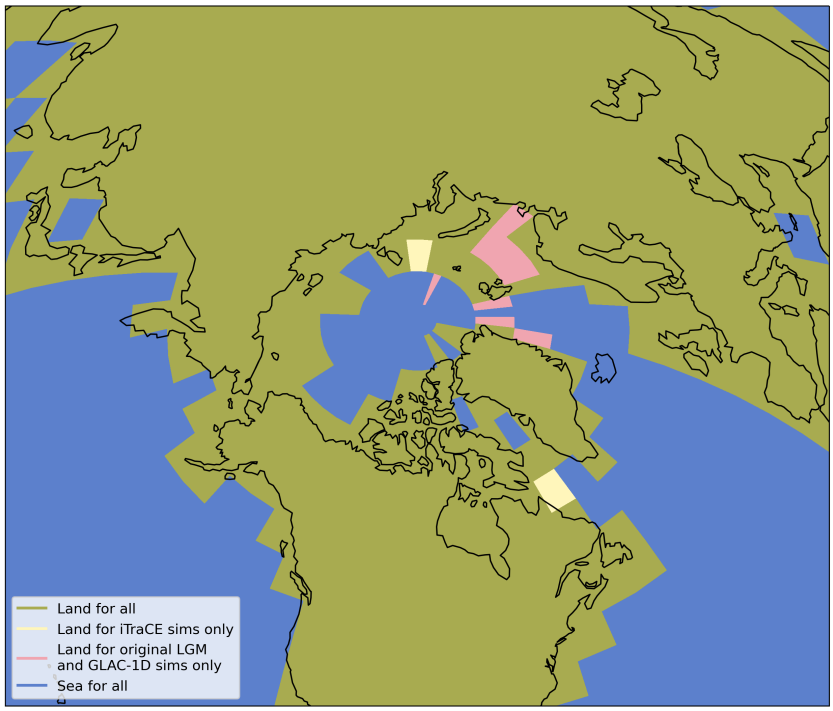

Figure 4.18: Land-sea mask used for each simulation.

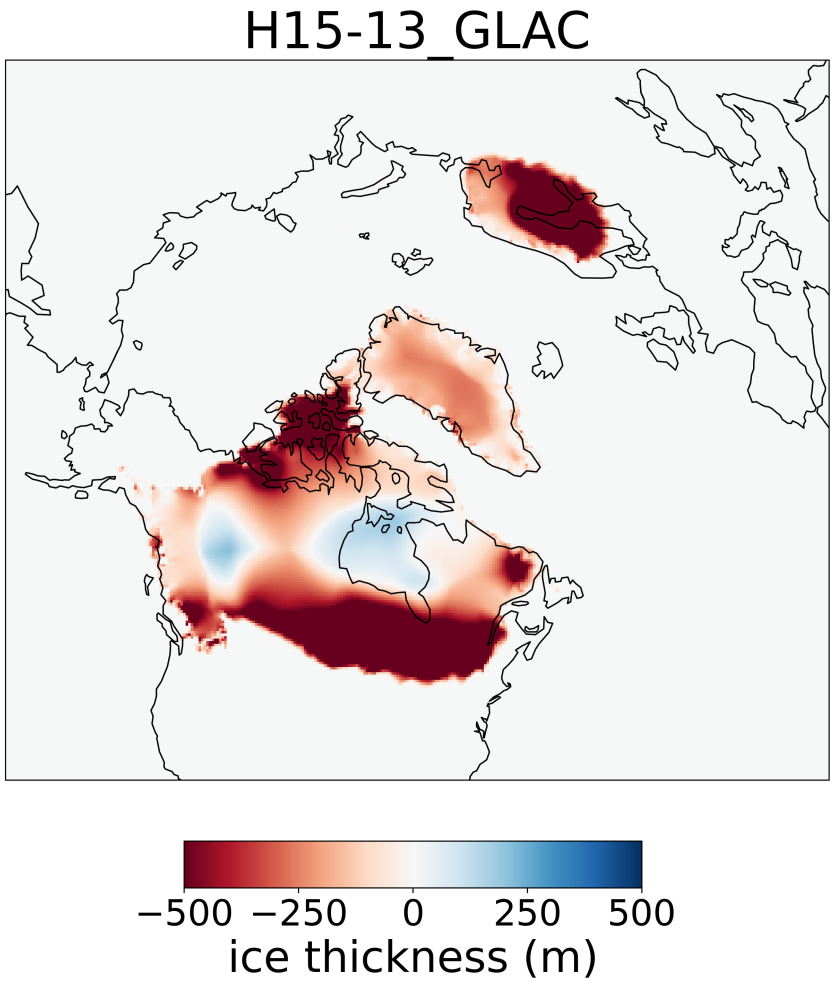

Figure 4.19: Ice thickness anomaly from between 14.7 ka BP and 14.1 ka BP for *H15-13_GLAC*.

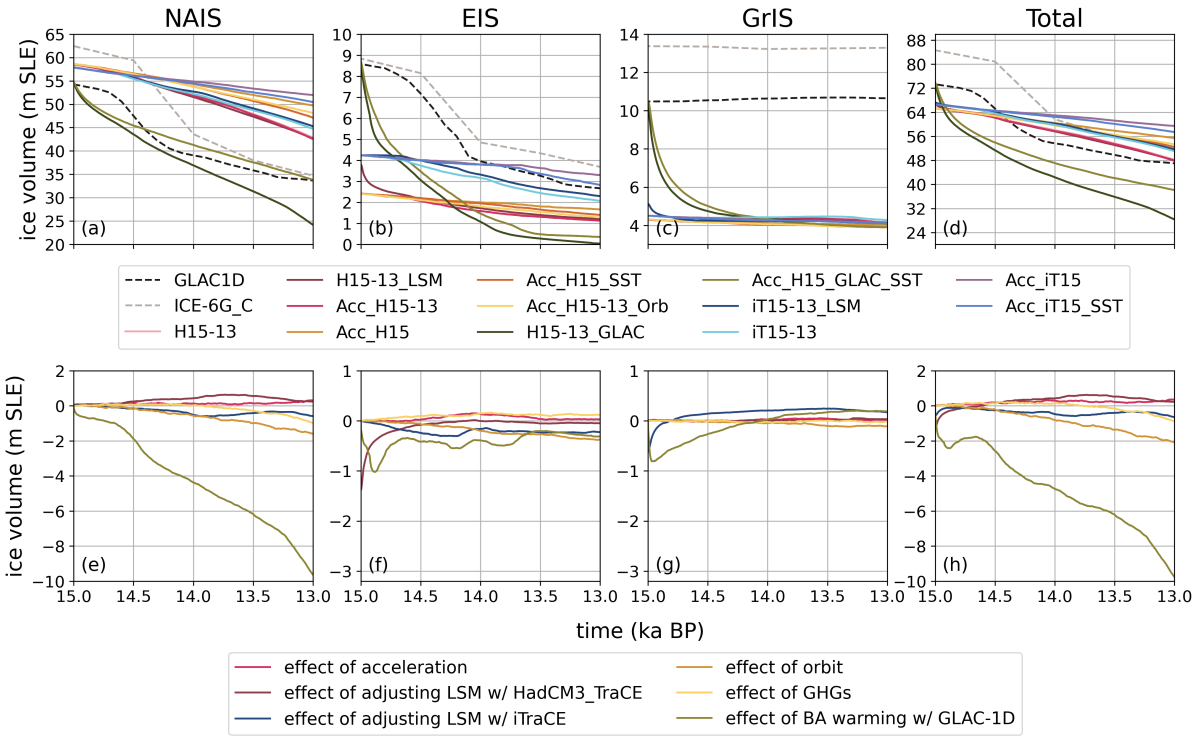

Figure 4.20: (a)-(d) Absolute ice volume for each simulation averaged over the North American ice sheet (NAIS), the Eurasian ice sheet (EIS), the Greenland ice sheet (GrIS) and the three ice sheets in total. (e)-(h) Ice volume anomalies between simulations in this study (see Table 4.5 for how each curve is calculated) for the same locations as (a)-(d). See Figure 4.21b for the area used to define each ice sheet.

Curve label in Figure 4.20	**Anomaly calculation**
Effect of acceleration	H15-13 - Acc_H15-13
Effect of adjusting LSM with HadCM3_TraCE	H15-13 - H15-13_LSM
Effect of adjusting LSM with iTraCE	iT15-13 - iT15-13_LSM
Effect of orbit	Acc_H15-13_Orb - Acc_H15
Effect of GHGs	Acc_H15_SST - Acc_H15-13_Orb
Effect of BA warming with GLAC-1D	H15-13_GLAC - Acc_H15_GLAC_SST

Table 4.5: Label key for Figure 4.20. *Acc_H15-13_Orb* has only transient orbit, *Acc_H15* has all forcings constant at 15 ka BP conditions, and *Acc_H15_SST* has only constant ocean forcing.

H15-13_GLAC undergoes the most ice loss of all the simulations between 14.7 and 14.1 ka BP– approximately 13.7 m SLE total (∼8 m SLE greater than *H15-13*; Figure 4.19 and 4.20). The North American ice sheet is the largest source of ice loss (∼9.8 m SLE), whilst the Eurasian ice sheet loses ∼3 m SLE and Greenland loses ∼0.9 m SLE. We can remove the impact of the adjustment period of the *H15-13_GLAC* ice sheet and isolate the effect of the abrupt warming caused by sea surface temperature changes with *Acc_H15_GLAC_SST*. There is 5.5 m SLE less ice volume loss over the total Northern Hemisphere in *Acc_H15_GLAC_SST* than with transient ocean forcings (as in *H15-13_GLAC*), suggesting that the Bølling Warming had a 5.5 m SLE impact on the ice sheets between 14.7 and 14.1 ka BP.

The significantly larger-scale melt in *H15-13_GLAC* mostly occurs in the first 500 years, suggesting there is a potential disequilibrium with the climate. For each of the ice sheets, though most noticeable in Eurasia and Greenland, there is a rapid melting of ∼5-10 m SLE within the first 500 years. The ice loss then levels out and melt occurs at a slower pace throughout the rest of the simulation (i.e., 1.6 m SLE per 100 years between 14.5 and 13 ka BP as opposed to 4.4 m SLE per 100 years between 15 and 14.5 ka BP). We thus consider the period 15 - 14.5 ka BP to be a period of adjustment (i.e., spin-up) of the initial GLAC-1D ice sheet topography to the climate simulated by FAMOUS. The same pattern occurs when sea surface temperatures are kept constant in *Acc_H15_GLAC_SST*.

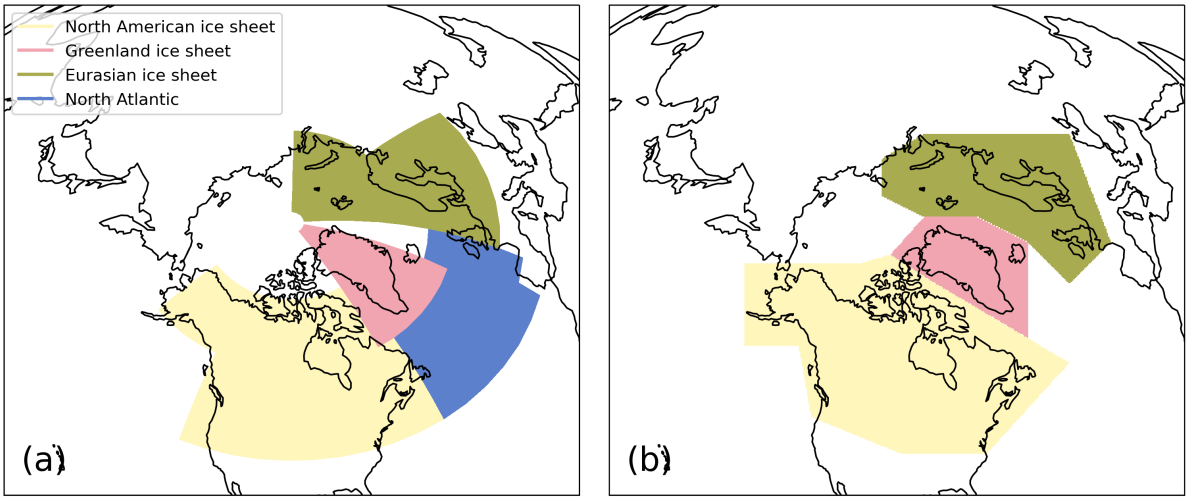

Figure 4.21: (a) Bounds for FAMOUS output at 37x48 resolution for each ice sheet and the North Atlantic. (b) The same as (a), but for BISICLES output on the Lambert azimuthal equal-area projection.

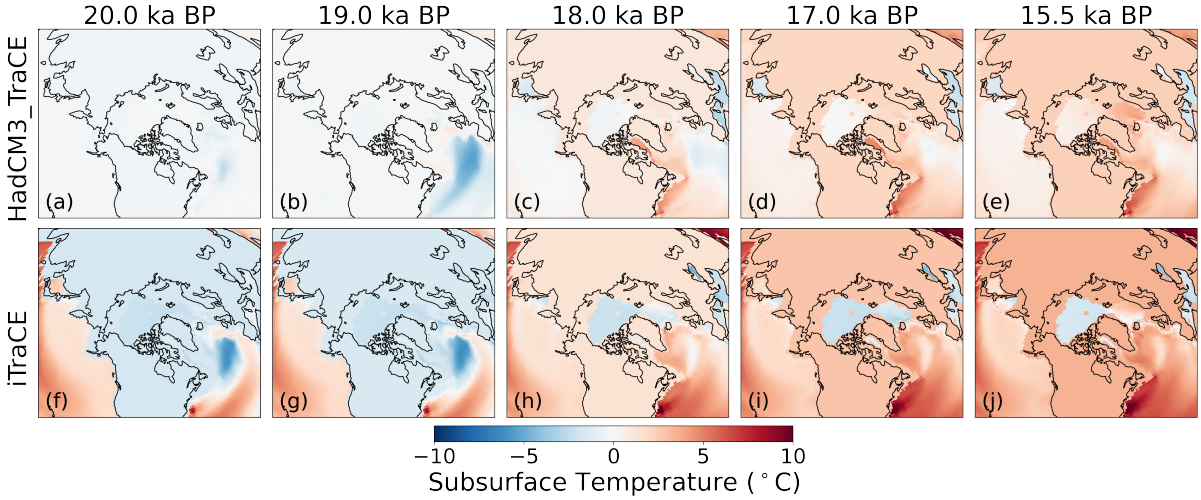

Figure 4.22: Prescribed sub-surface temperature from the *HadCM3_TraCE* and *iTraCE* simulations at the time labelled as anomalies from *HadCM3_TraCE* at 21 ka BP.

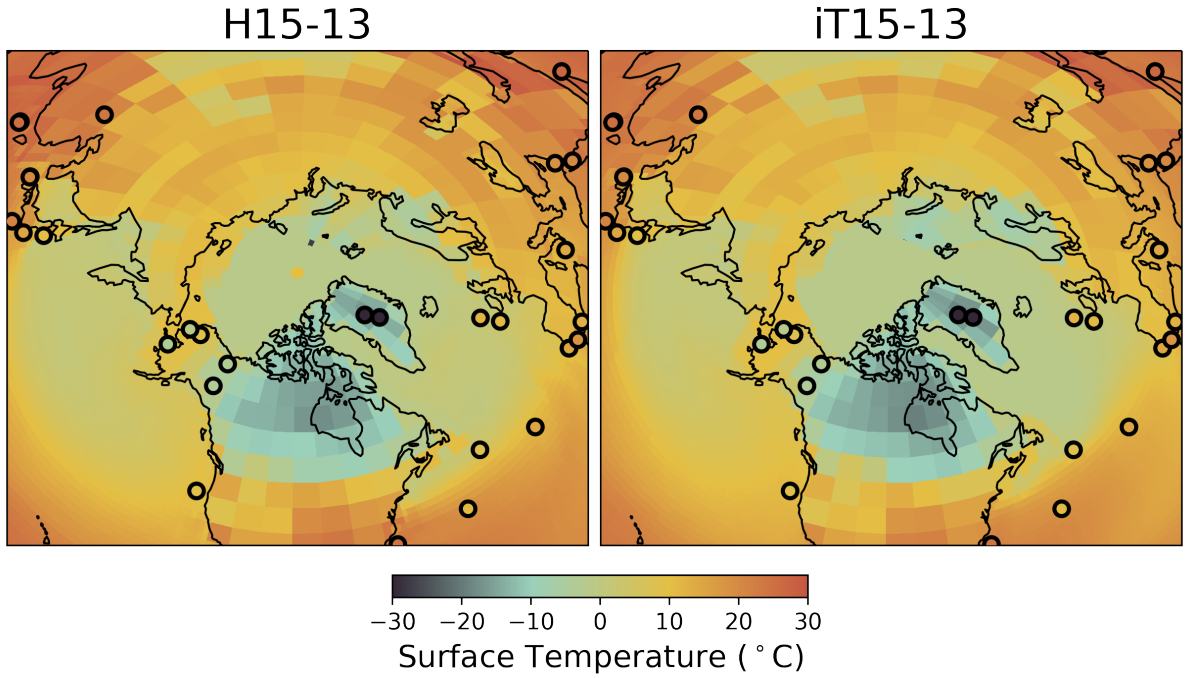

Figure 4.23: Surface decadal temperature at 15 ka BP (or the start of the Bølling Warming runs). Filled circles show the proxy surface temperature stack from Shakun et al. (2012) on the same colour scale.

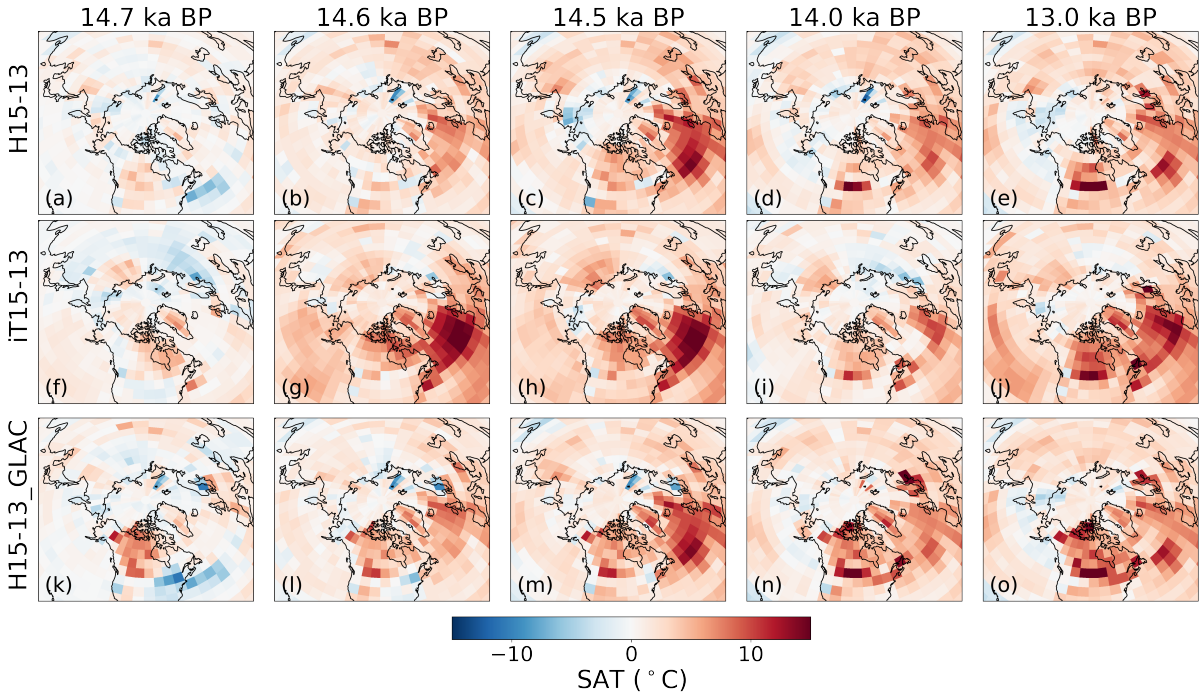

Figure 4.24: Boreal summer (June-July-August) surface air temperature anomaly from 15 ka BP for three simulations (*H15-13*, *iT15-13*, and *H15-13_GLAC)*.

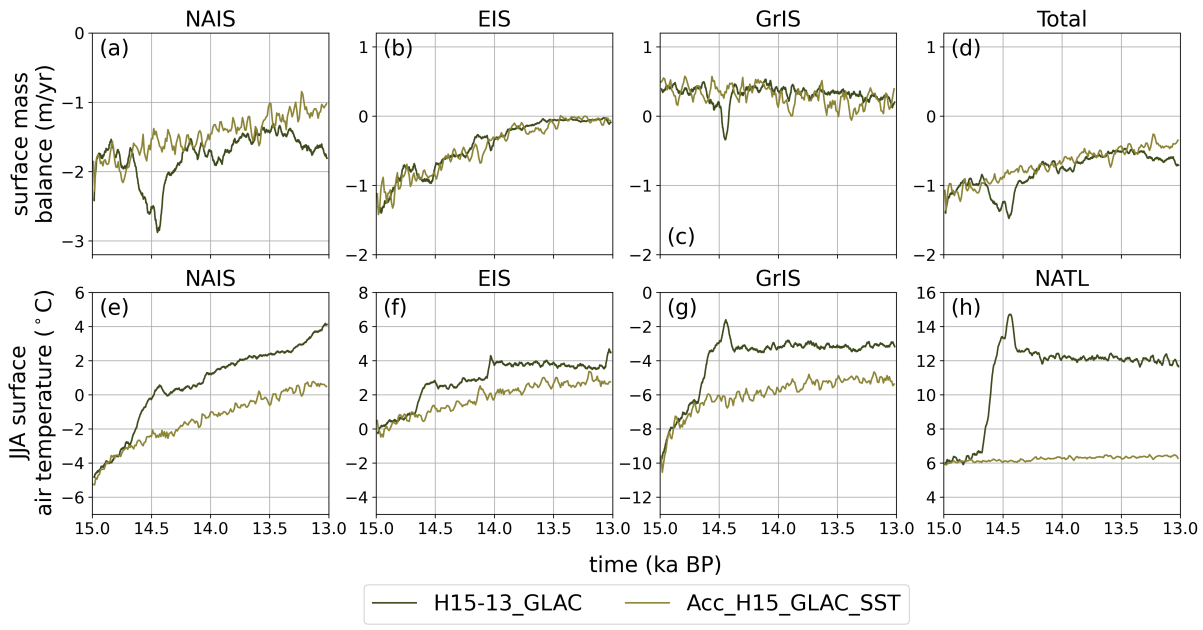

Figure 4.25: (a)-(d) Surface mass balance averaged over the North American ice sheet (NAIS), Eurasian ice sheet (EIS), Greenland ice sheet (GrIS), and all three ice sheets for each simulation. (e)-(h) Boreal summer (June-July-August; JJA) and lapse rate corrected (see section 4.2.1) surface air temperature for each simulation averaged over the NAIS, EIS and GrIS for panels (e), (f), and (g) and the North Atlantic (NATL) region in panel (h). All data are shown as the 30-year running mean. See Figure 4.21 for the area used to define each region.

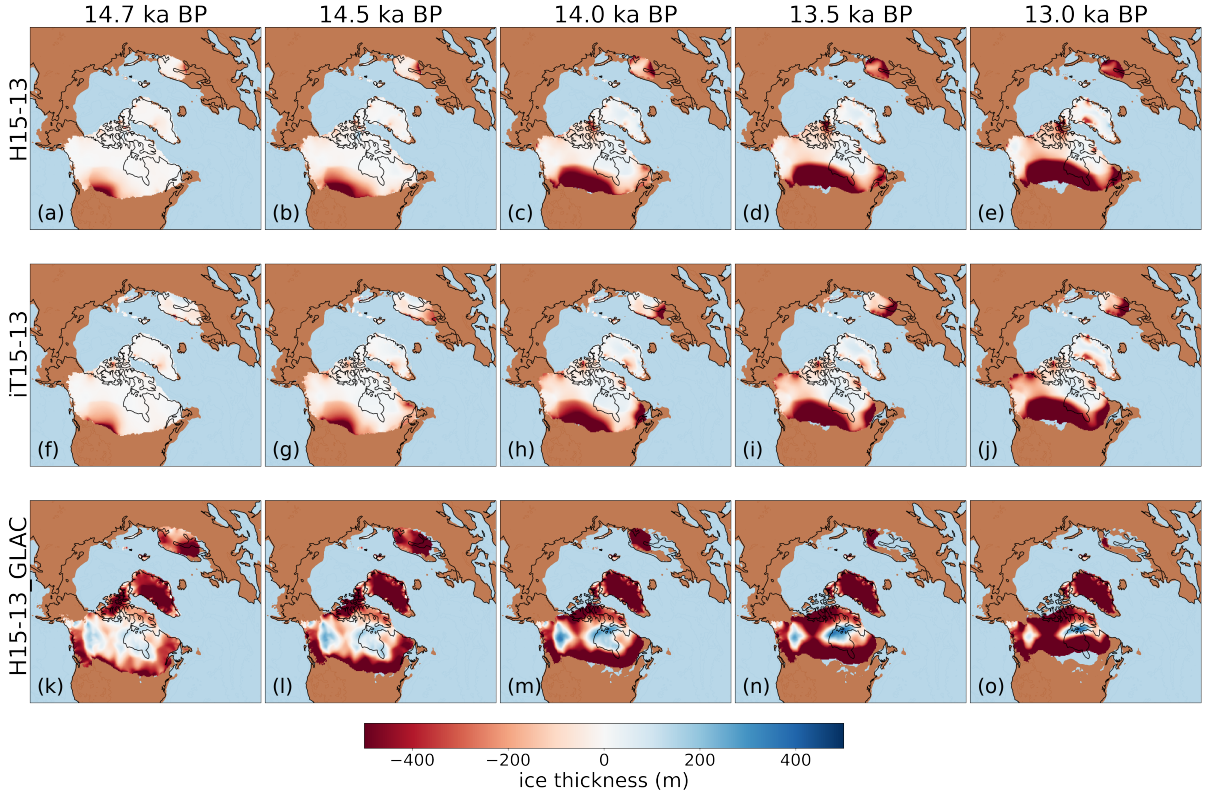

Figure 4.26: Ice thickness anomaly between the simulation labelled and its respective control simulation, i.e., *Acc_H15_SST* for *H15-13*, *Acc_iT15_SST* for *iT15-13*, and *Acc_H15_GLAC_SST* for *H15-13_GLAC*.

Figure 4.27: Absolute ice thickness of each simulation compared to reconstructions. The yellow-green curve is ICE-6G_C, the pale pink curve is GLAC-1D, and the deep-pink curve is by Dalton et al. (2023) for the North American and Greenland ice sheets and Hughes et al. (2015) for the Eurasian ice sheet.

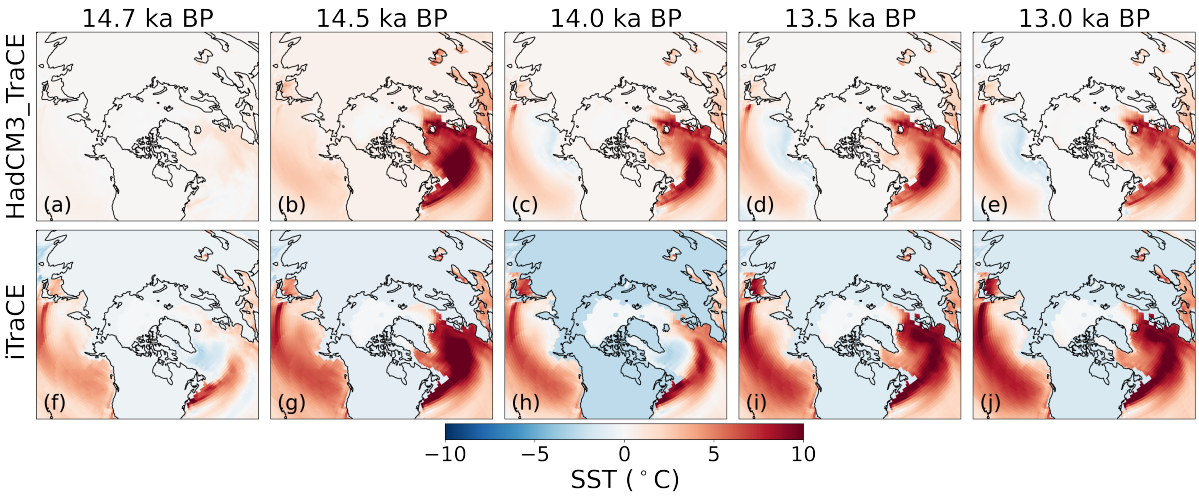

Figure 4.28: Prescribed sea surface temperature from the *HadCM3_TraCE* and *iTraCE* simulations at the time labelled as anomalies from *HadCM3_TraCE* at 15 ka BP

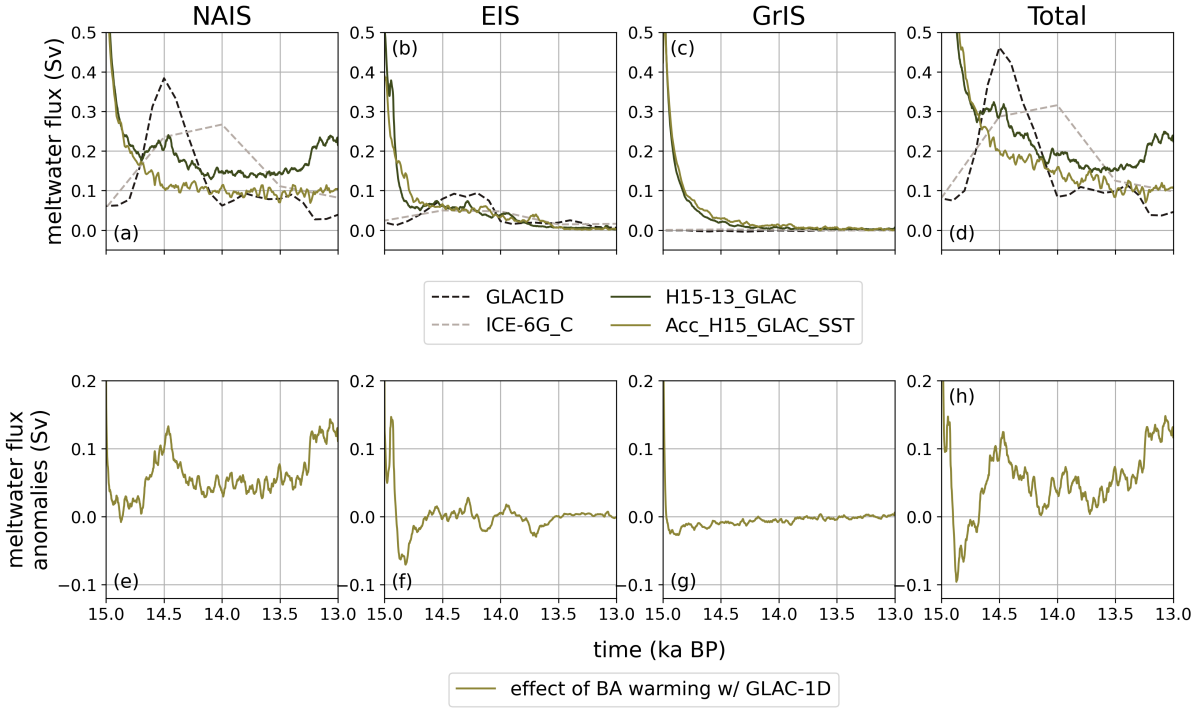

Figure 4.29: (a)-(d) Meltwater flux as derived from the ice sheet volume curve for each ice sheet (North American ice sheet; NAIS, Eurasian ice sheet; EIS, and Greenland ice sheet; GrIS) and all ice sheets in total for each simulation. (e)-(h) Meltwater flux anomalies between simulations in this study (see Table 4.5 for how each curve is calculated) for the same locations as (a)-(d). See Figure 4.21b for the area used to define each ice sheet.

CHAPTER 5

Discussion and conclusion

5.1 Summary

Through this thesis, I aimed *to investigate AMOC evolution and its role in abrupt climate change during the Last Glacial Period using different modelling approaches.* This was done by analysing a collection of simulations following the Palaeoclimate Modelling Intercomparison Project phase 4 last deglaciation protocol version 1 (PMIP4 LDv1), determining the robustness of Atlantic Meridional Overturning Circulation (AMOC) oscillations to changes in background conditions in HadCM3 simulations, and testing the impact of the Northern Hemisphere ice sheets to abrupt climate changes using a coupled climate-ice sheet model.

To answer **RQ1: What is the influence of transient ice sheet meltwater histories on the occurrence of abrupt climate change, such as Heinrich Stadial 1?**, I partook in a multi-model intercomparison project of last deglaciation simulations that had not previously been collectively analysed. The results of this analysis, found in Chapter 2, concluded that the meltwater discharge prescription chosen by the modelling group significantly affected the timing of the deglaciation, the impact of other transient forcings, and the replication of observed abrupt climate events. The difficulty reconciling a weak AMOC during the early deglaciation and Heinrich Stadial 1 or a strong AMOC during the Bølling Warming with a glaciologically consistent meltwater flux defines the 'meltwater paradox', where the freshwater forcing required by models to produce recorded climate change is broadly in opposition to the meltwater history reconstructed from ice sheet and sea level records. The unresolved meltwater paradox highlights the remaining uncertainty as to the chain of deglacial events, i.e., the timing, location, and amount of freshwater discharge during the deglaciation (Chapter 4) and how the AMOC, under evolving background conditions, is impacted by it (Chapter 3), demonstrating the importance of answering RQ2 and RQ3.

To answer **RQ2: How do changes in Earth's orbital configuration and atmospheric CO_2 impact abrupt transitions from weak to strong AMOC modes?**, I tested the resilience of AMOC oscillations to changes in the background climate. I did this by varying atmospheric CO_2 concentration and orbital configuration with HadCM3 simulations in which Romé et al. (2022) previously found oscillatory behaviour. The results of these sensitivity

tests, presented in Chapter 3, determined that an increase in CO_2 concentration ended the AMOC oscillations, whereas a CO_2 decrease shortened the duration of the interstadial mode. Boreal seasonality increases also led to a decrease in the warm interstadial mode, but the AMOC under the strongest seasonality remained oscillating within the warm mode attributed to differences in obliquity. I determine that the timing of an AMOC transition from weak to strong modes or vice versa is modulated by sea ice, adding on to the convection-advection mechanisms of Romé (2024). I demonstrated, through these results, that small changes in background conditions control whether spontaneous abrupt transitions in the AMOC can occur and if so, how the mechanism is impacted, highlighting the need to consider background conditions when evaluating drivers of rapid climate changes.

To answer **RQ3: How sensitive are the Northern Hemisphere ice sheets to the Bølling Warming under transient conditions?**, I transitioned from investigating the climatic controls on abrupt climate events to determining the impact of them on the ice sheets. I utilised the coupled atmosphere-only climate-ice sheet model, FAMOUS-BISICLES, to perform multiple simulations of the last deglaciation with prescribed surface ocean forcing that included abrupt climate events like Heinrich Stadial 1 and the Bølling Warming. The results of these simulations, presented in Chapter 4, sought to alleviate some of the temporal and spatial uncertainty as to the melting of the ice sheets and the resulting freshwater flux dealt with in Chapter 2. The conclusions demonstrated that more ice sheet volume loss occurred as a result of the Bølling Warming compared to when a gradual deglaciation is simulated, but the amount of additional melt is dependent on the starting ice sheet and surface ocean forcing used. The saddle collapse between the Laurentide and Cordilleran ice sheets is not simulated, but the North American ice sheet is still the largest contributor to Meltwater Pulse 1a, with most melt originating from the southern margin of the ice sheet.

The answers to each of these research questions highlight the importance of considering the background climate when evaluating causal mechanisms to abrupt climate changes during the Last Glacial Period. This is further discussed in the comprehensive discussion and conclusions section whilst connecting the results to the broader research. The discussion is followed by a critical evaluation of the limitations of the thesis and potential avenues to reduce the remaining gaps in knowledge.

5.2 What are the climatic controls on AMOC evolution and our ability to predict abrupt climate change events?

Despite the main events of the Last Glacial Period being fairly well constrained (Clark et al. 2012), the existing uncertainties of their magnitude and geographical extent emphasise the benefit of modelling to fill the knowledge gaps. For instance, earth system modelling can assist with the ongoing debate as to the state of the overturning circulation during the Last Glacial Maximum (LGM) (Muglia and Schmittner 2021; Repschläger et al. 2021; Pöppelmeier et al. 2023b), as well as determining the evolution of the ice sheets (Tarasov et al. 2012; Peltier et al. 2015; Batchelor et al. 2019; Gowan et al. 2021). The remaining uncertainty on ice

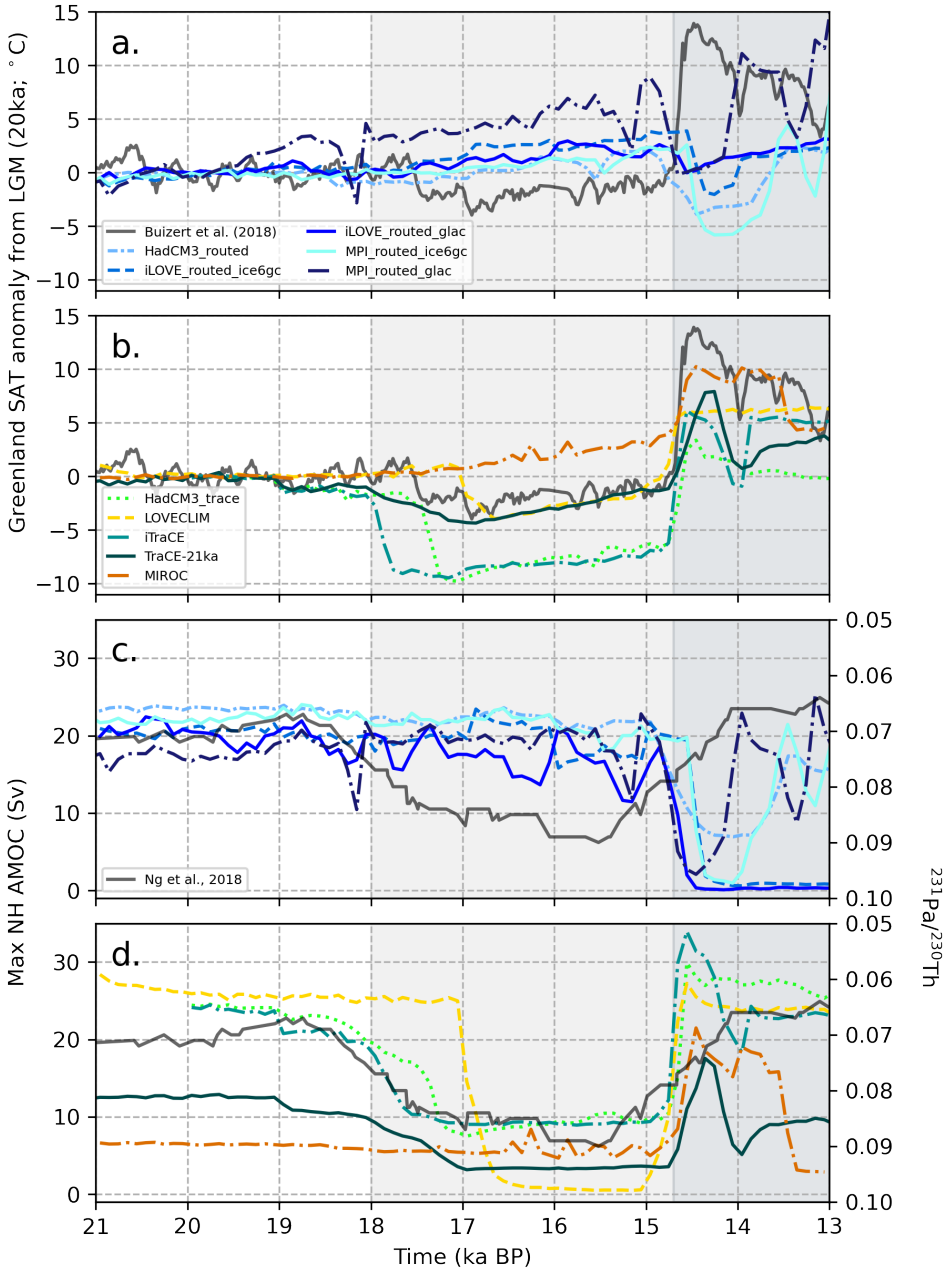

Figure 5.1: PMIP4 LDv1 simulations from Chapter 2. (a)-(b) Centennial mean Greenland surface air temperature (SAT) as an anomaly from the LGM (in this case 20 ka BP) for the *melt-routed* simulations (a) and the *TraCE-like* simulations and *MIROC* (b). (a)-(b) also includes the Greenland proxy temperature record of Buizert et al. (2018) in black. (c)-(d) The same as in (a)-(b) but for the maximum Northern Hemisphere (NH) AMOC strength. (c)-(d) also includes the Pa/Th convection proxy of Ng et al. (2018) in black.

sheet geometries during the Last Glacial Period has also led to a limited certainty on freshwater discharge, which is shown, as in Chapter 2, to be restricting when it comes to climate simulations and being able to reconstruct the chain of events (and causality). The climate model simulations in Chapter 2, conducted following the PMIP4 LDv1, underscore the critical role of freshwater fluxes in shaping the deglacial evolution. Modelling groups that prescribed a freshwater flux derived from the current known evolution of the ice sheets failed to reproduce the abrupt climate

events (Figure 5.1a; e.g., Kapsch et al. 2022; Snoll et al. 2022; Bouttes et al. 2023). Only groups that used a meltwater scenario that modulates the AMOC to achieve a set of target ocean circulation and surface temperature conditions (with significantly larger amounts of freshwater input than ice sheet reconstructions suggest) could successfully replicate these events (Figure 5.1b; e.g., Liu et al. 2009; He et al. 2021), except for the PMIP4 LDv1 MIROC simulation.

The need for a more than 'realistic' freshwater input aligns with the argument that the AMOC has too muted a response to meltwater during Heinrich Stadial 1 under certain conditions in climate models (Valdes 2011; Liu et al. 2014), rather than too sensitive (e.g., He and Clark 2022). However, if that were true, it presents a conundrum for Meltwater Pulse 1a (MWP1a). The simulations that do follow the ice sheet history force a cooling event in Greenland on the scale of 10 °C at the timing of MWP1a (specifically, the MPI and HadCM3 simulations; the AMOC in the iLOVECLIM simulations collapses and does not recover for several thousand years and the associated Greenland temperature changes are smaller than with MPI and HadCM3). If models are too muted to freshwater forcings, then a 'better' climate model could potentially simulate an even larger scale abrupt cooling at ∼14.7 ka BP (unless the AMOC is already weak) which would still contradict the abrupt warming occurring in Greenland at this time (Buizert et al. 2018). The disconnection between the model sensitivity and the AMOC's current modelled response to meltwater discharge in transient simulations of the last deglaciation suggests that there is still a gap in knowledge about the climatic controls on the AMOC.

One particular aspect of research on abrupt climate change that is often overlooked is the initial state of the AMOC and its influence on subsequent climate change. The last deglaciation simulation performed by the MIROC climate model, provides an opportunity to reach a new level of understanding. The MIROC LDv1 simulation is unique in that it simulates a weak AMOC and cold surface air temperatures of Heinrich Stadial 1 as well as the resumption of the AMOC for the Bølling Warming without releasing unrealistically large amounts of freshwater (Figure 5.1b). I determine in Chapter 2, that MIROC displays a different sensitivity to freshwater input compared to the rest of the deglaciation ensemble, likely due to the simulation of a very weak AMOC at the LGM. Obase and Abe-Ouchi (2019) show that without the meltwater flux, in a similar MIROC simulation, the presumably unstable, weak AMOC (aligned with the results of Tziperman 2000; Arzel et al. 2012) would have abruptly transitioned to a strong mode by 19 ka BP solely due to increasing insolation and greenhouse gases. Thus, the timing of the abrupt increase in the AMOC is dependent on the meltwater release. The MIROC AMOC is likely close to a stability threshold because only a small meltwater perturbation was needed to result in a large change in the system, and additionally, there is an increase in noise or temporal variability ahead of the abrupt AMOC increase (Figure 5.1d). This is coincides with Kapsch et al. (2022), Klockmann et al. (2018), and Oka et al. (2012) who propose that a weaker AMOC is more sensitive to perturbations. Their simulations begin with a strong LGM AMOC that is examined for its likelihood to weaken. The stronger AMOC, in this case, is deemed to be more stable (Tziperman 2000; Arzel et al. 2012) and therefore farther from a stability threshold and more difficult to perturb.

In the case of the oscillating simulations presented in Chapter 3, the AMOC strength at the start

of the simulations is ∼15 Sv. This is ∼7 Sv weaker than at the LGM (21 ka BP) in the PMIP4 LDv1 simulations performed with the same model (HadCM3). The HadCM3 LGM constant control run has a weaker AMOC than a transient HadCM3 simulation at the LGM because of the difference in ice sheet topography between ICE-6G_C and GLAC-1D (Izumi et al. 2023), indicating the role ice sheet topography has in modulating AMOC strength (e.g., Ullman et al. 2014; Löfverström and Lora 2017; Gregoire et al. 2018; Sherriff-Tadano et al. 2018; Bakker et al. 2020; Kapsch et al. 2022; Bouttes et al. 2023). The AMOC in the constant LGM control run (Romé et al. 2022) is also more easily perturbed by a freshwater flux. Once a 0.084 Sv flux is added to the system (equivalent to 0.731 m SLE), the AMOC begins to spontaneously oscillate with a periodicity of ∼1,500 years (Romé et al. 2022, Chapter 3). This is not dissimilar from the meltwater flux in the PMIP4 LDv1 MIROC simulation that modulates the timing of an abrupt increase in the AMOC. Whereas, a similar freshwater flux applied to the *HadCM3_routed* PMIP4 LDv1 experiment, does not perturb the AMOC for ∼3,000 years (Figure 5.1c). It is not until CO_2 concentrations begin to rise ∼18 ka BP that we see a noticeable deviation in AMOC strength in that simulation, suggesting that either the increasing insolation and/or difference in simulated conditions at 21 ka BP play a critical role in the AMOC's stability.

The role of orbital forcing and insolation on the sensitivity of the AMOC and modulating glacial-interglacial cycles (e.g., Berger 1988; Vettoretti and Peltier 2011; Yin and Berger 2012; Gregoire et al. 2015) is further demonstrated by the impact of orbital forcing on the magnitude and periodicity of AMOC oscillations (Chapter 3) and confirmed by previous studies (e.g., Rial and Yang 2007; Brown and Galbraith 2016; Yin et al. 2021; Zhang et al. 2021; Kuniyoshi et al. 2022). More specifically, when investigating the likelihood of millennial-scale variability, increases in boreal seasonality (due to the combination of orbital parameters) increases the periodicity of AMOC oscillations in climate model simulations (Brown and Galbraith 2016; Kuniyoshi et al. 2022, Chapter 3). The change in insolation in the simulations presented in Chapter 3 moderately align with the shape of D-O cycles at each corresponding time (Figure 5.2a; inspired by Rial and Yang (2007)). For instance, the *Orbit_30k* simulation, with an orbital configuration representing 30 ka BP conditions, has rapid and sharp transitions in Greenland temperature, similar to the D-O cycles occurring around this time. The *Orbit_10k* simulation, on the other hand, matches with the smaller-scale variability in Greenland surface air temperature of the Holocene interglacial period after 11 ka BP. The *REF* simulation with 21 ka BP orbital conditions, is the least representative of the the Greenland temperature record at 21 ka BP; however, the length of these oscillations are longer, more like that of the variability that occurs during the deglaciation (e.g., the Bølling Warming and Younger Dryas). The differences in the shape of the oscillations also coincide with changes in how the AMOC reaches an internal tipping point (e.g., the balance between salinity increase from brine rejection and salinity decrease from lack of convective transport discussed in Chapter 3), meaning that individual D-O cycles might be governed by mechanisms that are not all the same. These simulations were very idealised, and the differences in amplitude, periodicity, and frequency between the oscillations introduced in Chapter 3 and the temperature variability observed in Greenland at the respective times could be influenced by factors not accounted for in my simulations such as differences in the ice sheet topography and atmospheric greenhouse gases.

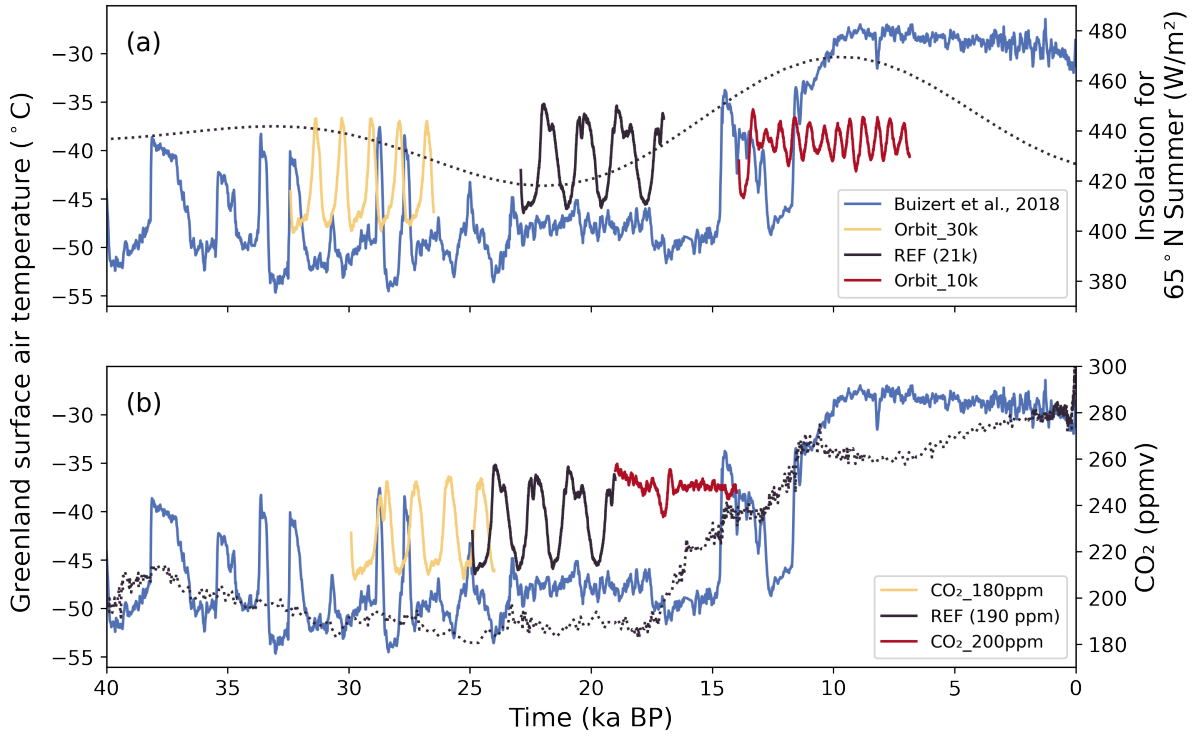

Figure 5.2: (a) Greenland surface air temperature proxy record (blue; Buizert et al. 2018) plotted alongside summer insolation at 65° N latitude (Berger 1978) and Greenland surface air temperature from Chapter 3 orbital configuration sensitivity experiments. (b) Greenland surface air temperature proxy record (blue) plotted alongside the CO_2 concentration proxy record (Bereiter et al. 2015) and the results from the Chapter 3 CO_2 tests. The Chapter 3 experiments are plotted on the x-axis centred as close as possible to the timing of the respective orbital configuration or CO_2 concentration.

Chapter 3 also illustrates the importance of greenhouse gas concentrations, specifically CO_2, in creating optimal background conditions to promote abrupt climate change. The simulated Greenland temperature from my different CO_2 scenarios are less representative of observed D-O cycles than with the orbital configuration changes (Figure 5.2b), but the transition from 190 ppm to 200 ppm displays a familiar pattern–i.e., the transition from Heinrich Stadial 1 to the Bølling Warming and then the Older Dryas, or the transition from the Younger Dryas into the Holocene and then the 8.2 kyr event (an abrupt cooling of 1-3 °C that lasted ∼160 years in the Northern Hemisphere; Thomas et al. 2007; Morrill et al. 2013). Furthermore, the relatively small change in CO_2 concentration (10 ppm) moved the background state from within the 'sweet spot' of millennial-scale variability (Barker and Knorr 2021) to outside it, indicating that small changes can be instrumental in allowing the AMOC to spontaneously strengthen or weaken. The CO_2 concentration at which the transition from within the 'window of opportunity' to outside it occurs is dependent on other background conditions. Malmierca-Vallet et al. (2024) empirically identified an atmospheric CO_2 sweet spot for AMOC oscillations in three different climate models (one of which is HadCM3, used in Chapter 3). However, their defined range (185 - 230 ppm) sits with higher CO_2 concentrations than our results ($<$ 200 ppm; I do not have enough simulations to identify a low end of the range), demonstrating that their CO_2 window for AMOC instability is not universally applicable. There are multiple differences in

the initial and boundary conditions between the simulations reviewed by Malmierca-Vallet et al. (2024) and my simulations from Chapter 3 (e.g., my simulations have a meltwater flux, larger ice sheets, and a different orbital configuration), suggesting that the 'window of opportunity' for unforced AMOC transitions (their occurrence, frequency, and amplitude) is multi-dimensional and controlled by the combination of background conditions, and thus caution must be applied when defining a range for one or a few individual climate variables (such as CO_2).

The nuances of the connection between the background climate and AMOC behaviour might be easier to identify in quasi-idealised climate experiments, such as those presented in this thesis, but it is critical to consider transient contexts. Outside of idealised experiments, multiple aspects of the background climate are consistently changing. The impact of transient forcings is emphasised by the results from Chapter 2 and the PMIP4 LDv1 experiments that do not produce an oscillating AMOC nor any unforced abrupt climate changes. In addition, the model or model configuration can influence whether the AMOC responds linearly to meltwater fluxes or not (e.g., the response of the decrease in AMOC strength in the MPI and HadCM3 PMIP4 LDv1 simulations due to Meltwater Pulse 1a versus the collapsed AMOC in the iLOVECLIM simulations, as well as the lack of AMOC response in *HadCM3_routed* to a small meltwater flux versus the oscillatory behaviour of Romé et al. (2022)'s *20.7k* simulation with a similar amount of meltwater and utilising the same model). Changes in background conditions can also spontaneously move the AMOC through modes of bistability (Chapter 3; Vettoretti et al. 2022). Although, the uncertainty as to the timing, location, and amount of freshwater discharge that would have occurred during this time period makes it difficult to determine whether abrupt climate changes in the Last Glacial Period (such as, Heinrich Stadial 1 or the Bølling Warming) were forced by meltwater discharge with a linear response of the AMOC, a non-linear response of the AMOC, or were unforced.

Chapter 4 attempts to reduce the meltwater discharge uncertainty by diagnosing the impact of abrupt climate changes on the Northern Hemisphere ice sheets. Two different ocean forcings were prescribed from transient simulations of the last deglaciation from the *TraCE-like* group of the PMIP4 LDv1 simulations–*iTraCE* and *HadCM3_TraCE* (Figure 5.1)–to an atmosphere-only coupled climate-ice sheet model. The freshwater scenarios used for *iTraCE* and *HadCM3_TraCE* are 'trained' to replicate the AMOC and Greenland temperature proxy records and are, therefore, not 'realistic', but both simulations produce Bølling Warming events that match relatively well with the magnitude of observations (Buizert et al. 2018), providing the opportunity to test the impact of the abrupt event on the ice sheets.

The abrupt Bølling Warming causes an additional 2-3 m SLE of ice sheet melt (Chapter 4), but the magnitude of the effect and overall contribution to Meltwater Pulse 1a depends on the initial ice sheet configuration and the oceanic forcings. The results further highlight the importance of background conditions on the state of the climate as well as model uncertainty and biases. For instance, *iTraCE* and *HadCM3_TraCE* have very similar experimental designs, except for the marginally larger meltwater flux in *iTraCE*, but employ different models (iCESM; Hurrell et al., 2013; and HadCM3; Valdes et al., 2017, respectively), allowing us to test the impact of different (but still plausible within the realms of possibility, and with a physical basis) sea

surface temperature and sea ice forcings. Specifically, the AMOC's response to the meltwater flux and the resulting temperature in deeper layers of the ocean and Northern Hemisphere sea ice concentration differ between the models, causing variations in the simulated surface mass balance of the Northern Hemisphere ice sheets (Chapter 4) and emphasising the benefit of testing model biases with MIPs.

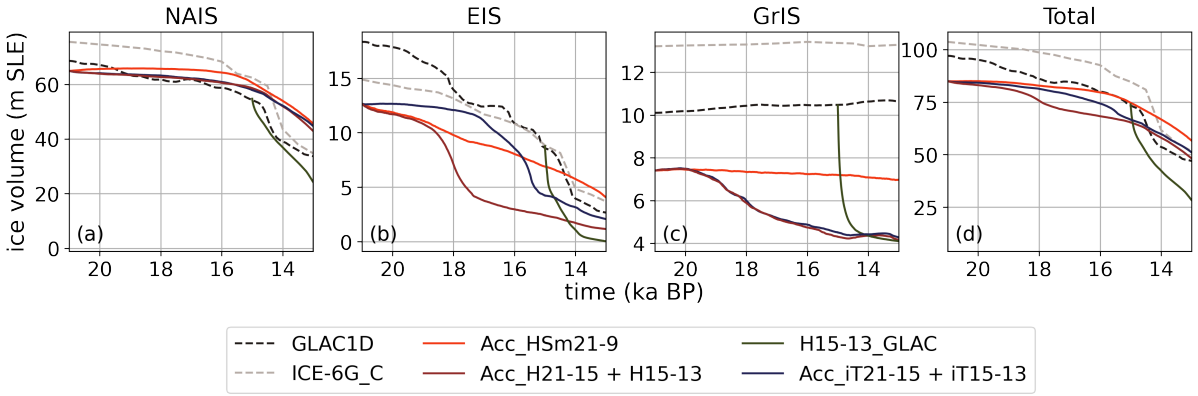

Figure 5.3: Ice sheet volume from 21-13 ka BP averaged over each ice sheet (North American ice sheet; NAIS, Eurasian ice sheet; EIS, and Greenland ice sheet; GrIS) and all Northern Hemisphere ice sheets in total for the simulations performed in this study, GLAC-1D and ICE-6G_C ice sheet reconstructions, and the *Acc_HSm21-9* simulations performed by Patterson et al. (Thesis).

In addition, substantially more melt occurred during the Bølling Warming when starting from the GLAC-1D 15 ka BP ice sheet rather than a simulated ice sheet because the GLAC-1D ice sheet was thinner and presumably not equilibrated with the climate (Figure 5.3). Differences in ice sheet topography have proven to be crucial for the existence of spontaneous abrupt climate changes (e.g., Chapter 3 results versus the results of Armstrong et al., 2022 as well as their 28 ka BP simulation versus their 30 ka BP simulation; Klockmann et al. 2018; Kapsch et al. 2022; Bouttes et al. 2023), but Chapter 4 confirms that the evolution of the ice sheet geometry not only directly affects the climate but also how the ice sheets respond to abrupt climate changes and thus the amount of meltwater deposited into the North Atlantic, sea level rise, and the AMOC. Small changes in the amount of meltwater discharge and location of the freshwater flux can be the determining factor between millennial-scale variability occurring or not (Romé et al. 2022). Driving ice sheet models or coupled climate-ice sheet simulations with abrupt climate events, as opposed to gradual deglacial forcings (e.g., Patterson et al., Thesis; Quiquet et al. 2021b) have proven to cause significant differences in ice sheet evolution (Chapter 4; Gregoire et al. 2016). For instance, I determine that ∼5 m SLE more ice volume is lost during the deglaciation (between 21 and 13 ka BP) in simulations forced with abrupt climate events (Heinrich Stadial 1 and the Bølling Warming) versus with a gradual warming, as performed by Patterson et al. (Thesis) with the same coupled climate-ice sheet model (Figure 5.3). However, notably, the opposite is true in the simulations by (Gregoire et al. 2016), though their results are strongly dependent on the timing of the simulated Cordilleran-Laurentide saddle collapse, which I do not successfully replicate. Their results, and those of Gregoire et al. (2012) and Gomez et al. (2015), suggest that simulating the saddle collapse at the time of the Bølling

Warming would increase the meltwater discharge from the North American ice sheet (i.e., from ∼5 m SLE between 14.7 to 14.1 ka BP; Chapter 4) and its contribution to Meltwater Pulse 1a, but the timing and therefore the contribution of the Cordilleran-Laurentide saddle collapse to the meltwater event is still debated (e.g., Reyes et al. 2024; Coonin et al. 2025).

Future work is necessary to further pursue the investigations brought forth in this thesis and continue learning about atmosphere-ocean-ice interactions, the timing and magnitude of events, and the influence of climatic variables on the occurrence of AMOC transitions and abrupt climate changes.

5.3 Implications for current and future climate

The results of this thesis highlight the critical importance of model dependency as well as background condition dependency. The conclusions presented in Chapters 2, 3, and 4 are contingent on the model used, the background climate, and the climate forcings prescribed. In addition, they demonstrate paradoxical behaviour (i.e., between meltwater pulses and climate events) that signal to potential gaps in our knowledge of physical processes in the North Atlantic. It is evident from past climate records as well as from model simulations that tipping points in the AMOC can and have previously occurred, but the specific conditions of the climate that are necessary for a tipping point are less clear due to the dependencies explored throughout this thesis. For example, as little as 10 ppm of CO_2 can move the AMOC in and out of a window of possible tipping, but the level of CO_2 concentration is dependent on the model used and background climate. If we have difficulty robustly simulating climate changes in which we have some record of their existence and the background conditions at the time, there are implications for how reliable our predictions can be for the future, a time period where we have no records for evaluation.

5.4 Limitations and future work

Each of the research questions posed as part of this thesis used different methodology with their own limitations and strategies for moving forward.

5.4.1 RQ1: PMIP4 LDv1

Answering RQ1 was limited by the design of the PMIP4 LDv1 protocol (Ivanovic et al. 2016). The flexibility of the protocol was advantageous in tackling two objectives in one–determining the influence of the experimental design as well as the impact of the model–whilst acknowledging the uncertainty of the time period and incorporating more needs and desires of various modelling groups. However, it also restricted the ability to draw conclusions across the ensemble and make direct model-to-model comparisons. Because most of the model simulations did not have the exact same experimental design, it became challenging to determine what differences in the climate output were due to model sensitivity versus the differences in boundary conditions. Grouping the simulations into categories based on similarities in experimental design was helpful and allowed for RQ1 to be answered; however it would be ideal to be able to compare more

simulations with the same experimental design and more scenarios tested by the same model to learn more about model sensitivities as well as test additional plausible scenarios of climate changes and AMOC states during the last deglaciation.

Therefore, the work of Chapter 2 can provide a foundation for developing new last deglaciation MIP protocols. I recommend that one of the protocols focuses on narrowing down the uncertainties regarding the 'meltwater paradox' that exists between the choice of large and geologically inconsistent meltwater forcings that successfully produce abrupt climate events versus glaciologically realistic meltwater fluxes that do not. This could initially begin by employing the various freshwater fluxes that modelling groups used previously and determining the impact of a different meltwater scenario on a new model (i.e., the groups that originally employed a 'trained' meltwater flux instead prescribing a glaciologically consistent flux). It would be interesting to determine what 'trained' meltwater fluxes were required for each model to replicate the AMOC and Greenland proxy records as the *TraCE-like* groups have and the MIROC simulation has done. Additionally, it would be critical to try these with different ice sheet reconstructions (based on the work of Kapsch et al. 2022; Bouttes et al. 2023; Izumi et al. 2023) . Most importantly, having more simulations with the same experimental design will allow for more direct model-to-model comparisons and investigating individual AMOC sensitivities.

To perform this many transient last deglaciation simulations, however, is very computationally and time expensive. Therefore, additional analysis can also be performed on the PMIP LDv1 simulations that are already available. Chapter 2 was focussed on the early deglaciation (until 15 ka BP) out of interest in comparing simulations when there was less variability. However, the time period between 15 and 11 ka BP has the largest disparity (Figure 5.1) due different methods of simulating the paradoxical occurrence of the Bølling Warming and AMOC strengthening alongside freshwater inputs from MWP1a that should be driving AMOC weakening and Northern Hemisphere cooling. Thus, the latter half of the deglaciation provides the opportunity to further investigate AMOC sensitivity to freshwater fluxes in particular models because more, and more diverse, AMOC responses are happening. For instance, the community could inquire into the muted response of the AMOC in CCSM3 (simulating *TraCE-21ka*) compared to HadCM3 (simulating *HadCM3_TraCE*) despite using the same freshwater flux, or the more sensitive AMOC in EMICs; i.e., LOVECLIM and iLOVECLIM show higher magnitude shifts in the AMOC and an AMOC collapse, respectively, despite using similar freshwater fluxes as other models.

Ultimately, the 'meltwater paradox' cannot be resolved with climate models alone. Temporal uncertainty in proxy reconstructions makes statistical processes such as history matching (adjusting a model so that it matches observed data) and data assimilation (combining observations with model data) challenging for palaeoclimate modelling, highlighting the difficulty in evaluating model performance. Developments in ice sheet reconstructions, such as constraining ice sheet melt (e.g., for the Cordilleran ice sheet), and proxy data availability, such as higher temporal resolution data, will significantly increase our understanding of AMOC sensitivity. In addition the inclusion of ice sheet models in transient climate simulations, as discussed further in section 5.4.3 will increase the community's ability to understand atmosphere-ocean-ice

interactions and how they contribute to abrupt climate events.

5.4.2 RQ2: AMOC oscillations in HadCM3 glacial simulations

Malmierca-Vallet et al. (2024) show that three different models produce D-O-like oscillations under the same range of CO_2 concentrations. At first glance, this suggests that there is consistency between models, but upon deeper analysis, each modelling group has a different experimental design with different background conditions. In Chapter 3, I utilised the HadCM3 climate model, one of the three discussed by Malmierca-Vallet et al. (2024), to similarly test the impact of different CO_2 concentrations on AMOC oscillations, but I use a different experimental design (i.e., different ice sheet topography, orbital configuration, and inclusion of a meltwater flux) and do not produce D-O-like oscillations under the same range of CO_2 concentrations. In addition, Malmierca-Vallet et al. (2024) describe how no climate properties (e.g., mean AMOC strength, North Atlantic salinity, subsurface temperature, and global mean ocean and surface temperature) except for North Atlantic sea ice show commonality amongst the models in their impact on D-O cycles, suggesting that the modelled mechanisms for D-O cycles are likely to be model and background condition dependent (consistent with my conclusions from Chapter 3 as changing the background conditions changed the oscillatory mechanism). The combination of the Chapter 3 study and the work of Malmierca-Vallet et al. (2024) highlights the importance of background conditions on the 'window of opportunity' (Barker and Knorr 2021).

Because of this, the Chapter 3 conclusions bring forth ideas for how to take the work forwards and expand it. In principle, it would be ideal to conduct as many climate simulations as possible, systematically varying different models, ice sheet conditions, greenhouse gas concentrations, orbital configuration, and meltwater fluxes. However, this is usually not feasible due to the computational expense, especially because it is necessary to perform the simulation for thousands of years to confirm the continuation or lack of an oscillating AMOC.

One way forward to narrow down the amount of possible simulations would be to focus on a particular set of background conditions. There is a large amount of evidence from proxy records (North Greenland Ice Core Project members 2004; Dome Fuji Ice Core Project Members: et al. 2017; Buizert et al. 2018) and model studies (e.g., Dome Fuji Ice Core Project Members: et al. 2017; Zhang et al. 2017; Zhang and Prange 2020) that millennial-scale variability and tipping points in the AMOC are more likely to occur during periods of intermediate glacial conditions rather than full glacial conditions (such as the LGM) or full interglacial conditions (such as the pre-industrial; Barker and Knorr 2021) (i.e., we identify more abrupt events during Marine Isotope Stage (MIS3) than during the LGM and more during the deglaciation than during the Holocene). In addition, modelling studies have shown that D-O-like behaviour tends to occur under orbital conditions like that of MIS3 (i.e., low obliquity and moderate eccentricity; Chapter 2; Zhang et al. 2021; Kuniyoshi et al. 2022), with intermediate or low MIS3 CO_2 concentrations (Zhang et al. 2014; Brown and Galbraith 2016; Klockmann et al. 2018; Vettoretti et al. 2022), with smaller-than-LGM ice sheets (Dome Fuji Ice Core Project Members: et al. 2017; Zhang and Prange 2020; Armstrong et al. 2022), and with intermediate freshwater fluxes (Dome Fuji Ice Core Project Members: et al. 2017; Zhang and Prange 2020; Romé et al. 2022). On

the back of these previous findings, Malmierca-Vallet et al. (2023) developed a baseline MIS3 experiment protocol in which to gather a larger number of standardised MIS3 simulations, whether they include AMOC oscillations or not. Having more simulations under intermediate, MIS3 conditions, when most of the recorded D-O cycles occurred can help the community explore the existence of the 'window of opportunity' whilst determining if current climate models are capable of representing unforced abrupt events under more realistic conditions.

However, this protocol suggests, to reduce computational time and increase feasibility, that an 1,000-year spin-up plus a minimum of a 2,000-year long run is sufficient, but the simulations with less consistent variability (e.g., Romé et al. (2022)'s *18.2k* simulation and my *200ppm* simulation) demonstrate that an integration length of only 2,000-3,000 years long would not capture spontaneous abrupt events that are equally as valuable as steady oscillations, if not more comparable to the temperature patterns recorded in Greenland (Buizert et al. 2018). In addition, whilst following this protocol, models might further prove themselves to be too stable and struggle to simulate abrupt climate transitions under MIS3 conditions, suggesting that the protocol could be too restrictive with current models if the goal is to achieve AMOC oscillations.

Abrupt climate events are similarly challenging to replicate under deglacial conditions with transient forcings, as I demonstrated in Chapter 2 and 4, and transient forcings are not considered in the MIS3 D-O protocol. A different method for including transient forcings and other combinations of background conditions as well as testing model stability, could be to conduct simulations like those of (Zhang et al. 2021) but instead of altering a few glacial conditions at once, only change one boundary condition at each chosen stage of the simulation and allow for the climate to re-equilibrate each time. This guarantees that only one forcing or condition is changing at a time, which is not the case for my simulations in Chapter 3 (see list below). The method of (Zhang et al. 2021) considers transient forcings in an idealised framework. In reality, the climate does not equilibrate to transient forcings, but it gives the modeller the time to diagnose the impact and ensure that no other variables are interfering with the conclusions.

Finally, and perhaps the easiest, the simulations of Chapter 3 could be redone with a few changes or additions:

1. Allowing there to be time in between the addition of the freshwater flux and the new condition. For Chapter 3, the simulations all begin from the LGM constant run, meaning that both the meltwater flux and the boundary condition change occurs at the same time. Changing one condition at a time and allowing the model time to adjust to the perturbed forcing would ensure the results were due to the change in background condition as opposed to the combination of the condition and the freshwater flux.

2. Changing the ice sheet topography to a smaller or intermediate ice sheet from a large LGM ice sheet to determine if the AMOC oscillations are sustainable under other ice sheet conditions and to compare with other oscillating simulations, following the advice of Malmierca-Vallet et al. (2023).

3. Changing the boundary condition at different points in the oscillation (i.e., when the AMOC is strong, weak, or in a transitional mode) to test the impact of initial AMOC

conditions, as shown to be important by Chapter 2 and previous studies (e.g., Kageyama et al. 2013; Kageyama et al. 2021).

4. Testing lower CO_2 concentrations to develop a more comprehensive window (i.e., determining at what low CO_2 the oscillations would stop again and how the AMOC would be impacted) to compare to Malmierca-Vallet et al. (2024).

5. Adding the freshwater flux second (i.e., after the change in the boundary condition), instead of first, to test the impact of a freshwater flux on the AMOC when already in a different background climate. This is a quasi-idealised way to test if the AMOC's ability to reach a tipping point due to a freshwater forcing is dependent on CO_2 concentration, orbital configuration, or ice sheet height, as opposed to testing whether the AMOC will *stay* in an oscillatory state if the background climate changes.

5.4.3 RQ3: FAMOUS-BISICLES simulations

Both Chapter 2 and Chapter 3 do not consider the impact of ice sheet feedbacks because the ice sheets are only prescribed. Ideally, all of the aforementioned future model work would include a dynamic ice sheet model, but unfortunately, this is technically challenging and can amplify model biases through coupled feedbacks. In addition, as demonstrated in Chapter 4, climate-ice sheet model parameter combinations that produce the best match to ice volume and extent for one time period do not necessarily perform well for other time periods–e.g., the best parameter combination for the LGM (Patterson et al. 2025) was too stable to deglaciate well enough after 21 ka BP and also did not match any of the parameter combinations used for the modern Greenland (Lang et al. 2023)–highlighting the importance of performing transient simulations of ice sheet evolution to make sure, for instance, the model is able to simulate ice sheet change. In the case of Chapter 4, I do not test model uncertainty, so it is undetermined how the results of the study would be impacted by different model parameters. Previous work suggests that changing the parameters would have a strong influence (Quiquet et al. 2021b; Patterson et al. 2024; Sherriff-Tadano et al. 2024; Patterson et al. 2025), e.g., decreasing sub-shelf melt rate forcing results in a lower contribution from ocean loss, and increasing the sensitivity of snow albedo to increasing snow/ice grain size intensifies surface ablation across all ice sheets (Patterson et al., Thesis), though these are not tested with abrupt climate forcings. Thus, a perturbed parameter ensemble would be beneficial with transient forcings and abrupt climate changes to determine what parameter combinations are ideal for simulating the best match to ice volume and extent for the deglaciation and why. Although ideally, it would be more efficient to start from the LGM ice sheet and perform a perturbed parameter ensemble for the entire deglaciation, to avoid high computational costs, the sensitivity tests could first be performed for the period 15-13 ka BP (after initialising the ice sheet at 15 ka BP, as I did in Chapter 4) and with accelerated forcings (as this proved to not significantly impact the results; Chapter 4). These simulations would then only be 2,000 ice sheet years and 200 climate years, a length that is significantly shorter (by 3,000 ice sheet years and 300 climate years) than the parameter ensemble performed by (Patterson et al. 2025). The saved computational time could instead be used to also test different ocean forcings, as these also proved to be critical (Chapter 4).

However, starting from the beginning of the deglaciation would provide a higher likelihood of diagnosing the chain of events, i.e., the timing and amount of meltwater discharge that would enter the Arctic and North Atlantic and potentially perturb the AMOC. For instance, I do not successfully simulate the Cordilleran-Laurentide saddle collapse, which is replicated by other ice sheet model simulations (e.g., Gregoire et al. 2012; Gowan et al. 2016; Gregoire et al. 2016; Obase et al. 2021), as well as with the same ice sheet model (Patterson et al. 2025) but at the wrong time, suggesting that modelling the saddle collapse is dependent on the selected combination of parameter values.

Modelling the saddle collapse could also be dependent on the coupling to a climate model. It is easier to replicate behaviour identified in proxy reconstructions, such as meltwater pulses (Quiquet et al. 2021a), with stand-alone ice sheet models compared to coupled climate-ice sheet models. In a stand-alone ice sheet model experiment, the interface with the ocean or atmosphere is prescribed uni-directionally (i.e., from climate to ice sheet), strongly imposing a forced scenario without the coupled interaction. Whereas, in coupled atmosphere-ocean-ice sheet models, abrupt climate changes rarely occur unforced (only Mikolajewicz et al. (2024) have successfully done so), similar to the dilemma faced in Chapter 2. To simulate abrupt climate changes in Chapter 4, I used an atmosphere-only climate-ice model and prescribed sea surface temperature and sea ice fields that included Heinrich Stadial 1 and the Bølling Warming. However, not incorporating a dynamic ocean limited my ability to fully investigate atmosphere-ocean-ice interactions.

To build on my work, it would be interesting to prescribe the results of the ice sheet model (i.e., the transient ice sheet topography and resulting meltwater discharge) to an atmosphere-ocean general circulation model (AOGCM). It would be best to do this with HadCM3, as it already has the same model physics as FAMOUS but at a finer resolution, and also after performing the perturbed parameter ensemble to ensure the best matching ice sheet and freshwater evolution for the deglaciation. Running this simulation would allow the community to diagnose the impact of a freshwater forcing that has already been influenced by abrupt climate change events on the AMOC, allowing the ocean-ice interactions to come full circle with a strong degree of self-consistency (in contrast to the *TraCE-like* simulations of Chapter 2, for example).

Furthermore, it would be beneficial to conduct the same simulations as those presented in Chapter 4, but employing an atmosphere model with finer resolution. Running these simulations with FAMOUS, as opposed to with an EMIC, was beneficial because GCMs include a more detailed representation of physical processes, such as surface mass balance, in the climate system. However, the still relatively coarse resolution of FAMOUS (7.5° longitude by 5° latitude) introduced biases in the atmospheric physics such as precipitation overestimations. Precipitation is not downscaled in the FAMOUS-ice version of FAMOUS, which can lead to a more widely distributed spread of precipitation instead of a more realistic concentration of snowfall on the slopes of ice margins, for example (Smith et al. 2021). Thus, the combination of the ice sheet topography in the region and the low resolution of the atmospheric model could have forced the ice to be too thick across the Cordilleran-Laurentide saddle, inhibiting collapse. FAMOUS-ice also has a known cold bias over the northwestern region of Canada and Alaska,

also due to the coarse resolution, which causes excess ice growth over this area (Sherriff-Tadano et al. 2024; Patterson et al. 2025). To resolve these biases, it would be beneficial to increase the resolution of the atmosphere in the model or to down-scale precipitation to better represent surface mass balance in regions of large ice sheet changes (e.g., the saddle region and over the Hudson Bay).

Lastly, it would be useful to have more coupled climate-ice sheet simulations prescribing abrupt climate changes (e.g., through the ocean forcing) to diagnose the impact on the ice sheets. In general, having more transient ice sheet simulations will help to fill in the gaps in our knowledge of the chain of events of the deglaciation–i.e., what the elevation of the Laurentide ice sheet was at different stages of the deglaciation, when the Cordilleran-Laurentide saddle collapse occurred, how much melt occurred and where at different times of the deglaciation, and what ocean basins this meltwater would have most likely drained into. These answers will be transformational for understanding AMOC evolution and our ability to predict abrupt climate events.

References

Abe-Ouchi, A., Saito, F., Kageyama, M., Braconnot, P., Harrison, S. P., Lambeck, K., Otto-Bliesner, B. L., Peltier, W. R., Tarasov, L., Peterschmitt, J.-Y., and Takahashi, K. (Nov. 6, 2015). "Ice-sheet configuration in the CMIP5/PMIP3 Last Glacial Maximum experiments". In: *Geoscientific Model Development* 8.11, pp. 3621–3637. ISSN: 1991-9603. DOI: 10.5194/gmd-8-3621-2015. URL: https://gmd.copernicus.org/articles/8/3621/2015/ (visited on 01/28/2022).

Abe-Ouchi, A., Segawa, T., and Saito, F. (July 19, 2007). "Climatic Conditions for modelling the Northern Hemisphere ice sheets throughout the ice age cycle". In: *Climate of the Past* 3.3. Publisher: Copernicus GmbH, pp. 423–438. ISSN: 1814-9324. DOI: 10.5194/cp-3-423-2007. URL: https://cp.copernicus.org/articles/3/423/2007/ (visited on 01/31/2025).

Adolphi, Florian, Bronk Ramsey, Christopher, Erhardt, Tobias, Edwards, R. Lawrence, Cheng, Hai, Turney, Chris S. M., Cooper, Alan, Svensson, Anders, Rasmussen, Sune O., Fischer, Hubertus, and Muscheler, Raimund (Nov. 20, 2018). "Connecting the Greenland ice-core and U/Th timescales via cosmogenic radionuclides: testing the synchroneity of Dansgaard–Oeschger events". In: *Climate of the Past* 14.11. Publisher: Copernicus GmbH, pp. 1755–1781. ISSN: 1814-9324. DOI: 10.5194/cp-14-1755-2018. URL: https://cp.copernicus.org/articles/14/1755/2018/ (visited on 02/23/2024).

Alvarez-Solas, Jorge, Banderas, Rubén, Robinson, Alexander, and Montoya, Marisa (June 4, 2019). "Ocean-driven millennial-scale variability of the Eurasian ice sheet during the last glacial period simulated with a hybrid ice-sheet–shelf model". In: *Climate of the Past* 15.3. Publisher: Copernicus GmbH, pp. 957–979. ISSN: 1814-9324. DOI: 10.5194/cp-15-957-2019. URL: https://cp.copernicus.org/articles/15/957/2019/ (visited on 01/10/2025).

Andersen, Katrine K., Svensson, Anders, Johnsen, Sigfus J., Rasmussen, Sune O., Bigler, Matthias, Röthlisberger, Regine, Ruth, Urs, Siggaard-Andersen, Marie-Louise, Peder Steffensen, Jørgen, Dahl-Jensen, Dorthe, Vinther, Bo M., and Clausen, Henrik B. (Dec. 1, 2006). "The Greenland Ice Core Chronology 2005, 15–42 ka. Part 1: constructing the time scale". In: *Quaternary Science Reviews*. Critical Quaternary Stratigraphy 25.23, pp. 3246–3257. ISSN: 0277-3791. DOI: 10.1016/j.quascirev.2006.08.002. URL: https://www.sciencedirect.com/science/article/pii/S0277379106002587 (visited on 02/22/2024).

Annan, James D., Hargreaves, Julia C., and Mauritsen, Thorsten (Aug. 18, 2022). "A new global surface temperature reconstruction for the Last Glacial Maximum". In: *Climate of the Past* 18.8, pp. 1883–1896. ISSN: 1814-9332. DOI: 10.5194/cp-18-1883-2022. URL: https://cp.copernicus.org/articles/18/1883/2022/ (visited on 09/01/2023).

Argus, Donald F., Peltier, W. R., Drummond, R., and Moore, Angelyn W. (July 1, 2014). "The Antarctica component of postglacial rebound model ICE-6G_C (VM5a) based on GPS positioning, exposure age dating of ice thicknesses, and relative sea level histories". In: *Geophysical Journal International* 198.1, pp. 537–563. ISSN: 0956-540X, 1365-246X. DOI: 10.1093/gji/ggu140. URL: http://academic.oup.com/gji/article/198/1/537/2874192/The-Antarctica-component-of-postglacial-rebound (visited on 01/27/2022).

Armstrong, Edward, Hopcroft, Peter O., and Valdes, Paul J. (Nov. 7, 2019). "A simulated Northern Hemisphere terrestrial climate dataset for the past 60,000 years". In: *Scientific Data* 6.1. Publisher: Nature Publishing Group, p. 265. ISSN: 2052-4463. DOI: 10.1038/s41597-019-0277-1. URL: https://www.nature.com/articles/s41597-019-0277-1 (visited on 01/17/2025).

Armstrong, Edward, Izumi, Kenji, and Valdes, Paul (Nov. 3, 2022). "Identifying the mechanisms of DO-scale oscillations in a GCM: a salt oscillator triggered by the Laurentide ice sheet". In: *Climate Dynamics*. ISSN: 0930-7575, 1432-0894. DOI: 10.1007/s00382-022-06564-y. URL: https://link.springer.com/10.1007/s00382-022-06564-y (visited on 03/21/2023).

Arzel, Olivier, England, Matthew H., Verdière, Alain Colin de, and Huck, Thierry (July 1, 2012). "Abrupt millennial variability and interdecadal-interstadial oscillations in a global coupled model: sensitivity to the background climate state". In: *Climate Dynamics* 39.1, pp. 259–275. ISSN: 1432-0894. DOI: 10.1007/s00382-011-1117-y. URL: https://doi.org/10.1007/s00382-011-1117-y (visited on 02/03/2025).

Asmerom, Yemane, Polyak, Victor J., and Burns, Stephen J. (Feb. 2010). "Variable winter moisture in the southwestern United States linked to rapid glacial climate shifts". In: *Nature Geoscience* 3.2. Number: 2 Publisher: Nature Publishing Group, pp. 114–117. ISSN: 1752-0908. DOI: 10.1038/ngeo754. URL: https://www.nature.com/articles/ngeo754 (visited on 02/23/2024).

Bakker, Pepijn, Rogozhina, Irina, Merkel, Ute, and Prange, Matthias (Feb. 18, 2020). "Hypersensitivity of glacial summer temperatures in Siberia". In: *Climate of the Past* 16.1. Publisher: Copernicus GmbH, pp. 371–386. ISSN: 1814-9324. DOI: 10.5194/cp-16-371-2020. URL: https://cp.copernicus.org/articles/16/371/2020/ (visited on 02/25/2025).

Bard, Edouard, Rostek, Frauke, Turon, Jean-Louis, and Gendreau, Sandra (Aug. 25, 2000). "Hydrological Impact of Heinrich Events in the Subtropical Northeast Atlantic". In: *Science* 289.5483, pp. 1321–1324. ISSN: 0036-8075, 1095-9203. DOI: 10.1126/science.289.5483.1321. URL: https://www.science.org/doi/10.1126/science.289.5483.1321 (visited on 01/28/2022).

Barker, Stephen, Chen, James, Gong, Xun, Jonkers, Lukas, Knorr, Gregor, and Thornalley, David (Apr. 2015). "Icebergs not the trigger for North Atlantic cold events". In: *Nature* 520.7547. Number: 7547 Publisher: Nature Publishing Group, pp. 333–336. ISSN: 1476-4687. DOI: 10.1038/nature14330. URL: https://www.nature.com/articles/nature14330 (visited on 02/26/2024).

Barker, Stephen and Knorr, Gregor (Dec. 2021). "Millennial scale feedbacks determine the shape and rapidity of glacial termination". In: *Nature Communications* 12.1, p. 2273. ISSN: 2041-1723. DOI: 10.1038/s41467-021-22388-6. URL: http://www.nature.com/articles/s41467-021-22388-6 (visited on 09/09/2021).

Batchelor, Christine L., Margold, Martin, Krapp, Mario, Murton, Della K., Dalton, April S., Gibbard, Philip L., Stokes, Chris R., Murton, Julian B., and Manica, Andrea (Aug. 16, 2019). "The configuration of Northern Hemisphere ice sheets through the Quaternary". In: *Nature Communications* 10.1. Publisher: Nature Publishing Group, p. 3713. ISSN: 2041-1723. DOI: 10.1038/s41467-019-11601-2. URL: https://www.nature.com/articles/s41467-019-11601-2 (visited on 02/03/2025).

Beaulieu, J.-L. de and Reille, M. (Jan. 1992). "The last climatic cycle at La Grande Pile (Vosges, France) a new pollen profile". In: *Quaternary Science Reviews* 11.4, pp. 431–438. ISSN: 02773791. DOI: 10.1016/0277-3791(92)90025-4. URL: https://linkinghub.elsevier.com/retrieve/pii/0277379192900254 (visited on 09/02/2021).

Beckmann, A and Goosse, H (Jan. 1, 2003). "A parameterization of ice shelf–ocean interaction for climate models". In: *Ocean Modelling* 5.2, pp. 157–170. ISSN: 1463-5003. DOI: 10.1016/S1463-5003(02)00019-7. URL: https://www.sciencedirect.com/science/article/pii/S1463500302000197 (visited on 02/14/2025).

Bereiter, Bernhard, Eggleston, Sarah, Schmitt, Jochen, Nehrbass-Ahles, Christoph, Stocker, Thomas F., Fischer, Hubertus, Kipfstuhl, Sepp, and Chappellaz, Jerome (Jan. 28, 2015). "Revision of the EPICA Dome C CO $_2$ record from 800 to 600 kyr before present: Analytical bias in the EDC CO2 record". In: *Geophysical Research Letters* 42.2, pp. 542–549. ISSN: 00948276. DOI: 10.1002/2014GL061957. URL: http://doi.wiley.com/10.1002/2014GL061957 (visited on 09/02/2021).

Berger, A. (1988). "Milankovitch Theory and climate". In: *Reviews of Geophysics* 26.4. _eprint: https://onlinelibrary.wiley.com/doi/pdf/10.1029/RG026i004p00624, pp. 624–657. ISSN: 1944-9208. DOI: 10.1029/RG026i004p00624. URL: https://onlinelibrary.wiley.com/doi/abs/10.1029/RG026i004p00624 (visited on 01/24/2025).

Berger, A. and Loutre, M.F. (Jan. 1991). "Insolation values for the climate of the last 10 million years". In: *Quaternary Science Reviews* 10.4, pp. 297–317. ISSN: 02773791. DOI: 10.1016/0277-3791(91)90033-Q. URL: https://linkinghub.elsevier.com/retrieve/pii/027737919190033Q (visited on 01/28/2022).

Berger, AndréL. (Dec. 1978). "Long-Term Variations of Daily Insolation and Quaternary Climatic Changes". In: *Journal of the Atmospheric Sciences* 35.12, pp. 2362–2367. ISSN: 0022-4928, 1520-0469. DOI: 10.1175/1520-0469(1978)035<2362:LTVODI>2.0.CO;2. URL: http://journals.ametsoc.org/doi/10.1175/1520-0469(1978)035<2362:LTVODI>2.0.CO;2 (visited on 01/28/2022).

Berk, Jelle van den, Drijfhout, Sybren, and Hazeleger, Wilco (Jan. 18, 2021). "Characterisation of Atlantic meridional overturning hysteresis using Langevin dynamics". In: *Earth System Dynamics* 12.1. Publisher: Copernicus GmbH, pp. 69–81. ISSN: 2190-4979. DOI: 10.5194/esd-12-69-2021. URL: https://esd.copernicus.org/articles/12/69/2021/ (visited on 08/06/2024).

Bethke, Ingo, Li, Camille, and Nisancioglu, Kerim H. (June 2012). "Can we use ice sheet reconstructions to constrain meltwater for deglacial simulations?: MELTWATER IN DEGLACIAL SIMULATIONS". In: *Paleoceanography* 27.2, n/a–n/a. ISSN: 08838305. DOI: 10.1029/2011PA002258. URL: http://doi.wiley.com/10.1029/2011PA002258 (visited on 09/02/2021).

Bitz, C. M., Chiang, J. C. H., Cheng, W., and Barsugli, J. J. (Apr. 11, 2007). "Rates of thermohaline recovery from freshwater pulses in modern, Last Glacial Maximum, and greenhouse warming climates". In: *Geophysical Research Letters* 34.7, p. L07708. ISSN: 0094-8276. DOI: 10.1029/2006GL029237. URL: http://doi.wiley.com/10.1029/2006GL029237 (visited on 09/02/2021).

Blunier, T., Chappellaz, J., Schwander, J., Dällenbach, A., Stauffer, B., Stocker, T. F., Raynaud, D., Jouzel, J., Clausen, H. B., Hammer, C. U., and Johnsen, S. J. (Aug. 1998). "Asynchrony of Antarctic and Greenland climate change during the last glacial period". In: *Nature* 394.6695. Publisher: Nature Publishing Group, pp. 739–743. ISSN: 1476-4687. DOI: 10.1038/29447. URL: https://www.nature.com/articles/29447 (visited on 01/24/2025).

Blunier, T., Schwander, J., Stauffer, B., Stocker, T., Dällenbach, A., Indermühle, A., Tschumi, J., Chappellaz, J., Raynaud, D., and Barnola, J.-M. (1997). "Timing of the Antarctic cold reversal and the atmospheric CO2 increase with respect to the Younger Dryas Event". In: *Geophysical Research Letters* 24.21. _eprint: https://onlinelibrary.wiley.com/doi/pdf/10.1029/97GL02658, pp. 2683–2686. ISSN: 1944-8007. DOI: 10.1029/97GL02658. URL: https://onlinelibrary.wiley.com/doi/abs/10.1029/97GL02658 (visited on 01/24/2025).

Bond, Gerard C. and Lotti, Rusty (Feb. 17, 1995). "Iceberg Discharges into the North Atlantic on Millennial Time Scales During the Last Glaciation". In: *Science* 267.5200. Publisher: American Association for the Advancement of Science, pp. 1005–1010. DOI: 10.1126/science.267.5200.1005. URL: https://www.science.org/doi/10.1126/science.267.5200.1005 (visited on 01/24/2025).

Bond, Gerard, Broecker, Wallace, Johnsen, Sigfus, McManus, Jerry, Labeyrie, Laurent, Jouzel, Jean, and Bonani, Georges (Sept. 1993). "Correlations between climate records from North Atlantic sediments and Greenland ice". In: *Nature* 365.6442, pp. 143–147. ISSN: 0028-0836,

1476-4687. DOI: 10.1038/365143a0. URL: http://www.nature.com/articles/365143a0 (visited on 01/27/2022).

Bond, Gerard, Heinrich, Hartmut, Broecker, Wallace, Labeyrie, Laurent, McManus, Jerry, Andrews, John, Huon, Sylvain, Jantschik, Ruediger, Clasen, Silke, Simet, Christine, Tedesco, Kathy, Klas, Mieczyslawa, Bonani, Georges, and Ivy, Susan (Nov. 1992). "Evidence for massive discharges of icebergs into the North Atlantic ocean during the last glacial period". In: *Nature* 360.6401, pp. 245–249. ISSN: 0028-0836, 1476-4687. DOI: 10.1038/360245a0. URL: http://www.nature.com/articles/360245a0 (visited on 01/27/2022).

Booth, Alice, Goodwin, Philip, and Cael, B. B. (2024). "Ice Sheet-Albedo Feedback Estimated From Most Recent Deglaciation". In: *Geophysical Research Letters* 51.15. _eprint: https://onlinelibrary.wiley.com/doi/pdf/10.1029/2024GL109953, e2024GL109953. ISSN: 1944-8007. DOI: 10.1029/2024GL109953. URL: https://onlinelibrary.wiley.com/doi/abs/10.1029/2024GL109953 (visited on 02/21/2025).

Bouttes, Nathaelle, Lhardy, Fanny, Quiquet, Aurélien, Paillard, Didier, Goosse, Hugues, and Roche, Didier M. (May 26, 2023). "Deglacial climate changes as forced by different ice sheet reconstructions". In: *Climate of the Past* 19.5, pp. 1027–1042. ISSN: 1814-9332. DOI: 10.5194/cp-19-1027-2023. URL: https://cp.copernicus.org/articles/19/1027/2023/ (visited on 05/31/2023).

Braconnot, Pascale, Harrison, Sandy P., Kageyama, Masa, Bartlein, Patrick J., Masson-Delmotte, Valerie, Abe-Ouchi, Ayako, Otto-Bliesner, Bette, and Zhao, Yan (June 2012). "Evaluation of climate models using palaeoclimatic data". In: *Nature Climate Change* 2.6, pp. 417–424. ISSN: 1758-678X, 1758-6798. DOI: 10.1038/nclimate1456. URL: http://www.nature.com/articles/nclimate1456 (visited on 04/22/2022).

Bradtmiller, Louisa I., McManus, Jerry F., and Robinson, Laura F. (Dec. 2014). "231Pa/230Th evidence for a weakened but persistent Atlantic meridional overturning circulation during Heinrich Stadial 1". In: *Nature Communications* 5.1, p. 5817. ISSN: 2041-1723. DOI: 10.1038/ncomms6817. URL: http://www.nature.com/articles/ncomms6817 (visited on 09/27/2021).

Brendryen, Jo, Haflidason, Haflidi, Yokoyama, Yusuke, Haaga, Kristian Agasøster, and Hannisdal, Bjarte (May 2020). "Eurasian Ice Sheet collapse was a major source of Meltwater Pulse 1A 14,600 years ago". In: *Nature Geoscience* 13.5, pp. 363–368. ISSN: 1752-0894, 1752-0908. DOI: 10.1038/s41561-020-0567-4. URL: http://www.nature.com/articles/s41561-020-0567-4 (visited on 07/12/2022).

Briggs, Robert D., Pollard, David, and Tarasov, Lev (Nov. 2014). "A data-constrained large ensemble analysis of Antarctic evolution since the Eemian". In: *Quaternary Science Reviews* 103, pp. 91–115. ISSN: 02773791. DOI: 10.1016/j.quascirev.2014.09.003. URL: https://linkinghub.elsevier.com/retrieve/pii/S0277379114003448 (visited on 09/02/2021).

Broecker, Wallace S. (Nov. 28, 1997). "Thermohaline Circulation, the Achilles Heel of Our Climate System: Will Man-Made CO2 Upset the Current Balance?" In: *Science* 278.5343. Publisher: American Association for the Advancement of Science, pp. 1582–1588. DOI: 10.1126/science.278.5343.1582. URL: https://www.science.org/doi/full/10.1126/science.278.5343.1582 (visited on 01/24/2025).

– (Apr. 1998). "Paleocean circulation during the Last Deglaciation: A bipolar seesaw?" In: *Paleoceanography* 13.2, pp. 119–121. ISSN: 08838305. DOI: 10.1029/97PA03707. URL: http://doi.wiley.com/10.1029/97PA03707 (visited on 09/02/2021).

Broecker, Wallace S., Bond, Gerard, Klas, Millie, Bonani, Georges, and Wolfli, Willy (1990). "A salt oscillator in the glacial Atlantic? 1. The concept". In: *Paleoceanography* 5.4. _eprint: https://onlinelibrary.wiley.com/doi/pdf/10.1029/PA005i004p00469, pp. 469–477. ISSN: 1944-9186. DOI: 10.1029/PA005i004p00469. URL: https://onlinelibrary.wiley.com/doi/abs/10.1029/PA005i004p00469 (visited on 01/28/2025).

Broecker, Wallace S., Denton, George H., Edwards, R. Lawrence, Cheng, Hai, Alley, Richard B., and Putnam, Aaron E. (May 1, 2010). "Putting the Younger Dryas cold event into context". In: *Quaternary Science Reviews* 29.9, pp. 1078–1081. ISSN: 0277-3791. DOI: 10.1016/j.quascirev.2010.02.019. URL: https://www.sciencedirect.com/science/article/pii/S027737911000051X (visited on 02/26/2024).

Broecker, Wally and Putnam, Aaron E. (Dec. 2012). "How did the hydrologic cycle respond to the two-phase mystery interval?" In: *Quaternary Science Reviews* 57, pp. 17–25. ISSN: 02773791. DOI: 10.1016/j.quascirev.2012.09.024. URL: https://linkinghub.elsevier.com/retrieve/pii/S0277379112003757 (visited on 01/28/2022).

Brown, Nicolas and Galbraith, Eric D. (Aug. 18, 2016). "Hosed vs. unhosed: interruptions of the Atlantic Meridional Overturning Circulation in a global coupled model, with and without freshwater forcing". In: *Climate of the Past* 12.8, pp. 1663–1679. ISSN: 1814-9332. DOI: 10.5194/cp-12-1663-2016. URL: https://cp.copernicus.org/articles/12/1663/2016/ (visited on 02/14/2022).

Buckley, Martha W. and Marshall, John (2016). "Observations, inferences, and mechanisms of the Atlantic Meridional Overturning Circulation: A review". In: *Reviews of Geophysics* 54.1. _eprint: https://onlinelibrary.wiley.com/doi/pdf/10.1002/2015RG000493, pp. 5–63. ISSN: 1944-9208. DOI: 10.1002/2015RG000493. URL: https://onlinelibrary.wiley.com/doi/abs/10.1002/2015RG000493 (visited on 01/24/2025).

Buizert, C., Gkinis, V., Severinghaus, J. P., He, F., Lecavalier, B. S., Kindler, P., Leuenberger, M., Carlson, A. E., Vinther, B., Masson-Delmotte, V., White, J. W. C., Liu, Z., Otto-Bliesner, B., and Brook, E. J. (Sept. 5, 2014). "Greenland temperature response to climate forcing during the last deglaciation". In: *Science* 345.6201, pp. 1177–1180. ISSN: 0036-8075, 1095-9203. DOI: 10.1126/science.1254961. URL: https://www.sciencemag.org/lookup/doi/10.1126/science.1254961 (visited on 09/02/2021).

Buizert, C., Keisling, B. A., Box, J. E., He, F., Carlson, A. E., Sinclair, G., and DeConto, R. M. (Feb. 28, 2018). "Greenland-Wide Seasonal Temperatures During the Last Deglaciation". In: *Geophysical Research Letters* 45.4. Publisher: John Wiley & Sons, Ltd, pp. 1905–1914. ISSN: 1944-8007. DOI: 10.1002/2017GL075601. URL: https://agupubs.onlinelibrary.wiley.com/doi/10.1002/2017GL075601 (visited on 11/30/2023).

Buizert, Christo, Adrian, Betty, Ahn, Jinho, Albert, Mary, Alley, Richard B., Baggenstos, Daniel, Bauska, Thomas K., Bay, Ryan C., Bencivengo, Brian B., Bentley, Charles R., Brook, Edward J., Chellman, Nathan J., Clow, Gary D., Cole-Dai, Jihong, Conway, Howard, Cravens, Eric, Cuffey, Kurt M., Dunbar, Nelia W., Edwards, Jon S., Fegyveresi, John M., Ferris, Dave G., Fitzpatrick, Joan J., Fudge, T. J., Gibson, Chris J., Gkinis, Vasileios, Goetz, Joshua J., Gregory, Stephanie, Hargreaves, Geoffrey M., Iverson, Nels, Johnson, Jay A., Jones, Tyler R., Kalk, Michael L., Kippenhan, Matthew J., Koffman, Bess G., Kreutz, Karl, Kuhl, Tanner W., Lebar, Donald A., Lee, James E., Marcott, Shaun A., Markle, Bradley R., Maselli, Olivia J., McConnell, Joseph R., McGwire, Kenneth C., Mitchell, Logan E., Mortensen, Nicolai B., Neff, Peter D., Nishiizumi, Kunihiko, Nunn, Richard M., Orsi, Anais J., Pasteris, Daniel R., Pedro, Joel B., Pettit, Erin C., Buford Price, P., Priscu, John C., Rhodes, Rachael H., Rosen, Julia L., Schauer, Andrew J., Schoenemann, Spruce W., Sendelbach, Paul J., Severinghaus, Jeffrey P., Shturmakov, Alexander J., Sigl, Michael, Slawny, Kristina R., Souney, Joseph M., Sowers, Todd A., Spencer, Matthew K., Steig, Eric J., Taylor, Kendrick C., Twickler, Mark S., Vaughn, Bruce H., Voigt, Donald E., Waddington, Edwin D., Welten, Kees C., Wendricks, Anthony W., White, James W. C., Winstrup, Mai, Wong, Gifford J., Woodruff, Thomas E., and WAIS Divide Project Members (Apr. 2015). "Precise interpolar phasing of abrupt climate change during the last ice age". In: *Nature* 520.7549. Publisher: Nature Publishing Group, pp. 661–665. ISSN: 1476-4687. DOI: 10.1038/nature14401. URL: https://www.nature.com/articles/nature14401 (visited on 02/27/2025).

Böhm, E., Lippold, J., Gutjahr, M., Frank, M., Blaser, P., Antz, B., Fohlmeister, J., Frank, N., Andersen, M. B., and Deininger, M. (Jan. 2015). "Strong and deep Atlantic meridional overturning circulation during the last glacial cycle". In: *Nature* 517.7532, pp. 73–76. ISSN: 0028-0836, 1476-4687. DOI: 10.1038/nature14059. URL: http://www.nature.com/articles/nature14059 (visited on 11/30/2022).

Carlson, Anders E. and Clark, Peter U. (Dec. 22, 2012). "Ice sheet sources of sea level rise and freshwater discharge during the last deglaciation". In: *Reviews of Geophysics* 50.4, RG4007. ISSN: 8755-1209. DOI: 10.1029/2011RG000371. URL: http://doi.wiley.com/10.1029/2011RG000371 (visited on 11/28/2022).

Carlson, Anders E., Ullman, David J., Anslow, Faron S., He, Feng, Clark, Peter U., Liu, Zhengyu, and Otto-Bliesner, Bette L. (Jan. 15, 2012). "Modeling the surface mass-balance response of the Laurentide Ice Sheet to Bølling warming and its contribution to Meltwater Pulse 1A". In: *Earth and Planetary Science Letters*. Sea Level and Ice Sheet Evolution: A PALSEA Special Edition 315-316, pp. 24–29. ISSN: 0012-821X. DOI: 10.1016/j.epsl.2011.07.008.

URL: https://www.sciencedirect.com/science/article/pii/S0012821X11004237 (visited on 02/13/2025).

Charbit, Sylvie, Kageyama, Masa, Roche, Didier, Ritz, Catherine, and Ramstein, Gilles (Oct. 1, 2005). "Investigating the mechanisms leading to the deglaciation of past continental northern hemisphere ice sheets with the CLIMBER–GREMLINS coupled model". In: *Global and Planetary Change* 48.4, pp. 253–273. ISSN: 0921-8181. DOI: 10.1016/j.gloplacha.2005.01.002. URL: https://www.sciencedirect.com/science/article/pii/S0921818105000329 (visited on 10/17/2024).

Cheng, Hai, Edwards, R. Lawrence, Sinha, Ashish, Spötl, Christoph, Yi, Liang, Chen, Shitao, Kelly, Megan, Kathayat, Gayatri, Wang, Xianfeng, Li, Xianglei, Kong, Xinggong, Wang, Yongjin, Ning, Youfeng, and Zhang, Haiwei (June 2016). "The Asian monsoon over the past 640,000 years and ice age terminations". In: *Nature* 534.7609. Publisher: Nature Publishing Group, pp. 640–646. ISSN: 1476-4687. DOI: 10.1038/nature18591. URL: https://www.nature.com/articles/nature18591 (visited on 01/29/2025).

Cheng, Wei, Bitz, Cecilia M., and Chiang, John C. H. (2007). "Adjustment of the global climate to an abrupt slowdown of the Atlantic meridional overturning circulation". In: *Geophysical Monograph Series*. Ed. by Andreas Schmittner, John C. H. Chiang, and Sidney R. Hemming. Vol. 173. Washington, D. C.: American Geophysical Union, pp. 295–313. ISBN: 978-0-87590-438-2. DOI: 10.1029/173GM19. URL: http://www.agu.org/books/gm/v173/173GM19/173GM19.shtml (visited on 09/02/2021).

Cheng, Wei, Weijer, Wilbert, Kim, Who M., Danabasoglu, Gokhan, Yeager, Steve G., Gent, Peter R., Zhang, Dongxiao, Chiang, John C. H., and Zhang, Jiaxu (Aug. 15, 2018). "Can the Salt-Advection Feedback Be Detected in Internal Variability of the Atlantic Meridional Overturning Circulation?" In: *Journal of Climate* 31.16. Publisher: American Meteorological Society Section: Journal of Climate, pp. 6649–6667. ISSN: 0894-8755, 1520-0442. DOI: 10.1175/JCLI-D-17-0825.1. URL: https://journals.ametsoc.org/view/journals/clim/31/16/jcli-d-17-0825.1.xml (visited on 06/12/2024).

Clark, P. U., Shakun, J. D., Baker, P. A., Bartlein, P. J., Brewer, S., Brook, E., Carlson, A. E., Cheng, H., Kaufman, D. S., Liu, Z., Marchitto, T. M., Mix, A. C., Morrill, C., Otto-Bliesner, B. L., Pahnke, K., Russell, J. M., Whitlock, C., Adkins, J. F., Blois, J. L., Clark, J., Colman, S. M., Curry, W. B., Flower, B. P., He, F., Johnson, T. C., Lynch-Stieglitz, J., Markgraf, V., McManus, J., Mitrovica, J. X., Moreno, P. I., and Williams, J. W. (May 8, 2012). "Global climate evolution during the last deglaciation". In: *Proceedings of the National Academy of Sciences* 109.19, E1134–E1142. ISSN: 0027-8424, 1091-6490. DOI: 10.1073/pnas.1116619109. URL: http://www.pnas.org/cgi/doi/10.1073/pnas.1116619109 (visited on 09/02/2021).

Clark, Peter U., Alley, Richard B., Keigwin, Lloyd D., Licciardi, Joseph M., Johnsen, Sigfus J., and Wang, Huaxiao (1996). "Origin of the first global meltwater pulse following the Last Glacial Maximum". In: *Paleoceanography* 11.5. _eprint: https://onlinelibrary.wiley.com/doi/pdf/10.1029/96P

pp. 563–577. ISSN: 1944-9186. DOI: 10.1029/96PA01419. URL: https://onlinelibrary.wiley.com/doi/abs/10.1029/96PA01419 (visited on 11/28/2024).

Clark, Peter U., Dyke, Arthur S., Shakun, Jeremy D., Carlson, Anders E., Clark, Jorie, Wohlfarth, Barbara, Mitrovica, Jerry X., Hostetler, Steven W., and McCabe, A. Marshall (Aug. 7, 2009). "The Last Glacial Maximum". In: *Science* 325.5941, pp. 710–714. ISSN: 0036-8075, 1095-9203. DOI: 10.1126/science.1172873. URL: https://www.science.org/doi/10.1126/science.1172873 (visited on 06/02/2023).

Clark, Peter U., He, Feng, Golledge, Nicholas R., Mitrovica, Jerry X., Dutton, Andrea, Hoffman, Jeremy S., and Dendy, Sarah (Jan. 2020). "Oceanic forcing of penultimate deglacial and last interglacial sea-level rise". In: *Nature* 577.7792. Publisher: Nature Publishing Group, pp. 660–664. ISSN: 1476-4687. DOI: 10.1038/s41586-020-1931-7. URL: https://www.nature.com/articles/s41586-020-1931-7 (visited on 01/21/2025).

Clarke, Garry K. C., Bush, Andrew B. G., and Bush, John W. M. (Apr. 15, 2009). "Freshwater Discharge, Sediment Transport, and Modeled Climate Impacts of the Final Drainage of Glacial Lake Agassiz". In: *Journal of Climate* 22.8, pp. 2161–2180. ISSN: 1520-0442, 0894-8755. DOI: 10.1175/2008JCLI2439.1. URL: http://journals.ametsoc.org/doi/10.1175/2008JCLI2439.1 (visited on 06/01/2023).

Collins, William D., Bitz, Cecilia M., Blackmon, Maurice L., Bonan, Gordon B., Bretherton, Christopher S., Carton, James A., Chang, Ping, Doney, Scott C., Hack, James J., Henderson, Thomas B., Kiehl, Jeffrey T., Large, William G., McKenna, Daniel S., Santer, Benjamin D., and Smith, Richard D. (June 1, 2006). "The Community Climate System Model Version 3 (CCSM3)". In: *Journal of Climate* 19.11, pp. 2122–2143. ISSN: 1520-0442, 0894-8755. DOI: 10.1175/JCLI3761.1. URL: http://journals.ametsoc.org/doi/10.1175/JCLI3761.1 (visited on 09/29/2021).

Condron, Alan and Winsor, Peter (Dec. 4, 2012). "Meltwater routing and the Younger Dryas". In: *Proceedings of the National Academy of Sciences* 109.49, pp. 19928–19933. ISSN: 0027-8424, 1091-6490. DOI: 10.1073/pnas.1207381109. URL: https://pnas.org/doi/full/10.1073/pnas.1207381109 (visited on 01/06/2023).

Coonin, Allie N., Lau, Harriet C. P., and Coulson, Sophie (Feb. 18, 2025). "Meltwater Pulse 1A sea-level-rise patterns explained by global cascade of ice loss". In: *Nature Geoscience*. Publisher: Nature Publishing Group, pp. 1–6. ISSN: 1752-0908. DOI: 10.1038/s41561-025-01648-w. URL: https://www.nature.com/articles/s41561-025-01648-w (visited on 02/25/2025).

Cornford, S. L., Martin, D. F., Payne, A. J., Ng, E. G., Le Brocq, A. M., Gladstone, R. M., Edwards, T. L., Shannon, S. R., Agosta, C., Broeke, M. R. van den, Hellmer, H. H., Krinner, G., Ligtenberg, S. R. M., Timmermann, R., and Vaughan, D. G. (Aug. 18, 2015). "Century-scale simulations of the response of the West Antarctic Ice Sheet to a warming climate". In: *The Cryosphere* 9.4. Publisher: Copernicus GmbH, pp. 1579–1600. ISSN: 1994-0416. DOI:

10.5194/tc-9-1579-2015. URL: https://tc.copernicus.org/articles/9/1579/2015/ (visited on 02/14/2025).

Cornford, Stephen L., Martin, Daniel F., Graves, Daniel T., Ranken, Douglas F., Le Brocq, Anne M., Gladstone, Rupert M., Payne, Antony J., Ng, Esmond G., and Lipscomb, William H. (Jan. 1, 2013). "Adaptive mesh, finite volume modeling of marine ice sheets". In: *Journal of Computational Physics* 232.1, pp. 529–549. ISSN: 0021-9991. DOI: 10.1016/j.jcp.2012.08.037. URL: https://www.sciencedirect.com/science/article/pii/S0021999112005050 (visited on 10/17/2024).

Crivellari, Stefano, Chiessi, Cristiano Mazur, Kuhnert, Henning, Häggi, Christoph, Costa Portilho-Ramos, Rodrigo da, Zeng, Jing-Ying, Zhang, Yancheng, Schefuß, Enno, Mollenhauer, Gesine, Hefter, Jens, Alexandre, Felipe, Sampaio, Gilvan, and Mulitza, Stefan (Feb. 2018). "Increased Amazon freshwater discharge during late Heinrich Stadial 1". In: *Quaternary Science Reviews* 181, pp. 144–155. ISSN: 02773791. DOI: 10.1016/j.quascirev.2017.12.005. URL: https://linkinghub.elsevier.com/retrieve/pii/S0277379117307345 (visited on 01/28/2022).

Cuzzone, Joshua K., Clark, Peter U., Carlson, Anders E., Ullman, David J., Rinterknecht, Vincent R., Milne, Glenn A., Lunkka, Juha-Pekka, Wohlfarth, Barbara, Marcott, Shaun A., and Caffee, Marc (Aug. 2016). "Final deglaciation of the Scandinavian Ice Sheet and implications for the Holocene global sea-level budget". In: *Earth and Planetary Science Letters* 448, pp. 34–41. ISSN: 0012821X. DOI: 10.1016/j.epsl.2016.05.019. URL: https://linkinghub.elsevier.com/retrieve/pii/S0012821X16302369 (visited on 06/02/2023).

Dalton, April S., Dulfer, Helen E., Margold, Martin, Heyman, Jakob, Clague, John J., Froese, Duane G., Gauthier, Michelle S., Hughes, Anna L.C., Jennings, Carrie E., Norris, Sophie L., and Stoker, Benjamin J. (Dec. 2023). "Deglaciation of the north American ice sheet complex in calendar years based on a comprehensive database of chronological data: NADI-1". In: *Quaternary Science Reviews* 321, p. 108345. ISSN: 02773791. DOI: 10.1016/j.quascirev.2023.108345. URL: https://linkinghub.elsevier.com/retrieve/pii/S0277379123003931 (visited on 05/07/2024).

Dansgaard, W., Clausen, H. B., Gundestrup, N., Hammer, C. U., Johnsen, S. F., Kristinsdottir, P. M., and Reeh, N. (Dec. 24, 1982). "A New Greenland Deep Ice Core". In: *Science* 218.4579, pp. 1273–1277. ISSN: 0036-8075, 1095-9203. DOI: 10.1126/science.218.4579.1273. URL: https://www.science.org/doi/10.1126/science.218.4579.1273 (visited on 01/27/2022).

Davies-Barnard, Taraka, Ridgwell, Andy, Singarayer, Joy, and Valdes, Paul (Oct. 26, 2017). "Quantifying the influence of the terrestrial biosphere on glacial–interglacial climate dynamics". In: *Climate of the Past* 13.10, pp. 1381–1401. ISSN: 1814-9332. DOI: 10.5194/cp-13-1381-2017. URL: https://cp.copernicus.org/articles/13/1381/2017/ (visited on 03/03/2022).

Dentith, Jennifer E., Ivanovic, Ruza F., Gregoire, Lauren J., Tindall, Julia C., and Smith, Robin S. (Feb. 1, 2019). "Ocean circulation drifts in multi-millennial climate simulations: the role of salinity corrections and climate feedbacks". In: *Climate Dynamics* 52.3, pp. 1761–1781. ISSN: 1432-0894. DOI: 10.1007/s00382-018-4243-y. URL: https://doi.org/10.1007/s00382-018-4243-y (visited on 01/20/2025).

Deplazes, Gaudenz, Lückge, Andreas, Peterson, Larry C., Timmermann, Axel, Hamann, Yvonne, Hughen, Konrad A., Röhl, Ursula, Laj, Carlo, Cane, Mark A., Sigman, Daniel M., and Haug, Gerald H. (Mar. 2013). "Links between tropical rainfall and North Atlantic climate during the last glacial period". In: *Nature Geoscience* 6.3, pp. 213–217. ISSN: 1752-0894, 1752-0908. DOI: 10.1038/ngeo1712. URL: http://www.nature.com/articles/ngeo1712 (visited on 01/27/2022).

Deschamps, Pierre, Durand, Nicolas, Bard, Edouard, Hamelin, Bruno, Camoin, Gilbert, Thomas, Alexander L., Henderson, Gideon M., Okuno, Jun'ichi, and Yokoyama, Yusuke (Mar. 2012). "Ice-sheet collapse and sea-level rise at the Bølling warming 14,600 years ago". In: *Nature* 483.7391, pp. 559–564. ISSN: 0028-0836, 1476-4687. DOI: 10.1038/nature10902. URL: http://www.nature.com/articles/nature10902 (visited on 09/02/2021).

Dima, M., Lohmann, G., and Knorr, G. (2018). "North Atlantic Versus Global Control on Dansgaard-Oeschger Events". In: *Geophysical Research Letters* 45.23. _eprint: https://onlinelibrary.wiley.com pp. 12,991–12,998. ISSN: 1944-8007. DOI: 10.1029/2018GL080035. URL: https://onlinelibrary.wiley.com/doi/abs/10.1029/2018GL080035 (visited on 01/24/2025).

Dokken, Trond M., Nisancioglu, Kerim H., Li, Camille, Battisti, David S., and Kissel, Catherine (Sept. 2013). "Dansgaard-Oeschger cycles: Interactions between ocean and sea ice intrinsic to the Nordic seas: D-O CYCLES AS SEEN IN THE NORDIC SEAS". In: *Paleoceanography* 28.3, pp. 491–502. ISSN: 08838305. DOI: 10.1002/palo.20042. URL: http://doi.wiley.com/10.1002/palo.20042 (visited on 06/10/2022).

Dome Fuji Ice Core Project Members: Kawamura, Kenji, Abe-Ouchi, Ayako, Motoyama, Hideaki, Ageta, Yutaka, Aoki, Shuji, Azuma, Nobuhiko, Fujii, Yoshiyuki, Fujita, Koji, Fujita, Shuji, Fukui, Kotaro, Furukawa, Teruo, Furusaki, Atsushi, Goto-Azuma, Kumiko, Greve, Ralf, Hirabayashi, Motohiro, Hondoh, Takeo, Hori, Akira, Horikawa, Shinichiro, Horiuchi, Kazuho, Igarashi, Makoto, Iizuka, Yoshinori, Kameda, Takao, Kanda, Hiroshi, Kohno, Mika, Kuramoto, Takayuki, Matsushi, Yuki, Miyahara, Morihiro, Miyake, Takayuki, Miyamoto, Atsushi, Nagashima, Yasuo, Nakayama, Yoshiki, Nakazawa, Takakiyo, Nakazawa, Fumio, Nishio, Fumihiko, Obinata, Ichio, Ohgaito, Rumi, Oka, Akira, Okuno, Jun'ichi, Okuyama, Junichi, Oyabu, Ikumi, Parrenin, Frédéric, Pattyn, Frank, Saito, Fuyuki, Saito, Takashi, Saito, Takeshi, Sakurai, Toshimitsu, Sasa, Kimikazu, Seddik, Hakime, Shibata, Yasuyuki, Shinbori, Kunio, Suzuki, Keisuke, Suzuki, Toshitaka, Takahashi, Akiyoshi, Takahashi, Kunio, Takahashi, Shuhei, Takata, Morimasa, Tanaka, Yoichi, Uemura, Ryu, Watanabe, Genta, Watanabe, Okitsugu, Yamasaki, Tetsuhide, Yokoyama, Kotaro, Yoshimori, Masakazu, and Yoshimoto, Takayasu (Feb. 3, 2017). "State dependence of climatic instability over the past 720,000 years

from Antarctic ice cores and climate modeling". In: *Science Advances* 3.2, e1600446. ISSN: 2375-2548. DOI: 10.1126/sciadv.1600446. URL: https://www.science.org/doi/10.1126/sciadv.1600446 (visited on 01/27/2022).

Drijfhout, Sybren S., Weber, Susanne L., and Swaluw, Eric van der (Oct. 1, 2011). "The stability of the MOC as diagnosed from model projections for pre-industrial, present and future climates". In: *Climate Dynamics* 37.7, pp. 1575–1586. ISSN: 1432-0894. DOI: 10.1007/s00382-010-0930-z. URL: https://doi.org/10.1007/s00382-010-0930-z (visited on 01/28/2025).

Drijfhout, Sybren, Gleeson, Emily, Dijkstra, Henk A., and Livina, Valerie (Dec. 3, 2013). "Spontaneous abrupt climate change due to an atmospheric blocking–sea-ice–ocean feedback in an unforced climate model simulation". In: *Proceedings of the National Academy of Sciences* 110.49. Publisher: Proceedings of the National Academy of Sciences, pp. 19713–19718. DOI: 10.1073/pnas.1304912110. URL: https://www.pnas.org/doi/abs/10.1073/pnas.1304912110 (visited on 02/26/2024).

Druzhinina, Olga, Rudinskaya, Anna, Filippova, Ksenia, Lazukova, Lyudmila, Lavrova, Nadezhda, Zharov, Anton, Skhodnov, Ivan, Burko, Aleksey, and Berghe, Kasper van den (June 5, 2023). "The Bølling–Allerød Transition in the Eastern Baltic: Environmental Responses to Climate Change". In: *Biology* 12.6, p. 821. ISSN: 2079-7737. DOI: 10.3390/biology12060821. URL: https://www.ncbi.nlm.nih.gov/pmc/articles/PMC10295734/ (visited on 02/17/2025).

Dyke, Arthur S. (2004). "An outline of North American deglaciation with emphasis on central and northern Canada". In: *Developments in Quaternary Sciences*. Vol. 2. Elsevier, pp. 373–424. ISBN: 978-0-444-51592-6. DOI: 10.1016/S1571-0866(04)80209-4. URL: https://linkinghub.elsevier.com/retrieve/pii/S1571086604802094 (visited on 01/27/2022).

EPICA Community Members, The, Barbante, C., Barnola, J.-M., Becagli, S., Beer, J., Bigler, M., Boutron, C., Blunier, T., Castellano, E., Cattani, O., Chappellaz, J., Dahl-Jensen, D., Debret, M., Delmonte, B., Dick, Dorothee, Falourd, S., Faria, S., Federer, U., Fischer, Hubertus, Freitag, Johannes, Frenzel, Andreas, Fritzsche, Diedrich, Fundel, Felix, Gabrielli, P., Gaspari, V., Gersonde, Rainer, Graf, W., Grigoriev, D., Hamann, Ilka, Hansson, M., Hoffmann, G., Hutterli, M. A., Huybrechts, Philippe, Isaksson, E., Johnsen, S., Jouzel, J., Kaczmarska, M., Karlin, T., Kaufmann, P., Kipfstuhl, Sepp, Kohno, Mika, Lambert, F., Lambrecht, Anja, Lambrecht, Astrid, Landais, A., Lawer, G., Leuenberger, M., Littot, G., Loulergue, L., Lüthi, D., Maggi, V., Marino, F., Masson-Delmotte, V., Meyer, Hanno, Miller, Heinrich, Mulvaney, R., Narcisi, B., Oerlemans, J., Oerter, Hans, Parrenin, F., Petit, J.-R., Raisbeck, G., Raynaud, D., Röthlisberger, R., Ruth, Urs, Rybak, Oleg, Severi, M., Schmitt, Jochen, Schwander, J., Siegenthaler, U., Siggaard-Andersen, M.-L., Spahni, R., Steffensen, J. P., Stenni, B., Stocker, T. F., Tison, J.-L., Traversi, R., Udisti, R., Valero-Delgado, Fernando, Broeke, M. R. van den, Wal, R. S. W. van de, Wagenbach, D., Wegner, Anna, Weiler, K., Wilhelms, Frank, Winther, J.-G., and Wolff, E. (2006). "One-to-one coupling of glacial climate variability in Greenland and Antarctica". In: *Nature* 444.7116. Number: 7116, pp. 195–198. ISSN: 0028-0836.

DOI: 10.1038/nature05301. URL: http://dx.doi.org/10.1038/nature05301 (visited on 01/24/2025).

Erb, Michael P., Broccoli, Anthony J., and Clement, Amy C. (Aug. 15, 2013). "The Contribution of Radiative Feedbacks to Orbitally Driven Climate Change". In: *Journal of Climate* 26.16. Publisher: American Meteorological Society Section: Journal of Climate, pp. 5897–5914. ISSN: 0894-8755, 1520-0442. DOI: 10.1175/JCLI-D-12-00419.1. URL: https://journals.ametsoc.org/view/journals/clim/26/16/jcli-d-12-00419.1.xml (visited on 07/24/2023).

Fairbanks, Richard G. (Dec. 1989). "A 17,000-year glacio-eustatic sea level record: influence of glacial melting rates on the Younger Dryas event and deep-ocean circulation". In: *Nature* 342.6250, pp. 637–642. ISSN: 0028-0836, 1476-4687. DOI: 10.1038/342637a0. URL: http://www.nature.com/articles/342637a0 (visited on 10/31/2022).

Favier, Vincent, Krinner, Gerhard, Amory, Charles, Gallée, Hubert, Beaumet, Julien, and Agosta, Cécile (Dec. 1, 2017). "Antarctica-Regional Climate and Surface Mass Budget". In: *Current Climate Change Reports* 3.4. Company: Springer Distributor: Springer Institution: Springer Label: Springer Number: 4 Publisher: Springer International Publishing, pp. 303–315. ISSN: 2198-6061. DOI: 10.1007/s40641-017-0072-z. URL: https://link.springer.com/article/10.1007/s40641-017-0072-z (visited on 02/13/2025).

Fletcher, William J., Sánchez Goñi, Maria Fernanda, Allen, Judy R. M., Cheddadi, Rachid, Combourieu-Nebout, Nathalie, Huntley, Brian, Lawson, Ian, Londeix, Laurent, Magri, Donatella, Margari, Vasiliki, Müller, Ulrich C., Naughton, Filipa, Novenko, Elena, Roucoux, Katy, and Tzedakis, P. C. (Oct. 1, 2010). "Millennial-scale variability during the last glacial in vegetation records from Europe". In: *Quaternary Science Reviews*. Vegetation Response to Millennial-scale Variability during the Last Glacial 29.21, pp. 2839–2864. ISSN: 0277-3791. DOI: 10.1016/j.quascirev.2009.11.015. URL: https://www.sciencedirect.com/science/article/pii/S0277379109003886 (visited on 02/22/2024).

Frajka-Williams, Eleanor, Ansorge, Isabelle J., Baehr, Johanna, Bryden, Harry L., Chidichimo, Maria Paz, Cunningham, Stuart A., Danabasoglu, Gokhan, Dong, Shenfu, Donohue, Kathleen A., Elipot, Shane, Heimbach, Patrick, Holliday, N. Penny, Hummels, Rebecca, Jackson, Laura C., Karstensen, Johannes, Lankhorst, Matthias, Le Bras, Isabela A., Lozier, M. Susan, McDonagh, Elaine L., Meinen, Christopher S., Mercier, Herlé, Moat, Bengamin I., Perez, Renellys C., Piecuch, Christopher G., Rhein, Monika, Srokosz, Meric A., Trenberth, Kevin E., Bacon, Sheldon, Forget, Gael, Goni, Gustavo, Kieke, Dagmar, Koelling, Jannes, Lamont, Tarron, McCarthy, Gerard D., Mertens, Christian, Send, Uwe, Smeed, David A., Speich, Sabrina, Berg, Marcel van den, Volkov, Denis, and Wilson, Chris (June 7, 2019). "Atlantic Meridional Overturning Circulation: Observed Transport and Variability". In: *Frontiers in Marine Science* 6. Publisher: Frontiers. ISSN: 2296-7745. DOI: 10.3389/fmars.2019.00260. URL: https://www.frontiersin.org/journals/marine-science/articles/10.3389/fmars.2019.00260/full (visited on 01/24/2025).

Fritz, S. C., Baker, P. A., Ekdahl, E., Seltzer, G. O., and Stevens, L. R. (Apr. 1, 2010). "Millennial-scale climate variability during the Last Glacial period in the tropical Andes". In: *Quaternary Science Reviews* 29.7, pp. 1017–1024. ISSN: 0277-3791. DOI: 10.1016/j.quascirev.2010.01.001. URL: https://www.sciencedirect.com/science/article/pii/S0277379110000028 (visited on 02/22/2024).

Fyke, Jeremy, Sergienko, Olga, Löfverström, Marcus, Price, Stephen, and Lenaerts, Jan T. M. (2018). "An Overview of Interactions and Feedbacks Between Ice Sheets and the Earth System". In: *Reviews of Geophysics* 56.2. _eprint: https://onlinelibrary.wiley.com/doi/pdf/10.1029/2018RG00060 pp. 361–408. ISSN: 1944-9208. DOI: 10.1029/2018RG000600. URL: https://onlinelibrary.wiley.com/doi/abs/10.1029/2018RG000600 (visited on 02/17/2025).

Galbraith, Eric and Lavergne, Casimir de (Jan. 2019). "Response of a comprehensive climate model to a broad range of external forcings: relevance for deep ocean ventilation and the development of late Cenozoic ice ages". In: *Climate Dynamics* 52.1, pp. 653–679. ISSN: 0930-7575, 1432-0894. DOI: 10.1007/s00382-018-4157-8. URL: http://link.springer.com/10.1007/s00382-018-4157-8 (visited on 11/30/2022).

Gandy, N., Astfalck, L. C., Gregoire, L. J., Ivanovic, R. F., Patterson, V. L., Sherriff-Tadano, S., Smith, R. S., Williamson, D., and Rigby, R. (2023). "De-Tuning Albedo Parameters in a Coupled Climate Ice Sheet Model to Simulate the North American Ice Sheet at the Last Glacial Maximum". In: *Journal of Geophysical Research: Earth Surface* 128.8. _eprint: https://onlinelibrary.wiley.com/doi/pdf/10.1029/2023JF007250, e2023JF007250. ISSN: 2169-9011. DOI: 10.1029/2023JF007250. URL: https://onlinelibrary.wiley.com/doi/abs/10.1029/2023JF007250 (visited on 10/17/2024).

Gandy, Niall, Gregoire, Lauren J., Ely, Jeremy C., Clark, Christopher D., Hodgson, David M., Lee, Victoria, Bradwell, Tom, and Ivanovic, Ruza F. (Nov. 23, 2018). "Marine ice sheet instability and ice shelf buttressing of the Minch Ice Stream, northwest Scotland". In: *The Cryosphere* 12.11. Publisher: Copernicus GmbH, pp. 3635–3651. ISSN: 1994-0416. DOI: 10.5194/tc-12-3635-2018. URL: https://tc.copernicus.org/articles/12/3635/2018/ (visited on 02/14/2025).

Gandy, Niall, Gregoire, Lauren J., Ely, Jeremy C., Cornford, Stephen L., Clark, Christopher D., and Hodgson, David M. (Nov. 1, 2019). "Exploring the ingredients required to successfully model the placement, generation, and evolution of ice streams in the British-Irish Ice Sheet". In: *Quaternary Science Reviews* 223, p. 105915. ISSN: 0277-3791. DOI: 10.1016/j.quascirev.2019.105915. URL: https://www.sciencedirect.com/science/article/pii/S0277379119304962 (visited on 01/23/2025).

– (2021). "Collapse of the Last Eurasian Ice Sheet in the North Sea Modulated by Combined Processes of Ice Flow, Surface Melt, and Marine Ice Sheet Instabilities". In: *Journal of Geophysical Research: Earth Surface* 126.4. _eprint: https://onlinelibrary.wiley.com/doi/pdf/10.1029/2020JF0057

e2020JF005755. ISSN: 2169-9011. DOI: 10.1029/2020JF005755. URL: https://onlinelibrary.wiley.com/doi/abs/10.1029/2020JF005755 (visited on 02/14/2025).

Ganopolski, Andrey and Brovkin, Victor (Nov. 29, 2017). "Simulation of climate, ice sheets and CO_2 evolution during the last four glacial cycles with an Earth system model of intermediate complexity". In: *Climate of the Past* 13.12. Publisher: Copernicus GmbH, pp. 1695–1716. ISSN: 1814-9324. DOI: 10.5194/cp-13-1695-2017. URL: https://cp.copernicus.org/articles/13/1695/2017/ (visited on 10/17/2024).

Ganopolski, Andrey and Rahmstorf, Stefan (Jan. 2001). "Rapid changes of glacial climate simulated in a coupled climate model". In: *Nature* 409.6817, pp. 153–158. ISSN: 0028-0836, 1476-4687. DOI: 10.1038/35051500. URL: http://www.nature.com/articles/35051500 (visited on 10/05/2021).

Gao, Yang, Liu, Jian, Wen, Qin, Chen, Deliang, Sun, Weiyi, Ning, Liang, and Yan, Mi (2024). "The Influence of Increased CO2 Concentrations on AMOC Interdecadal Variability Under the LGM Background". In: *Journal of Geophysical Research: Atmospheres* 129.3. _eprint: https://onlinelibrary.wiley.com/doi/pdf/10.1029/2023JD039976, e2023JD039976. ISSN: 2169-8996. DOI: 10.1029/2023JD039976. URL: https://onlinelibrary.wiley.com/doi/abs/10.1029/2023JD039976 (visited on 03/15/2024).

García-Alix, Antonio, Jiménez-Moreno, Gonzalo, Jiménez-Espejo, Francisco J., García-García, Fernando, and Delgado Huertas, Antonio (Mar. 1, 2014). "An environmental snapshot of the Bølling interstadial in Southern Iberia". In: *Quaternary Research* 81.2, pp. 284–294. ISSN: 0033-5894. DOI: 10.1016/j.yqres.2014.01.009. URL: https://www.sciencedirect.com/science/article/pii/S003358941400012X (visited on 02/17/2025).

Gherardi, J.-M., Labeyrie, L., Nave, S., Francois, R., McManus, J. F., and Cortijo, E. (June 2009). "Glacial-interglacial circulation changes inferred from ^{231} Pa/ ^{230} Th sedimentary record in the North Atlantic region: MOC CHANGES INFERRED FROM Pa/Th RECORDS". In: *Paleoceanography* 24.2, n/a–n/a. ISSN: 08838305. DOI: 10.1029/2008PA001696. URL: http://doi.wiley.com/10.1029/2008PA001696 (visited on 11/30/2022).

Gherardi, J, Labeyrie, L, Mcmanus, J, Francois, R, Skinner, L, and Cortijo, E (Dec. 15, 2005). "Evidence from the Northeastern Atlantic basin for variability in the rate of the meridional overturning circulation through the last deglaciation". In: *Earth and Planetary Science Letters* 240.3, pp. 710–723. ISSN: 0012821X. DOI: 10.1016/j.epsl.2005.09.061. URL: https://linkinghub.elsevier.com/retrieve/pii/S0012821X05006576 (visited on 11/19/2021).

Giorgetta, Marco A., Jungclaus, Johann, Reick, Christian H., Legutke, Stephanie, Bader, Jürgen, Böttinger, Michael, Brovkin, Victor, Crueger, Traute, Esch, Monika, Fieg, Kerstin, Glushak, Ksenia, Gayler, Veronika, Haak, Helmuth, Hollweg, Heinz-Dieter, Ilyina, Tatiana, Kinne, Stefan, Kornblueh, Luis, Matei, Daniela, Mauritsen, Thorsten, Mikolajewicz, Uwe, Mueller, Wolfgang, Notz, Dirk, Pithan, Felix, Raddatz, Thomas, Rast, Sebastian, Redler, Rene, Roeckner, Erich, Schmidt, Hauke, Schnur, Reiner, Segschneider, Joachim, Six, Katharina D., Stock-

hause, Martina, Timmreck, Claudia, Wegner, Jörg, Widmann, Heinrich, Wieners, Karl-H., Claussen, Martin, Marotzke, Jochem, and Stevens, Bjorn (July 2013). "Climate and carbon cycle changes from 1850 to 2100 in MPI-ESM simulations for the Coupled Model Intercomparison Project phase 5: Climate Changes in MPI-ESM". In: *Journal of Advances in Modeling Earth Systems* 5.3, pp. 572–597. ISSN: 19422466. DOI: 10.1002/jame.20038. URL: http://doi.wiley.com/10.1002/jame.20038 (visited on 10/01/2021).

Golledge, N. R., Menviel, L., Carter, L., Fogwill, C. J., England, M. H., Cortese, G., and Levy, R. H. (Sept. 29, 2014). "Antarctic contribution to meltwater pulse 1A from reduced Southern Ocean overturning". In: *Nature Communications* 5.1. Number: 1 Publisher: Nature Publishing Group, pp. 1–10. ISSN: 2041-1723. DOI: 10.1038/ncomms6107. URL: https://www.nature.com/articles/ncomms6107 (visited on 01/03/2024).

Gomez, N., Gregoire, L. J., Mitrovica, J. X., and Payne, A. J. (May 28, 2015). "Laurentide-Cordilleran Ice Sheet saddle collapse as a contribution to meltwater pulse 1A". In: *Geophysical Research Letters* 42.10, pp. 3954–3962. ISSN: 0094-8276, 1944-8007. DOI: 10.1002/2015GL063960. URL: https://onlinelibrary.wiley.com/doi/abs/10.1002/2015GL063960 (visited on 09/09/2021).

Gomez, Natalya, Mitrovica, Jerry X., Huybers, Peter, and Clark, Peter U. (Dec. 2010). "Sea level as a stabilizing factor for marine-ice-sheet grounding lines". In: *Nature Geoscience* 3.12. Publisher: Nature Publishing Group, pp. 850–853. ISSN: 1752-0908. DOI: 10.1038/ngeo1012. URL: https://www.nature.com/articles/ngeo1012 (visited on 02/14/2025).

Gong, Xun, Zhang, Xiangdong, Lohmann, Gerrit, Wei, Wei, Zhang, Xu, and Pfeiffer, Madlene (July 2015). "Higher Laurentide and Greenland ice sheets strengthen the North Atlantic ocean circulation". In: *Climate Dynamics* 45.1, pp. 139–150. ISSN: 0930-7575, 1432-0894. DOI: 10.1007/s00382-015-2502-8. URL: http://link.springer.com/10.1007/s00382-015-2502-8 (visited on 05/26/2022).

Goosse, H., Brovkin, V., Fichefet, T., Haarsma, R., Huybrechts, P., Jongma, J., Mouchet, A., Selten, F., Barriat, P.-Y., Campin, J.-M., Deleersnijder, E., Driesschaert, E., Goelzer, H., Janssens, I., Loutre, M.-F., Morales Maqueda, M. A., Opsteegh, T., Mathieu, P.-P., Munhoven, G., Pettersson, E. J., Renssen, H., Roche, D. M., Schaeffer, M., Tartinville, B., Timmermann, A., and Weber, S. L. (Nov. 2, 2010). "Description of the Earth system model of intermediate complexity LOVECLIM version 1.2". In: *Geoscientific Model Development* 3.2, pp. 603–633. ISSN: 1991-9603. DOI: 10.5194/gmd-3-603-2010. URL: https://gmd.copernicus.org/articles/3/603/2010/ (visited on 09/29/2021).

Gorbarenko, Sergey A., Shi, Xuefa, Bosin, Aleksandr A., Liu, Yanguang, Artemova, Antonina V., Zou, Jianjun, Yanchenko, Elena A., Vasilenko, Yuriy P., Wu, Yonghua, and Vladimirov, Anton S. (Mar. 2022). "Relative sea level changes during the Last Glacial Maximum and deglaciation (33–15 ka) inferred from the 18O records of planktic foraminifera from the Sea of Japan". In: *Quaternary Science Reviews* 279, p. 107386. ISSN: 02773791. DOI: 10.1016/

j.quascirev.2022.107386. URL: https://linkinghub.elsevier.com/retrieve/pii/S0277379122000178 (visited on 06/07/2023).

Gordon, C., Cooper, C., Senior, C. A., Banks, H., Gregory, J. M., Johns, T. C., Mitchell, J. F. B., and Wood, R. A. (Feb. 4, 2000). "The simulation of SST, sea ice extents and ocean heat transports in a version of the Hadley Centre coupled model without flux adjustments". In: *Climate Dynamics* 16.2, pp. 147–168. ISSN: 0930-7575, 1432-0894. DOI: 10.1007/s003820050010. URL: http://link.springer.com/10.1007/s003820050010 (visited on 01/27/2022).

Gowan, Evan J., Tregoning, Paul, Purcell, Anthony, Montillet, Jean-Philippe, and McClusky, Simon (May 1, 2016). "A model of the western Laurentide Ice Sheet, using observations of glacial isostatic adjustment". In: *Quaternary Science Reviews* 139, pp. 1–16. ISSN: 0277-3791. DOI: 10.1016/j.quascirev.2016.03.003. URL: https://www.sciencedirect.com/science/article/pii/S0277379116300646 (visited on 02/06/2025).

Gowan, Evan J., Zhang, Xu, Khosravi, Sara, Rovere, Alessio, Stocchi, Paolo, Hughes, Anna L. C., Gyllencreutz, Richard, Mangerud, Jan, Svendsen, John-Inge, and Lohmann, Gerrit (Dec. 2021). "A new global ice sheet reconstruction for the past 80 000 years". In: *Nature Communications* 12.1, p. 1199. ISSN: 2041-1723. DOI: 10.1038/s41467-021-21469-w. URL: http://www.nature.com/articles/s41467-021-21469-w (visited on 09/09/2021).

Goñi, María Fernanda Sánchez (Jan. 2020). "Regional impacts of climate change and its relevance to human evolution". In: *Evolutionary Human Sciences* 2, e55. ISSN: 2513-843X. DOI: 10.1017/ehs.2020.56. URL: https://www.cambridge.org/core/journals/evolutionary-human-sciences/article/regional-impacts-of-climate-change-and-its-relevance-to-human-evolution/F48FC5562D7FF05FEB172158E60B8894 (visited on 01/31/2025).

Grafenstein, Ulrich von, Erlenkeuser, Helmut, Brauer, Achim, Jouzel, Jean, and Johnsen, Sigfus J. (June 4, 1999). "A Mid-European Decadal Isotope-Climate Record from 15,500 to 5000 Years B.P." In: *Science* 284.5420. Publisher: American Association for the Advancement of Science, pp. 1654–1657. DOI: 10.1126/science.284.5420.1654. URL: https://www.science.org/doi/full/10.1126/science.284.5420.1654 (visited on 02/17/2025).

Gregoire, Lauren J (2010). "Modelling the Northern Hemisphere Climate and Ice Sheets during the Last Deglaciation". In.

Gregoire, Lauren J., Ivanovic, Ruza F., Maycock, Amanda C., Valdes, Paul J., and Stevenson, Samantha (Nov. 2018). "Holocene lowering of the Laurentide ice sheet affects North Atlantic gyre circulation and climate". In: *Climate Dynamics* 51.9, pp. 3797–3813. ISSN: 0930-7575, 1432-0894. DOI: 10.1007/s00382-018-4111-9. URL: http://link.springer.com/10.1007/s00382-018-4111-9 (visited on 05/26/2022).

Gregoire, Lauren J., Otto-Bliesner, Bette, Valdes, Paul J., and Ivanovic, Ruza (Sept. 16, 2016). "Abrupt Bølling warming and ice saddle collapse contributions to the Meltwater Pulse 1a

rapid sea level rise: North American MWP1a Contribution". In: *Geophysical Research Letters* 43.17, pp. 9130–9137. ISSN: 00948276. DOI: 10.1002/2016GL070356. URL: http://doi.wiley.com/10.1002/2016GL070356 (visited on 10/05/2021).

Gregoire, Lauren J., Payne, Antony J., and Valdes, Paul J. (July 2012). "Deglacial rapid sea level rises caused by ice-sheet saddle collapses". In: *Nature* 487.7406, pp. 219–222. ISSN: 0028-0836, 1476-4687. DOI: 10.1038/nature11257. URL: http://www.nature.com/articles/nature11257 (visited on 09/09/2021).

Gregoire, Lauren J., Valdes, Paul J., and Payne, Antony J. (Nov. 28, 2015). "The relative contribution of orbital forcing and greenhouse gases to the North American deglaciation: DRIVERS OF N. AMERICAN DEGLACIATION". In: *Geophysical Research Letters* 42.22, pp. 9970–9979. ISSN: 00948276. DOI: 10.1002/2015GL066005. URL: http://doi.wiley.com/10.1002/2015GL066005 (visited on 07/11/2022).

Grist, Jeremy P., Josey, Simon A., and Sinha, Bablu (2007). "Impact on the ocean of extreme Greenland Sea heat loss in the HadCM3 coupled ocean-atmosphere model". In: *Journal of Geophysical Research: Oceans* 112 (C4). ISSN: 2156-2202. DOI: 10.1029/2006JC003629. URL: https://onlinelibrary.wiley.com/doi/abs/10.1029/2006JC003629 (visited on 07/28/2025).

Grootes, P. M., Stuiver, M., White, J. W. C., Johnsen, S., and Jouzel, J. (Dec. 1993). "Comparison of oxygen isotope records from the GISP2 and GRIP Greenland ice cores". In: *Nature* 366.6455, pp. 552–554. ISSN: 0028-0836, 1476-4687. DOI: 10.1038/366552a0. URL: http://www.nature.com/articles/366552a0 (visited on 06/10/2022).

Gu, Sifan, Liu, Zhengyu, Oppo, Delia W., Lynch-Stieglitz, Jean, Jahn, Alexandra, Zhang, Jiaxu, and Wu, Lixin (July 1, 2020). "Assessing the potential capability of reconstructing glacial Atlantic water masses and AMOC using multiple proxies in CESM". In: *Earth and Planetary Science Letters* 541, p. 116294. ISSN: 0012-821X. DOI: 10.1016/j.epsl.2020.116294. URL: https://www.sciencedirect.com/science/article/pii/S0012821X20302375 (visited on 11/20/2023).

Hanna, Edward, Cropper, Thomas E., Hall, Richard J., and Cappelen, John (2016). "Greenland Blocking Index 1851–2015: a regional climate change signal". In: *International Journal of Climatology* 36.15. _eprint: https://onlinelibrary.wiley.com/doi/pdf/10.1002/joc.4673, pp. 4847–4861. ISSN: 1097-0088. DOI: 10.1002/joc.4673. URL: https://onlinelibrary.wiley.com/doi/abs/10.1002/joc.4673 (visited on 02/21/2025).

Harrison, S. P., Bartlein, P. J., Brewer, S., Prentice, I. C., Boyd, M., Hessler, I., Holmgren, K., Izumi, K., and Willis, K. (Aug. 1, 2014). "Climate model benchmarking with glacial and mid-Holocene climates". In: *Climate Dynamics* 43.3, pp. 671–688. ISSN: 1432-0894. DOI: 10.1007/s00382-013-1922-6. URL: https://doi.org/10.1007/s00382-013-1922-6 (visited on 02/21/2025).

Harrison, S. P., Bartlein, P. J., Izumi, K., Li, G., Annan, J., Hargreaves, J., Braconnot, P., and Kageyama, M. (Aug. 2015). "Evaluation of CMIP5 palaeo-simulations to improve climate projections". In: *Nature Climate Change* 5.8, pp. 735–743. ISSN: 1758-678X, 1758-6798. DOI: 10.1038/nclimate2649. URL: https://www.nature.com/articles/nclimate2649 (visited on 06/01/2023).

Harrison, Sandy P., Braconnot, Pascale, Joussaume, Sylvie, Hewitt, Chris, and Stouffer, Ronald J. (2002). "PMIP Workshop 4 : launching PMIP Phase II". In: *EOS* 83, pp. 447–447. URL: https://pmip1.lsce.ipsl.fr/publications/local/eos_pmipiilaunch.html (visited on 02/01/2022).

He, Chengfei, Liu, Zhengyu, Otto-Bliesner, Bette L., Brady, Esther C., Zhu, Chenyu, Tomas, Robert, Buizert, Christo, and Severinghaus, Jeffrey P. (June 2021). "Abrupt Heinrich Stadial 1 cooling missing in Greenland oxygen isotopes". In: *Science Advances* 7.25, eabh1007. ISSN: 2375-2548. DOI: 10.1126/sciadv.abh1007. URL: https://advances.sciencemag.org/lookup/doi/10.1126/sciadv.abh1007 (visited on 10/11/2021).

He, Feng (2011). "Simulating transient climate evolution of the last deglaciation with CCSM 3." In: 72.10.

He, Feng and Clark, Peter U. (May 2022). "Freshwater forcing of the Atlantic Meridional Overturning Circulation revisited". In: *Nature Climate Change* 12.5. Number: 5 Publisher: Nature Publishing Group, pp. 449–454. ISSN: 1758-6798. DOI: 10.1038/s41558-022-01328-2. URL: https://www.nature.com/articles/s41558-022-01328-2 (visited on 01/23/2024).

He, Feng, Shakun, Jeremy D., Clark, Peter U., Carlson, Anders E., Liu, Zhengyu, Otto-Bliesner, Bette L., and Kutzbach, John E. (Feb. 7, 2013). "Northern Hemisphere forcing of Southern Hemisphere climate during the last deglaciation". In: *Nature* 494.7435, pp. 81–85. ISSN: 0028-0836, 1476-4687. DOI: 10.1038/nature11822. URL: http://www.nature.com/articles/nature11822 (visited on 05/03/2023).

Heinemann, M., Timmermann, A., Elison Timm, O., Saito, F., and Abe-Ouchi, A. (Aug. 27, 2014). "Deglacial ice sheet meltdown: orbital pacemaking and CO_2 effects". In: *Climate of the Past* 10.4. Publisher: Copernicus GmbH, pp. 1567–1579. ISSN: 1814-9324. DOI: 10.5194/cp-10-1567-2014. URL: https://cp.copernicus.org/articles/10/1567/2014/ (visited on 10/17/2024).

Heinrich, Hartmut (Mar. 1988). "Origin and Consequences of Cyclic Ice Rafting in the Northeast Atlantic Ocean During the Past 130,000 Years". In: *Quaternary Research* 29.2, pp. 142–152. ISSN: 0033-5894, 1096-0287. DOI: 10.1016/0033-5894(88)90057-9. URL: https://www.cambridge.org/core/journals/quaternary-research/article/abs/origin-and-consequences-of-cyclic-ice-rafting-in-the-northeast-atlantic-ocean-during-the-past-130000-years/4F38BE7643FFAB17EB2214C3A5E124FA (visited on 02/23/2024).

Hemming, Sidney R. (Mar. 2004). "Heinrich events: Massive late Pleistocene detritus layers of the North Atlantic and their global climate imprint: HEINRICH EVENTS". In: *Reviews of Geophysics* 42.1. ISSN: 87551209. DOI: 10.1029/2003RG000128. URL: http://doi.wiley.com/10.1029/2003RG000128 (visited on 01/27/2022).

Heymsfield, Andrew J. (Feb. 1, 1977). "Precipitation Development in Stratiform Ice Clouds: A Microphysical and Dynamical Study". In: Section: Journal of the Atmospheric Sciences. ISSN: 1520-0469. URL: https://journals.ametsoc.org/view/journals/atsc/34/2/1520-0469_1977_034_0367_pdisic_2_0_co_2.xml (visited on 01/23/2025).

Hodell, David A., Nicholl, Joseph A., Bontognali, Tomaso R. R., Danino, Steffan, Dorador, Javier, Dowdeswell, Julian A., Einsle, Joshua, Kuhlmann, Holger, Martrat, Belen, Mleneck-Vautravers, Maryline J., Rodríguez-Tovar, Francisco Javier, and Röhl, Ursula (2017). "Anatomy of Heinrich Layer 1 and its role in the last deglaciation". In: *Paleoceanography* 32.3. _eprint: https://onlinelibrary.wiley.com/doi/pdf/10.1002/2016PA003028, pp. 284–303. ISSN: 1944-9186. DOI: 10.1002/2016PA003028. URL: https://onlinelibrary.wiley.com/doi/abs/10.1002/2016PA003028 (visited on 01/24/2025).

Hoek, Wim Z. (2009). "Bølling-Allerød Interstadial". In: *Encyclopedia of Paleoclimatology and Ancient Environments*. Ed. by Vivien Gornitz. Dordrecht: Springer Netherlands, pp. 100–103. ISBN: 978-1-4020-4411-3. DOI: 10.1007/978-1-4020-4411-3_26. URL: https://doi.org/10.1007/978-1-4020-4411-3_26 (visited on 02/17/2025).

Hormes, Anne, Gjermundsen, Endre Før, and Rasmussen, Tine Lander (Sept. 1, 2013). "From mountain top to the deep sea – Deglaciation in 4D of the northwestern Barents Sea ice sheet". In: *Quaternary Science Reviews* 75, pp. 78–99. ISSN: 0277-3791. DOI: 10.1016/j.quascirev.2013.04.009. URL: https://www.sciencedirect.com/science/article/pii/S0277379113001418 (visited on 11/28/2024).

Huang, Jie, Wan, Shiming, Li, Anchun, and Li, Tiegang (Oct. 2019). "Two-phase structure of tropical hydroclimate during Heinrich Stadial 1 and its global implications". In: *Quaternary Science Reviews* 222, p. 105900. ISSN: 02773791. DOI: 10.1016/j.quascirev.2019.105900. URL: https://linkinghub.elsevier.com/retrieve/pii/S0277379119303798 (visited on 01/28/2022).

Huang, Kuo-Fang, Oppo, Delia W., and Curry, William B. (Mar. 2014). "Decreased influence of Antarctic intermediate water in the tropical Atlantic during North Atlantic cold events". In: *Earth and Planetary Science Letters* 389, pp. 200–208. ISSN: 0012821X. DOI: 10.1016/j.epsl.2013.12.037. URL: https://linkinghub.elsevier.com/retrieve/pii/S0012821X13007528 (visited on 01/28/2022).

Hubbard, Alun, Bradwell, Tom, Golledge, Nicholas, Hall, Adrian, Patton, Henry, Sugden, David, Cooper, Rhys, and Stoker, Martyn (Apr. 1, 2009). "Dynamic cycles, ice streams and their impact on the extent, chronology and deglaciation of the British–Irish ice sheet". In: *Quaternary Science Reviews*. Quaternary Glaciodynamics 28.7, pp. 758–776. ISSN: 0277-3791. DOI:

10.1016/j.quascirev.2008.12.026. URL: https://www.sciencedirect.com/science/article/pii/S0277379109000201 (visited on 01/30/2025).

Huber, Christof, Leuenberger, Markus, Spahni, Renato, Flückiger, Jacqueline, Schwander, Jakob, Stocker, Thomas F., Johnsen, Sigfus, Landais, Amaelle, and Jouzel, Jean (Mar. 30, 2006). "Isotope calibrated Greenland temperature record over Marine Isotope Stage 3 and its relation to CH4". In: *Earth and Planetary Science Letters* 243.3, pp. 504–519. ISSN: 0012-821X. DOI: 10.1016/j.epsl.2006.01.002. URL: https://www.sciencedirect.com/science/article/pii/S0012821X06000392 (visited on 02/22/2024).

Hughes, Anna L C, Gyllencreutz, Richard, Lohne, Øystein S, Mangerud, Jan, and Svendsen, John Inge (2015). *DATED-1: compilation of dates and time-slice reconstruction of the build-up and retreat of the last Eurasian (British-Irish, Scandinavian, Svalbard-Barents-Kara Seas) Ice Sheets 40-10 ka*. In collab. with University Of Bergen Department Of Earth Science. Artwork Size: 24 data points Pages: 24 data points. DOI: 10.1594/PANGAEA.848117. URL: https://doi.pangaea.de/10.1594/PANGAEA.848117 (visited on 06/07/2023).

Hughes, Anna L. C., Gyllencreutz, Richard, Lohne, Øystein S., Mangerud, Jan, and Svendsen, John Inge (Jan. 2016). "The last Eurasian ice sheets – a chronological database and time-slice reconstruction, DATED-1". In: *Boreas* 45.1, pp. 1–45. ISSN: 0300-9483, 1502-3885. DOI: 10.1111/bor.12142. URL: https://onlinelibrary.wiley.com/doi/10.1111/bor.12142 (visited on 11/22/2022).

Huntley, Brian, Allen, Judy R. M., Forrest, Matthew, Hickler, Thomas, Ohlemüller, Ralf, Singarayer, Joy S., and Valdes, Paul J. (2023). "Global biome patterns of the Middle and Late Pleistocene". In: *Journal of Biogeography* 50.8. _eprint: https://onlinelibrary.wiley.com/doi/pdf/10.1111/jbi.1 pp. 1352–1372. ISSN: 1365-2699. DOI: 10.1111/jbi.14619. URL: https://onlinelibrary.wiley.com/doi/abs/10.1111/jbi.14619 (visited on 01/17/2025).

Hurrell, James W., Holland, M. M., Gent, P. R., Ghan, S., Kay, Jennifer E., Kushner, P. J., Lamarque, J.-F., Large, W. G., Lawrence, D., Lindsay, K., Lipscomb, W. H., Long, M. C., Mahowald, N., Marsh, D. R., Neale, R. B., Rasch, P., Vavrus, S., Vertenstein, M., Bader, D., Collins, W. D., Hack, J. J., Kiehl, J., and Marshall, S. (Sept. 2013). "The Community Earth System Model: A Framework for Collaborative Research". In: *Bulletin of the American Meteorological Society* 94.9, pp. 1339–1360. ISSN: 0003-0007, 1520-0477. DOI: 10.1175/BAMS-D-12-00121.1. URL: http://journals.ametsoc.org/doi/10.1175/BAMS-D-12-00121.1 (visited on 09/29/2021).

Huybrechts, Philippe (Jan. 1, 2002). "Sea-level changes at the LGM from ice-dynamic reconstructions of the Greenland and Antarctic ice sheets during the glacial cycles". In: *Quaternary Science Reviews*. EPILOG 21.1, pp. 203–231. ISSN: 0277-3791. DOI: 10.1016/S0277-3791(01)00082-8. URL: https://www.sciencedirect.com/science/article/pii/S0277379101000828 (visited on 02/23/2025).

Häkkinen, Sirpa, Rhines, Peter B., and Worthen, Denise L. (Nov. 4, 2011). "Atmospheric Blocking and Atlantic Multidecadal Ocean Variability". In: *Science* 334.6056. Publisher: American Association for the Advancement of Science, pp. 655–659. DOI: 10.1126/science.1205683. URL: https://www.science.org/doi/full/10.1126/science.1205683 (visited on 02/21/2025).

Ivanovic, R. F., Gregoire, L. J., Burke, A., Wickert, A. D., Valdes, P. J., Ng, H. C., Robinson, L. F., McManus, J. F., Mitrovica, J. X., Lee, L., and Dentith, J. E. (July 2018a). "Acceleration of Northern Ice Sheet Melt Induces AMOC Slowdown and Northern Cooling in Simulations of the Early Last Deglaciation". In: *Paleoceanography and Paleoclimatology* 33.7, pp. 807–824. ISSN: 2572-4517, 2572-4525. DOI: 10.1029/2017PA003308. URL: https://onlinelibrary.wiley.com/doi/abs/10.1029/2017PA003308 (visited on 09/09/2021).

Ivanovic, R. F., Gregoire, L. J., Wickert, A. D., and Burke, A. (2018b). "Climatic Effect of Antarctic Meltwater Overwhelmed by Concurrent Northern Hemispheric Melt". In: *Geophysical Research Letters* 45.11. _eprint: https://onlinelibrary.wiley.com/doi/pdf/10.1029/2018GL077623, pp. 5681–5689. ISSN: 1944-8007. DOI: 10.1029/2018GL077623. URL: https://onlinelibrary.wiley.com/doi/abs/10.1029/2018GL077623 (visited on 01/30/2025).

Ivanovic, Ruza F., Gregoire, Lauren J., Kageyama, Masa, Roche, Didier M., Valdes, Paul J., Burke, Andrea, Drummond, Rosemarie, Peltier, W. Richard, and Tarasov, Lev (July 29, 2016). "Transient climate simulations of the deglaciation 21–9 thousand years beforepresent (version 1) – PMIP4 Core experiment design and boundary conditions". In: *Geoscientific Model Development* 9.7, pp. 2563–2587. ISSN: 1991-9603. DOI: 10.5194/gmd-9-2563-2016. URL: https://gmd.copernicus.org/articles/9/2563/2016/ (visited on 09/02/2021).

Ivanovic, Ruza F., Gregoire, Lauren J., Wickert, Andrew D., Valdes, Paul J., and Burke, Andrea (Jan. 16, 2017). "Collapse of the North American ice saddle 14,500 years ago caused widespread cooling and reduced ocean overturning circulation: Ice Collapse Caused Cooling ˜14.5 ka". In: *Geophysical Research Letters* 44.1, pp. 383–392. ISSN: 00948276. DOI: 10.1002/2016GL071849. URL: http://doi.wiley.com/10.1002/2016GL071849 (visited on 09/02/2021).

Izumi, Kenji, Valdes, Paul, Ivanovic, Ruza, and Gregoire, Lauren (Apr. 1, 2023). "Impacts of the PMIP4 ice sheets on Northern Hemisphere climate during the last glacial period". In: *Climate Dynamics* 60.7, pp. 2481–2499. ISSN: 1432-0894. DOI: 10.1007/s00382-022-06456-1. URL: https://doi.org/10.1007/s00382-022-06456-1 (visited on 08/05/2024).

Jackson, Laura C., Biastoch, Arne, Buckley, Martha W., Desbruyères, Damien G., Frajka-Williams, Eleanor, Moat, Ben, and Robson, Jon (Apr. 2022). "The evolution of the North Atlantic Meridional Overturning Circulation since 1980". In: *Nature Reviews Earth & Environment* 3.4. Publisher: Nature Publishing Group, pp. 241–254. ISSN: 2662-138X. DOI: 10.1038/s43017-022-00263-2. URL: https://www.nature.com/articles/s43017-022-00263-2 (visited on 10/24/2024).

Ji, Weiwen, Robel, Alexander, Tziperman, Eli, and Yang, Jun (2021). "Laurentide Ice Saddle Mergers Drive Rapid Sea Level Drops During Glaciations". In: *Geophysical Research Letters* 48.14. _eprint: https://onlinelibrary.wiley.com/doi/pdf/10.1029/2021GL094263, e2021GL094263. ISSN: 1944-8007. DOI: 10.1029/2021GL094263. URL: https://onlinelibrary.wiley.com/doi/abs/10.1029/2021GL094263 (visited on 12/12/2024).

Jiménez-Moreno, Gonzalo, Anderson, R. Scott, Desprat, Stéphanie, Grigg, Laurie D., Grimm, Eric C., Heusser, Linda E., Jacobs, Bonnie F., López-Martínez, Constancia, Whitlock, Cathy L., and Willard, Debra A. (Oct. 1, 2010). "Millennial-scale variability during the last glacial in vegetation records from North America". In: *Quaternary Science Reviews*. Vegetation Response to Millennial-scale Variability during the Last Glacial 29.21, pp. 2865–2881. ISSN: 0277-3791. DOI: 10.1016/j.quascirev.2009.12.013. URL: https://www.sciencedirect.com/science/article/pii/S0277379109004326 (visited on 02/27/2025).

Joos, F. and Spahni, R. (Feb. 5, 2008). "Rates of change in natural and anthropogenic radiative forcing over the past 20,000 years". In: *Proceedings of the National Academy of Sciences* 105.5, pp. 1425–1430. ISSN: 0027-8424, 1091-6490. DOI: 10.1073/pnas.0707386105. URL: http://www.pnas.org/cgi/doi/10.1073/pnas.0707386105 (visited on 01/28/2022).

Jouzel, J., Masson-Delmotte, V., Cattani, O., Dreyfus, G., Falourd, S., Hoffmann, G., Minster, B., Nouet, J., Barnola, J. M., Chappellaz, J., Fischer, H., Gallet, J. C., Johnsen, S., Leuenberger, M., Loulergue, L., Luethi, D., Oerter, H., Parrenin, F., Raisbeck, G., Raynaud, D., Schilt, A., Schwander, J., Selmo, E., Souchez, R., Spahni, R., Stauffer, B., Steffensen, J. P., Stenni, B., Stocker, T. F., Tison, J. L., Werner, M., and Wolff, E. W. (Aug. 10, 2007). "Orbital and Millennial Antarctic Climate Variability over the Past 800,000 Years". In: *Science*. Publisher: American Association for the Advancement of Science. DOI: 10.1126/science.1141038. URL: https://www.science.org/doi/abs/10.1126/science.1141038 (visited on 02/02/2022).

Jóhannesson, Tómas, Raymond, Charles, and Waddington, Ed (Jan. 1989). "Time–Scale for Adjustment of Glaciers to Changes in Mass Balance". In: *Journal of Glaciology* 35.121, pp. 355–369. ISSN: 0022-1430, 1727-5652. DOI: 10.3189/S002214300000928X. URL: https://www.cambridge.org/core/journals/journal-of-glaciology/article/timescale-for-adjustment-of-glaciers-to-changes-in-mass-balance/B34E832DC10EADCF6DF4220695F34B9A (visited on 01/13/2025).

Kachuck, S. B., Martin, D. F., Bassis, J. N., and Price, S. F. (2020). "Rapid Viscoelastic Deformation Slows Marine Ice Sheet Instability at Pine Island Glacier". In: *Geophysical Research Letters* 47.10. _eprint: https://onlinelibrary.wiley.com/doi/pdf/10.1029/2019GL086446, e2019GL086446. ISSN: 1944-8007. DOI: 10.1029/2019GL086446. URL: https://onlinelibrary.wiley.com/doi/abs/10.1029/2019GL086446 (visited on 02/14/2025).

Kageyama, M., Merkel, U., Otto-Bliesner, B., Prange, M., Abe-Ouchi, A., Lohmann, G., Ohgaito, R., Roche, D. M., Singarayer, J., Swingedouw, D., and X Zhang (Apr. 9, 2013). "Climatic

impacts of fresh water hosing under Last Glacial Maximum conditions: a multi-model study". In: *Climate of the Past* 9.2, pp. 935–953. ISSN: 1814-9332. DOI: 10.5194/cp-9-935-2013. URL: https://cp.copernicus.org/articles/9/935/2013/ (visited on 09/24/2021).

Kageyama, Masa, Albani, Samuel, Braconnot, Pascale, Harrison, Sandy P., Hopcroft, Peter O., Ivanovic, Ruza F., Lambert, Fabrice, Marti, Olivier, Peltier, W. Richard, Peterschmitt, Jean-Yves, Roche, Didier M., Tarasov, Lev, Zhang, Xu, Brady, Esther C., Haywood, Alan M., LeGrande, Allegra N., Lunt, Daniel J., Mahowald, Natalie M., Mikolajewicz, Uwe, Nisancioglu, Kerim H., Otto-Bliesner, Bette L., Renssen, Hans, Tomas, Robert A., Zhang, Qiong, Abe-Ouchi, Ayako, Bartlein, Patrick J., Cao, Jian, Li, Qiang, Lohmann, Gerrit, Ohgaito, Rumi, Shi, Xiaoxu, Volodin, Evgeny, Yoshida, Kohei, Zhang, Xiao, and Zheng, Weipeng (Nov. 7, 2017). "The PMIP4 contribution to CMIP6 – Part 4: Scientific objectives and experimental design of the PMIP4-CMIP6 Last Glacial Maximum experiments and PMIP4 sensitivity experiments". In: *Geoscientific Model Development* 10.11, pp. 4035–4055. ISSN: 1991-9603. DOI: 10.5194/gmd-10-4035-2017. URL: https://gmd.copernicus.org/articles/10/4035/2017/ (visited on 11/27/2023).

Kageyama, Masa, Sime, Louise C., Sicard, Marie, Guarino, Maria-Vittoria, Vernal, Anne de, Stein, Ruediger, Schroeder, David, Malmierca-Vallet, Irene, Abe-Ouchi, Ayako, Bitz, Cecilia, Braconnot, Pascale, Brady, Esther C., Cao, Jian, Chamberlain, Matthew A., Feltham, Danny, Guo, Chuncheng, LeGrande, Allegra N., Lohmann, Gerrit, Meissner, Katrin J., Menviel, Laurie, Morozova, Polina, Nisancioglu, Kerim H., Otto-Bliesner, Bette L., O'ishi, Ryouta, Ramos Buarque, Silvana, Melia, David Salas y, Sherriff-Tadano, Sam, Stroeve, Julienne, Shi, Xiaoxu, Sun, Bo, Tomas, Robert A., Volodin, Evgeny, Yeung, Nicholas K. H., Zhang, Qiong, Zhang, Zhongshi, Zheng, Weipeng, and Ziehn, Tilo (Jan. 11, 2021). "A multi-model CMIP6-PMIP4 study of Arctic sea ice at 127 ka: sea ice data compilation and model differences". In: *Climate of the Past* 17.1, pp. 37–62. ISSN: 1814-9332. DOI: 10.5194/cp-17-37-2021. URL: https://cp.copernicus.org/articles/17/37/2021/ (visited on 09/24/2021).

Kapsch, Marie-Luise, Mikolajewicz, Uwe, Ziemen, Florian A., Rodehacke, Christian B., and Schannwell, Clemens (Mar. 3, 2021). "Analysis of the surface mass balance for deglacial climate simulations". In: *The Cryosphere* 15.2, pp. 1131–1156. ISSN: 1994-0424. DOI: 10.5194/tc-15-1131-2021. URL: https://tc.copernicus.org/articles/15/1131/2021/ (visited on 05/04/2023).

Kapsch, Marie-Luise, Mikolajewicz, Uwe, Ziemen, Florian, and Schannwell, Clemens (Jan. 24, 2022). "Ocean response in transient simulations of the last deglaciation dominated by underlying ice-sheet reconstruction and method of meltwater distribution". In: *Geophysical Research Letters*. ISSN: 0094-8276, 1944-8007. DOI: 10.1029/2021GL096767. URL: https://onlinelibrary.wiley.com/doi/10.1029/2021GL096767 (visited on 01/27/2022).

Kawamura, Kenji, Parrenin, Frédéric, Lisiecki, Lorraine, Uemura, Ryu, Vimeux, Françoise, Severinghaus, Jeffrey P., Hutterli, Manuel A., Nakazawa, Takakiyo, Aoki, Shuji, Jouzel, Jean, Raymo, Maureen E., Matsumoto, Koji, Nakata, Hisakazu, Motoyama, Hideaki, Fujita, Shuji,

Goto-Azuma, Kumiko, Fujii, Yoshiyuki, and Watanabe, Okitsugu (Aug. 2007). "Northern Hemisphere forcing of climatic cycles in Antarctica over the past 360,000 years". In: *Nature* 448.7156. Publisher: Nature Publishing Group, pp. 912–916. ISSN: 1476-4687. DOI: 10.1038/nature06015. URL: https://www.nature.com/articles/nature06015 (visited on 01/23/2025).

Kindler, P., Guillevic, M., Baumgartner, M., Schwander, J., Landais, A., and Leuenberger, M. (Apr. 30, 2014). "Temperature reconstruction from 10 to 120 kyr b2k from the NGRIP ice core". In: *Climate of the Past* 10.2. Publisher: Copernicus GmbH, pp. 887–902. ISSN: 1814-9324. DOI: 10.5194/cp-10-887-2014. URL: https://cp.copernicus.org/articles/10/887/2014/ (visited on 02/22/2024).

Kleppin, Hannah, Jochum, Markus, Otto-Bliesner, Bette, Shields, Christine A., and Yeager, Stephen (Oct. 1, 2015). "Stochastic Atmospheric Forcing as a Cause of Greenland Climate Transitions". In: *Journal of Climate* 28.19. Publisher: American Meteorological Society Section: Journal of Climate, pp. 7741–7763. ISSN: 0894-8755, 1520-0442. DOI: 10.1175/JCLI-D-14-00728.1. URL: https://journals.ametsoc.org/view/journals/clim/28/19/jcli-d-14-00728.1.xml (visited on 02/26/2024).

Klockmann, M., Mikolajewicz, U., Kleppin, H., and Marotzke, J. (Nov. 16, 2020). "Coupling of the Subpolar Gyre and the Overturning Circulation During Abrupt Glacial Climate Transitions". In: *Geophysical Research Letters* 47.21. ISSN: 0094-8276, 1944-8007. DOI: 10.1029/2020GL090361. URL: https://onlinelibrary.wiley.com/doi/10.1029/2020GL090361 (visited on 08/23/2022).

Klockmann, Marlene, Mikolajewicz, Uwe, and Marotzke, Jochem (Sept. 8, 2016). "The effect of greenhouse gas concentrations and ice sheets on the glacial AMOC in a coupled climate model". In: *Climate of the Past* 12.9, pp. 1829–1846. ISSN: 1814-9332. DOI: 10.5194/cp-12-1829-2016. URL: https://cp.copernicus.org/articles/12/1829/2016/ (visited on 08/24/2022).

– (Oct. 2018). "Two AMOC States in Response to Decreasing Greenhouse Gas Concentrations in the Coupled Climate Model MPI-ESM". In: *Journal of Climate* 31.19, pp. 7969–7984. ISSN: 0894-8755, 1520-0442. DOI: 10.1175/JCLI-D-17-0859.1. URL: https://journals.ametsoc.org/doi/10.1175/JCLI-D-17-0859.1 (visited on 08/24/2022).

Knorr, Gregor and Lohmann, Gerrit (July 2003). "Southern Ocean origin for the resumption of Atlantic thermohaline circulation during deglaciation". In: *Nature* 424.6948. Publisher: Nature Publishing Group, pp. 532–536. ISSN: 1476-4687. DOI: 10.1038/nature01855. URL: https://www.nature.com/articles/nature01855 (visited on 01/24/2025).

Knutti, R., Flückiger, J., Stocker, T. F., and Timmermann, A. (Aug. 2004). "Strong hemispheric coupling of glacial climate through freshwater discharge and ocean circulation". In: *Nature* 430.7002, pp. 851–856. ISSN: 0028-0836, 1476-4687. DOI: 10.1038/nature02786. URL: http://www.nature.com/articles/nature02786 (visited on 02/14/2022).

Kopp, Robert E., DeConto, Robert M., Bader, Daniel A., Hay, Carling C., Horton, Radley M., Kulp, Scott, Oppenheimer, Michael, Pollard, David, and Strauss, Benjamin H. (2017). "Evolving Understanding of Antarctic Ice-Sheet Physics and Ambiguity in Probabilistic Sea-Level Projections". In: *Earth's Future* 5.12. _eprint: https://onlinelibrary.wiley.com/doi/pdf/10.1002/2017EF00066 pp. 1217–1233. ISSN: 2328-4277. DOI: 10.1002/2017EF000663. URL: https://onlinelibrary.wiley.com/doi/abs/10.1002/2017EF000663 (visited on 01/30/2025).

Kuniyoshi, Yuta, Abe-Ouchi, Ayako, Sherriff-Tadano, Sam, Chan, Wing-Le, and Saito, Fuyuki (Mar. 28, 2022). "Effect of Climatic Precession on Dansgaard-Oeschger-Like Oscillations". In: *Geophysical Research Letters* 49.6. ISSN: 0094-8276, 1944-8007. DOI: 10.1029/2021GL095695. URL: https://onlinelibrary.wiley.com/doi/10.1029/2021GL095695 (visited on 07/10/2023).

Köhler, Peter, Nehrbass-Ahles, Christoph, Schmitt, Jochen, Stocker, Thomas F., and Fischer, Hubertus (June 20, 2017). "A 156 kyr smoothed history of the atmospheric greenhouse gases CO₂, CH₄, and N₂O and their radiative forcing". In: *Earth System Science Data* 9.1, pp. 363–387. ISSN: 1866-3516. DOI: 10.5194/essd-9-363-2017. URL: https://essd.copernicus.org/articles/9/363/2017/ (visited on 01/28/2022).

Lambeck, K., Rouby, H., Purcell, A., Sun, Y., and Sambridge, M. (Oct. 28, 2014). "Sea level and global ice volumes from the Last Glacial Maximum to the Holocene". In: *Proceedings of the National Academy of Sciences* 111.43, pp. 15296–15303. ISSN: 0027-8424, 1091-6490. DOI: 10.1073/pnas.1411762111. URL: http://www.pnas.org/cgi/doi/10.1073/pnas.1411762111 (visited on 01/27/2022).

Lambeck, Kurt, Purcell, Anthony, and Zhao, S. (Feb. 15, 2017). "The North American Late Wisconsin ice sheet and mantle viscosity from glacial rebound analyses". In: *Quaternary Science Reviews* 158, pp. 172–210. ISSN: 0277-3791. DOI: 10.1016/j.quascirev.2016.11.033. URL: https://www.sciencedirect.com/science/article/pii/S0277379116306047 (visited on 02/17/2025).

Lang, Charlotte, Edwards, Tamsin, Owen, Jonathan, Sherriff-Tadano, Sam, Gregory, Jonathan, Ivanovic, Ruza, Gregoire, Lauren, and Smith, Robin S. (May 1, 2023). "Sensitivity of of coupled climate and ice sheet of modern Greenland to atmospheric, snow and ice sheet parameters". In: Conference Name: EGU General Assembly Conference Abstracts ADS Bibcode: 2023EGUGA..2514666L, EGU–14666. DOI: 10.5194/egusphere-egu23-14666. URL: https://ui.adsabs.harvard.edu/abs/2023EGUGA..2514666L (visited on 02/06/2025).

Lea, David W., Pak, Dorothy K., Peterson, Larry C., and Hughen, Konrad A. (Sept. 5, 2003). "Synchroneity of Tropical and High-Latitude Atlantic Temperatures over the Last Glacial Termination". In: *Science* 301.5638, pp. 1361–1364. ISSN: 0036-8075, 1095-9203. DOI: 10.1126/science.1088470. URL: https://www.science.org/doi/10.1126/science.1088470 (visited on 05/26/2022).

Lee, Victoria, Cornford, Stephen L., and Payne, Antony J. (Jan. 2015). "Initialization of an ice-sheet model for present-day Greenland". In: *Annals of Glaciology* 56.70, pp. 129–140. ISSN: 0260-3055, 1727-5644. DOI: 10.3189/2015AoG70A121. URL: https://www.cambridge.org/core/journals/annals-of-glaciology/article/initialization-of-an-icesheet-model-for-presentday-greenland/8514FB24D7B4FD95F3EA00FD8A54E83D (visited on 02/14/2025).

Lenaerts, Jan T. M., Medley, Brooke, Broeke, Michiel R. van den, and Wouters, Bert (2019). "Observing and Modeling Ice Sheet Surface Mass Balance". In: *Reviews of Geophysics* 57.2. _eprint: https://onlinelibrary.wiley.com/doi/pdf/10.1029/2018RG000622, pp. 376–420. ISSN: 1944-9208. DOI: 10.1029/2018RG000622. URL: https://onlinelibrary.wiley.com/doi/abs/10.1029/2018RG000622 (visited on 01/31/2025).

Li, Camille, Battisti, David S., and Bitz, Cecilia M. (Oct. 15, 2010). "Can North Atlantic Sea Ice Anomalies Account for Dansgaard–Oeschger Climate Signals?*". In: *Journal of Climate* 23.20, pp. 5457–5475. ISSN: 1520-0442, 0894-8755. DOI: 10.1175/2010JCLI3409.1. URL: http://journals.ametsoc.org/doi/10.1175/2010JCLI3409.1 (visited on 06/10/2022).

Li, Camille and Born, Andreas (Jan. 2019). "Coupled atmosphere-ice-ocean dynamics in Dansgaard-Oeschger events". In: *Quaternary Science Reviews* 203, pp. 1–20. ISSN: 02773791. DOI: 10.1016/j.quascirev.2018.10.031. URL: https://linkinghub.elsevier.com/retrieve/pii/S0277379118305705 (visited on 12/07/2022).

Lin, Yucheng, Hibbert, Fiona D., Whitehouse, Pippa L., Woodroffe, Sarah A., Purcell, Anthony, Shennan, Ian, and Bradley, Sarah L. (Dec. 2021). "A reconciled solution of Meltwater Pulse 1A sources using sea-level fingerprinting". In: *Nature Communications* 12.1, p. 2015. ISSN: 2041-1723. DOI: 10.1038/s41467-021-21990-y. URL: http://www.nature.com/articles/s41467-021-21990-y (visited on 10/31/2022).

Lippold, Jörg, Pöppelmeier, Frerk, Süfke, Finn, Gutjahr, Marcus, Goepfert, Tyler J., Blaser, Patrick, Friedrich, Oliver, Link, Jasmin M., Wacker, Lukas, Rheinberger, Stefan, and Jaccard, Samuel L. (Oct. 28, 2019). "Constraining the Variability of the Atlantic Meridional Overturning Circulation During the Holocene". In: *Geophysical Research Letters* 46.20, pp. 11338–11346. ISSN: 0094-8276, 1944-8007. DOI: 10.1029/2019GL084988. URL: https://onlinelibrary.wiley.com/doi/10.1029/2019GL084988 (visited on 06/02/2023).

Liu, Jean, Milne, Glenn A., Kopp, Robert E., Clark, Peter U., and Shennan, Ian (Feb. 2016). "Sea-level constraints on the amplitude and source distribution of Meltwater Pulse 1A". In: *Nature Geoscience* 9.2, pp. 130–134. ISSN: 1752-0894, 1752-0908. DOI: 10.1038/ngeo2616. URL: http://www.nature.com/articles/ngeo2616 (visited on 07/12/2022).

Liu, Wei, Liu, Zhengyu, and Brady, Esther C. (Mar. 15, 2014). "Why is the AMOC Monostable in Coupled General Circulation Models?" In: *Journal of Climate* 27.6. Publisher: American Meteorological Society Section: Journal of Climate, pp. 2427–2443. ISSN: 0894-8755, 1520-0442. DOI: 10.1175/JCLI-D-13-00264.1. URL: https://journals.ametsoc.org/view/journals/clim/27/6/jcli-d-13-00264.1.xml (visited on 12/04/2023).

Liu, Z., Otto-Bliesner, B. L., He, F., Brady, E. C., Tomas, R., Clark, P. U., Carlson, A. E., Lynch-Stieglitz, J., Curry, W., Brook, E., Erickson, D., Jacob, R., Kutzbach, J., and Cheng, J. (July 17, 2009). "Transient Simulation of Last Deglaciation with a New Mechanism for Bolling-Allerod Warming". In: *Science* 325.5938, pp. 310–314. ISSN: 0036-8075, 1095-9203. DOI: 10.1126/science.1171041. URL: https://www.sciencemag.org/lookup/doi/10.1126/science.1171041 (visited on 09/02/2021).

Liu, Zhengyu, Bao, Yuntao, Thompson, Lonnie G., Mosley-Thompson, Ellen, Tabor, Clay, Zhang, Guang J., Yan, Mi, Lofverstrom, Marcus, Montanez, Isabel, and Oster, Jessica (Nov. 8, 2023). "Tropical mountain ice core 18O: A Goldilocks indicator for global temperature change". In: *Science Advances* 9.45. Publisher: American Association for the Advancement of Science, eadi6725. DOI: 10.1126/sciadv.adi6725. URL: https://www.science.org/doi/full/10.1126/sciadv.adi6725 (visited on 09/10/2024).

Liu, Zhengyu, Carlson, Anders E., He, Feng, Brady, Esther C., Otto-Bliesner, Bette L., Briegleb, Bruce P., Wehrenberg, Mark, Clark, Peter U., Wu, Shu, Cheng, Jun, Zhang, Jiaxu, Noone, David, and Zhu, Jiang (July 10, 2012). "Younger Dryas cooling and the Greenland climate response to CO2". In: *Proceedings of the National Academy of Sciences* 109.28. Publisher: Proceedings of the National Academy of Sciences, pp. 11101–11104. DOI: 10.1073/pnas.1202183109. URL: https://www.pnas.org/doi/10.1073/pnas.1202183109 (visited on 02/21/2025).

Lohmann, Johannes and Ditlevsen, Peter D. (Sept. 27, 2019). "Objective extraction and analysis of statistical features of Dansgaard–Oeschger events". In: *Climate of the Past* 15.5. Publisher: Copernicus GmbH, pp. 1771–1792. ISSN: 1814-9324. DOI: 10.5194/cp-15-1771-2019. URL: https://cp.copernicus.org/articles/15/1771/2019/ (visited on 01/24/2025).

Loulergue, Laetitia, Schilt, Adrian, Spahni, Renato, Masson-Delmotte, Valérie, Blunier, Thomas, Lemieux, Bénédicte, Barnola, Jean-Marc, Raynaud, Dominique, Stocker, Thomas F., and Chappellaz, Jérôme (May 2008). "Orbital and millennial-scale features of atmospheric CH4 over the past 800,000 years". In: *Nature* 453.7193, pp. 383–386. ISSN: 0028-0836, 1476-4687. DOI: 10.1038/nature06950. URL: http://www.nature.com/articles/nature06950 (visited on 01/27/2022).

Lozier, M. S., Li, F., Bacon, S., Bahr, F., Bower, A. S., Cunningham, S. A., Jong, M. F. de, Steur, L. de, deYoung, B., Fischer, J., Gary, S. F., Greenan, B. J. W., Holliday, N. P., Houk, A., Houpert, L., Inall, M. E., Johns, W. E., Johnson, H. L., Johnson, C., Karstensen, J., Koman, G., Le Bras, I. A., Lin, X., Mackay, N., Marshall, D. P., Mercier, H., Oltmanns, M., Pickart, R. S., Ramsey, A. L., Rayner, D., Straneo, F., Thierry, V., Torres, D. J., Williams, R. G., Wilson, C., Yang, J., Yashayaev, I., and Zhao, J. (Feb. 2019). "A sea change in our view of overturning in the subpolar North Atlantic". In: *Science* 363.6426, pp. 516–521. DOI: 10.1126/science.aau6592. URL: https://www.science.org/doi/full/10.1126/science.aau6592 (visited on 07/28/2025).

Lunt, D. J., Dunkley Jones, T., Heinemann, M., Huber, M., LeGrande, A., Winguth, A., Loptson, C., Marotzke, J., Roberts, C. D., Tindall, J., Valdes, P., and Winguth, C. (Oct. 29, 2012). "A model–data comparison for a multi-model ensemble of early Eocene atmosphere–ocean simulations: EoMIP". In: *Climate of the Past* 8.5, pp. 1717–1736. ISSN: 1814-9332. DOI: 10.5194/cp-8-1717-2012. URL: https://cp.copernicus.org/articles/8/1717/2012/ (visited on 05/27/2022).

Lynch-Stieglitz, Jean (Jan. 3, 2017). "The Atlantic Meridional Overturning Circulation and Abrupt Climate Change". In: *Annual Review of Marine Science* 9.1, pp. 83–104. ISSN: 1941-1405, 1941-0611. DOI: 10.1146/annurev-marine-010816-060415. URL: https://www.annualreviews.org/doi/10.1146/annurev-marine-010816-060415 (visited on 05/03/2023).

Lynch-Stieglitz, Jean, Adkins, Jess F., Curry, William B., Dokken, Trond, Hall, Ian R., Herguera, Juan Carlos, Hirschi, Joël J.-M., Ivanova, Elena V., Kissel, Catherine, Marchal, Olivier, Marchitto, Thomas M., McCave, I. Nicholas, McManus, Jerry F., Mulitza, Stefan, Ninnemann, Ulysses, Peeters, Frank, Yu, Ein-Fen, and Zahn, Rainer (Apr. 6, 2007). "Atlantic Meridional Overturning Circulation During the Last Glacial Maximum". In: *Science* 316.5821, pp. 66–69. ISSN: 0036-8075, 1095-9203. DOI: 10.1126/science.1137127. URL: https://www.science.org/doi/10.1126/science.1137127 (visited on 01/27/2022).

Löfverström, M., Caballero, R., Nilsson, J., and Kleman, J. (July 31, 2014). "Evolution of the large-scale atmospheric circulation in response to changing ice sheets over the last glacial cycle". In: *Climate of the Past* 10.4, pp. 1453–1471. ISSN: 1814-9332. DOI: 10.5194/cp-10-1453-2014. URL: https://cp.copernicus.org/articles/10/1453/2014/ (visited on 06/16/2022).

Löfverström, Marcus and Lora, Juan M. (Aug. 16, 2017). "Abrupt regime shifts in the North Atlantic atmospheric circulation over the last deglaciation". In: *Geophysical Research Letters* 44.15, pp. 8047–8055. ISSN: 0094-8276, 1944-8007. DOI: 10.1002/2017GL074274. URL: https://onlinelibrary.wiley.com/doi/10.1002/2017GL074274 (visited on 05/26/2022).

Lüthi, Dieter, Le Floch, Martine, Bereiter, Bernhard, Blunier, Thomas, Barnola, Jean-Marc, Siegenthaler, Urs, Raynaud, Dominique, Jouzel, Jean, Fischer, Hubertus, Kawamura, Kenji, and Stocker, Thomas F. (May 2008). "High-resolution carbon dioxide concentration record 650,000–800,000 years before present". In: *Nature* 453.7193, pp. 379–382. ISSN: 0028-0836, 1476-4687. DOI: 10.1038/nature06949. URL: http://www.nature.com/articles/nature06949 (visited on 01/27/2022).

Malmierca-Vallet, Irene, Sime, Louise C., Valdes, Paul J., Klockmann, Marlene, Vettoretti, Guido, and Slattery, John (2024). "The Impact of CO2 and Climate State on Whether Dansgaard–Oeschger Type Oscillations Occur in Climate Models". In: DOI: 10.1029/2024GL110068. URL: https://agupubs.onlinelibrary.wiley.com/doi/10.1029/2024GL110068 (visited on 07/10/2024).

Malmierca-Vallet, Irene, Sime, Louise C., and the D–O community members (May 8, 2023). "Dansgaard–Oeschger events in climate models: review and baseline Marine Isotope Stage 3 (MIS3) protocol". In: *Climate of the Past* 19.5, pp. 915–942. ISSN: 1814-9332. DOI: 10.5194/cp-19-915-2023. URL: https://cp.copernicus.org/articles/19/915/2023/ (visited on 07/14/2023).

Mangerud, Jan (Jan. 1, 1970). "Late Weichselian Vegetation and Ice-Front Oscillations in the Bergen District, Western Norway". In: *Norsk Geografisk Tidsskrift - Norwegian Journal of Geography* 24.3. Publisher: Routledge _eprint: https://doi.org/10.1080/00291957008551900, pp. 121–148. ISSN: 0029-1951. DOI: 10.1080/00291957008551900. URL: https://doi.org/10.1080/00291957008551900 (visited on 02/21/2025).

Markle, Bradley R., Steig, Eric J., Buizert, Christo, Schoenemann, Spruce W., Bitz, Cecilia M., Fudge, T. J., Pedro, Joel B., Ding, Qinghua, Jones, Tyler R., White, James W. C., and Sowers, Todd (Jan. 2017). "Global atmospheric teleconnections during Dansgaard–Oeschger events". In: *Nature Geoscience* 10.1. Publisher: Nature Publishing Group, pp. 36–40. ISSN: 1752-0908. DOI: 10.1038/ngeo2848. URL: https://www.nature.com/articles/ngeo2848 (visited on 01/24/2025).

Martin, Kaden C., Buizert, Christo, Edwards, Jon S., Kalk, Michael L., Riddell-Young, Ben, Brook, Edward J., Beaudette, Ross, Severinghaus, Jeffrey P., and Sowers, Todd A. (May 2023). "Bipolar impact and phasing of Heinrich-type climate variability". In: *Nature* 617.7959. Number: 7959 Publisher: Nature Publishing Group, pp. 100–104. ISSN: 1476-4687. DOI: 10.1038/s41586-023-05875-2. URL: https://www.nature.com/articles/s41586-023-05875-2 (visited on 11/30/2023).

Martin, Torge, Park, Wonsun, and Latif, Mojib (Apr. 1, 2015). "Southern Ocean forcing of the North Atlantic at multi-centennial time scales in the Kiel Climate Model". In: *Deep Sea Research Part II: Topical Studies in Oceanography*. Southern Ocean Dynamics and Biogeochemistry in a Changing Climate 114, pp. 39–48. ISSN: 0967-0645. DOI: 10.1016/j.dsr2.2014.01.018. URL: https://www.sciencedirect.com/science/article/pii/S0967064514000320 (visited on 02/26/2024).

Martinson, Douglas G., Pisias, Nicklas G., Hays, James D., Imbrie, John, Jr, Theodore C. Moore, and Shackleton, Nicholas J. (Jan. 1987). "Age Dating and the Orbital Theory of the Ice Ages: Development of a High-Resolution 0 to 300,000-Year Chronostratigraphy". In: *Quaternary Research* 27.1, pp. 1–29. ISSN: 0033-5894, 1096-0287. DOI: 10.1016/0033-5894(87)90046-9. URL: https://www.cambridge.org/core/journals/quaternary-research/article/abs/%20highresolution-0-to-300000year-chronostratigraphy-1/057D5EDADC9D16A353C9E48DC3A5A5D7 (visited on 02/01/2025).

Matero, I. S. O., Gregoire, L. J., Ivanovic, R. F., Tindall, J. C., and Haywood, A. M. (Sept. 1, 2017). "The 8.2 ka cooling event caused by Laurentide ice saddle collapse". In: *Earth and Planetary Science Letters* 473, pp. 205–214. ISSN: 0012-821X. DOI: 10.1016/j.epsl.2017.06.011.

URL: https://www.sciencedirect.com/science/article/pii/S0012821X17303205 (visited on 02/26/2024).

Matero, Ilkka S. O., Gregoire, Lauren J., and Ivanovic, Ruza F. (Sept. 25, 2020). "Simulating the Early Holocene demise of the Laurentide Ice Sheet with BISICLES (public trunk revision 3298)". In: *Geoscientific Model Development* 13.9. Publisher: Copernicus GmbH, pp. 4555–4577. ISSN: 1991-959X. DOI: 10.5194/gmd-13-4555-2020. URL: https://gmd.copernicus.org/articles/13/4555/2020/ (visited on 02/14/2025).

McCarthy, Gerard, Smeed, David, Cunningham, Stuart, and Roberts, Chris (2017). "Atlantic Meridonal Overturning Circulation". In: *MCCIP Science Review 2017*. Artwork Size: 7 pages Medium: pdf Publisher: Marine Climate Change Impacts Partnership (MCCIP), Lowestoft, UK, 7 pages. DOI: 10.14465/2017.ARC10.002-ATL. URL: http://www.mccip.org.uk/impacts-report-cards/full-report-cards/2017-10-year-report-card/climate-of-the-marine-environment/atlantic-meridional-overturning-circulation-amoc/ (visited on 01/27/2022).

McManus, J. F., Francois, R., Gherardi, J.-M., Keigwin, L. D., and Brown-Leger, S. (Apr. 2004). "Collapse and rapid resumption of Atlantic meridional circulation linked to deglacial climate changes". In: *Nature* 428.6985, pp. 834–837. ISSN: 0028-0836, 1476-4687. DOI: 10.1038/nature02494. URL: http://www.nature.com/articles/nature02494 (visited on 10/07/2021).

Members, CAPE-Last Interglacial Project (July 2006). "Last Interglacial Arctic warmth confirms polar amplification of climate change". In: *Quaternary Science Reviews* 25.13, pp. 1383–1400. ISSN: 02773791. DOI: 10.1016/j.quascirev.2006.01.033. URL: https://linkinghub.elsevier.com/retrieve/pii/S0277379106000990 (visited on 01/24/2023).

Menounos, B., Goehring, B. M., Osborn, G., Margold, M., Ward, B., Bond, J., Clarke, G. K. C., Clague, J. J., Lakeman, T., Koch, J., Caffee, M. W., Gosse, J., Stroeven, A. P., Seguinot, J., and Heyman, J. (Nov. 10, 2017). "Cordilleran Ice Sheet mass loss preceded climate reversals near the Pleistocene Termination". In: *Science* 358.6364. Publisher: American Association for the Advancement of Science, pp. 781–784. DOI: 10.1126/science.aan3001. URL: https://www.science.org/doi/abs/10.1126/science.aan3001 (visited on 01/20/2025).

Menviel, L., Joos, F., and Ritz, S.P. (Nov. 2012). "Simulating atmospheric CO2, 13C and the marine carbon cycle during the Last Glacial–Interglacial cycle: possible role for a deepening of the mean remineralization depth and an increase in the oceanic nutrient inventory". In: *Quaternary Science Reviews* 56, pp. 46–68. ISSN: 02773791. DOI: 10.1016/j.quascirev.2012.09.012. URL: https://linkinghub.elsevier.com/retrieve/pii/S0277379112003496 (visited on 06/05/2023).

Menviel, L., Timmermann, A., Timm, O. Elison, and Mouchet, A. (2010). "Climate and biogeochemical response to a rapid melting of the West Antarctic Ice Sheet during interglacials and implications for future climate". In: *Paleoceanography* 25.4. _eprint: https://onlinelibrary.wiley.com/doi/pdf/1

ISSN: 1944-9186. DOI: 10.1029/2009PA001892. URL: https://onlinelibrary.wiley.com/doi/abs/10.1029/2009PA001892 (visited on 11/28/2024).

Menviel, L., Timmermann, A., Timm, O. Elison, and Mouchet, A. (May 2011). "Deconstructing the Last Glacial termination: the role of millennial and orbital-scale forcings". In: *Quaternary Science Reviews* 30.9, pp. 1155–1172. ISSN: 02773791. DOI: 10.1016/j.quascirev.2011.02.005. URL: https://linkinghub.elsevier.com/retrieve/pii/S0277379111000539 (visited on 09/09/2021).

Menviel, L., Yu, J., Joos, F., Mouchet, A., Meissner, K. J., and England, M. H. (Jan. 2017). "Poorly ventilated deep ocean at the Last Glacial Maximum inferred from carbon isotopes: A data-model comparison study". In: *Paleoceanography* 32.1, pp. 2–17. ISSN: 0883-8305, 1944-9186. DOI: 10.1002/2016PA003024. URL: https://onlinelibrary.wiley.com/doi/10.1002/2016PA003024 (visited on 06/05/2023).

Menviel, Laurie C., Skinner, Luke C., Tarasov, Lev, and Tzedakis, Polychronis C. (Nov. 3, 2020). "An ice–climate oscillatory framework for Dansgaard–Oeschger cycles". In: *Nature Reviews Earth & Environment* 1.12, pp. 677–693. ISSN: 2662-138X. DOI: 10.1038/s43017-020-00106-y. URL: https://www.nature.com/articles/s43017-020-00106-y (visited on 12/09/2022).

Merz, Niklaus, Raible, Christoph C., and Woollings, Tim (May 15, 2015). "North Atlantic Eddy-Driven Jet in Interglacial and Glacial Winter Climates". In: *Journal of Climate* 28.10, pp. 3977–3997. ISSN: 0894-8755, 1520-0442. DOI: 10.1175/JCLI-D-14-00525.1. URL: http://journals.ametsoc.org/doi/10.1175/JCLI-D-14-00525.1 (visited on 06/16/2022).

Mikolajewicz, Uwe, Kapsch, Marie-Luise, Schannwell, Clemens, Six, Katharina D., Ziemen, Florian A., Bagge, Meike, Baudouin, Jean-Philippe, Erokhina, Olga, Gayler, Veronika, Klemann, Volker, Meccia, Virna L., Mouchet, Anne, and Riddick, Thomas (Aug. 7, 2024). "Deglaciation and abrupt events in a coupled comprehensive atmosphere–ocean–ice sheet–solid earth model". In: *Climate of the Past Discussions*. Publisher: Copernicus GmbH, pp. 1–46. DOI: 10.5194/cp-2024-55. URL: https://cp.copernicus.org/preprints/cp-2024-55/ (visited on 01/09/2025).

Mix, Alan C., Bard, Edouard, and Schneider, Ralph (Feb. 1, 2001). "Environmental processes of the ice age: land, oceans, glaciers (EPILOG)". In: *Quaternary Science Reviews* 20.4. Publisher: Pergamon, pp. 627–657. ISSN: 0277-3791. DOI: 10.1016/S0277-3791(00)00145-1. URL: https://www.sciencedirect.com/science/article/pii/S0277379100001451 (visited on 09/10/2024).

Montoya, Marisa, Born, Andreas, and Levermann, Anders (Mar. 2011). "Reversed North Atlantic gyre dynamics in present and glacial climates". In: *Climate Dynamics* 36.5, pp. 1107–1118. ISSN: 0930-7575, 1432-0894. DOI: 10.1007/s00382-009-0729-y. URL: http://link.springer.com/10.1007/s00382-009-0729-y (visited on 11/18/2022).

Morrill, C., Anderson, D. M., Bauer, B. A., Buckner, R., Gille, E. P., Gross, W. S., Hartman, M., and Shah, A. (Feb. 19, 2013). "Proxy benchmarks for intercomparison of 8.2 ka simulations". In: *Climate of the Past* 9.1. Publisher: Copernicus GmbH, pp. 423–432. ISSN: 1814-9324. DOI: 10.5194/cp-9-423-2013. URL: https://cp.copernicus.org/articles/9/423/2013/ (visited on 08/15/2024).

Muglia, Juan and Schmittner, Andreas (Nov. 28, 2015). "Glacial Atlantic overturning increased by wind stress in climate models: WIND STRESS AND GLACIAL AMOC". In: *Geophysical Research Letters* 42.22, pp. 9862–9868. ISSN: 00948276. DOI: 10.1002/2015GL064583. URL: http://doi.wiley.com/10.1002/2015GL064583 (visited on 01/27/2022).

– (Apr. 2021). "Carbon isotope constraints on glacial Atlantic meridional overturning: Strength vs depth". In: *Quaternary Science Reviews* 257, p. 106844. ISSN: 02773791. DOI: 10.1016/j.quascirev.2021.106844. URL: https://linkinghub.elsevier.com/retrieve/pii/S0277379121000512 (visited on 11/18/2022).

Muntjewerf, Laura, Petrini, Michele, Vizcaino, Miren, Silva, Carolina Ernani da, Sellevold, Raymond, Scherrenberg, Meike D. W., Thayer-Calder, Katherine, Bradley, Sarah L., Lenaerts, Jan T. M., Lipscomb, William H., and Lofverstrom, Marcus (2020). "Greenland Ice Sheet Contribution to 21st Century Sea Level Rise as Simulated by the Coupled CESM2.1-CISM2.1". In: *Geophysical Research Letters* 47.9. _eprint: https://onlinelibrary.wiley.com/doi/pdf/10.1029/2019GL086836, e2019GL086836. ISSN: 1944-8007. DOI: 10.1029/2019GL086836. URL: https://onlinelibrary.wiley.com/doi/abs/10.1029/2019GL086836 (visited on 01/09/2025).

Murton, Julian B., Bateman, Mark D., Dallimore, Scott R., Teller, James T., and Yang, Zhirong (Apr. 2010). "Identification of Younger Dryas outburst flood path from Lake Agassiz to the Arctic Ocean". In: *Nature* 464.7289. Publisher: Nature Publishing Group, pp. 740–743. ISSN: 1476-4687. DOI: 10.1038/nature08954. URL: https://www.nature.com/articles/nature08954 (visited on 02/21/2025).

Ménot, Guillemette, Bard, Edouard, Rostek, Frauke, Weijers, Johan W. H., Hopmans, Ellen C., Schouten, Stefan, and Damsté, Jaap S. Sinninghe (Sept. 15, 2006). "Early Reactivation of European Rivers During the Last Deglaciation". In: *Science* 313.5793. Publisher: American Association for the Advancement of Science, pp. 1623–1625. DOI: 10.1126/science.1130511. URL: https://www.science.org/doi/10.1126/science.1130511 (visited on 02/20/2025).

Naughton, Filipa, Toucanne, Samuel, Landais, Amaelle, Rodrigues, Teresa, Riveiros, Natalia Vazquez, and Sánchez-Goñi, María F. (Jan. 1, 2023). "Chapter 5 - Heinrich Stadial 1". In: *European Glacial Landscapes*. Ed. by David Palacios, Philip D. Hughes, José M. García-Ruiz, and Nuria Andrés. Elsevier, pp. 37–44. ISBN: 978-0-323-91899-2. DOI: 10.1016/B978-0-323-91899-2.00049-8. URL: https://www.sciencedirect.com/science/article/pii/B9780323918992000498 (visited on 02/10/2025).

Nebbia, Giorgio and Menozzi, Gabriella Nebbia (Jan. 1, 1968). "Early experiments on water desalination by freezing". In: *Desalination* 5.1, pp. 49–54. ISSN: 0011-9164. DOI: 10.1016/

S0011-9164(00)80191-5. URL: https://www.sciencedirect.com/science/article/pii/S0011916400801915 (visited on 01/24/2025).

Ng, Hong Chin, Robinson, Laura F., McManus, Jerry F., Mohamed, Kais J., Jacobel, Allison W., Ivanovic, Ruza F., Gregoire, Lauren J., and Chen, Tianyu (Dec. 2018). "Coherent deglacial changes in western Atlantic Ocean circulation". In: *Nature Communications* 9.1, p. 2947. ISSN: 2041-1723. DOI: 10.1038/s41467-018-05312-3. URL: http://www.nature.com/articles/s41467-018-05312-3 (visited on 01/28/2022).

Nias, I. J., Cornford, S. L., and Payne, A. J. (2018). "New Mass-Conserving Bedrock Topography for Pine Island Glacier Impacts Simulated Decadal Rates of Mass Loss". In: *Geophysical Research Letters* 45.7. _eprint: https://onlinelibrary.wiley.com/doi/pdf/10.1002/2017GL076493, pp. 3173–3181. ISSN: 1944-8007. DOI: 10.1002/2017GL076493. URL: https://onlinelibrary.wiley.com/doi/abs/10.1002/2017GL076493 (visited on 02/14/2025).

Niu, Lu, Lohmann, Gerrit, Hinck, Sebastian, Gowan, Evan J., and Krebs-Kanzow, Uta (Aug. 2019). "The sensitivity of Northern Hemisphere ice sheets to atmospheric forcing during the last glacial cycle using PMIP3 models". In: *Journal of Glaciology* 65.252, pp. 645–661. ISSN: 0022-1430, 1727-5652. DOI: 10.1017/jog.2019.42. URL: https://www.cambridge.org/core/journals/journal-of-glaciology/article/sensitivity-of-northern-hemisphere-ice-sheets-to-atmospheric-forcing-during-the-last-glacial-cycle-using-pmip3-models/37419685605BAD5D63851ACFEFF8BB4E (visited on 02/21/2025).

North Greenland Ice Core Project members (Sept. 2004). "High-resolution record of Northern Hemisphere climate extending into the last interglacial period". In: *Nature* 431.7005, pp. 147–151. ISSN: 0028-0836, 1476-4687. DOI: 10.1038/nature02805. URL: http://www.nature.com/articles/nature02805 (visited on 02/01/2022).

Nowicki, Sophie M. J., Payne, Anthony, Larour, Eric, Seroussi, Helene, Goelzer, Heiko, Lipscomb, William, Gregory, Jonathan, Abe-Ouchi, Ayako, and Shepherd, Andrew (Dec. 21, 2016). "Ice Sheet Model Intercomparison Project (ISMIP6) contribution to CMIP6". In: *Geoscientific Model Development* 9.12. Publisher: Copernicus GmbH, pp. 4521–4545. ISSN: 1991-959X. DOI: 10.5194/gmd-9-4521-2016. URL: https://gmd.copernicus.org/articles/9/4521/2016/ (visited on 02/13/2025).

Nürnberg, Dirk, Bijma, Jelle, and Hemleben, Christoph (Mar. 1, 1996). "Assessing the reliability of magnesium in foraminiferal calcite as a proxy for water mass temperatures". In: *Geochimica et Cosmochimica Acta* 60.5, pp. 803–814. ISSN: 0016-7037. DOI: 10.1016/0016-7037(95)00446-7. URL: https://www.sciencedirect.com/science/article/pii/0016703795004467 (visited on 01/29/2025).

Obase, Takashi, Abe-Ouchi, Ayako, and Saito, Fuyuki (Nov. 25, 2021). "Abrupt climate changes in the last two deglaciations simulated with different Northern ice sheet discharge and insolation". In: *Scientific Reports* 11.1. Number: 1 Publisher: Nature Publishing Group, pp. 1–11.

ISSN: 2045-2322. DOI: 10.1038/s41598-021-01651-2. URL: https://www.nature.com/articles/s41598-021-01651-2 (visited on 01/22/2024).

Obase, Takashi and Abe-Ouchi, Ayako (Oct. 28, 2019). "Abrupt Bølling-Allerød Warming Simulated under Gradual Forcing of the Last Deglaciation". In: *Geophysical Research Letters* 46.20, pp. 11397–11405. ISSN: 0094-8276, 1944-8007. DOI: 10.1029/2019GL084675. URL: https://onlinelibrary.wiley.com/doi/10.1029/2019GL084675 (visited on 09/02/2021).

Oka, A., Hasumi, H., and Abe-Ouchi, A. (May 2012). "The thermal threshold of the Atlantic meridional overturning circulation and its control by wind stress forcing during glacial climate: THE THERMAL THRESHOLD OF THE AMOC". In: *Geophysical Research Letters* 39.9, n/a–n/a. ISSN: 00948276. DOI: 10.1029/2012GL051421. URL: http://doi.wiley.com/10.1029/2012GL051421 (visited on 01/27/2022).

Otto-Bliesner, Bette L. and Brady, Esther C. (Jan. 2010). "The sensitivity of the climate response to the magnitude and location of freshwater forcing: last glacial maximum experiments". In: *Quaternary Science Reviews* 29.1, pp. 56–73. ISSN: 02773791. DOI: 10.1016/j.quascirev.2009.07.004. URL: https://linkinghub.elsevier.com/retrieve/pii/S0277379109002340 (visited on 01/06/2023).

Paillard, D. and Labeyriet, L. (Nov. 1994). "Role of the thermohaline circulation in the abrupt warming after Heinrich events". In: *Nature* 372.6502. Publisher: Nature Publishing Group, pp. 162–164. ISSN: 1476-4687. DOI: 10.1038/372162a0. URL: https://www.nature.com/articles/372162a0 (visited on 01/28/2025).

Park, Hyo-Seok, Kim, Seong-Joong, Stewart, Andrew L., Son, Seok-Woo, and Seo, Kyong-Hwan (Dec. 6, 2019). "Mid-Holocene Northern Hemisphere warming driven by Arctic amplification". In: *Science Advances* 5.12, eaax8203. ISSN: 2375-2548. DOI: 10.1126/sciadv.aax8203. URL: https://www.science.org/doi/10.1126/sciadv.aax8203 (visited on 01/24/2023).

Patterson, Violet L., Gregoire, Lauren J., Ivanovic, Ruza F., Gandy, Niall, Cornford, Stephen, Owen, Jonathan, Sherriff-Tadano, Sam, and Smith, Robin S. (Feb. 14, 2025). "Exploring the sensitivity of the Northern Hemisphere ice sheets at the last two glacial maxima to coupled climate-ice sheet model parameters". In: *EGUsphere*. Publisher: Copernicus GmbH, pp. 1–59. DOI: 10.5194/egusphere-2024-3896. URL: https://egusphere.copernicus.org/preprints/2025/egusphere-2024-3896/ (visited on 02/27/2025).

Patterson, Violet L., Gregoire, Lauren J., Ivanovic, Ruza F., Gandy, Niall, Owen, Jonathan, Smith, Robin S., Pollard, Oliver G., Astfalck, Lachlan C., and Valdes, Paul J. (Oct. 2, 2024). "Contrasting the Penultimate Glacial Maximum and the Last Glacial Maximum (140 and 21 ka) using coupled climate–ice sheet modelling". In: *Climate of the Past* 20.10. Publisher: Copernicus GmbH, pp. 2191–2218. ISSN: 1814-9324. DOI: 10.5194/cp-20-2191-2024. URL: https://cp.copernicus.org/articles/20/2191/2024/ (visited on 10/17/2024).

Patton, Henry, Hubbard, Alun, Andreassen, Karin, Winsborrow, Monica, and Stroeven, Arjen P. (Dec. 1, 2016). "The build-up, configuration, and dynamical sensitivity of the Eurasian ice-sheet complex to Late Weichselian climatic and oceanic forcing". In: *Quaternary Science Reviews* 153, pp. 97–121. ISSN: 0277-3791. DOI: 10.1016/j.quascirev.2016.10.009. URL: https://www.sciencedirect.com/science/article/pii/S0277379116304498 (visited on 02/12/2025).

Pattyn, F., Schoof, C., Perichon, L., Hindmarsh, R. C. A., Bueler, E., Fleurian, B. de, Durand, G., Gagliardini, O., Gladstone, R., Goldberg, D., Gudmundsson, G. H., Huybrechts, P., Lee, V., Nick, F. M., Payne, A. J., Pollard, D., Rybak, O., Saito, F., and Vieli, A. (May 30, 2012). "Results of the Marine Ice Sheet Model Intercomparison Project, MISMIP". In: *The Cryosphere* 6.3. Publisher: Copernicus GmbH, pp. 573–588. ISSN: 1994-0416. DOI: 10.5194/tc-6-573-2012. URL: https://tc.copernicus.org/articles/6/573/2012/ (visited on 01/30/2025).

Pedro, J. B., Andersson, C., Vettoretti, G., Voelker, A. H. L., Waelbroeck, C., Dokken, T. M., Jensen, M. F., Rasmussen, S. O., Sessford, E. G., Jochum, M., and Nisancioglu, K. H. (Aug. 1, 2022). "Dansgaard-Oeschger and Heinrich event temperature anomalies in the North Atlantic set by sea ice, frontal position and thermocline structure". In: *Quaternary Science Reviews* 289, p. 107599. ISSN: 0277-3791. DOI: 10.1016/j.quascirev.2022.107599. URL: https://www.sciencedirect.com/science/article/pii/S027737912200230X (visited on 02/20/2025).

Pedro, Joel B., Bostock, Helen C., Bitz, Cecilia M., He, Feng, Vandergoes, Marcus J., Steig, Eric J., Chase, Brian M., Krause, Claire E., Rasmussen, Sune O., Markle, Bradley R., and Cortese, Giuseppe (Jan. 2016). "The spatial extent and dynamics of the Antarctic Cold Reversal". In: *Nature Geoscience* 9.1. Publisher: Nature Publishing Group, pp. 51–55. ISSN: 1752-0908. DOI: 10.1038/ngeo2580. URL: https://www.nature.com/articles/ngeo2580 (visited on 01/24/2025).

Pelt, Ward J. J. Van and Oerlemans, Johannes (Jan. 2012). "Numerical simulations of cyclic behaviour in the Parallel Ice Sheet Model (PISM)". In: *Journal of Glaciology* 58.208, pp. 347–360. ISSN: 0022-1430, 1727-5652. DOI: 10.3189/2012JoG11J217. URL: https://www.cambridge.org/core/journals/journal-of-glaciology/article/numerical-simulations-of-cyclic-behaviour-in-the-parallel-ice-sheet-model-pism/B74F3BEC1FE836E5D69C49ADF4E539AF (visited on 02/14/2025).

Peltier, W. R., Argus, D. F., and Drummond, R. (Jan. 2015). "Space geodesy constrains ice age terminal deglaciation: The global ICE-6G_C (VM5a) model: Global Glacial Isostatic Adjustment". In: *Journal of Geophysical Research: Solid Earth* 120.1, pp. 450–487. ISSN: 21699313. DOI: 10.1002/2014JB011176. URL: http://doi.wiley.com/10.1002/2014JB011176 (visited on 01/27/2022).

Peltier, W. Richard and Vettoretti, Guido (Oct. 28, 2014). "Dansgaard-Oeschger oscillations predicted in a comprehensive model of glacial climate: A "kicked" salt oscillator in the Atlantic: Dansgaard-Oeschger Oscillations". In: *Geophysical Research Letters* 41.20, pp. 7306–7313. ISSN: 00948276. DOI: 10.1002/2014GL061413. URL: http://doi.wiley.com/10.1002/2014GL061413 (visited on 09/09/2021).

Peltier, W.R. (May 19, 2004). "GLOBAL GLACIAL ISOSTASY AND THE SURFACE OF THE ICE-AGE EARTH: The ICE-5G (VM2) Model and GRACE". In: *Annual Review of Earth and Planetary Sciences* 32.1, pp. 111–149. ISSN: 0084-6597, 1545-4495. DOI: 10.1146/annurev.earth.32.082503.144359. URL: https://www.annualreviews.org/doi/10.1146/annurev.earth.32.082503.144359 (visited on 01/27/2022).

– (Aug. 2005). "On the hemispheric origins of meltwater pulse 1a". In: *Quaternary Science Reviews* 24.14, pp. 1655–1671. ISSN: 02773791. DOI: 10.1016/j.quascirev.2004.06.023. URL: https://linkinghub.elsevier.com/retrieve/pii/S0277379105000788 (visited on 07/12/2022).

Peltier, W.R. and Fairbanks, R.G. (Dec. 2006). "Global glacial ice volume and Last Glacial Maximum duration from an extended Barbados sea level record". In: *Quaternary Science Reviews* 25.23, pp. 3322–3337. ISSN: 02773791. DOI: 10.1016/j.quascirev.2006.04.010. URL: https://linkinghub.elsevier.com/retrieve/pii/S0277379106001788 (visited on 09/10/2024).

Pelto, Ben M. and Menounos, Brian (July 19, 2021). "Surface Mass-Balance Gradients From Elevation and Ice Flux Data in the Columbia Basin, Canada". In: *Frontiers in Earth Science* 9. Publisher: Frontiers. ISSN: 2296-6463. DOI: 10.3389/feart.2021.675681. URL: https://www.frontiersin.org/journals/earth-science/articles/10.3389/feart.2021.675681/full (visited on 02/21/2025).

Petit, Tillys, Lozier, M. Susan, Josey, Simon A., and Cunningham, Stuart A. (2020). "Atlantic Deep Water Formation Occurs Primarily in the Iceland Basin and Irminger Sea by Local Buoyancy Forcing". In: *Geophysical Research Letters* 47.22, e2020GL091028. ISSN: 1944-8007. DOI: 10.1029/2020GL091028. URL: https://onlinelibrary.wiley.com/doi/abs/10.1029/2020GL091028 (visited on 07/28/2025).

Petrini, Michele, Colleoni, Florence, Kirchner, Nina, Hughes, Anna L. C., Camerlenghi, Angelo, Rebesco, Michele, Lucchi, Renata G., Forte, Emanuele, Colucci, Renato R., and Noormets, Riko (May 8, 2018). "Interplay of grounding-line dynamics and sub-shelf melting during retreat of the Bjørnøyrenna Ice Stream". In: *Scientific Reports* 8.1. Publisher: Nature Publishing Group, p. 7196. ISSN: 2045-2322. DOI: 10.1038/s41598-018-25664-6. URL: https://www.nature.com/articles/s41598-018-25664-6 (visited on 01/21/2025).

Petrini, Michele, Colleoni, Florence, Kirchner, Nina, Hughes, Anna L. C., Camerlenghi, Angelo, Rebesco, Michele, Lucchi, Renata G., Forte, Emanuele, Colucci, Renato R., Noormets, Riko, and Mangerud, Jan (June 15, 2020). "Simulated last deglaciation of the Barents Sea Ice Sheet

primarily driven by oceanic conditions". In: *Quaternary Science Reviews* 238, p. 106314. ISSN: 0277-3791. DOI: 10.1016/j.quascirev.2020.106314. URL: https://www.sciencedirect.com/science/article/pii/S0277379120302766 (visited on 02/05/2025).

Pickart, Robert S. and Spall, Michael A. (Sept. 1, 2007). "Impact of Labrador Sea Convection on the North Atlantic Meridional Overturning Circulation". In: Section: Journal of Physical Oceanography. DOI: 10.1175/JPO3178.1. URL: https://journals.ametsoc.org/view/journals/phoc/37/9/jpo3178.1.xml (visited on 01/27/2025).

Pollard, D. and DeConto, R. M. (Oct. 17, 2012). "Description of a hybrid ice sheet-shelf model, and application to Antarctica". In: *Geoscientific Model Development* 5.5. Publisher: Copernicus GmbH, pp. 1273–1295. ISSN: 1991-959X. DOI: 10.5194/gmd-5-1273-2012. URL: https://gmd.copernicus.org/articles/5/1273/2012/ (visited on 02/14/2025).

Pollard, Oliver G., Barlow, Natasha L. M., Gregoire, Lauren J., Gomez, Natalya, Cartelle, Víctor, Ely, Jeremy C., and Astfalck, Lachlan C. (Nov. 10, 2023). "Quantifying the uncertainty in the Eurasian ice-sheet geometry at the Penultimate Glacial Maximum (Marine Isotope Stage 6)". In: *The Cryosphere* 17.11. Publisher: Copernicus GmbH, pp. 4751–4777. ISSN: 1994-0416. DOI: 10.5194/tc-17-4751-2023. URL: https://tc.copernicus.org/articles/17/4751/2023/ (visited on 02/21/2025).

Pope, V. D., Gallani, M. L., Rowntree, P. R., and Stratton, R. A. (Feb. 4, 2000). "The impact of new physical parametrizations in the Hadley Centre climate model: HadAM3". In: *Climate Dynamics* 16.2, pp. 123–146. ISSN: 0930-7575, 1432-0894. DOI: 10.1007/s003820050009. URL: http://link.springer.com/10.1007/s003820050009 (visited on 01/27/2022).

Pöppelmeier, Frerk, Baggenstos, Daniel, Grimmer, Markus, Liu, Zhijun, Schmitt, Jochen, Fischer, Hubertus, and Stocker, Thomas F. (Mar. 28, 2023a). "The Effect of Past Saturation Changes on Noble Gas Reconstructions of Mean Ocean Temperature". In: *Geophysical Research Letters* 50.6, e2022GL102055. ISSN: 0094-8276, 1944-8007. DOI: 10.1029/2022GL102055. URL: https://agupubs.onlinelibrary.wiley.com/doi/10.1029/2022GL102055 (visited on 05/03/2023).

Pöppelmeier, Frerk, Jeltsch-Thömmes, Aurich, Lippold, Jörg, Joos, Fortunat, and Stocker, Thomas F. (Apr. 2023b). "Multi-proxy constraints on Atlantic circulation dynamics since the last ice age". In: *Nature Geoscience* 16.4, pp. 349–356. ISSN: 1752-0894, 1752-0908. DOI: 10.1038/s41561-023-01140-3. URL: https://www.nature.com/articles/s41561-023-01140-3 (visited on 05/31/2023).

Quiquet, Aurélien, Dumas, Christophe, Paillard, Didier, Ramstein, Gilles, Ritz, Catherine, and Roche, Didier M. (2021a). "Deglacial Ice Sheet Instabilities Induced by Proglacial Lakes". In: *Geophysical Research Letters* 48.9. _eprint: https://onlinelibrary.wiley.com/doi/pdf/10.1029/2020GL092141, e2020GL092141. ISSN: 1944-8007. DOI: 10.1029/2020GL092141. URL: https://onlinelibrary.wiley.com/doi/abs/10.1029/2020GL092141 (visited on 02/05/2025).

Quiquet, Aurélien and Roche, Didier M. (June 25, 2024). "Investigating similarities and differences of the penultimate and last glacial terminations with a coupled ice sheet–climate model". In: *Climate of the Past* 20.6. Publisher: Copernicus GmbH, pp. 1365–1385. ISSN: 1814-9324. DOI: 10.5194/cp-20-1365-2024. URL: https://cp.copernicus.org/articles/20/1365/2024/ (visited on 01/09/2025).

Quiquet, Aurélien, Roche, Didier M., Dumas, Christophe, Bouttes, Nathaëlle, and Lhardy, Fanny (Oct. 19, 2021b). "Climate and ice sheet evolutions from the last glacial maximum to the pre-industrial period with an ice-sheet–climate coupled model". In: *Climate of the Past* 17.5. Publisher: Copernicus GmbH, pp. 2179–2199. ISSN: 1814-9324. DOI: 10.5194/cp-17-2179-2021. URL: https://cp.copernicus.org/articles/17/2179/2021/ (visited on 12/05/2024).

Rahmstorf, S. (Nov. 1, 1996). "On the freshwater forcing and transport of the Atlantic thermohaline circulation". In: *Climate Dynamics* 12.12, pp. 799–811. ISSN: 1432-0894. DOI: 10.1007/s003820050144. URL: https://doi.org/10.1007/s003820050144 (visited on 01/27/2025).

Rahmstorf, Stefan (1999). "Decadal Variability of the Thermohaline Ocean Circulation". In: *Beyond El Niño*. Ed. by Antonio Navarra. Berlin, Heidelberg: Springer Berlin Heidelberg, pp. 309–331. ISBN: 978-3-642-63556-4 978-3-642-58369-8. DOI: 10.1007/978-3-642-58369-8_15. URL: http://link.springer.com/10.1007/978-3-642-58369-8_15 (visited on 02/14/2022).

– (2000). "The Thermohaline Ocean Circulation: A System with Dangerous Thresholds?found]". In: *Climatic Change* 46.3, pp. 247–256. ISSN: 01650009. DOI: 10.1023/A:1005648404783. URL: http://link.springer.com/10.1023/A:1005648404783 (visited on 08/06/2024).

– (Sept. 2002). "Ocean circulation and climate during the past 120,000 years". In: *Nature* 419.6903, pp. 207–214. ISSN: 0028-0836, 1476-4687. DOI: 10.1038/nature01090. URL: https://www.nature.com/articles/nature01090 (visited on 06/19/2023).

Rasmussen, Sune O., Bigler, Matthias, Blockley, Simon P., Blunier, Thomas, Buchardt, Susanne L., Clausen, Henrik B., Cvijanovic, Ivana, Dahl-Jensen, Dorthe, Johnsen, Sigfus J., Fischer, Hubertus, Gkinis, Vasileios, Guillevic, Myriam, Hoek, Wim Z., Lowe, J. John, Pedro, Joel B., Popp, Trevor, Seierstad, Inger K., Steffensen, Jørgen Peder, Svensson, Anders M., Vallelonga, Paul, Vinther, Bo M., Walker, Mike J.C., Wheatley, Joe J., and Winstrup, Mai (Dec. 2014). "A stratigraphic framework for abrupt climatic changes during the Last Glacial period based on three synchronized Greenland ice-core records: refining and extending the INTIMATE event stratigraphy". In: *Quaternary Science Reviews* 106, pp. 14–28. ISSN: 02773791. DOI: 10.1016/j.quascirev.2014.09.007. URL: https://linkinghub.elsevier.com/retrieve/pii/S0277379114003485 (visited on 01/27/2022).

Repschläger, Janne, Zhao, Ning, Rand, Devin, Lisiecki, Lorraine, Muglia, Juan, Mulitza, Stefan, Schmittner, Andreas, Cartapanis, Olivier, Bauch, Henning A., Schiebel, Ralf, and Haug, Gerald H. (Oct. 2021). "Active North Atlantic deepwater formation during Heinrich Sta-

dial 1". In: *Quaternary Science Reviews* 270, p. 107145. ISSN: 02773791. DOI: 10.1016/j.quascirev.2021.107145. URL: https://linkinghub.elsevier.com/retrieve/pii/S0277379121003528 (visited on 09/13/2021).

Reyes, Alberto V., Carlson, Anders E., Clark, Jorie, Guillaume, Louise, Milne, Glenn A., Tarasov, Lev, Carlson, Elizabeth C. B., He, Feng, Caffee, Marc W., Wilcken, Klaus M., and Rood, Dylan H. (Mar. 15, 2024). "Timing of Cordilleran-Laurentide ice-sheet separation: Implications for sea-level rise". In: *Quaternary Science Reviews* 328, p. 108554. ISSN: 0277-3791. DOI: 10.1016/j.quascirev.2024.108554. URL: https://www.sciencedirect.com/science/article/pii/S0277379124000556 (visited on 03/05/2024).

Rial, J. A. and Yang, M. (2007). "Is the Frequency of Abrupt Climate Change Modulated by The Orbital Insolation?" In: *Ocean Circulation: Mechanisms and Impacts—Past and Future Changes of Meridional Overturning.* _eprint: https://onlinelibrary.wiley.com/doi/pdf/10.1029/173GM12. American Geophysical Union (AGU), pp. 167–174. ISBN: 978-1-118-66624-1. DOI: 10.1029/173GM12. URL: https://onlinelibrary.wiley.com/doi/abs/10.1029/173GM12 (visited on 02/05/2025).

Riddick, Thomas, Brovkin, Victor, Hagemann, Stefan, and Mikolajewicz, Uwe (Oct. 19, 2018). "Dynamic hydrological discharge modelling for coupled climate model simulations of the last glacial cycle: the MPI-DynamicHD model version 3.0". In: *Geoscientific Model Development* 11.10, pp. 4291–4316. ISSN: 1991-9603. DOI: 10.5194/gmd-11-4291-2018. URL: https://gmd.copernicus.org/articles/11/4291/2018/ (visited on 06/19/2023).

Ridley, J. K., Huybrechts, P., Gregory, J. M., and Lowe, J. A. (Sept. 1, 2005). "Elimination of the Greenland Ice Sheet in a High CO2 Climate". In: Section: Journal of Climate. DOI: 10.1175/JCLI3482.1. URL: https://journals.ametsoc.org/view/journals/clim/18/17/jcli3482.1.xml (visited on 01/09/2025).

Roberts, Natalie L., Piotrowski, Alexander M., McManus, Jerry F., and Keigwin, Lloyd D. (Jan. 2010). "Synchronous Deglacial Overturning and Water Mass Source Changes". In: *Science* 327.5961, pp. 75–78. ISSN: 0036-8075, 1095-9203. DOI: 10.1126/science.1178068. URL: https://www.science.org/doi/10.1126/science.1178068 (visited on 05/26/2022).

Roberts, William H. G. and Valdes, Paul J. (May 15, 2017). "Green Mountains and White Plains: The Effect of Northern Hemisphere Ice Sheets on the Global Energy Budget". In: *Journal of Climate* 30.10, pp. 3887–3905. ISSN: 0894-8755, 1520-0442. DOI: 10.1175/JCLI-D-15-0846.1. URL: http://journals.ametsoc.org/doi/10.1175/JCLI-D-15-0846.1 (visited on 06/16/2022).

Roberts, William H. G., Valdes, Paul J., and Payne, Antony J. (Jan. 15, 2014). "A new constraint on the size of Heinrich Events from an iceberg/sediment model". In: *Earth and Planetary Science Letters* 386, pp. 1–9. ISSN: 0012-821X. DOI: 10.1016/j.epsl.2013.10.020. URL: https://www.sciencedirect.com/science/article/pii/S0012821X13005839 (visited on 02/21/2025).

Roche, D. M., Dumas, C., Bügelmayer, M., Charbit, S., and Ritz, C. (July 10, 2014). "Adding a dynamical cryosphere to *i*LOVECLIM (version 1.0): coupling with the GRISLI ice-sheet model". In: *Geoscientific Model Development* 7.4. Publisher: Copernicus GmbH, pp. 1377–1394. ISSN: 1991-959X. DOI: 10.5194/gmd-7-1377-2014. URL: https://gmd.copernicus.org/articles/7/1377/2014/ (visited on 10/17/2024).

Roche, D. M., Renssen, H., Paillard, D., and Levavasseur, G. (2011). "Deciphering the spatio-temporal complexity of climate change of the last deglaciation: a model analysis". In: *Climate of the Past* 7.2, pp. 591–602. DOI: 10.5194/cp-7-591-2011. URL: https://cp.copernicus.org/articles/7/591/2011/.

Roche, Didier M., Renssen, Hans, Weber, Susanne L., and Goosse, Hugues (Dec. 29, 2007). "Could meltwater pulses have been sneaked unnoticed into the deep ocean during the last glacial?" In: *Geophysical Research Letters* 34.24, p. L24708. ISSN: 0094-8276. DOI: 10.1029/2007GL032064. URL: http://doi.wiley.com/10.1029/2007GL032064 (visited on 01/06/2023).

Roche, Didier M., Wiersma, Ane P., and Renssen, Hans (June 2010). "A systematic study of the impact of freshwater pulses with respect to different geographical locations". In: *Climate Dynamics* 34.7, pp. 997–1013. ISSN: 0930-7575, 1432-0894. DOI: 10.1007/s00382-009-0578-8. URL: http://link.springer.com/10.1007/s00382-009-0578-8 (visited on 01/06/2023).

Romé, Yvan M., Ivanovic, Ruza F., Gregoire, Lauren J., Sherriff-Tadano, Sam, and Valdes, Paul J. (Oct. 2022). "Millennial-Scale Climate Oscillations Triggered by Deglacial Meltwater Discharge in Last Glacial Maximum Simulations". In: *Paleoceanography and Paleoclimatology* 37.10. ISSN: 2572-4517, 2572-4525. DOI: 10.1029/2022PA004451. URL: https://onlinelibrary.wiley.com/doi/10.1029/2022PA004451 (visited on 01/06/2023).

Romé, Yvan M., Ivanovic, Ruza F., Gregoire, Lauren J., Swingedouw, Didier, Sherriff-Tadano, Sam, and Börner, Reyk (Mar. 7, 2025). "Simulated millennial-scale climate variability driven by a convection–advection oscillator". In: *Climate Dynamics* 63.3, p. 150. ISSN: 1432-0894. DOI: 10.1007/s00382-025-07630-x. URL: https://doi.org/10.1007/s00382-025-07630-x (visited on 05/21/2025).

Romé, Yvan Malo, Ivanovic, Ruza F., Gregoire, Lauren J., Swingedouw, Didier, Sherriff-Tadano, Sam, and Börner, Reyk (Oct. 10, 2024). *Simulated millennial-scale climate variability driven by a convection-advection oscillator*. ISSN: 2693-5015. DOI: 10.21203/rs.3.rs-5045536/v1. URL: https://www.researchsquare.com/article/rs-5045536/v1 (visited on 12/10/2024).

Romé, Yvan (Jan. 2024). "Abrupt climate changes during the last ice age: a study of millennial-scale variability in climate simulations". PhD thesis. University of Leeds. URL: https://etheses.whiterose.ac.uk/34761/ (visited on 08/14/2024).

Rousseau, Denis-Didier, Boers, Niklas, Sima, Adriana, Svensson, Anders, Bigler, Matthias, Lagroix, France, Taylor, Samuel, and Antoine, Pierre (Aug. 1, 2017). "(MIS3 & 2) millennial oscillations in Greenland dust and Eurasian aeolian records – A paleosol perspec-

tive". In: *Quaternary Science Reviews* 169, pp. 99–113. ISSN: 0277-3791. DOI: 10.1016/j.quascirev.2017.05.020. URL: https://www.sciencedirect.com/science/article/pii/S0277379116304115 (visited on 02/23/2024).

Roy, Keven and Peltier, W.R. (Mar. 2018). "Relative sea level in the Western Mediterranean basin: A regional test of the ICE-7G_NA (VM7) model and a constraint on late Holocene Antarctic deglaciation". In: *Quaternary Science Reviews* 183, pp. 76–87. ISSN: 02773791. DOI: 10.1016/j.quascirev.2017.12.021. URL: https://linkinghub.elsevier.com/retrieve/pii/S027737911730642X (visited on 06/07/2023).

Ruddiman, William F. (Dec. 1, 1977). "Late Quaternary deposition of ice-rafted sand in the subpolar North Atlantic (lat 40° to 65°N)". In: *GSA Bulletin* 88.12, pp. 1813–1827. ISSN: 0016-7606. DOI: 10.1130/0016-7606(1977)88<1813:LQDOIS>2.0.CO;2. URL: https://doi.org/10.1130/0016-7606(1977)88<1813:LQDOIS>2.0.CO;2 (visited on 01/28/2025).

Sanchez Goñi, Maria Fernanda and Harrison, Sandy P. (Oct. 1, 2010). "Millennial-scale climate variability and vegetation changes during the Last Glacial: Concepts and terminology". In: *Quaternary Science Reviews*. Vegetation Response to Millennial-scale Variability during the Last Glacial 29.21, pp. 2823–2827. ISSN: 0277-3791. DOI: 10.1016/j.quascirev.2009.11.014. URL: https://www.sciencedirect.com/science/article/pii/S0277379109003874 (visited on 02/23/2024).

Schilt, Adrian, Baumgartner, Matthias, Schwander, Jakob, Buiron, Daphné, Capron, Emilie, Chappellaz, Jérôme, Loulergue, Laetitia, Schüpbach, Simon, Spahni, Renato, Fischer, Hubertus, and Stocker, Thomas F. (Nov. 2010). "Atmospheric nitrous oxide during the last 140,000years". In: *Earth and Planetary Science Letters* 300.1, pp. 33–43. ISSN: 0012821X. DOI: 10.1016/j.epsl.2010.09.027. URL: https://linkinghub.elsevier.com/retrieve/pii/S0012821X10006023 (visited on 01/27/2022).

Schmidt, G. A., Jungclaus, J. H., Ammann, C. M., Bard, E., Braconnot, P., Crowley, T. J., Delaygue, G., Joos, F., Krivova, N. A., Muscheler, R., Otto-Bliesner, B. L., Pongratz, J., Shindell, D. T., Solanki, S. K., Steinhilber, F., and Vieira, L. E. A. (Jan. 30, 2012). "Climate forcing reconstructions for use in PMIP simulations of the Last Millennium (v1.1)". In: *Geoscientific Model Development* 5.1, pp. 185–191. ISSN: 1991-9603. DOI: 10.5194/gmd-5-185-2012. URL: https://gmd.copernicus.org/articles/5/185/2012/ (visited on 01/06/2023).

Schmittner, A. and Lund, D. C. (July 9, 2014). *Carbon isotopes support Atlantic meridional overturning circulation decline as a trigger for early deglacial CO₂ rise*. preprint. Ocean Dynamics/Marine Archives/Millenial/D-O. DOI: 10.5194/cpd-10-2857-2014. URL: https://cp.copernicus.org/preprints/10/2857/2014/cpd-10-2857-2014.pdf (visited on 01/28/2022).

– (Feb. 5, 2015). "Early deglacial Atlantic overturning decline and its role in atmospheric CO₂ rise inferred from carbon isotopes (¹³C)".

In: *Climate of the Past* 11.2, pp. 135–152. ISSN: 1814-9332. DOI: 10.5194/cp-11-135-2015. URL: https://cp.copernicus.org/articles/11/135/2015/ (visited on 03/26/2024).

Schneider, Stephen H. and Dickinson, Robert E. (1974). "Climate modeling". In: *Reviews of Geophysics* 12.3. _eprint: https://onlinelibrary.wiley.com/doi/pdf/10.1029/RG012i003p00447, pp. 447–493. ISSN: 1944-9208. DOI: 10.1029/RG012i003p00447. URL: https://onlinelibrary.wiley.com/doi/abs/10.1029/RG012i003p00447 (visited on 01/23/2025).

Schoof, Christian (June 2006). "A variational approach to ice stream flow". In: *Journal of Fluid Mechanics* 556, pp. 227–251. ISSN: 1469-7645, 0022-1120. DOI: 10.1017/S0022112006009591. URL: https://www.cambridge.org/core/journals/journal-of-fluid-mechanics/article/abs/variational-approach-to-ice-stream-flow/BB9932ED80D7056388F07C311D6201D9 (visited on 02/14/2025).

Schoof, Christian and Hindmarsh, Richard C. A. (Feb. 1, 2010). "Thin-Film Flows with Wall Slip: An Asymptotic Analysis of Higher Order Glacier Flow Models". In: *The Quarterly Journal of Mechanics and Applied Mathematics* 63.1, pp. 73–114. ISSN: 0033-5614. DOI: 10.1093/qjmam/hbp025. URL: https://doi.org/10.1093/qjmam/hbp025 (visited on 10/17/2024).

Schulz, Michael (2002). "On the 1470-year pacing of Dansgaard-Oeschger warm events". In: *Paleoceanography* 17.2. _eprint: https://onlinelibrary.wiley.com/doi/pdf/10.1029/2000PA000571, pp. 4–1–4–9. ISSN: 1944-9186. DOI: 10.1029/2000PA000571. URL: https://onlinelibrary.wiley.com/doi/abs/10.1029/2000PA000571 (visited on 08/06/2024).

Seroussi, Hélène, Nowicki, Sophie, Payne, Antony J., Goelzer, Heiko, Lipscomb, William H., Abe-Ouchi, Ayako, Agosta, Cécile, Albrecht, Torsten, Asay-Davis, Xylar, Barthel, Alice, Calov, Reinhard, Cullather, Richard, Dumas, Christophe, Galton-Fenzi, Benjamin K., Gladstone, Rupert, Golledge, Nicholas R., Gregory, Jonathan M., Greve, Ralf, Hattermann, Tore, Hoffman, Matthew J., Humbert, Angelika, Huybrechts, Philippe, Jourdain, Nicolas C., Kleiner, Thomas, Larour, Eric, Leguy, Gunter R., Lowry, Daniel P., Little, Chistopher M., Morlighem, Mathieu, Pattyn, Frank, Pelle, Tyler, Price, Stephen F., Quiquet, Aurélien, Reese, Ronja, Schlegel, Nicole-Jeanne, Shepherd, Andrew, Simon, Erika, Smith, Robin S., Straneo, Fiammetta, Sun, Sainan, Trusel, Luke D., Van Breedam, Jonas, Wal, Roderik S. W. van de, Winkelmann, Ricarda, Zhao, Chen, Zhang, Tong, and Zwinger, Thomas (Sept. 17, 2020). "ISMIP6 Antarctica: a multi-model ensemble of the Antarctic ice sheet evolution over the 21st century". In: *The Cryosphere* 14.9. Publisher: Copernicus GmbH, pp. 3033–3070. ISSN: 1994-0416. DOI: 10.5194/tc-14-3033-2020. URL: https://tc.copernicus.org/articles/14/3033/2020/ (visited on 02/13/2025).

Severinghaus, Jeffrey P. and Brook, Edward J. (Oct. 29, 1999). "Abrupt Climate Change at the End of the Last Glacial Period Inferred from Trapped Air in Polar Ice". In: *Science* 286.5441, pp. 930–934. ISSN: 0036-8075, 1095-9203. DOI: 10.1126/science.286.5441.930. URL: https://www.science.org/doi/10.1126/science.286.5441.930 (visited on 05/26/2022).

Shakun, Jeremy D., Clark, Peter U., He, Feng, Marcott, Shaun A., Mix, Alan C., Liu, Zhengyu, Otto-Bliesner, Bette, Schmittner, Andreas, and Bard, Edouard (Apr. 2012). "Global warming preceded by increasing carbon dioxide concentrations during the last deglaciation". In: *Nature* 484.7392, pp. 49–54. ISSN: 0028-0836, 1476-4687. DOI: 10.1038/nature10915. URL: http://www.nature.com/articles/nature10915 (visited on 06/13/2022).

Sherriff-Tadano, Sam and Abe-Ouchi, Ayako (Apr. 15, 2020). "Roles of Sea Ice–Surface Wind Feedback in Maintaining the Glacial Atlantic Meridional Overturning Circulation and Climate". In: *Journal of Climate* 33.8. Publisher: American Meteorological Society Section: Journal of Climate, pp. 3001–3018. ISSN: 0894-8755, 1520-0442. DOI: 10.1175/JCLI-D-19-0431.1. URL: https://journals.ametsoc.org/view/journals/clim/33/8/jcli-d-19-0431.1.xml (visited on 02/26/2024).

Sherriff-Tadano, Sam, Abe-Ouchi, Ayako, Oka, Akira, Mitsui, Takahito, and Saito, Fuyuki (Sept. 28, 2021). "Does a difference in ice sheets between Marine Isotope Stages 3 and 5a affect the duration of stadials? Implications from hosing experiments". In: *Climate of the Past* 17.5. Publisher: Copernicus GmbH, pp. 1919–1936. ISSN: 1814-9324. DOI: 10.5194/cp-17-1919-2021. URL: https://cp.copernicus.org/articles/17/1919/2021/ (visited on 08/05/2024).

Sherriff-Tadano, Sam, Abe-Ouchi, Ayako, Yoshimori, Masakazu, Ohgaito, Rumi, Vadsaria, Tristan, Chan, Wing-Le, Hotta, Haruka, Kikuchi, Maki, Kodama, Takanori, Oka, Akira, and Suzuki, Kentaroh (June 1, 2023). "Southern Ocean Surface Temperatures and Cloud Biases in Climate Models Connected to the Representation of Glacial Deep Ocean Circulation". In: *Journal of Climate* 36.11, pp. 3849–3866. ISSN: 0894-8755, 1520-0442. DOI: 10.1175/JCLI-D-22-0221.1. URL: https://journals.ametsoc.org/view/journals/clim/36/11/JCLI-D-22-0221.1.xml (visited on 07/24/2023).

Sherriff-Tadano, Sam, Abe-Ouchi, Ayako, Yoshimori, Masakazu, Oka, Akira, and Chan, Wing-Le (Apr. 2018). "Influence of glacial ice sheets on the Atlantic meridional overturning circulation through surface wind change". In: *Climate Dynamics* 50.7, pp. 2881–2903. ISSN: 0930-7575, 1432-0894. DOI: 10.1007/s00382-017-3780-0. URL: http://link.springer.com/10.1007/s00382-017-3780-0 (visited on 11/30/2022).

Sherriff-Tadano, Sam, Ivanovic, Ruza, Gregoire, Lauren, Lang, Charlotte, Gandy, Niall, Gregory, Jonathan, Edwards, Tamsin L., Pollard, Oliver, and Smith, Robin S. (July 15, 2024). "Large-ensemble simulations of the North American and Greenland ice sheets at the Last Glacial Maximum with a coupled atmospheric general circulation–ice sheet model". In: *Climate of the Past* 20.7. Publisher: Copernicus GmbH, pp. 1489–1512. ISSN: 1814-9324. DOI: 10.5194/cp-20-1489-2024. URL: https://cp.copernicus.org/articles/20/1489/2024/ (visited on 10/17/2024).

Siahaan, Antony, Smith, Robin S., Holland, Paul R., Jenkins, Adrian, Gregory, Jonathan M., Lee, Victoria, Mathiot, Pierre, Payne, Antony J., Ridley, Jeff K., and Jones, Colin G. (Oct. 7,

2022). “The Antarctic contribution to 21st-century sea-level rise predicted by the UK Earth System Model with an interactive ice sheet”. In: *The Cryosphere* 16.10. Publisher: Copernicus GmbH, pp. 4053–4086. ISSN: 1994-0416. DOI: 10.5194/tc-16-4053-2022. URL: https://tc.copernicus.org/articles/16/4053/2022/ (visited on 02/14/2025).

Siegenthaler, Urs, Stocker, Thomas F., Monnin, Eric, Lüthi, Dieter, Schwander, Jakob, Stauffer, Bernhard, Raynaud, Dominique, Barnola, Jean-Marc, Fischer, Hubertus, Masson-Delmotte, Valérie, and Jouzel, Jean (Nov. 25, 2005). “Stable Carbon CycleClimate Relationship During the Late Pleistocene”. In: *Science* 310.5752. Publisher: American Association for the Advancement of Science, pp. 1313–1317. DOI: 10.1126/science.1120130. URL: https://www.science.org/doi/10.1126/science.1120130 (visited on 01/23/2025).

Sigmond, Michael, Fyfe, John C., Saenko, Oleg A., and Swart, Neil C. (July 2020). “Ongoing AMOC and related sea-level and temperature changes after achieving the Paris targets”. In: *Nature Climate Change* 10.7, pp. 672–677. ISSN: 1758-678X, 1758-6798. DOI: 10.1038/s41558-020-0786-0. URL: http://www.nature.com/articles/s41558-020-0786-0 (visited on 02/07/2023).

Smith, R. N. B. (1990). “A scheme for predicting layer clouds and their water content in a general circulation model”. In: *Quarterly Journal of the Royal Meteorological Society* 116.492. _eprint: https://onlinelibrary.wiley.com/doi/pdf/10.1002/qj.49711649210, pp. 435–460. ISSN: 1477-870X. DOI: 10.1002/qj.49711649210. URL: https://onlinelibrary.wiley.com/doi/abs/10.1002/qj.49711649210 (visited on 01/23/2025).

Smith, R. S., Gregory, J. M., and Osprey, A. (Dec. 12, 2008). “A description of the FAMOUS (version XDBUA) climate model and control run”. In: *Geoscientific Model Development* 1.1, pp. 53–68. ISSN: 1991-9603. DOI: 10.5194/gmd-1-53-2008. URL: https://gmd.copernicus.org/articles/1/53/2008/ (visited on 05/10/2023).

Smith, Robin S., George, Steve, and Gregory, Jonathan M. (Sept. 17, 2021). “FAMOUS version xotzt (FAMOUS-ice): a general circulation model (GCM) capable of energy- and water-conserving coupling to an ice sheet model”. In: *Geoscientific Model Development* 14.9. Publisher: Copernicus GmbH, pp. 5769–5787. ISSN: 1991-959X. DOI: 10.5194/gmd-14-5769-2021. URL: https://gmd.copernicus.org/articles/14/5769/2021/ (visited on 09/12/2024).

Smith, Robin S. and Gregory, Jonathan M. (Aug. 16, 2009). “A study of the sensitivity of ocean overturning circulation and climate to freshwater input in different regions of the North Atlantic: SENSITIVITY OF MOC TO HOSING REGION”. In: *Geophysical Research Letters* 36.15, n/a–n/a. ISSN: 00948276. DOI: 10.1029/2009GL038607. URL: http://doi.wiley.com/10.1029/2009GL038607 (visited on 01/06/2023).

Snoll, Brooke, Ivanovic, Ruza F., Valdes, Paul J., Maycock, Amanda C., and Gregoire, Lauren J. (Feb. 19, 2022). “Effect of orographic gravity wave drag on Northern Hemisphere climate in transient simulations of the last deglaciation”. In: *Climate Dynamics* 59, pp. 2067–2079. ISSN:

0930-7575, 1432-0894. DOI: 10.1007/s00382-022-06196-2. URL: https://link.springer.com/10.1007/s00382-022-06196-2 (visited on 06/16/2022).

Snoll, Brooke, Ivanovic, Ruza, Gregoire, Lauren, Sherriff-Tadano, Sam, Menviel, Laurie, Obase, Takashi, Abe-Ouchi, Ayako, Bouttes, Nathaelle, He, Chengfei, He, Feng, Kapsch, Marie, Mikolajewicz, Uwe, Muglia, Juan, and Valdes, Paul (Apr. 5, 2024). "A multi-model assessment of the early last deglaciation (PMIP4 LDv1): a meltwater perspective". In: *Climate of the Past* 20.4. Publisher: Copernicus GmbH, pp. 789–815. ISSN: 1814-9324. DOI: 10.5194/cp-20-789-2024. URL: https://cp.copernicus.org/articles/20/789/2024/ (visited on 04/09/2024).

Snow, K., Goldberg, D. N., Holland, P. R., Jordan, J. R., Arthern, R. J., and Jenkins, A. (2017). "The Response of Ice Sheets to Climate Variability". In: *Geophysical Research Letters* 44.23. _eprint: https://onlinelibrary.wiley.com/doi/pdf/10.1002/2017GL075745, pp. 11,878–11,885. ISSN: 1944-8007. DOI: 10.1002/2017GL075745. URL: https://onlinelibrary.wiley.com/doi/abs/10.1002/2017GL075745 (visited on 01/10/2025).

Solas, J. Álvarez, Montoya, M., Ritz, C., Ramstein, G., Charbit, S., Dumas, C., Nisancioglu, K., Dokken, T., and Ganopolski, A. (Nov. 29, 2011). "Heinrich event 1: an example of dynamical ice-sheet reaction to oceanic changes". In: *Climate of the Past* 7.4. Publisher: Copernicus GmbH, pp. 1297–1306. ISSN: 1814-9324. DOI: 10.5194/cp-7-1297-2011. URL: https://cp.copernicus.org/articles/7/1297/2011/ (visited on 01/10/2025).

Stanford, J. D., Rohling, E. J., Bacon, S., Roberts, A. P., Grousset, F. E., and Bolshaw, M. (May 1, 2011). "A new concept for the paleoceanographic evolution of Heinrich event 1 in the North Atlantic". In: *Quaternary Science Reviews* 30.9, pp. 1047–1066. ISSN: 0277-3791. DOI: 10.1016/j.quascirev.2011.02.003. URL: https://www.sciencedirect.com/science/article/pii/S0277379111000400 (visited on 02/20/2025).

Steffensen, Jørgen Peder, Andersen, Katrine K., Bigler, Matthias, Clausen, Henrik B., Dahl-Jensen, Dorthe, Fischer, Hubertus, Goto-Azuma, Kumiko, Hansson, Margareta, Johnsen, Sigfús J., Jouzel, Jean, Masson-Delmotte, Valérie, Popp, Trevor, Rasmussen, Sune O., Röthlisberger, Regine, Ruth, Urs, Stauffer, Bernhard, Siggaard-Andersen, Marie-Louise, Sveinbjörnsdóttir, Árný E., Svensson, Anders, and White, James W. C. (Aug. 2008). "High-Resolution Greenland Ice Core Data Show Abrupt Climate Change Happens in Few Years". In: *Science* 321.5889, pp. 680–684. ISSN: 0036-8075, 1095-9203. DOI: 10.1126/science.1157707. URL: https://www.science.org/doi/10.1126/science.1157707 (visited on 06/10/2022).

Stenni, Barbara, Masson-Delmotte, Valerie, Johnsen, Sigfus, Jouzel, Jean, Longinelli, Antonio, Monnin, Eric, Röthlisberger, Regine, and Selmo, Enrico (Sept. 14, 2001). "An Oceanic Cold Reversal During the Last Deglaciation". In: *Science* 293.5537. Publisher: American Association for the Advancement of Science, pp. 2074–2077. DOI: 10.1126/science.1059702. URL: https://www.science.org/doi/full/10.1126/science.1059702 (visited on 01/24/2025).

Stocker, Thomas F. (Oct. 2, 1998). "The Seesaw Effect". In: *Science* 282.5386, pp. 61–62. ISSN: 0036-8075, 1095-9203. DOI: 10.1126/science.282.5386.61. URL: https://www.science.org/doi/10.1126/science.282.5386.61 (visited on 01/10/2023).

Stocker, Thomas F., Timmermann, Axel, Renold, Manuel, and Timm, Oliver (Dec. 15, 2007). "Effects of Salt Compensation on the Climate Model Response in Simulations of Large Changes of the Atlantic Meridional Overturning Circulation". In: *Journal of Climate* 20.24. Publisher: American Meteorological Society Section: Journal of Climate, pp. 5912–5928. ISSN: 0894-8755, 1520-0442. DOI: 10.1175/2007JCLI1662.1. URL: https://journals.ametsoc.org/view/journals/clim/20/24/2007jcli1662.1.xml (visited on 01/24/2024).

Stokes, Chris R. and Clark, Chris D. (July 1, 2001). "Palaeo-ice streams". In: *Quaternary Science Reviews* 20.13, pp. 1437–1457. ISSN: 0277-3791. DOI: 10.1016/S0277-3791(01)00003-8. URL: https://www.sciencedirect.com/science/article/pii/S0277379101000038 (visited on 01/30/2025).

Stokes, Chris R., Tarasov, Lev, Blomdin, Robin, Cronin, Thomas M., Fisher, Timothy G., Gyllencreutz, Richard, Hättestrand, Clas, Heyman, Jakob, Hindmarsh, Richard C. A., Hughes, Anna L. C., Jakobsson, Martin, Kirchner, Nina, Livingstone, Stephen J., Margold, Martin, Murton, Julian B., Noormets, Riko, Peltier, W. Richard, Peteet, Dorothy M., Piper, David J. W., Preusser, Frank, Renssen, Hans, Roberts, David H., Roche, Didier M., Saint-Ange, Francky, Stroeven, Arjen P., and Teller, James T. (Oct. 1, 2015). "On the reconstruction of palaeo-ice sheets: Recent advances and future challenges". In: *Quaternary Science Reviews* 125, pp. 15–49. ISSN: 0277-3791. DOI: 10.1016/j.quascirev.2015.07.016. URL: https://www.sciencedirect.com/science/article/pii/S027737911530055X (visited on 02/21/2025).

Stommel, Henry (1961). "Thermohaline Convection with Two Stable Regimes of Flow". In: *Tellus* 13.2. _eprint: https://onlinelibrary.wiley.com/doi/pdf/10.1111/j.2153-3490.1961.tb00079.x, pp. 224–230. ISSN: 2153-3490. DOI: 10.1111/j.2153-3490.1961.tb00079.x. URL: https://onlinelibrary.wiley.com/doi/abs/10.1111/j.2153-3490.1961.tb00079.x (visited on 01/27/2025).

Stouffer, Ronald J., Seidov, Dan, and Haupt, Bernd J. (Feb. 1, 2007). "Climate Response to External Sources of Freshwater: North Atlantic versus the Southern Ocean". In: Section: Journal of Climate. DOI: 10.1175/JCLI4015.1. URL: https://journals.ametsoc.org/view/journals/clim/20/3/jcli4015.1.xml (visited on 01/27/2025).

Su, Zhan, Ingersoll, Andrew P., and He, Feng (July 1, 2016). "On the Abruptness of Bølling–Allerød Warming". In: Section: Journal of Climate. DOI: 10.1175/JCLI-D-15-0675.1. URL: https://journals.ametsoc.org/view/journals/clim/29/13/jcli-d-15-0675.1.xml (visited on 02/21/2025).

Sun, Yuchen, Knorr, Gregor, Zhang, Xu, Tarasov, Lev, Barker, Stephen, Werner, Martin, and Lohmann, Gerrit (Mar. 2022). "Ice sheet decline and rising atmospheric CO2 control AMOC

sensitivity to deglacial meltwater discharge". In: *Global and Planetary Change* 210, p. 103755. ISSN: 09218181. DOI: 10.1016/j.gloplacha.2022.103755. URL: https://linkinghub.elsevier.com/retrieve/pii/S0921818122000224 (visited on 03/16/2022).

Svendsen, J (June 2004). "Late Quaternary ice sheet history of northern Eurasia". In: *Quaternary Science Reviews* 23.11, pp. 1229–1271. ISSN: 02773791. DOI: 10.1016/j.quascirev.2003.12.008. URL: https://linkinghub.elsevier.com/retrieve/pii/S0277379103003421 (visited on 01/27/2022).

Swingedouw, Didier, Fichefet, T., Goosse, H., and Loutre, M. F. (Aug. 1, 2009). "Impact of transient freshwater releases in the Southern Ocean on the AMOC and climate". In: *Climate Dynamics* 33.2, pp. 365–381. ISSN: 1432-0894. DOI: 10.1007/s00382-008-0496-1. URL: https://doi.org/10.1007/s00382-008-0496-1 (visited on 02/13/2025).

Sánchez Goñi, María Fernanda, Landais, Amaelle, Fletcher, William J., Naughton, Filipa, Desprat, Stéphanie, and Duprat, Josette (June 1, 2008). "Contrasting impacts of Dansgaard–Oeschger events over a western European latitudinal transect modulated by orbital parameters". In: *Quaternary Science Reviews* 27.11, pp. 1136–1151. ISSN: 0277-3791. DOI: 10.1016/j.quascirev.2008.03.003. URL: https://www.sciencedirect.com/science/article/pii/S0277379108000759 (visited on 02/20/2025).

Tabone, Ilaria, Blasco, Javier, Robinson, Alexander, Alvarez-Solas, Jorge, and Montoya, Marisa (Apr. 9, 2018). "The sensitivity of the Greenland Ice Sheet to glacial–interglacial oceanic forcing". In: *Climate of the Past* 14.4. Publisher: Copernicus GmbH, pp. 455–472. ISSN: 1814-9324. DOI: 10.5194/cp-14-455-2018. URL: https://cp.copernicus.org/articles/14/455/2018/ (visited on 01/10/2025).

Tarasov, L. and Peltier, W. R. (July 2002). "Greenland glacial history and local geodynamic consequences". In: *Geophysical Journal International* 150.1, pp. 198–229. ISSN: 0956540X, 1365246X. DOI: 10.1046/j.1365-246X.2002.01702.x. URL: https://academic.oup.com/gji/article-lookup/doi/10.1046/j.1365-246X.2002.01702.x (visited on 01/27/2022).

Tarasov, Lev, Dyke, Arthur S., Neal, Radford M., and Peltier, W.R. (Jan. 2012). "A data-calibrated distribution of deglacial chronologies for the North American ice complex from glaciological modeling". In: *Earth and Planetary Science Letters* 315-316, pp. 30–40. ISSN: 0012821X. DOI: 10.1016/j.epsl.2011.09.010. URL: https://linkinghub.elsevier.com/retrieve/pii/S0012821X11005243 (visited on 01/27/2022).

Thomas, Elizabeth R., Wolff, Eric W., Mulvaney, Robert, Johnsen, Sigfus J., Steffensen, Jorgen P., and Arrowsmith, Carol (2009). "Anatomy of a Dansgaard-Oeschger warming transition: High-resolution analysis of the North Greenland Ice Core Project ice core". In: *Journal of Geophysical Research: Atmospheres* 114 (D8). _eprint: https://onlinelibrary.wiley.com/doi/pdf/10.1029/2008JD0 ISSN: 2156-2202. DOI: 10.1029/2008JD011215. URL: https://onlinelibrary.wiley.com/doi/abs/10.1029/2008JD011215 (visited on 01/24/2025).

Thomas, Elizabeth R., Wolff, Eric W., Mulvaney, Robert, Steffensen, Jorgen P., Johnsen, Sigfus J., Arrowsmith, Carol, White, James W.C., Vaughn, Bruce, and Popp, Trevor (Jan. 2007). "The 8.2ka event from Greenland ice cores". In: *Quaternary Science Reviews* 26.1, pp. 70–81. ISSN: 02773791. DOI: 10.1016/j.quascirev.2006.07.017. URL: https://linkinghub.elsevier.com/retrieve/pii/S0277379106002393 (visited on 01/17/2023).

Thornalley, David J. R., McCave, I. Nick, and Elderfield, Harry (Mar. 2010). "Freshwater input and abrupt deglacial climate change in the North Atlantic: DEGLACIAL FRESHWATER INPUT AND CLIMATE". In: *Paleoceanography* 25.1. ISSN: 08838305. DOI: 10.1029/2009PA001772. URL: http://doi.wiley.com/10.1029/2009PA001772 (visited on 06/01/2023).

Toggweiler, J. R. and Russell, Joellen (Jan. 2008). "Ocean circulation in a warming climate". In: *Nature* 451.7176. Publisher: Nature Publishing Group, pp. 286–288. ISSN: 1476-4687. DOI: 10.1038/nature06590. URL: https://www.nature.com/articles/nature06590 (visited on 12/10/2024).

Toucanne, Samuel, Soulet, Guillaume, Freslon, Nicolas, Silva Jacinto, Ricardo, Dennielou, Bernard, Zaragosi, Sébastien, Eynaud, Frédérique, Bourillet, Jean-François, and Bayon, Germain (Sept. 1, 2015). "Millennial-scale fluctuations of the European Ice Sheet at the end of the last glacial, and their potential impact on global climate". In: *Quaternary Science Reviews* 123, pp. 113–133. ISSN: 0277-3791. DOI: 10.1016/j.quascirev.2015.06.010. URL: https://www.sciencedirect.com/science/article/pii/S0277379115300196 (visited on 02/20/2025).

Tsai, Victor C., Stewart, Andrew L., and Thompson, Andrew F. (Jan. 2015). "Marine ice-sheet profiles and stability under Coulomb basal conditions". In: *Journal of Glaciology* 61.226, pp. 205–215. ISSN: 0022-1430, 1727-5652. DOI: 10.3189/2015JoG14J221. URL: https://www.cambridge.org/core/journals/journal-of-glaciology/article/marine-icesheet-profiles-and-stability-under-coulomb-basal-conditions/21715D81380B20D4C72EBAC1F0953610 (visited on 02/14/2025).

Turner, John, Bracegirdle, Thomas J., Phillips, Tony, Marshall, Gareth J., and Hosking, J. Scott (Mar. 1, 2013). "An Initial Assessment of Antarctic Sea Ice Extent in the CMIP5 Models". In: DOI: 10.1175/JCLI-D-12-00068.1. URL: https://journals.ametsoc.org/view/journals/clim/26/5/jcli-d-12-00068.1.xml (visited on 07/28/2025).

Turney, Chris S. M., Thomas, Zoë A., Hutchinson, David K., Bradshaw, Corey J. A., Brook, Barry W., England, Matthew H., Fogwill, Christopher J., Jones, Richard T., Palmer, Jonathan, Hughen, Konrad A., and Cooper, Alan (2015). "Obliquity-driven expansion of North Atlantic sea ice during the last glacial". In: *Geophysical Research Letters* 42.23. _eprint: https://onlinelibrary.wiley.com pp. 10,382–10,390. ISSN: 1944-8007. DOI: 10.1002/2015GL066344. URL: https://onlinelibrary.wiley.com/doi/abs/10.1002/2015GL066344 (visited on 08/15/2024).

Tziperman, Eli (Jan. 1, 2000). "Proximity of the Present-Day Thermohaline Circulation to an Instability Threshold". In: Section: Journal of Physical Oceanography. ISSN: 1520-0485. URL:

https://journals.ametsoc.org/view/journals/phoc/30/1/1520-0485_2000_030_0090_potpdt_2.0.co_2.xml (visited on 02/03/2025).

Ullman, D. J., LeGrande, A. N., Carlson, A. E., Anslow, F. S., and Licciardi, J. M. (Mar. 13, 2014). "Assessing the impact of Laurentide Ice Sheet topography on glacial climate". In: *Climate of the Past* 10.2, pp. 487–507. ISSN: 1814-9332. DOI: 10.5194/cp-10-487-2014. URL: https://cp.copernicus.org/articles/10/487/2014/ (visited on 06/16/2022).

Ullman, David J., Carlson, Anders E., Hostetler, Steven W., Clark, Peter U., Cuzzone, Joshua, Milne, Glenn A., Winsor, Kelsey, and Caffee, Marc (Nov. 2016). "Final Laurentide ice-sheet deglaciation and Holocene climate-sea level change". In: *Quaternary Science Reviews* 152, pp. 49–59. ISSN: 02773791. DOI: 10.1016/j.quascirev.2016.09.014. URL: https://linkinghub.elsevier.com/retrieve/pii/S027737911630364X (visited on 06/01/2023).

Valdes, Paul J., Armstrong, Edward, Badger, Marcus P. S., Bradshaw, Catherine D., Bragg, Fran, Crucifix, Michel, Davies-Barnard, Taraka, Day, Jonathan J., Farnsworth, Alex, Gordon, Chris, Hopcroft, Peter O., Kennedy, Alan T., Lord, Natalie S., Lunt, Dan J., Marzocchi, Alice, Parry, Louise M., Pope, Vicky, Roberts, William H. G., Stone, Emma J., Tourte, Gregory J. L., and Williams, Jonny H. T. (Oct. 12, 2017). "The BRIDGE HadCM3 family of climate models: HadCM3@Bristol v1.0". In: *Geoscientific Model Development* 10.10, pp. 3715–3743. ISSN: 1991-9603. DOI: 10.5194/gmd-10-3715-2017. URL: https://gmd.copernicus.org/articles/10/3715/2017/ (visited on 01/27/2022).

Valdes, Paul (July 2011). "Built for stability". In: *Nature Geoscience* 4.7, pp. 414–416. ISSN: 1752-0894, 1752-0908. DOI: 10.1038/ngeo1200. URL: http://www.nature.com/articles/ngeo1200 (visited on 01/06/2023).

Vanneste, Heleen, De Vleeschouwer, François, Martínez-Cortizas, Antonio, Scheffer, Clemens von, Piotrowska, Natalia, Coronato, Andrea, and Le Roux, Gaël (July 1, 2015). "Late-glacial elevated dust deposition linked to westerly wind shifts in southern South America". In: *Scientific Reports* 5.1. Number: 1 Publisher: Nature Publishing Group, p. 11670. ISSN: 2045-2322. DOI: 10.1038/srep11670. URL: https://www.nature.com/articles/srep11670 (visited on 02/23/2024).

Veres, D., Bazin, L., Landais, A., Toyé Mahamadou Kele, H., Lemieux-Dudon, B., Parrenin, F., Martinerie, P., Blayo, E., Blunier, T., Capron, E., Chappellaz, J., Rasmussen, S. O., Severi, M., Svensson, A., Vinther, B., and Wolff, E. W. (Aug. 1, 2013). "The Antarctic ice core chronology (AICC2012): an optimized multi-parameter and multi-site dating approach for the last 120 thousand years". In: *Climate of the Past* 9.4, pp. 1733–1748. ISSN: 1814-9332. DOI: 10.5194/cp-9-1733-2013. URL: https://cp.copernicus.org/articles/9/1733/2013/ (visited on 06/16/2022).

Vettoretti, G. and Peltier, W.R. (Aug. 1, 2011). "The impact of insolation, greenhouse gas forcing and ocean circulation changes on glacial inception". In: *The Holocene* 21.5. Publisher:

SAGE Publications Ltd, pp. 803–817. ISSN: 0959-6836. DOI: 10.1177/0959683610394885. URL: https://doi.org/10.1177/0959683610394885 (visited on 02/04/2025).

Vettoretti, Guido, Ditlevsen, Peter, Jochum, Markus, and Rasmussen, Sune Olander (Apr. 2022). "Atmospheric CO2 control of spontaneous millennial-scale ice age climate oscillations". In: *Nature Geoscience* 15.4. Publisher: Nature Publishing Group, pp. 300–306. ISSN: 1752-0908. DOI: 10.1038/s41561-022-00920-7. URL: https://www.nature.com/articles/s41561-022-00920-7 (visited on 12/02/2024).

Vettoretti, Guido and Peltier, W. Richard (2016). "Thermohaline instability and the formation of glacial North Atlantic super polynyas at the onset of Dansgaard-Oeschger warming events". In: *Geophysical Research Letters* 43.10. _eprint: https://onlinelibrary.wiley.com/doi/pdf/10.1002/2016GL068 pp. 5336–5344. ISSN: 1944-8007. DOI: 10.1002/2016GL068891. URL: https://onlinelibrary.wiley.com/doi/abs/10.1002/2016GL068891 (visited on 01/28/2025).

– (May 1, 2018). "Fast Physics and Slow Physics in the Nonlinear Dansgaard–Oeschger Relaxation Oscillation". In: Section: Journal of Climate. DOI: 10.1175/JCLI-D-17-0559.1. URL: https://journals.ametsoc.org/view/journals/clim/31/9/jcli-d-17-0559.1.xml (visited on 12/09/2024).

Vidal, L., Labeyrie, L., Cortijo, E., Arnold, M., Duplessy, J. C., Michel, E., Becqué, S., and Weering, T. C. E. van (Jan. 1, 1997). "Evidence for changes in the North Atlantic Deep Water linked to meltwater surges during the Heinrich events". In: *Earth and Planetary Science Letters* 146.1, pp. 13–27. ISSN: 0012-821X. DOI: 10.1016/S0012-821X(96)00192-6. URL: https://www.sciencedirect.com/science/article/pii/S0012821X96001926 (visited on 01/28/2025).

Vizcaino, Miren, Mikolajewicz, Uwe, Ziemen, Florian, Rodehacke, Christian B., Greve, Ralf, and Broeke, Michiel R. van den (2015). "Coupled simulations of Greenland Ice Sheet and climate change up to A.D. 2300". In: *Geophysical Research Letters* 42.10. _eprint: https://onlinelibrary.wiley.com/doi/ pp. 3927–3935. ISSN: 1944-8007. DOI: 10.1002/2014GL061142. URL: https://onlinelibrary.wiley.com/doi/abs/10.1002/2014GL061142 (visited on 01/09/2025).

Waelbroeck, C., Labeyrie, L., Michel, E., Duplessy, J. C., McManus, J. F., Lambeck, K., Balbon, E., and Labracherie, M. (Jan. 1, 2002). "Sea-level and deep water temperature changes derived from benthic foraminifera isotopic records". In: *Quaternary Science Reviews*. EPILOG 21.1, pp. 295–305. ISSN: 0277-3791. DOI: 10.1016/S0277-3791(01)00101-9. URL: https://www.sciencedirect.com/science/article/pii/S0277379101001019 (visited on 01/21/2025).

Wang, Xianfeng, Auler, Augusto S., Edwards, R. Lawrence, Cheng, Hai, Cristalli, Patricia S., Smart, Peter L., Richards, David A., and Shen, Chuan-Chou (Dec. 2004). "Wet periods in northeastern Brazil over the past 210 kyr linked to distant climate anomalies". In: *Nature* 432.7018. Number: 7018 Publisher: Nature Publishing Group, pp. 740–743. ISSN: 1476-4687. DOI: 10.1038/nature03067. URL: https://www.nature.com/articles/nature03067 (visited on 02/23/2024).

Wang, Yongjin, Cheng, Hai, Edwards, R. Lawrence, Kong, Xinggong, Shao, Xiaohua, Chen, Shitao, Wu, Jiangyin, Jiang, Xiouyang, Wang, Xianfeng, and An, Zhisheng (Feb. 2008). "Millennial- and orbital-scale changes in the East Asian monsoon over the past 224,000 years". In: *Nature* 451.7182. Number: 7182 Publisher: Nature Publishing Group, pp. 1090–1093. ISSN: 1476-4687. DOI: 10.1038/nature06692. URL: https://www.nature.com/articles/nature06692 (visited on 02/23/2024).

Weaver, A. J. (Mar. 14, 2003). "Meltwater Pulse 1A from Antarctica as a Trigger of the Bolling-Allerod Warm Interval". In: *Science* 299.5613, pp. 1709–1713. ISSN: 00368075, 10959203. DOI: 10.1126/science.1081002. URL: https://www.sciencemag.org/lookup/doi/10.1126/science.1081002 (visited on 09/02/2021).

Weaver, Andrew J., Eby, Michael, Wiebe, Edward C., Bitz, Cecilia M., Duffy, Phil B., Ewen, Tracy L., Fanning, Augustus F., Holland, Marika M., MacFadyen, Amy, Matthews, H. Damon, Meissner, Katrin J., Saenko, Oleg, Schmittner, Andreas, Wang, Huaxiao, and Yoshimori, Masakazu (Dec. 1, 2001). "The UVic earth system climate model: Model description, climatology, and applications to past, present and future climates". In: *Atmosphere-Ocean* 39.4, pp. 361–428. ISSN: 0705-5900, 1480-9214. DOI: 10.1080/07055900.2001.9649686. URL: https://www.tandfonline.com/doi/full/10.1080/07055900.2001.9649686 (visited on 05/10/2023).

Weber, M. E., Clark, P. U., Kuhn, G., Timmermann, A., Sprenk, D., Gladstone, R., Zhang, X., Lohmann, G., Menviel, L., Chikamoto, M. O., Friedrich, T., and Ohlwein, C. (June 2014). "Millennial-scale variability in Antarctic ice-sheet discharge during the last deglaciation". In: *Nature* 510.7503. Number: 7503 Publisher: Nature Publishing Group, pp. 134–138. ISSN: 1476-4687. DOI: 10.1038/nature13397. URL: https://www.nature.com/articles/nature13397 (visited on 01/03/2024).

Weber, Susanne L. (2010). "The utility of Earth system Models of Intermediate Complexity (EMICs)". In: *WIREs Climate Change* 1.2. _eprint: https://onlinelibrary.wiley.com/doi/pdf/10.1002/wcc.24, pp. 243–252. ISSN: 1757-7799. DOI: 10.1002/wcc.24. URL: https://onlinelibrary.wiley.com/doi/abs/10.1002/wcc.24 (visited on 01/30/2025).

Wickert, Andrew D. (Nov. 8, 2016). "Reconstruction of North American drainage basins and river discharge since the Last Glacial Maximum". In: *Earth Surface Dynamics* 4.4, pp. 831–869. ISSN: 2196-632X. DOI: 10.5194/esurf-4-831-2016. URL: https://esurf.copernicus.org/articles/4/831/2016/ (visited on 05/11/2023).

Wickert, Andrew D., Williams, Carlie, Gregoire, Lauren J., Callaghan, Kerry L., Ivanović, Ruža F., Valdes, Paul J., Vetter, Lael, and Jennings, Carrie E. (2023). "Marine-Calibrated Chronology of Southern Laurentide Ice Sheet Advance and Retreat: 2,000-Year Cycles Paced by Meltwater–Climate Feedback". In: *Geophysical Research Letters* 50.10. _eprint: https://onlinelibrary.wiley.com/do e2022GL100391. ISSN: 1944-8007. DOI: 10.1029/2022GL100391. URL: https://onlinelibrary.wiley.com/doi/abs/10.1029/2022GL100391 (visited on 12/17/2024).

Wilmes, Sophie-Berenice, Green, J. A. Mattias, and Schmittner, Andreas (Aug. 18, 2021). "Enhanced vertical mixing in the glacial ocean inferred from sedimentary carbon isotopes". In: *Communications Earth & Environment* 2.1, p. 166. ISSN: 2662-4435. DOI: 10.1038/s43247-021-00239-y. URL: https://www.nature.com/articles/s43247-021-00239-y (visited on 06/05/2023).

Wolff, E. W., Chappellaz, J., Blunier, T., Rasmussen, S. O., and Svensson, A. (Oct. 1, 2010). "Millennial-scale variability during the last glacial: The ice core record". In: *Quaternary Science Reviews*. Vegetation Response to Millennial-scale Variability during the Last Glacial 29.21, pp. 2828–2838. ISSN: 0277-3791. DOI: 10.1016/j.quascirev.2009.10.013. URL: https://www.sciencedirect.com/science/article/pii/S0277379109003588 (visited on 02/22/2024).

Yang, Shiling and Ding, Zhongli (2014). "A 249 kyr stack of eight loess grain size records from northern China documenting millennial-scale climate variability". In: *Geochemistry, Geophysics, Geosystems* 15.3. _eprint: https://onlinelibrary.wiley.com/doi/pdf/10.1002/2013GC005113, pp. 798–814. ISSN: 1525-2027. DOI: 10.1002/2013GC005113. URL: https://onlinelibrary.wiley.com/doi/abs/10.1002/2013GC005113 (visited on 02/27/2025).

Yeung, N. K. H., Menviel, L., Meissner, K. J., and Sikes, E. (Dec. 1, 2019). "Assessing the Spatial Origin of Meltwater Pulse 1A Using Oxygen-Isotope Fingerprinting". In: *Paleoceanography and Paleoclimatology* 34.12. Publisher: John Wiley & Sons, Ltd, pp. 2031–2046. ISSN: 2572-4525. DOI: 10.1029/2019PA003599. URL: https://agupubs.onlinelibrary.wiley.com/doi/10.1029/2019PA003599 (visited on 01/04/2024).

Yin, Q. Z., Wu, Z. P., Berger, A., Goosse, H., and Hodell, D. (Aug. 27, 2021). "Insolation triggered abrupt weakening of Atlantic circulation at the end of interglacials". In: *Science*. Publisher: American Association for the Advancement of Science. DOI: 10.1126/science.abg1737. URL: https://www.science.org/doi/10.1126/science.abg1737 (visited on 06/14/2024).

Yin, Qiu Zhen and Berger, André (Feb. 1, 2012). "Individual contribution of insolation and CO2 to the interglacial climates of the past 800,000 years". In: *Climate Dynamics* 38.3, pp. 709–724. ISSN: 1432-0894. DOI: 10.1007/s00382-011-1013-5. URL: https://doi.org/10.1007/s00382-011-1013-5 (visited on 02/04/2025).

Yokoyama, Yusuke, Lambeck, Kurt, De Deckker, Patrick, Johnston, Paul, and Fifield, L. Keith (Aug. 17, 2000). "Timing of the Last Glacial Maximum from observed sea-level minima". In: *Nature* 406.6797, pp. 713–716. ISSN: 0028-0836, 1476-4687. DOI: 10.1038/35021035. URL: https://www.nature.com/articles/35021035 (visited on 06/02/2023).

Zhang, Xiao and Prange, Matthias (Aug. 15, 2020). "Stability of the Atlantic overturning circulation under intermediate (MIS3) and full glacial (LGM) conditions and its relationship with Dansgaard-Oeschger climate variability". In: *Quaternary Science Reviews* 242,

p. 106443. ISSN: 0277-3791. DOI: 10.1016/j.quascirev.2020.106443. URL: https://www.sciencedirect.com/science/article/pii/S0277379120304054 (visited on 02/05/2025).

Zhang, Xu, Barker, Stephen, Knorr, Gregor, Lohmann, Gerrit, Drysdale, Russell, Sun, Youbin, Hodell, David, and Chen, Fahu (Nov. 2021). "Direct astronomical influence on abrupt climate variability". In: *Nature Geoscience* 14.11. Number: 11 Publisher: Nature Publishing Group, pp. 819–826. ISSN: 1752-0908. DOI: 10.1038/s41561-021-00846-6. URL: https://www.nature.com/articles/s41561-021-00846-6 (visited on 02/26/2024).

Zhang, Xu, Knorr, Gregor, Lohmann, Gerrit, and Barker, Stephen (July 2017). "Abrupt North Atlantic circulation changes in response to gradual CO2 forcing in a glacial climate state". In: *Nature Geoscience* 10.7, pp. 518–523. ISSN: 1752-0894, 1752-0908. DOI: 10.1038/ngeo2974. URL: http://www.nature.com/articles/ngeo2974 (visited on 09/09/2021).

Zhang, Xu, Lohmann, Gerrit, Knorr, Gregor, and Purcell, Conor (Aug. 21, 2014). "Abrupt glacial climate shifts controlled by ice sheet changes". In: *Nature* 512.7514, pp. 290–294. ISSN: 0028-0836, 1476-4687. DOI: 10.1038/nature13592. URL: https://www.nature.com/articles/nature13592 (visited on 09/09/2021).

Zhu, Chenyu, Liu, Zhengyu, Zhang, Shaoqing, and Wu, Lixin (Sept. 1, 2021). "Global Oceanic Overturning Circulation Forced by the Competition between Greenhouse Gases and Continental Ice Sheets during the Last Deglaciation". In: *Journal of Climate* 34.18. Publisher: American Meteorological Society Section: Journal of Climate, pp. 7555–7570. ISSN: 0894-8755, 1520-0442. DOI: 10.1175/JCLI-D-21-0125.1. URL: https://journals.ametsoc.org/view/journals/clim/34/18/JCLI-D-21-0125.1.xml (visited on 11/20/2023).

Zhu, Jiang, Liu, Zhengyu, Zhang, Jiaxu, and Liu, Wei (June 1, 2015). "AMOC response to global warming: dependence on the background climate and response timescale". In: *Climate Dynamics* 44.11, pp. 3449–3468. ISSN: 1432-0894. DOI: 10.1007/s00382-014-2165-x. URL: https://doi.org/10.1007/s00382-014-2165-x (visited on 12/10/2024).

Ziemen, F. A., Rodehacke, C. B., and Mikolajewicz, U. (Oct. 7, 2014). "Coupled ice sheet–climate modeling under glacial and pre-industrial boundary conditions". In: *Climate of the Past* 10.5. Publisher: Copernicus GmbH, pp. 1817–1836. ISSN: 1814-9324. DOI: 10.5194/cp-10-1817-2014. URL: https://cp.copernicus.org/articles/10/1817/2014/ (visited on 09/18/2024).